

DESIGN AND ANALYSIS OF COMPOSITE STRUCTURES WITH APPLICATIONS TO AEROSPACE STRUCTURES

Christos Kassapoglou

Delft University of Technology, The Netherlands



A John Wiley and Sons, Ltd, Publication

DESIGN AND ANALYSIS OF COMPOSITE STRUCTURES

Aerospace Series List

Cooperative Path Planning of Unmanned Aerial Vehicles	Tsourdos et al	November 2010
Principles of Flight for Pilots	Swatton	October 2010
Air Travel and Health: A Systems Perspective	Seabridge et al	September 2010
Design and Analysis of Composite Structures: With Applications to Aerospace Structures	Kassapoglou	September 2010
Unmanned Aircraft Systems: UAVS Design, Development and Deployment	Austin	April 2010
Introduction to Antenna Placement & Installations	Macnamara	April 2010
Principles of Flight Simulation	Allerton	October 2009
Aircraft Fuel Systems	Langton et al	May 2009
The Global Airline Industry	Belobaba	April 2009
Computational Modelling and Simulation of Aircraft and the Environment: Volume 1 - Platform Kinematics and Synthetic Environment	Diston	April 2009
Handbook of Space Technology	Ley, Wittmann Hallmann	April 2009
Aircraft Performance Theory and Practice for Pilots	Swatton	August 2008
Surrogate Modelling in Engineering Design: A Practical Guide	Forrester, Sobester, Keane	August 2008
Aircraft Systems, 3rd Edition	Moir & Seabridge	March 2008
Introduction to Aircraft Aeroelasticity And Loads	Wright & Cooper	December 2007
Stability and Control of Aircraft Systems	Langton	September 2006
Military Avionics Systems	Moir & Seabridge	February 2006
Design and Development of Aircraft Systems	Moir & Seabridge	June 2004
Aircraft Loading and Structural Layout	Howe	May 2004
Aircraft Display Systems	Jukes	December 2003
Civil Avionics Systems	Moir & Seabridge	December 2002

DESIGN AND ANALYSIS OF COMPOSITE STRUCTURES WITH APPLICATIONS TO AEROSPACE STRUCTURES

Christos Kassapoglou

Delft University of Technology, The Netherlands



A John Wiley and Sons, Ltd, Publication

This edition first published 2010
© 2010, John Wiley & Sons, Ltd

Registered office

John Wiley & Sons Ltd, The Atrium, Southern Gate, Chichester, West Sussex, PO19 8SQ, United Kingdom

For details of our global editorial offices, for customer services and for information about how to apply for permission to reuse the copyright material in this book please see our website at www.wiley.com.

The right of the author to be identified as the author of this work has been asserted in accordance with the Copyright, Designs and Patents Act 1988.

All rights reserved. No part of this publication may be reproduced, stored in a retrieval system, or transmitted, in any form or by any means, electronic, mechanical, photocopying, recording or otherwise, except as permitted by the UK Copyright, Designs and Patents Act 1988, without the prior permission of the publisher.

Wiley also publishes its books in a variety of electronic formats. Some content that appears in print may not be available in electronic books.

Designations used by companies to distinguish their products are often claimed as trademarks. All brand names and product names used in this book are trade names, service marks, trademarks or registered trademarks of their respective owners. The publisher is not associated with any product or vendor mentioned in this book. This publication is designed to provide accurate and authoritative information in regard to the subject matter covered. It is sold on the understanding that the publisher is not engaged in rendering professional services. If professional advice or other expert assistance is required, the services of a competent professional should be sought.

Library of Congress Cataloging-in-Publication Data

Kassapoglou, Christos.

Design and analysis of composite structures: With applications to aerospace structures / Christos Kassapoglou.

p. cm.

Includes index.

ISBN 978-0-470-97263-2 (cloth)

1. Composite construction. I. Title.

TA664.K37 2010

624.1'8-dc22

2010019474

A catalogue record for this book is available from the British Library.

Print ISBN:9780470972632

ePDF ISBN:9780470972717

eBook ISBN: 9780470972700

Set in 10/12 Times, by Thomson Digital, Noida, India.

Contents

About the Author	ix
Series Preface	x
Preface	xi
1 Applications of Advanced Composites in Aircraft Structures	1
References	7
2 Cost of Composites: a Qualitative Discussion	9
2.1 Recurring Cost	10
2.2 Nonrecurring Cost	18
2.3 Technology Selection	20
2.4 Summary and Conclusions	27
Exercises	30
References	30
3 Review of Classical Laminated Plate Theory	33
3.1 Composite Materials: Definitions, Symbols and Terminology	33
3.2 Constitutive Equations in Three Dimensions	35
3.2.1 <i>Tensor Transformations</i>	37
3.3 Constitutive Equations in Two Dimensions: Plane Stress	39
Exercises	52
References	53
4 Review of Laminate Strength and Failure Criteria	55
4.1 Maximum Stress Failure Theory	57
4.2 Maximum Strain Failure Theory	58
4.3 Tsai–Hill Failure Theory	58
4.4 Tsai–Wu Failure Theory	59
4.5 Other Failure Theories	59
References	60
5 Composite Structural Components and Mathematical Formulation	63
5.1 Overview of Composite Airframe	63
5.1.1 <i>The Structural Design Process: The Analyst's Perspective</i>	64

5.1.2	<i>Basic Design Concept and Process/Material Considerations for Aircraft Parts</i>	69
5.1.3	<i>Sources of Uncertainty: Applied Loads, Usage and Material Scatter</i>	72
5.1.4	<i>Environmental Effects</i>	75
5.1.5	<i>Effect of Damage</i>	76
5.1.6	<i>Design Values and Allowables</i>	78
5.1.7	<i>Additional Considerations of the Design Process</i>	81
5.2	Governing Equations	82
5.2.1	<i>Equilibrium Equations</i>	82
5.2.2	<i>Stress–Strain Equations</i>	84
5.2.3	<i>Strain–Displacement Equations</i>	85
5.2.4	<i>von Karman Anisotropic Plate Equations for Large Deflections</i>	86
5.3	Reductions of Governing Equations: Applications to Specific Problems	91
5.3.1	<i>Composite Plate Under Localized in-Plane Load</i>	92
5.3.2	<i>Composite Plate Under Out-of-Plane Point Load</i>	103
5.4	Energy Methods	106
5.4.1	<i>Energy Expressions for Composite Plates</i>	107
	Exercises	113
	References	116
6	Buckling of Composite Plates	119
6.1	Buckling of Rectangular Composite Plate under Biaxial Loading	119
6.2	Buckling of Rectangular Composite Plate under Uniaxial Compression	122
6.2.1	<i>Uniaxial Compression, Three Sides Simply Supported, One Side Free</i>	124
6.3	Buckling of Rectangular Composite Plate under Shear	127
6.4	Buckling of Long Rectangular Composite Plates under Shear	129
6.5	Buckling of Rectangular Composite Plates under Combined Loads	132
6.6	Design Equations for Different Boundary Conditions and Load Combinations	138
	Exercises	141
	References	143
7	Post-Buckling	145
7.1	Post-Buckling Analysis of Composite Panels under Compression	149
7.1.1	<i>Application: Post-Buckled Panel Under Compression</i>	157
7.2	Post-Buckling Analysis of Composite Plates under Shear	159
7.2.1	<i>Post-buckling of Stiffened Composite Panels under Shear</i>	163
7.2.2	<i>Post-buckling of Stiffened Composite Panels under Combined Uniaxial and Shear Loading</i>	171
	Exercises	174
	References	177
8	Design and Analysis of Composite Beams	179
8.1	Cross-section Definition Based on Design Guidelines	179
8.2	Cross-sectional Properties	182
8.3	Column Buckling	188

8.4	Beam on an Elastic Foundation under Compression	189
8.5	Crippling	194
8.5.1	<i>One-Edge-Free (OEF) Crippling</i>	196
8.5.2	<i>No-Edge-Free (NEF) Crippling</i>	200
8.5.3	<i>Crippling under Bending Loads</i>	202
8.5.4	<i>Crippling of Closed-Section Beams</i>	207
8.6	Importance of Radius Regions at Flange Intersections	207
8.7	Inter-rivet Buckling of Stiffener Flanges	210
8.8	Application: Analysis of Stiffeners in a Stiffened Panel under Compression	215
	Exercises	218
	References	222
9	Skin-Stiffened Structure	223
9.1	Smearing of Stiffness Properties (Equivalent Stiffness)	223
9.1.1	<i>Equivalent Membrane Stiffnesses</i>	223
9.1.2	<i>Equivalent Bending Stiffnesses</i>	225
9.2	Failure Modes of a Stiffened Panel	227
9.2.1	<i>Local Buckling (Between Stiffeners) Versus Overall Panel Buckling (the Panel Breaker Condition)</i>	228
9.2.2	<i>Skin–Stiffener Separation</i>	236
9.3	Additional Considerations for Stiffened Panels	251
9.3.1	<i>'Pinching' of Skin</i>	251
9.3.2	<i>Co-Curing Versus Bonding Versus Fastening</i>	251
	Exercises	253
	References	258
10	Sandwich Structure	259
10.1	Sandwich Bending Stiffnesses	260
10.2	Buckling of Sandwich Structure	262
10.2.1	<i>Buckling of Sandwich Under Compression</i>	262
10.2.2	<i>Buckling of Sandwich Under Shear</i>	264
10.2.3	<i>Buckling of Sandwich Under Combined Loading</i>	265
10.3	Sandwich Wrinkling	265
10.3.1	<i>Sandwich Wrinkling Under Compression</i>	265
10.3.2	<i>Sandwich Wrinkling Under Shear</i>	276
10.3.3	<i>Sandwich Wrinkling Under Combined Loads</i>	276
10.4	Sandwich Crimping	278
10.4.1	<i>Sandwich Crimping Under Compression</i>	278
10.4.2	<i>Sandwich Crimping Under Shear</i>	278
10.5	Sandwich Intracellular Buckling (Dimpling) under Compression	278
10.6	Attaching Sandwich Structures	279
10.6.1	<i>Core Ramp-Down Regions</i>	280
10.6.2	<i>Alternatives to Core Ramp-Down</i>	282
	Exercises	284
	References	288

11 Good Design Practices and Design ‘Rules of Thumb’	289
11.1 Lay up/Stacking Sequence-related	289
11.2 Loading and Performance-related	290
11.3 Guidelines Related to Environmental Sensitivity and Manufacturing Constraints	292
11.4 Configuration and Layout-related	292
Exercises	294
References	295
Index	297

About the Author

Christos Kassapoglou received his BS degree in Aeronautics and Astronautics and two MS degrees (Aeronautics and Astronautics and Mechanical Engineering) all from Massachusetts Institute of Technology. Since 1984 he has worked in industry, first at Beech Aircraft on the all-composite Starship I and then at Sikorsky Aircraft in the Structures Research Group specializing on analysis of composite structures of the all-composite Comanche and other helicopters, and leading internally funded research and programs funded by NASA and the US Army. Since 2001 he has been consulting with various companies in the US on applications of composite structures on airplanes and helicopters. He joined the faculty of the Aerospace Engineering Department of the Delft University of Technology (Aerospace Structures) in 2007 as an Associate Professor. His interests include fatigue and damage tolerance of composites, analysis of sandwich structures, design and optimization for cost and weight, and technology optimization. He has over 40 journal papers and 3 issued or pending patents on related subjects. He is a member of AIAA, AHS, and SAMPE.

Series Preface

The field of aerospace is wide ranging and covers a variety of products, disciplines and domains, not merely in engineering but in many related supporting activities. These combine to enable the aerospace industry to produce exciting and technologically challenging products. A wealth of knowledge is contained by practitioners and professionals in the aerospace fields that is of benefit to other practitioners in the industry, and to those entering the industry from University.

The Aerospace Series aims to be a practical and topical series of books aimed at engineering professionals, operators, users and allied professions such as commercial and legal executives in the aerospace industry. The range of topics is intended to be wide ranging, covering design and development, manufacture, operation and support of aircraft as well as topics such as infrastructure operations, and developments in research and technology. The intention is to provide a source of relevant information that will be of interest and benefit to all those people working in aerospace.

The use of composite materials for aerospace structures has increased dramatically in the last three decades. The attractive strength-to-weight ratios, improved fatigue and corrosion resistance, and ability to tailor the geometry and fibre orientations, combined with recent advances in fabrication, have made composites a very attractive option for aerospace applications from both a technical and financial viewpoint. This has been tempered by problems associated with damage tolerance and detection, damage repair, environmental degradation and assembly joints. The anisotropic nature of composites also dramatically increases the number of variables that need to be considered in the design of any aerospace structure.

This book, *Design and Analysis of Composite Structures: With Application to Aerospace Structures*, provides a methodology of various analysis approaches that can be used for the preliminary design of aerospace structures without having to resort to finite elements. Representative types of composite structure are described, along with techniques to define the geometry and lay-up stacking sequence required to withstand the applied loads. The value of such a set of tools is to enable rapid initial trade-off preliminary design studies to be made, before using a detailed Finite Element analysis on the finalized design configurations.

Allan Seabridge, Roy Langton,
Jonathan Cooper and Peter Belobaba

Preface

This book is a compilation of analysis and design methods for structural components made of advanced composites. The term ‘advanced composites’ is used here somewhat loosely and refers to materials consisting of a high-performance fiber (graphite, glass, Kevlar®, etc) embedded in a polymeric matrix (epoxy, bismaleimide, PEEK etc). The material in this book is the product of lecture notes used in graduate-level classes in Advanced Composites Design and Optimization courses taught at the Delft University of Technology.

The book is aimed at fourth year undergraduate or graduate level students and starting engineering professionals in the composites industry. The reader is expected to be familiar with classical laminated-plate theory (CLPT) and first ply failure criteria. Also, some awareness of energy methods, and Rayleigh–Ritz approaches will make following some of the solution methods easier. In addition, basic applied mathematics knowledge such as Fourier series, simple solutions of partial differential equations, and calculus of variations are subjects that the reader should have some familiarity with.

A series of attractive properties of composites such as high stiffness and strength-to-weight ratios, reduced sensitivity to cyclic loads, improved corrosion resistance, and, above all, the ability to tailor the configuration (geometry and stacking sequence) to specific loading conditions for optimum performance has made them a prime candidate material for use in aerospace applications. In addition, the advent of automated fabrication methods such as advanced fiber/tow placement, automated tape laying, filament winding, etc. has made it possible to produce complex components at costs competitive with if not lower than metallic counterparts. This increase in the use of composites has brought to the forefront the need for reliable analysis and design methods that can assist engineers in implementing composites in aerospace structures. This book is a small contribution towards fulfilling that need.

The objective is to provide methodology and analysis approaches that can be used in preliminary design. The emphasis is on methods that do not use finite elements or other computationally expensive approaches in order to allow the rapid generation of alternative designs that can be traded against each other. This will provide insight in how different design variables and parameters of a problem affect the result.

The approach to preliminary design and analysis may differ according to the application and the persons involved. It combines a series of attributes such as experience, intuition, inspiration and thorough knowledge of the basics. Of these, intuition and inspiration cannot be captured in the pages of a book or itemized in a series of steps. For the first attribute, experience, an attempt can be made to collect previous best practices which can serve as guidelines for future work.

Only the last attribute, knowledge of the basics, can be formulated in such a way that the reader can learn and understand them and then apply them to his/her own applications. And doing that is neither easy nor guaranteed to be exhaustive. The wide variety of applications and the peculiarities that each may require in the approach, preclude any complete and in-depth presentation of the material. It is only hoped that the material presented here will serve as a starting point for most types of design and analysis problems.

Given these difficulties, the material covered in this book is an attempt to show representative types of composite structure and some of the approaches that may be used in determining the geometry and stacking sequences that meet applied loads without failure. It should be emphasized that not all methods presented here are equally accurate nor do they have the same range of applicability. Every effort has been made to present, along with each approach, its limitations. There are many more methods than the ones presented here and they vary in accuracy and range of applicability. Additional references are given where some of these methods can be found.

These methods cannot replace thorough finite element analyses which, when properly set up, will be more accurate than most of the methods presented here. Unfortunately, the complexity of some of the problems and the current (and foreseeable) computational efficiency in implementing finite element solutions precludes their extensive use during preliminary design or, even, early phases of the detailed design. There is not enough time to trade hundreds or thousands of designs in an optimization effort to determine the ‘best’ design if the analysis method is based on detailed finite elements. On the other hand, once the design configuration has been finalized or a couple of configurations have been down-selected using simpler, more efficient approaches, detailed finite elements can and should be used to provide accurate predictions for the performance, point to areas where revisions of the design are necessary, and, eventually, provide supporting analysis for the certification effort of a product.

Some highlights of composite applications from the 1950s to today are given in Chapter 1 with emphasis on nonmilitary applications. Recurring and nonrecurring cost issues that may affect design decisions are presented in Chapter 2 for specific fabrication processes. Chapter 3 provides a review of CLPT and Chapter 4 summarizes strength failure criteria for composite plates; these two chapters are meant as a quick refresher of some of the basic concepts and equations that will be used in subsequent chapters.

Chapter 5 presents the governing equations for anisotropic plates. It includes the von Karman large-deflection equations that are used later to generate simple solutions for post-buckled composite plates under compression. These are followed by a presentation of the types of composite parts found in aerospace structures and the design philosophy typically used to come up with a geometric shape. Design requirements and desired attributes are also discussed. This sets the stage for quantitative requirements that address uncertainties during the design and during service of a fielded structure. Uncertainties in applied loads, and variations in usage from one user to another are briefly discussed. A more detailed discussion about uncertainties in material performance (material scatter) leads to the introduction of statistically meaningful (A- and B-basis) design values or allowables. Finally, sensitivity to damage and environmental conditions is discussed and the use of knockdown factors for preliminary design is introduced.

Chapter 6 contains a discussion of buckling of composite plates. Plates are introduced first and beams follow (Chapter 8) because failure modes of beams such as crippling can

be introduced more easily as special cases of plate buckling and post-buckling. Buckling under compression is discussed first, followed by buckling under shear. Combined load cases are treated next and a table including different boundary conditions and load cases is provided.

Post-buckling under compression and shear is treated in Chapter 7. For applied compression, an approximate solution to the governing (von Karman) equations for large deflections of plates is presented. For applied shear, an approach that is a modification of the standard approach for metals undergoing diagonal tension is presented. A brief section follows suggesting how post-buckling under combined compression and shear could be treated.

Design and analysis of composite beams (stiffeners, stringers, panel breakers, etc.) are treated in Chapter 8. Calculation of equivalent membrane and bending stiffnesses for cross-sections consisting of members with different layups are presented first. These can be used with standard beam design equations and some examples are given. Buckling of beams and beams on elastic foundations is discussed next. This does not differentiate between metals and composites. The standard equations for metals can be used with appropriate (re)definition of terms such as membrane and bending stiffness. The effect of different end-conditions is also discussed. Crippling, or collapse after very-short-wavelength buckling, is discussed in detail deriving design equations from plate buckling presented earlier and from semi-empirical approaches. Finally, conditions for inter-rivet buckling are presented.

The two constituents, plates and beams are brought together in Chapter 9 where stiffened panels are discussed. The concept of smeared stiffness is introduced and its applicability discussed briefly. Then, special design conditions such as the panel breaker condition and failure modes such as skin–stiffener separation are analyzed in detail, concluding with design guidelines for stiffened panels derived from the previous analyses.

Sandwich structure is treated in Chapter 10. Aspects of sandwich modeling, in particular the effect of transverse shear on buckling, are treated first. Various failure modes such as wrinkling, crimping, and intracellular buckling are then discussed with particular emphasis on wrinkling with and without waviness. Interaction equations are introduced for analyzing sandwich structure under combined loading. A brief discussion on attachments including ramp-downs and associated design guidelines close this chapter.

The final chapter, Chapter 11, summarizes design guidelines and rules presented throughout the previous chapters. It also includes some additional rules, presented for the first time in this book, that have been found to be useful in designing composite structures.

To facilitate material coverage and in order to avoid having to read some chapters that may be considered of lesser interest or not directly related to the reader's needs, certain concepts and equations are presented in more than one place. This is minimized to avoid repetition and is done in such a way that reader does not have to interrupt reading a certain chapter and go back to find the original concept or equation on which the current derivation is based.

Specific problems are worked out in detail as examples of applications throughout the book. Representative exercises are given at the end of each chapter. These require the determination of geometry and/or stacking sequence for a specific structure not to fail under certain applied loads. Many of them are created in such a way that more than one answer is acceptable reflecting real-life situations. Depending on the assumptions made and design rules enforced, different but still acceptable designs can be created. Even though low weight is the primary objective of most of the exercises, situations where other issues are important and end up

driving the design are also given. For academic applications, experience has shown that students benefit the most if they work out some of these exercises in teams so design ideas and concepts can be discussed and an approach to a solution formulated.

It is recognized that analysis of composite structures is very much in a state of flux and new and better methods are being developed (for example failure theories with and without damage). The present edition includes what are felt to be the most useful approaches at this point in time. As better approaches mature in the future, it will be modified accordingly.

1

Applications of Advanced Composites in Aircraft Structures

Some of the milestones in the implementation of advanced composites on aircraft and rotorcraft are discussed in this chapter. Specific applications have been selected that highlight various phases that the composites industry went through while trying to extend the application of composites.

The application of composites in civilian or military aircraft followed the typical stages that every new technology goes through during its implementation. At the beginning, limited application on secondary structure minimized risk and improved understanding by collecting data from tests and fleet experience. This limited usage was followed by wider applications, first in smaller aircraft, capitalizing on the experience gained earlier. More recently, with the increased demand on efficiency and low operation costs, composites have been applied widely on larger aircraft.

Perhaps the first significant application of advanced composites was on the Akaflieg Phönix FS-24 (Figure 1.1) in the late 1950s. What started as a balsa wood and paper sailplane designed by professors at the University of Stuttgart and built by the students was later transformed into a fiberglass/balsa wood sandwich design. Eight planes were eventually built.

The helicopter industry was among the first to recognize the potential of the composite materials and use them on primary structure. The main and tail rotor blades with their beam-like behavior were one of the major structural parts designed and built with composites towards the end of the 1960s. One such example is the Aerospatiale Gazelle (Figure 1.2). Even though, to first order, helicopter blades can be modeled as beams, the loading complexity and the multiple static and dynamic performance requirements (strength, buckling, stiffness distribution, frequency placement, etc.) make for a very challenging design and manufacturing problem.

In the 1970s, with the composites usage on sailplanes and helicopters increasing, the first all-composite planes appeared. These were small recreational or aerobatic planes. Most notable among them were the Burt Rutan designs such as the Long EZ and Vari-Eze (Figure 1.3). These were largely co-cured and bonded constructions with very limited numbers of fasteners. Efficient aerodynamic designs with mostly laminar flow and light weight led to a combination of speed and agility.



Figure 1.1 Akaflieg Phönix FS-24 (Courtesy Deutsches Segelflugzeugmuseum; see Plate 1 for the colour figure)



Figure 1.2 Aerospatiale SA 341G Gazelle (Copyright Jenny Coffey printed with permission; see Plate 2 for the colour figure)



Figure 1.3 Long EZ and Vari-Eze. (Vari-Eze photo: courtesy Stephen Kearney; Long EZ photo: courtesy Ray McCrea; see Plate 3 for the colour figure)

Up to that point, usage of composites was limited and/or was applied to small aircraft with relatively easy structural requirements. In addition, the performance of composites was not completely understood. For example, their sensitivity to impact damage and its implications for design only came to the forefront in the late 1970s and early 1980s. At that time, efforts to build the first all-composite airplane of larger size began with the LearFan 2100 (Figure 1.4). This was the first civil aviation all-composite airplane to seek FAA certification (see Section 2.2).



Figure 1.4 Lear Avia LearFan 2100 (Copyright: Thierry Deutsch; see Plate 4 for the colour figure)

It used a pusher propeller and combined high speed and low weight with excellent range and fuel consumption. Unfortunately, while it met all the structural certification requirements, delays in certifying the drive system, and the death of Bill Lear the visionary designer and inventor behind the project, kept the LearFan from making it into production and the company, LearAvia, went bankrupt.

The Beech Starship I (Figure 1.5), which followed on the heels of the LearFan in the early 1980s was the first all-composite airplane to obtain FAA certification. It was designed to the new composite structure requirements specially created for it by the FAA. These requirements were the precursor of the structural requirements for composite aircraft as they are today. Unlike the LearFan which was a more conventional skin-stiffened structure with frames and stringers, the Starship fuselage was made of sandwich (graphite/epoxy facesheets with Nomex® core) and had a very limited number of frames, increasing cabin head room for a given cabin diameter, and minimizing fabrication cost. It was co-cured in large pieces that were bonded together and, in critical connections such as the wing-box or the main fuselage joints, were also fastened. Designed also by Burt Rutan the Starship was meant to have mostly laminar flow and increased range through the use efficient canard design and blended main wing. Two engines with pusher propellers located at the aft fuselage were to provide enough power for high cruising speed. In the end, the aerodynamic performance was not met and the fuel



Figure 1.5 Beech (Raytheon Aircraft) Starship I (Photo courtesy Brian Bartlett; see Plate 5 for the colour figure)



Figure 1.6 Airbus A-320 (Photo courtesy Brian Bartlett; see Plate 6 for the colour figure)

consumption and cruising speeds missed their targets by a small amount. Structurally however, the Starship I proved that all-composite aircraft could be designed and fabricated to meet the stringent FAA requirements. In addition, invaluable experience was gained in analysis and testing of large composite structures and new low-cost structurally robust concepts were developed for joints and sandwich structure in general.

With fuel prices rising, composites with their reduced weight became a very attractive alternative to metal structure. Applications in the large civilian transport category started in the early 1980s with the Boeing 737 horizontal stabilizer which was a sandwich construction, and continued with larger-scale application on the Airbus A-320 (Figure 1.6). The horizontal and vertical stabilizers as well as the control surfaces of the A-320 are made of composite materials.

The next significant application of composites on primary aircraft structure came in the 1990s with the Boeing 777 (Figure 1.7) where, in addition to the empennage and control surfaces, the main floor beams are also made out of composites.

Despite the use of innovative manufacturing technologies which started with early robotics applications on the A320 and continued with significant automation (tape layup) on the 777, the



Figure 1.7 Boeing 777 (Photo courtesy Brian Bartlett; see Plate 7 for the colour figure)



Figure 1.8 Airbus A-380 (Photo courtesy Bjoern Schmitt – World of Aviation.de; see Plate 8 for the colour figure)

cost of composite structures was not attractive enough to lead to an even larger-scale (e.g. entire fuselage and/or wing structure) application of composites at that time. The Airbus A-380 (Figure 1.8) in the new millennium, was the next major application with glass/aluminum (glare) composites on the upper portion of the fuselage and glass and graphite composites in the center wing-box, floor beams, and aft pressure bulkhead.

Already in the 1990s, the demand for more efficient aircraft with lower operation and maintenance costs made it clear that more usage of composites was necessary for significant reductions in weight in order to gain in fuel efficiency. In addition, improved fatigue lives and improved corrosion resistance compared with aluminum suggested that more composites on aircraft were necessary. This, despite the fact that the cost of composites was still not competitive with aluminum and the stringent certification requirements would lead to increased certification cost.

Boeing was the first to commit to a composite fuselage and wing with the 787 (Figure 1.9) launched in the first decade of the new millennium. Such extended use of composites, about 50% of the structure (combined with other advanced technologies) would give the efficiency improvement (increased range, reduced operation and maintenance costs) needed by the airline operators.



Figure 1.9 Boeing 787 Dreamliner (Courtesy of Agnes Blom; see Plate 9 for the colour figure)

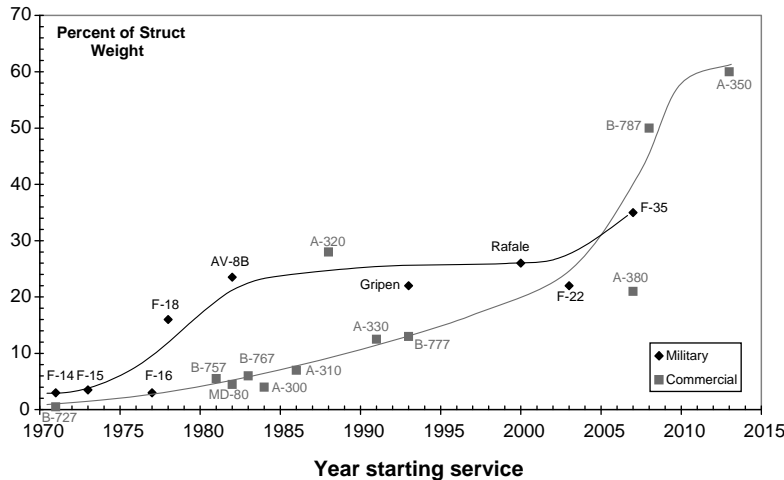


Figure 1.10 Applications of composites in military and civilian aircraft structures

The large number of orders (most successful launch in history) for the Boeing 787 led Airbus to start development of a competing design in the market segment covered by the 787 and the 777. This is the Airbus A-350, with all-composite fuselage and wings.

Another way to see the implementation of composites in aircraft structure over time is by examining the amount of composites (by weight) used in various aircraft models as a function of time. This is shown in Figure 1.10 for some civilian and military aircraft. It should be borne in mind that the numbers shown in Figure 1.10 are approximate as they had to be inferred from open literature data and interpretation of different company announcements [1–8].

Both military and civilian aircraft applications show the same basic trends. A slow start (corresponding to the period where the behavior of composite structures is still not well understood and limited low risk applications are selected) is followed by rapid growth as experience is gained reliable analysis and design tools are developed and verified by testing, and the need for reduced weight becomes more pressing. After the rapid growth period, the applicability levels off as: (a) it becomes harder to find parts of the structure that are amenable to use of composites; (b) the cost of further composite implementation becomes prohibitive; and (c) managerial decisions and other external factors (lack of funding, changes in research emphasis, investments already made in other technologies) favor alternatives. As might be expected, composite implementation in military aircraft leads the way. The fact that in recent years civilian applications seem to have overtaken military applications does not reflect true trends as much as lack of data on the military side (e.g several military programs such as the B-2 have very large composite applications, but the actual numbers are hard to find).

It is still unclear how well the composite primary structures in the most recent programs such as the Boeing 787 and the Airbus A-350 will perform and whether they will meet the design targets. In addition, several areas such as performance of composites after impact, fatigue, and damage tolerance are still the subjects of ongoing research. As our understanding in these areas improves, the development cost, which currently requires a large amount of testing to answer

questions where analysis is prohibitively expensive and/or not as accurate as needed to reduce the amount of testing, will drop significantly. In addition, further improvements in robotics technology and integration of parts into larger co-cured structures are expected to make the fabrication cost of composites more competitive compared with metal airplanes.

References

1. *Jane's All the World's Aircraft 2000–2001*, P. Jackson (ed.), Jane's Information Group, June 2000.
2. *NetComposites News*, 14 December 2000.
3. *Aerospace America*, May 2001, pp 45–47.
4. *Aerospace America*, September 2005.
5. www.compositesworld.com/hpc/issues/2005/May/865.
6. www.boeing.com/news/feature/concept/background.html.
7. www.4spe.org/pub/pe/articles/2005/august/08_toensmeier.pdf.
8. Watson, J.C. and Ostrodka, D.L., AV-8B Forward Fuselage Development, *Proc. 5th Conf. on Fibrous Composites in Structural Design*, New Orleans, LA, January 1981.

2

Cost of Composites: a Qualitative Discussion

Considering that cost is the most important aspect of an airframe structure (along with the weight), one would expect it to be among the best defined, most studied and most optimized quantities in a design. Unfortunately, it remains one of the least understood and ill-defined aspects of a structure. There are many reasons for this inconsistency some of which are: (a) cost data for different fabrication processes and types of parts are proprietary and only indirect or comparative values are usually released; (b) there seems to be no well-defined reliable method to relate design properties such as geometry and complexity to the cost of the resulting structure; (c) different companies have different methods of book-keeping the cost, and it is hard to make comparisons without knowing these differences (for example, the cost of the autoclave can be apportioned to the number of parts being cured at any given time or it may be accounted for as an overhead cost, included in the total overhead cost structure of the entire factory); (d) learning curve effects, which may or may not be included in the cost figures reported, tend to confuse the situation especially since different companies use different production run sizes in their calculations.

These issues are common to all types of manufacturing technologies and not just the aerospace sector. In the case of composites the situation is further complicated by the relative novelty of the materials and processes being used, the constant emergence of new processes or variations thereof that alter the cost structure, and the high nonrecurring cost associated with switching to the new processes that, usually, acts as a deterrent towards making the switch.

The discussion in this chapter attempts to bring up some of the cost considerations that may affect a design. This discussion is by no means exhaustive, in fact it is limited by the lack of extensive data and generic but accurate cost models. It serves mainly to alert or sensitize a designer to several issues that affect the cost. These issues, when appropriately accounted for, may lead to a robust design that minimizes the weight and is cost-competitive with the alternatives.

The emphasis is placed on recurring and nonrecurring cost. The recurring cost is the cost that is incurred every time a part is fabricated. The nonrecurring cost is the cost that is incurred once during the fabrication run.

2.1 Recurring Cost

The recurring cost includes the raw material cost (including scrap) for fabricating a specific part, the labor hours spent in fabricating the part, and cost of attaching it to the rest of the structure. The recurring cost is hard to quantify, especially for complex parts. There is no single analytical model that relates specific final part attributes such as geometry, weight, volume, area, or complexity to the cost of each process step and through the summation over all process steps to the total recurring cost. One of the reasons for these difficulties and, as a result, the multitude of cost models that have been proposed with varying degrees of accuracy and none of them all-encompassing, is the definition of complexity. One of the most rigorous and promising attempts to define complexity and its effect on recurring cost of composite parts was by Gutowski *et al.* [1, 2].

For the case of *hand layup*, averaging over a large quantity of parts of varying complexity ranging from simple flat laminates to compound curvature parts with co-cured stiffeners, the fraction of total cost taken up by the different process steps is shown in Figure 2.1 (taken from [3]).

It can be seen from Figure 2.1 that, by far, the costliest steps are locating the plies into the mold (42%) and assembling to the adjacent structure (29%). Over the years, cost-cutting and

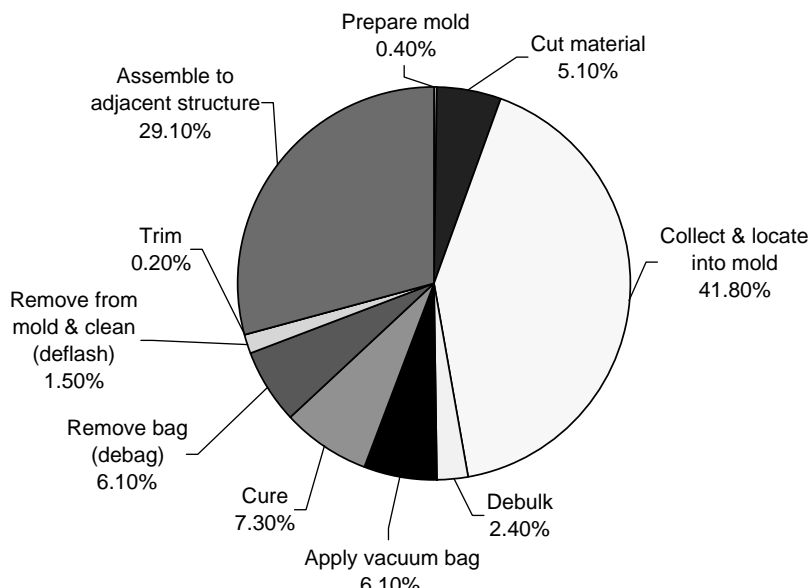


Figure 2.1 Process steps for hand layup and their cost as fractions of total recurring cost [3] (See Plate 10 for the colour figure)

optimization efforts have concentrated mostly on these two process steps. This is the reason for introducing automation. Robots, used for example in automated tape layup, take the cut plies and locate them automatically in the mold, greatly reducing the cost associated with that process step, improving the accuracy, and reducing or eliminating human error, thereby increasing consistency and quality. Since assembly accounts for about one-third of the total cost, increasing the amount of co-curing where various components are cured at the same time, reduces drastically the assembly cost. An example of this integration is shown in Figure 2.2.

These improvements as well as others associated with other process steps such as automated cutting (using lasers or water jets), trimming and drilling (using numerically controlled equipment) have further reduced the cost and improved quality by reducing the human involvement in the process. Hand layup and its automated or semi-automated variations can be used to fabricate just about any piece of airframe structure. An example of a complex part with compound curvature and parts intersecting in different directions is shown in Figure 2.3.

Further improvements have been brought to bear by taking advantage of the experience acquired in the textile industry. By working with fibers alone, several automated techniques such as knitting, weaving, braiding and stitching can be used to create a preform, which is then injected with resin. This is the *resin transfer molding(RTM) process*. The raw material cost can be less than half the raw material cost of pre-impregnated material (prepreg) used in hand layup or automated tape layup because the impregnation step needed to create the prepreg used in those processes is eliminated. On the other hand, ensuring that resin fully wets all fibers everywhere in the part and that the resin content is uniform and equal to the desired resin



Figure 2.2 Integration of various parts into a single co-cured part to minimize assembly cost (Courtesy Aurora Flight Sciences)

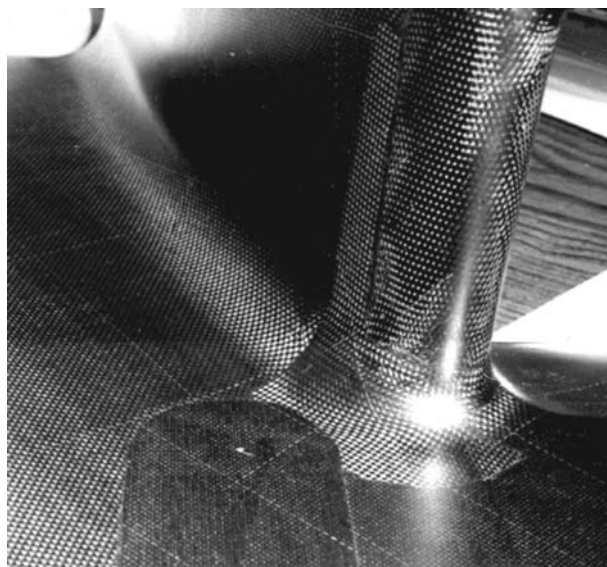


Figure 2.3 Portion of a three-dimensional composite part with compound curvature fabricated using hand layup

content can be hard for complex parts, and may require special tooling, complex design of injection and overflow ports, and use of high pressure. It is not uncommon, for complex RTM parts to have 10–15% less strength (especially in compression and shear) than their equivalent prepreg parts due to reduced resin content. Another problem with matched metal molding RTM is the high nonrecurring cost associated with the fabrication of the molds. For this reason, variations of the RTM process such as *vacuum-assisted RTM (VARTM)* where one of the tools is replaced by a flexible caul plate whose cost is much lower than an equivalent matched metal mold, or *resin film infusion (RFI)* where resin is drawn into dry fiber preforms from a pool or film located under it and/or from staged plies that already have resin in them, have been used successfully in several applications (Figure 2.4). Finally, due to the fact that the process operates with resin and fibers separately, the high amounts of scrap associated with hand layup can be significantly reduced.

Introduction of more automation led to the development of *automated fiber or tow placement*. This was a result of trying to improve filament winding (see below). Robotic heads can each dispense material as narrow as 3 mm and as wide as 100 mm by manipulating individual strips (or tows) each 3 mm wide. Tows are individually controlled so the amount of material laid down in the mold can vary in real time. Starting and stopping individual tows also allows the creation of cutouts ‘on the fly’. The robotic head can move in a straight line at very high rates (as high as 30 m/min). This makes automated fiber placement an ideal process for laying material down to create parts with large surface area and small variations in thickness or cutouts. For maximum efficiency, structural details (e.g. cutouts) that require starting and stopping the machine or cutting material while laying it down should be avoided. Material scrap is very low. Convex as well as concave tools can be used since the machine does not rely on constant fiber tension, as in filament winding, to lay material down. There are limitations



Figure 2.4 Curved stiffened panels made with the RTM process

with the process associated with the accuracy of starting and stopping when material is laid down at high rates and the size and shape of the tool when concave tools are used (in order to avoid interference of the robotic head with the tool). The ability to steer fibers on prescribed paths (Figure 2.5) can also be used as an advantage by transferring the loads efficiently across



Figure 2.5 Composite cylinder with steered fibers fabricated by automated fiber placement (made in a collaborative effort by TU Delft and NLR; see Plate 11 for the colour figure)

the part. This results in laminates where stiffness and strength are a function of location and provides an added means for optimization [4, 5].

Automated fiber placement is most efficient when making large parts. Parts such as stringers, fittings, small frames, that do not have at least one sizeable side where the advantage of the high lay-down rate of material by the robotic head can be brought to bear, are hard to make and/or not cost competitive. In addition, skins with large amounts of taper and number of cutouts may also not be amenable to this process.

In addition to the above processes that apply to almost any type of part (with some exceptions already mentioned for automated fiber placement) specialized processes that are very efficient for the fabrication of specific types parts or classes of parts have been developed. The most common of these are filament winding, pultrusion, and press molding using long discontinuous fibers and sheet molding compounds.

Filament winding, as already mentioned is the precursor to advanced fiber or tow placement. It is used to make pressure vessels and parts that can be wound on a convex mandrel. The use of a convex mandrel is necessary in order to maintain tension on the filaments being wound. The filaments are drawn from a spool without resin and are driven through a resin bath before they are wound around the mandrel. Due to the fact that tension must be maintained on the filaments, their paths can only be geodetic paths on the surface of the part being woven. This means that, for a cylindrical part, if the direction parallel to the cylinder axis is denoted as the zero direction, winding angles between 15° and 30° are hard to maintain (filaments tend to slide) and angles less than 15° cannot be wound at all. Thus, for a cylindrical part with conical closeouts at its ends, it is impossible to include 0° fibers using filament winding. 0° plies can be added by hand if necessary at a significant increase in cost. Since the material can be dispensed at high rates, filament winding is an efficient and low-cost process. In addition, fibers and matrix are used separately and the raw material cost is low. Material scrap is very low.

Pultrusion is a process where fibers are pulled through a resin bath and then through a heated die that gives the final shape. It is used for making long constant-cross-section parts such as stringers and stiffeners. Large cross-sections, measuring more than 25×25 cm are hard to make. Also, because fibers are pulled, if the pulling direction is denoted by 0° , it is not possible to obtain layups with angles greater than 45° (or more negative than -45°). Some recent attempts have shown it is possible to obtain longitudinal structures with some taper. The process is very low cost. Long parts can be made and then cut at the desired length. Material scrap is minimal.

With *press molding* it is possible to create small three-dimensional parts such as fittings. Typically, composite fittings made with hand layup or RTM without stitching suffer from low out-of-plane strength. There is at least one plane without any fibers crossing it and thus only the resin provides strength perpendicular to that plane. Since the resin strength is very low, the overall performance of the fitting is compromised. This is the reason some RTM parts are stitched. Press molding (Figure 2.6) provides an alternative with improved out-of-plane properties. The out-of-plane properties are not as good as those of a stitched RTM structure, but better than hand laid-up parts and the low cost of the process makes them very attractive for certain applications. The raw material is essentially a slurry of randomly oriented long discontinuous fibers in the form of chips. High pressure applied during cure forces the chips to completely cover the tool cavity. Their random orientation is, for the most part, maintained. As a result, there are chips in every direction with fibers providing



Figure 2.6 Portion of a composite fitting made by press molding

extra strength. Besides three-dimensional fittings, the process is also very efficient and reliable for making clips and shear ties. Material scrap is minimal. The size of the parts to be made is limited by the press size and the tool cost. If there are enough parts to be made, the high tooling cost is offset by the low recurring cost.

There are other fabrication methods or variations within a fabrication process that specialize in certain types of parts and/or part sizes. The ones mentioned above are the most representative. There is one more aspect that should be mentioned briefly; the effect of learning curves. Each fabrication method has its own learning curve which is specific to the process, the factory and equipment used, and the skill level of the personnel involved. The learning curve describes how the recurring cost for making the same part multiple times decreases as a function of the number of parts. It reflects the fact that the process is streamlined and people find more efficient ways to do the same task. Learning curves are important when comparing alternate fabrication processes. A process with a steep learning curve can start with a high unit cost but, after a sufficiently large number of parts, can yield unit costs much lower than another process, which starts with lower unit cost, but has shallower learning curve. As a result, the first process may result in lower average cost (total cost over all units divided by the number of units) than the first.

As a rule, fabrication processes with little or no automation have steeper learning curves and start with higher unit cost. This is because an automated process has fixed throughput rates while human labor can be streamlined and become more efficient over time as the skills of the people involved improve and ways of speeding up some of the process steps used in making the same part are found. The hand layup process would fall in this category with, typically, an 85% learning curve. An 85% learning curve means that the cost of unit $2n$ is 85% of the cost of unit n . Fabrication processes involving a lot of automation have shallower learning curves and start at lower unit cost. One such example is the automated fiber/tow placement process with, typically, a 92% learning curve. A discussion of some of these effects and the associated tradeoffs can be found in [3].

An example comparing a labor intensive process with 85% learning curve and cost of unit one 40% higher than an automated fabrication process with 92% learning curve, is given here to highlight some of the issues that are part of the design phase, in particular at early stages when the fabrication process or processes have not been finalized yet.

Assuming identical units, the cost of unit n , $C(n)$, is assumed to be given by a power law:

$$C(n) = \frac{C(1)}{n^r} \quad (2.1)$$

where $C(1)$ is the cost of unit 1 and r is an exponent that is a function of the fabrication process, factory capabilities, personnel skill etc.

If $p\%$ is the learning curve corresponding to the specific process, then

$$p = \frac{C(2n)}{C(n)} \quad (2.2)$$

Using Equation (2.1) to substitute in (2.2) and solving for r , it can be shown that,

$$r = -\frac{\ln p}{\ln 2} \quad (2.3)$$

For our example, with process A having $p_A = 0.85$ and process B having $p_B = 0.92$, substituting in Equation (2.3) gives $r_A = 0.2345$ and $r_B = 0.1203$. If the cost of unit 1 of process B is normalized to 1, $C_B(1) = 1$, then the cost of unit 1 of process A will be 1.4, based on our assumption stated earlier, so $C_A(1) = 1.4$. Putting it all together,

$$C_A(n) = \frac{1.4}{n^{0.2345}} \quad (2.4)$$

$$C_B(n) = \frac{1}{n^{0.1203}} \quad (2.5)$$

The cost as a function of n for each of the two processes can now be plotted in Figure 2.7. A logarithmic scale is used on the x axis to better show the differences between the two curves.

It can be seen from Figure 2.7 that a little after the 20th part, the unit cost of process A becomes less than that of process B suggesting that for sufficiently large runs, process A may be competitive with process B. To investigate this further, the average cost over a production run of N units is needed. If N is large enough, the average cost can be accurately approximated by:

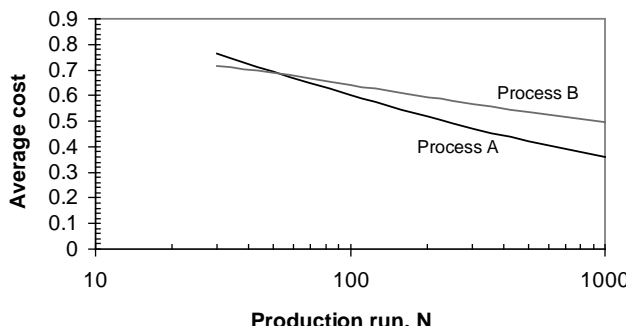


Figure 2.7 Unit recurring cost for a process with no automation (process A) and an automated process (process B)

$$C_{av} = \frac{1}{N} \sum_{n=1}^N C(n) \approx \frac{1}{N} \int_1^N C(n) dn \quad (2.6)$$

and using Equation (2.1),

$$C_{av} = \frac{1}{N} \int_1^N \frac{C(1)}{n^r} dn = \frac{C(1)}{1-r} \left(\frac{1}{N^r} - \frac{1}{1} \right) \quad (2.7)$$

Note that to derive Equation (2.7) the summation was approximated by an integral. This gives accurate results for $N > 30$. For smaller production runs ($N < 30$) the summation in Equation (2.6) should be used. Equation (2.7) is used to determine the average cost for Process A and Process B as a function of the size of the production run N . The results are shown in Figure 2.8.

As can be seen from Figure 2.8, Process B, with automation, has lower average cost as long as less than approximately 55 parts are made ($N < 55$). For $N > 55$, the steeper learning curve of Process A leads to lower average cost for that process. Based on these results, the less-automated process should be preferred for production runs with more than 50–60 parts. However, these results should be viewed only as preliminary, as additional factors that play a role were neglected in the above discussion. Some of these factors are briefly discussed below.

Process A, which has no automation, is prone to human errors. This means that: (a) the part consistency will vary more than in Process B; and (b) the quality and accuracy may not always be satisfactory requiring repairs, or scrapping of parts. In addition, process improvements, which the equations presented assume to be continuous and permanent, are not always possible. It is likely that after a certain number of parts, all possible improvements have been implemented. This would suggest that the learning curves typically reach a plateau after a while and cost cannot be reduced below that plateau without major changes in the process (new equipment, new process steps, etc.). These drastic changes are more likely in automated processes where new equipment is developed regularly than in a nonautomated process.

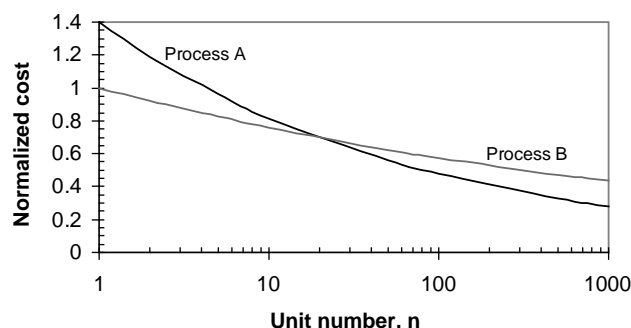


Figure 2.8 Average recurring cost for a process with no automation (process A) and a fully automated process (process B)

Therefore, while the conclusion that a less-automated process will give lower average cost over a sufficiently large production run, is valid, in reality may only occur under very special circumstances favoring continuous process improvement, consistent high part quality and part accuracy, etc. In general, automated processes are preferred because of their quality, consistency, and potential for continuous improvement.

The above is a very brief reference to some of the major composite fabrication processes. It serves to bring some aspects to the forefront as they relate to design decisions. More in-depth discussion of some of these processes and how they relate to design of composite parts can be found in [6, 7].

2.2 Nonrecurring Cost

The main components of nonrecurring cost follow the phases of the development of a program and are the following.

Design. Typically divided in stages (for example, conceptual, preliminary, and detail) it is the phase of creating the geometry of the various parts and coming up with the material(s) and fabrication processes (see Sections 5.1.1 and 5.1.2 for a more detailed discussion). For composites it is more involved than for metals because it includes detailed definition of each ply in a layup (material, orientation, location of boundaries, etc.). The design of press-molded parts would take less time than other fabrication processes as definition of the boundaries of each ply is not needed. Material under pressure fills the mold cavity and the concept of a ply is more loosely used.

Analysis. In parallel with the design effort, it determines applied loads for each part and comes up with the stacking sequence and geometry to meet the static and cyclic loads without failure and with minimum weight and cost. The multitude of failure modes specific to composites (delamination, matrix failure, fiber failure, etc.) makes this an involved process that may require special analytical tools and modeling approaches.

Tooling. This includes the design and fabrication of the entire tool string needed to produce the parts: Molds, assembly jigs and fixtures etc. For composite parts cured in the autoclave, extra care must be exercised to account for thermal coefficient mismatch (when metal tools are used) and spring-back phenomena where parts removed from the tools after cure tend to deform slightly to release some residual thermal and cure stresses. Special (and expensive) metal alloys (e.g. Invar) with low coefficients of thermal expansion can be used where dimensional tolerances are critical. Also careful planning of how heat is transmitted to the parts during cure for more uniform temperature distribution and curing is required. All these add to the cost, making tooling one of the biggest elements of the nonrecurring cost. In particular, if matched metal tooling is used, such as for RTM parts or press-molded parts, the cost can be prohibitive for short production runs. In such cases an attempt is made to combine as many parts as possible in a single co-cured component. An idea of tool complexity when local details of a wing-skin are accommodated accurately is shown in Figure 2.9.

Nonrecurring fabrication. This does not include routine fabrication during production that is part of the recurring cost. It includes: (a) one-off parts made to toolproof the tooling concepts; (b) test specimens to verify analysis and design and provide the data base needed to support design and analysis; and (c) producibility specimens to verify the fabrication approach and avoid surprises during production. This can be costly when large co-cured structures are involved with

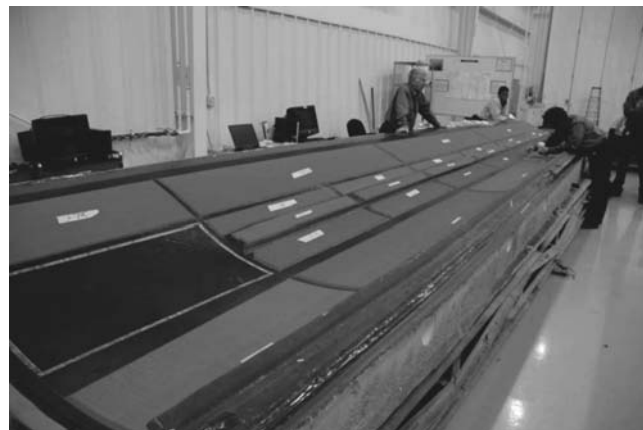


Figure 2.9 Co-cure of large complex parts (Courtesy Aurora Flight Sciences; see Plate 12 for the colour figure)

any of the processes already mentioned. It may take the form of a building-block approach where fabrication of subcomponents of the full co-cured structure is done first to check different tooling concepts and verify part quality. Once any problems (resin-rich, resin-poor areas, locations with insufficient degree of cure or pressure during cure, voids, local anomalies such as 'pinched' material, fiber misalignment), are resolved, more complex portions leading up to the full co-cured structure are fabricated to minimize risk and verify the design.

Testing. During this phase, the specimens fabricated during the previous phase are tested. This includes the tests needed to verify analysis methods and provide missing information for various failure modes. This does not include testing needed for certification (see next item). If the design has opted for large co-cured structures to minimize recurring cost, the cost of testing can be very high since it, typically, involves testing of various subcomponents first and then testing the full co-cured component. Creating the right boundary conditions and applying the desired load combinations in complex components results in expensive tests.

Certification. This is one of the most expensive nonrecurring cost items. Proving that the structure will perform as required, and providing relevant evidence to certifying agencies requires a combination of testing and analysis [8–10]. The associated test program can be extremely broad (and expensive). For this reason, a building-block approach is usually followed where tests of increasing complexity, but reduced in numbers follow simpler more numerous tests, each time building on the previous level in terms of information gained, increased confidence in the design performance, and reduction of risk associated with the full-scale article. In a broad level description going from simplest to most complex: (a) material qualification where thousands of coupons with different layups are fabricated and tested under different applied loads and environmental conditions with and without damage to provide statistically meaningful values (see Sections 5.1.3–5.1.5) for strength and stiffness of the material and stacking sequences to be used; (b) element tests of specific structural details isolating failure modes or interactions; (c) subcomponent and component tests verifying how the elements come together and providing missing (or hard to otherwise accurately quantify) information on failure loads and modes; (d) full-scale test. Associated with each test level, analysis is used to reduce test data, bridge structural performance from one level to the next and

justify the reduction of specimens at the next level of higher complexity. The tests include static and fatigue tests leading to the flight test program that is also part of the certification effort. When new fabrication methods are used, it is necessary to prove that they will generate parts of consistently high quality. This, sometimes, along with the investment in equipment purchasing and training, acts as a deterrent in switching from a proven method (e.g. hand layup) with high comfort level to a new method some aspects of which may not be well known (e.g. automated fiber placement).

The relative cost of each of the different phases described above is a strong function of the application, the fabrication process(es) selected and the size of the production run. It is, therefore, hard to create a generic pie chart that would show how the cost associated with each compares. In general, it can be said that certification tends to be the most costly followed by tooling, nonrecurring fabrication and testing.

2.3 Technology Selection

The discussion in the two previous sections shows that there is a wide variety of fabrication processes, each with its own advantages and disadvantages. Trading these and calculating the recurring and nonrecurring cost associated with each selection is paramount in coming up with the best choice. The problem becomes very complex when one considers large components such as the fuselage or the wing or entire aircraft. At this stage is it useful to define the term 'technology' as referring to any combination of material, fabrication process and design concept. For example, graphite/epoxy skins using fiber placement would be one technology. Similarly, sandwich skins with a mixture of glass/epoxy and graphite/epoxy plies made using hand layup would be another technology.

In a large-scale application such as an entire aircraft, it is extremely important to determine the optimum technology mix, i.e. the combination of technologies that will minimize weight and cost. This can be quite complicated since different technologies are more efficient for different types of part. For example, fiber-placed skins might give the lowest weight and recurring cost, but assembling the stringers as a separate step (bonding or fastening) might make the resulting skin/stiffened structure less cost competitive. On the other hand, using resin transfer molding to co-cure skin and stringers in one step might have lower overall recurring cost at a slight increase in weight (due to reduced strength and stiffness) and a significant increase in nonrecurring cost due to increased tooling cost. At the same time, fiber placement may require significant capital outlays to purchase automated fiber/tow placement machines. These expenditures require justification accounting for the size of the production run, availability of capital, and the extent to which capital investments already made on the factory floor for other fabrication methods have been amortized or not.

These tradeoffs and final selection of optimum technology mix for the entire structure of an aircraft are done early in the design process and 'lock in' most of the cost of an entire program. For this reason it is imperative that the designer be able to perform these trades in order to come up with the 'best alternatives'. As will be shown in this section these 'best alternatives' are a function of the amount of risk one is willing to take, the amount of investment available, and the relative importance of recurring, nonrecurring cost and weight [11–14].

In order to make the discussion more tractable, the airframe (load-bearing structure of an aircraft) is divided in part families. These are families of parts that perform the same function, have approximately the same shapes, are made with the same material(s) and can be fabricated

Table 2.1 Part families of an airframe

Part family	Description
Skins and covers	Two-dimensional parts with single curvature
Frames, bulkheads, beams, ribs, intercostals	Two-dimensional flat parts
Stringers, stiffeners, breakers	One-dimensional (long) parts
Fittings	Three-dimensional small parts connecting other parts
Decks and floors	Mostly flat parts
Doors and fairings	Parts with compound curvature
Miscellaneous	Seals, etc.

by the same manufacturing process. The simplest division into part families is shown in Table 2.1. In what follows the discussion will include metals for comparison purposes.

The technologies that can be used for each part family are then determined. This includes the material (metal or composite, and, if composite, the type of composite), fabrication process (built-up sheet metal, automated fiber placement, resin transfer molding, etc) and design concept (e.g. stiffened skin versus sandwich). In addition, the applicability of each technology to each part family is determined. This means determining what portion in the part family can be made by the technology in question. Usually, as the complexity of the parts in a part family increases, a certain technology becomes less applicable. For example, small skins with large changes in thickness across their length and width cannot be made by fiber placement and have low cost. Or pultrusion cannot be used (efficiently) to make tapering beams. A typical breakdown by part family and applicability by technology is shown in Table 2.2. For convenience, the following shorthand designations are used: SMT = (built-up) sheet metal, HSM = high-speed-machined aluminum, HLP = hand layup, AFP = automated fiber placement, RTM = resin transfer molding, ALP = automated (tape) layup, PLT = pultrusion. The numbers in Table 2.2 denote the percentage of the parts in the part family that can be made by the selected process and have acceptable (i.e. competitive) cost.

It is immediately obvious from Table 2.2 that no single technology can be used to make an entire airframe in the most cost-effective fashion. There are some portions of certain part families that are more efficiently made by another technology. While the numbers in Table 2.2 are subjective, they reflect what is perceived to be the reality of today and they can be modified according to specific preferences or expected improvements in specific technologies.

Given the applicabilities of Table 2.2, recurring and nonrecurring cost data are obtained or estimated by part family. This is done by calculating or estimating the average cost for a part of

Table 2.2 Applicability of fabrication processes by part family

Part family	SMT	HLP	HSM	AFP	RTM	PLT	ALP
Skins and covers	100	100	15	80	100	0	50
Frames, etc.	100	100	65	55	100	10	30
Stringers etc.	100	100	5	0	100	90	0
Fittings	100	85	5	0	100	0	0
Decks and floors	90	100	35	40	90	10	20
Doors and fairings	80	100	5	35	90	5	10

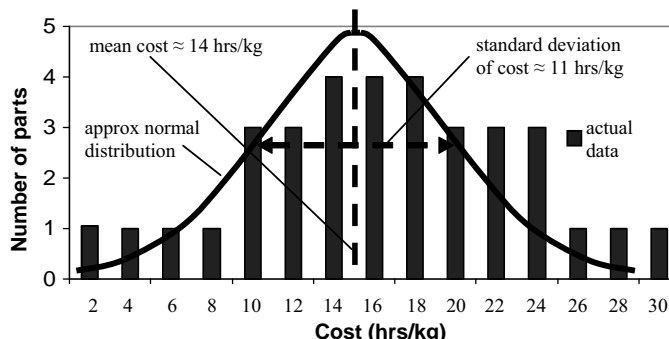


Figure 2.10 Distribution of recurring cost of HLP skins

medium complexity in the specific part family made by a selected process, and determining the standard deviation associated with the distribution of cost around that average as the part complexity ranges from simple to complex parts. This can be done using existing data as is shown in Figure 2.10, for technologies already implemented such as HLP, or by extrapolating and approximating limited data from producibility evaluations, vendor information, and anticipated improvements for new technologies or technologies with which a particular factory has not had enough experience.

In the case of the data shown in Figure 2.10, data over 34 different skin parts made with hand layup shows an average (or mean) cost of 14 hr/kg of finished product and a standard deviation around that mean of about 11 hr/kg (the horizontal arrows in Figure 2.10 cover approximately two standard deviations). This scatter around the mean cost is mostly due to variations in complexity. A simple skin (flat, constant thickness, no cutouts) can cost as little as 1 hr/kg while a complex skin (curved, with ply dropoffs, with cutouts) can cost as high as 30 hr/kg. In addition to part complexity, there is a contribution to the standard deviation due to uncertainty. This uncertainty results mainly from two sources [12]: (a) not having enough experience with the process, and applying it to types of part to which it has not been applied before; this is referred to as production-readiness; and (b) operator or equipment variability. Determining the portion of the standard deviation caused by uncertainty is necessary in order to proceed with the selection of the best technology for an application. One way to separate uncertainty from complexity is to use a reliable cost model to predict the cost of parts of different complexity for which actual data are available. The difference between the predictions and the actual data is attributed to uncertainty. By normalizing the prediction by the actual cost for all parts available, a distribution is obtained the standard deviation of which is a measure of the uncertainty associated with the process in question. This standard deviation (or its square, the variance) is an important parameter because it can be associated with the risk. If the predicted cost divided by actual cost data were all in a narrow band around the mean, the risk in using this technology (e.g. HLP) for this part family (e.g. skins) would be very low since the expected cost range would be narrow. Since narrow distributions have low variances, the lower the variance the lower the risk.

It is more convenient, instead of using absolute cost numbers to use cost savings numbers obtained by comparing each technology of interest with a baseline technology. In what follows, SMT is used as the baseline technology. Positive cost savings numbers denote cost reduction below SMT cost and negative cost savings numbers denote cost increase above SMT costs.

Also, generalizing the results from Figure 2.10, it will be assumed that the cost savings for a certain technology applied to a certain part family is normally distributed. Other statistical distributions can be used and, in some cases, will be more accurate. For the purposes of this discussion, the simplicity afforded by assuming a normal distribution is sufficient to show the basic trends and draw the most important conclusions.

By examining data published in the open literature, inferring numbers from trend lines, and using experience, the mean cost savings and variances associated with the technologies given in Table 2.2 can be compiled. The results are shown in Table 2.3. Note that these results reflect a specific instant in time and they comprise the best estimate of current costs for a given technology. This means that some learning curve effects are already included in the numbers. For example, HLP and RTM parts have been used fairly widely in industry and factories have come down their respective learning curves. Other technologies such as AFP have not been used as extensively and the numbers quoted are fairly high up in the respective learning curves.

For each technology/part family combination in Table 2.3, two numbers are given. The first is the cost savings as a fraction (i.e. 0.17 implies 17% cost reduction compared to SMT) and the second is the variance (square of standard deviation) of the cost savings population. Negative cost savings numbers imply increase in cost over SMT. They are included here because the weight savings may justify use of the technology even if, on average, the cost is higher. For SMT and some HLP cases, the variance is set to a very low number, 0.0001 to reflect the fact that the cost for these technologies and part families is well understood and there is little uncertainty associated with it. This means the technology has already been in use for that part family for some time. Some of the data in Table 2.3 are highlighted to show some of the implications: (a) HLP skins have 17% lower cost than SMT skin mostly due to co-curing large pieces and eliminating or minimizing assembly; (b) ALP has the lowest cost numbers, but limited applicability (see Table 2.2); (c) the variance in some cases such as ALP decks and floors or AFP doors and fairings is high because for many parts in these families additional nonautomated steps are necessary to complete fabrication. This is typical of parts containing core where core processing involves manual labor and increases the cost. Manual labor increases the uncertainty due to the operator variability already mentioned.

Table 2.3 Typical cost data by technology by part family [14]

Part family	SMT	HLP	HSM	AFP	RTM	PLT	ALP
Skins and covers	0.0	0.17	0.2	0.25	0.08	0.08	0.32
	0.0001	0.0061	0.02	0.009	0.003	0.06	0.01
Frames, etc.	0.0	0.1	0.28	0.1	0.18		0.40
	0.0001	0.0001	0.006	0.06	0.008		0.08
Stringers, etc.	0.0	-0.05	(in skins)		0.05	0.40	0.35
	0.0001	0.0001			0.002	0.001	0.09
Fittings	0.0		0.2		-0.10		
	0.0001		0.005			0.015	
Decks and floors	0.0	-0.01		0.15	-0.15		0.20
	0.0001	0.0001		0.01	0.008		0.02
Doors and fairings	0.0	0.1		0.25	-0.10		0.35
	0.0001	0.0021		0.026	0.01		0.05

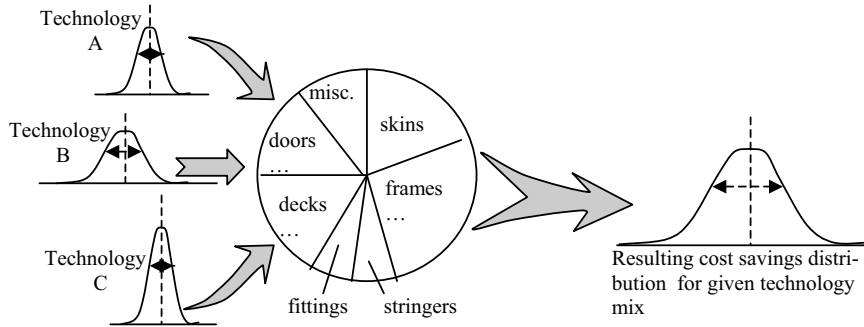


Figure 2.11 Combining different technologies to an airframe and expected cost distribution

Given the data in Tables 2.2 and 2.3, one can combine different technologies to make a part family. Doing that over all part families results in a technology mix. This technology mix has an overall mean cost savings and variance associated with it that can be calculated using the data from Tables 2.2 and 2.3 and using the percentages of how much of each part family is made by each technology [12, 13]. This process is shown in Figure 2.11. Obviously, some technology mixes are better than others because they have lower recurring cost and/or lower risk. An optimization scheme can then be set up [13] that aims at determining the technology mix that minimizes the overall recurring cost savings (below the SMT baseline) keeping the associated variance (and thus the risk) below a preselected value. By changing that preselected value from very small (low risk) to very high (high risk) different optimum mixes can be obtained. A typical result of this process is shown in Figure 2.12 for the case of a fuselage and wing of a 20-passenger commuter plane.

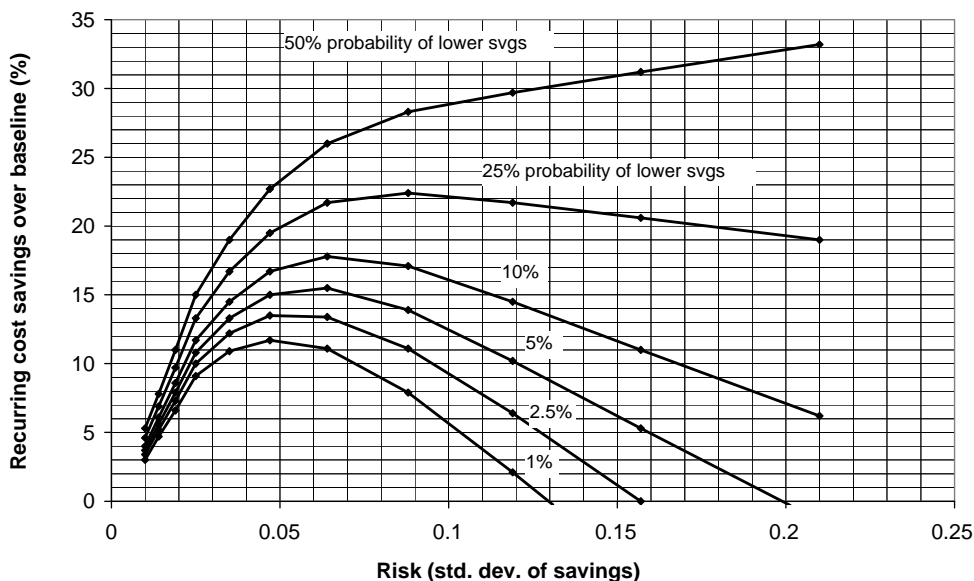


Figure 2.12 Recurring cost savings as a function of risk

The risk is shown in Figure 2.12 on the x axis as the square root of the variance, or standard deviation of the cost savings of the resulting technology mix. For each value of risk, the optimization process results in a technology mix that maximizes cost savings. Assuming that the cost savings of each technology mix is normally distributed, the corresponding probabilities that the cost savings will be lower than a specified value can be determined [13]. These different probabilities trace the different curves shown in Figure 2.12. For example, if the risk is set at 0.05 on the x axis, the resulting optimum mix has 1% probability of not achieving 11.5% savings, 2.5% probability of not achieving 13.5% savings, 5% probability of not achieving 15% savings and so on. Note that all curves, except the 50% probability curve go through a maximum. This maximum can be used for selecting the optimum technology mix to be used. For example, if a specific factory/management team is risk averse it would probably go with the 1% curve which goes through a maximum at a risk value slightly less than 0.05. The team would expect savings of at least 11.5%. A more aggressive team might be comfortable with 25% probability that the cost savings is lower and would use the 25% curve. This has a maximum at a risk value of 0.09 with corresponding savings of 22.5%. However, there is a 25% probability that this level of savings will not be met. That is, if this technology mix were to be implemented a large number of times, it would meet or exceed the 22.5% savings target only 75% of the time. It is up to the management team and factory to decide which risk level and curve they should use. It should be noted that for very high risk values, beyond 0.1, the cost savings curves eventually become negative. For example the 1% curve becomes negative at a risk value of 0.13. This means that the technology mix corresponding to a risk value of 0.13 has so much uncertainty that there is 99% probability that the cost savings will be negative, i.e. the cost will be higher than the SMT baseline.

Once a risk level is selected from Figure 2.12, the corresponding technology mix is known from the optimization process. Examples for low and high risk values are shown in Figures 2.13 and 2.14.

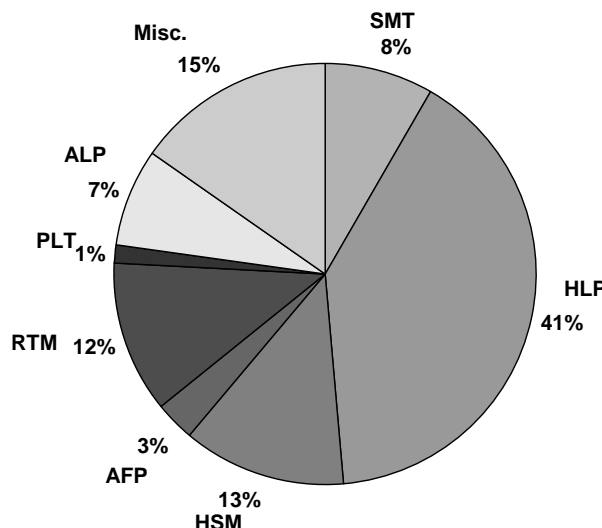


Figure 2.13 Optimum mix of technologies for small airplane (low risk)

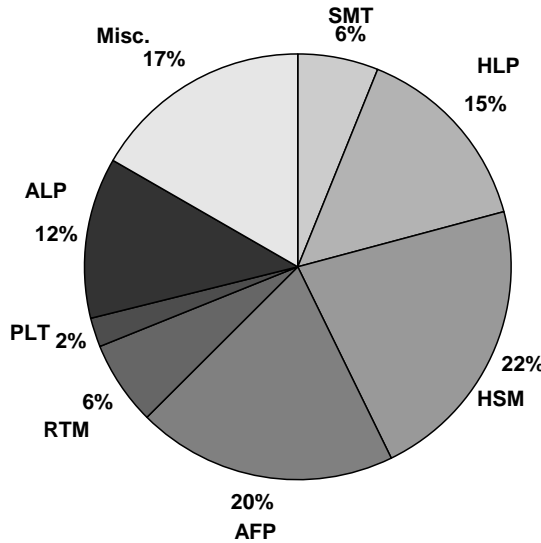


Figure 2.14 Optimum mix of technologies for small airplane (high risk)

For the low risk optimum mix of Figure 2.13, there is a 10% probability of not achieving 12.5% cost savings. For the high risk optimum mix of Figure 2.14 there is a 10% probability of not achieving 7% cost savings. The only reason to go with the high risk optimum mix is that, at higher probability values (greater than 25%) it exceeds the cost savings of the low-risk optimum mix.

A comparison of Figures 2.14 and 2.13 shows that as the risk increases, the percentage usage of baseline SMT and low-risk low-return HLP and RTM decreases while the usage of higher-risk high-return AFP and ALP increases. ALP usage doubles from 6 to 12% and AFP usage increases by a factor of almost 7, from 3 to 20%. The amount of PLT also increases (in fact doubles) but since PLT is only limited to stringers in this example, the overall impact of using PLT is quite small. It should be noted that there is a portion of the airframe denoted by ‘Misc’. These are miscellaneous parts such as seals, or parts for which applicability is unclear, and mixing technologies (for example pultruded stringers co-bonded on fiber-placed skins) might be a better option, but no data were available for generating predictions.

Finally, the breakdown by part family for one of the cases, the low-risk optimum mix of Figure 2.13 is shown in Table 2.4. For example, 21.1% of the frames are made by HLP, 32.4% by

Table 2.4 Low-risk technology mix by part family and technology

	%SMT	%HLP	%HSM	%AFP	%RTM	%PLT	%ALP
Skins + ...	0	81	0	4.9	3.6	0	10.5
Frames + ...	0	21.1	32.4	0	40.5	0	6
Stringers	79.3	0	0	0	0	20.7	0
Fittings	44.1	0	55.5	0	0	0	0.4
Decks + ...	0	76.5	0	8.4	3.1	0	12
Doors + ...	0	81	0	10	0	0	9

HSM, 40.5% by RTM and 6% by ALP. Note that SMT is only used for three quarters of the stringers and almost half the fittings. Note that these percentages are the results of the optimization mentioned earlier and do not exactly determine which parts will be made with what process, only that a certain percentage of parts for each part family is made by a certain process. It is up to the designers and manufacturing personnel to decide how these percentages can be achieved or, if not possible, determine what the best compromise will be. For example, 6% of the frames and bulkheads made by ALP would probably correspond to the pressure bulkheads and any frames with deep webs where automated layup can be used effectively.

The above discussion focused on recurring cost as a driver. The optimum technology mixes determined have a certain weight and nonrecurring cost associated with them. If weight or nonrecurring cost were the drivers different optimum technology mixes would be obtained. Also, the optimized results are frozen in time in the sense that the applicabilities of Table 2.2 and the cost figures of Table 2.3 are assumed constant. Over time, as technologies improve, these data will change and the associated optimum technology mixes will change. Results for the time-dependent problem with different drivers such as nonrecurring cost or optimum return on investment can be found in the references [11, 14].

It should be kept in mind that some of the data used in this section are subjective or based on expectations of what certain technologies will deliver in the future. As such, the results should be viewed as trends that will change with different input data. What is important here is that an approach has been developed that can be used to trade weight, recurring cost and nonrecurring cost and determine the optimum mix of technologies given certain cost data. The interested user of the approach can use his/her own data and degree of comfort in coming up with the optimum mix of technologies for his/her application.

2.4 Summary and Conclusions

An attempt to summarize the above discussion by fabrication process and collect some of the qualitative considerations that should be taken into account during the design and analysis phases of a program using composite materials is shown in Table 2.5. For reference, sheet metal built-up structure and high-speed-machining (aluminum or titanium) are also included. This table is meant to be a rough set of guidelines and it is expected that different applications and manufacturing experiences can deviate significantly from its conclusions.

As shown in the previous section, there is no single process that can be applied to all types of parts and result in the lowest recurring and/or nonrecurring costs. A combination of processes is necessary. In many cases, combining two or more processes in fabricating a single part, thus creating a hybrid process (for example automated fiber-placed skins with staged pultruded stiffeners, all co-cured in one cure cycle) appears to be the most efficient approach. In general, co-curing as large parts as possible and combining with as much automation as possible seems to have the most promise for parts of low cost, high quality and consistency. Of course, the degree to which this can be done depends on how much risk is considered acceptable in a specific application and to what extent the investment required to implement more than one fabrication processes is justified by the size of the production run. These combinations of processes and process improvements have already started to pay off and, for certain applications [15] the cost of composite airframe is comparable if not lower than that of equivalent metal structure.

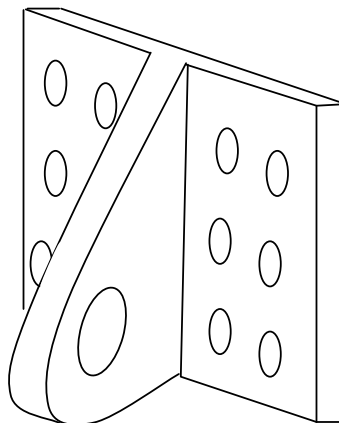
Table 2.5 Qualitative cost considerations affecting design/analysis decisions

Process	Application	Comments
Sheet metal	All airframe structure	Assembly intensive, relatively heavy. Moderate tooling costs including fit-out and assembly jigs
High-speed machining	Frames, bulkheads, ribs, beams, decks and floors. In general, parts with one flat surface that can be created via machining	Very low tooling cost. Very low recurring cost. Can generate any desired thickness greater than 0.6 mm. Moderate raw material cost due to the use of special alloys. Extremely high scrap rate (more than 99% of the raw material ends up recycled as machined chips). Limited due to vibrations to part thicknesses greater than 0.6–0.7 mm. Issues with damage tolerance (no built-in crack stoppers) repair methods, and low damping; Size of billet limits size of part that can be fabricated
Hand Layup	All airframe structure	Weight reductions over equivalent metal of at least 15%. Recurring cost competitive with sheet metal when large amount of co-curing is used. Moderate scrap. High raw material cost. High tooling cost. Hard to fabricate 3-D fittings. Reduced out-of-plane strength (important in fittings and parts with out-of-plane loading)
Automated fiber/tow placement	Skins, decks, floors, doors, fairings, bulkheads, large ribs and beams. In general, parts with large surface area	Weight reductions similar to hand layup. Recurring cost can be less than metal baseline if the number of starts and stops for the machine are minimized (few cutouts, plydrops, etc.). Less scrap than hand layup., High tooling cost. For parts made on concave tools, limited by size of robotic head (interference with tool). Fiber steering is promising for additional weight savings but is limited by maximum radius of curvature the machine can turn without buckling the tows
RTM	All airframe structure	Weight reductions somewhat less than hand layup due to decreased fiber volume for complex parts. Combined with automated preparation of fiber performs it can result in low recurring fabrication cost. Relatively low scrap rate. Very high tooling cost if matched metal tooling is used. Less so for vacuum-assisted RTM (half of the tool is a semi-rigid caul plate) or resin film infusion. To use unidirectional plies, some carrier or tackifier is needed for the fibers, increasing the recurring cost somewhat

Pultrusion	Constant cross-section parts: stiffeners, stringers, small beams	Weight reductions somewhat less than hand layup due to the fact that not all layups are possible (plies with 45° orientation or higher when 0 is aligned with the long axis of the part). Very low recurring cost and relatively low tooling cost compared with other fabrication processes. Reduced strength and stiffness in shear and transverse directions due to inability to generate any desired layup
Filament winding	Concave parts wound on a rotating mandrel: pressure vessels, cylinders, channels (wound and then cut)	Weight reductions somewhat less than hand layup due to difficulty in achieving the required fiber volume and due to inability to achieve certain stacking sequences. Low scrap rate, low raw material cost. Low recurring fabrication cost. Moderate tooling cost. Only convex parts wound on a mandrel where the tension in the fibers can be maintained during fabrication. Cannot wind angles shallower than geodetic lines (angles less than 15° not possible for long slender parts with 0 aligned with the long axis of the part). Reduced strength and stiffness
Press molding	Fittings, clips, shear ties, small beams, ribs, intercostals	Weight reductions in the range 10–20% over aluminum baseline (weight savings potential limited due to the use of discontinuous fibers). Very low recurring cost with very short production cycle (minutes to a couple of hours). Low material scrap. Limited by the size of the press. Very high tooling cost for the press mold. Reduced strength due to the use of long discontinuous fibers, but good out-of-plane strength due to interlocking [*] of fibers

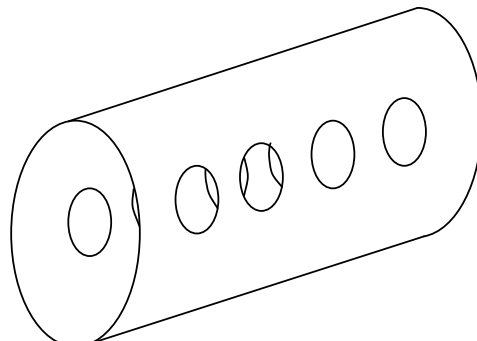
Exercises

2.1 Hand layup, resin transfer molding and press molding are considered as the candidate processes for the following part:



Discuss qualitatively how each choice may affect the structural performance and the weight of the final product. Include size effects, out-of-plane load considerations, load path continuity around corners, etc.

2.2 Hand layup, automated fiber placement, and filament winding are proposed as candidate processes for the following part:



Discuss qualitatively how each choice may affect the structural performance and the weight of the final product. Include size effects, load path continuity, etc. in your discussion. Assume there are no local reinforcements (e.g. around window cutouts) or attachments to adjacent structure.

References

1. Gutowski, T.G., Hoult, D., Dillon, G., Mutter, S., Kim, E., Tse, M., and Neoh, E.T., Development of a Theoretical Cost Model for Advanced Composite Fabrication, *Proc. 4th NASA/DoD Advanced Composites Technology Conf.*, Salt Lake City, UT, 1993.

2. Gutowski, T.G., Neoh, E.T., and Dillon, G., Scaling Laws for Advanced Composites Fabrication Cost, *Proc. 5th NASA/DoD Advanced Composites Technology Conf.*, Seattle, WA, 1994, pp. 205–233.
3. Apostolopoulos, P., and Kassapoglou, C., Cost Minimization of Composite Laminated Structures – Optimum Part Size as a Function of Learning Curve Effects and Assembly, *Journal of Composite Materials*, **36**(4) 501–518 (2002).
4. Tatting, B., and Gürdal, Z., Design and Manufacture of Elastically Tailored Tow-Placed Plates, NASA CR 2002 211919, August 2002.
5. Jegley, D., Tatting, B., and Gürdal, Z., Optimization of Elastically Tailored Tow-Placed Plates with Holes, *44th AIAA/ASME/ASCE/AHS Structures, Structural Dynamics and Materials Conf.*, Norfolk VA, 2003, also paper AIAA-2003-1420.
6. *1st NASA Advanced Composites Technology Conf.*, NASA CP 3104, Seattle WA, 1990.
7. *2nd NASA Advanced Composites Technology Conf.*, NASA CP 3154, Lake Tahoe, NV, 1991.
8. Abbott, R., Design and certification of the all-composite airframe. *Society of Automotive Engineers Technical Paper Series – Paper No 892210*; 1989.
9. Whitehead, R.S., Kan, H.P., Cordero, R. and Saether E.S., Certification testing methodology for composite structures: volume I – Data analysis. *Naval Air Development Center Report 87042-60 (DOT/FAA/CT-86-39)*; 1986.
10. Whitehead, R.S., Kan, H.P., Cordero, R. and Saether E.S., Certification testing methodology for composite structures: volume II – Methodology development. *Naval Air Development Center Report 87042-60 (DOT/FAA/CT-86-39)*; 1986.
11. Kassapoglou, C., Determination of the Optimum Implementation Plan for Manufacturing Technologies – The case of a Helicopter Fuselage, *Journal of Manufacturing Systems*, **19**, 121–133 (2000).
12. Kassapoglou, C., Selection of Manufacturing Technologies for Fuselage Structures for Minimum Cost and Low Risk: Part A – Problem Formulation, *Journal of Composites Technology and Research*, **21**, 183–188 (1999).
13. Kassapoglou, C., Selection of Manufacturing Technologies for Fuselage Structures for Minimum Cost and Low risk: Part B – Solution and Results, *Journal of Composites Technology and Research*, **21**, 189–196 (1999).
14. Sarkar, P. and Kassapoglou, C., An ROI-Based Strategy for Implementation of Existing and Emerging Technologies, *Spring Research Conf. on Statistics in Industry and Technology*, Minneapolis St Paul MN, June 1999. Also *IEEE Transactions on Engineering Management*, **48**, 414–427 (1999).
15. McGettrick, M., and Abbott, R., To MRB or not to be: Intrinsic manufacturing variabilities and effects on load carrying capacity, *Proc. 10th DoD/NASA/FAA Conf. on Fibrous Composites in Structural Design*, Hilton Head, SC, 1993, pp 5–39.

3

Review of Classical Laminated Plate Theory

This chapter gives some basic laminate definitions and a brief summary of the classical laminated-plate theory (CLPT). Aspects of CLPT, in particular the laminate stiffness matrices are used throughout the remainder of this book.

3.1 Composite Materials: Definitions, Symbols and Terminology

A composite material is any material that consists of at least two constituents. In this book, the term ‘composite material’ refers to a mixture of fibers and matrix resulting in a configuration that combines some of the best characteristics of the two constituents. There is a large variety of possible combinations. For fibers, some of the options include, E- or S-glass, quartz, graphite, Kevlar®, boron, silicon, etc, appearing in long continuous or short discontinuous form. The matrix materials, cover a wide range of thermoset (epoxy, polyester, phenolics, polyimides, bismaleimids) or thermoplastic resins, or metals such as aluminum or steel. The building block of a composite material is the ply or lamina. Plies or laminae are stacked together (different orientations and materials can be combined) to make a laminate.

The most common plies used are unidirectional plies (where all fibers are aligned in one direction) or fabric plies (plain weave, satins, etc.) where fibers are oriented in two mutually perpendicular directions. If each ply in the stacking sequence or layup making up a laminate is denoted by its orientation θ (in degrees) relative to a reference axis ($-90^\circ < \theta \leq +90^\circ$), as shown for example in Figure 3.1, then a laminate can be denoted by its stacking sequence (or layup):

$$[\theta_1/\theta_2/\theta_3 \dots]$$

where θ_1, θ_2 etc are the angles of successive plies starting from the top of the laminate.

If more than one material types are used in the same laminate the angular orientation can be followed by a symbol that denotes the material type. For example, in the following stacking sequence,

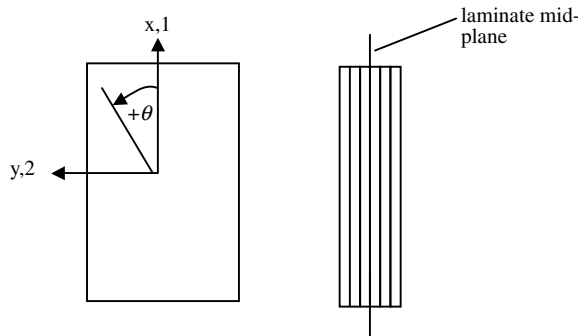


Figure 3.1 Laminate axes and definition of positive θ orientation

$$[\theta_1(T)/\theta_2(F)/\theta_3(T)\dots]$$

the first and third plies are made with unidirectional tape material and the second with fabric material.

When fabric material is used, it is also common to indicate the two orientations in each ply in parentheses such as

$$(0/90), (\pm 45), (20/-70)$$

where the first denotes a fabric ply with fibers oriented in the 0° and 90° directions, the second denotes a ply with fibers in the $+45^\circ$ and -45° directions and the third a ply with fibers in the $+20^\circ$ and -70° directions.

There are several special laminate types often encountered in practice some of which are:
(a) symmetric, (b) balanced, (c) cross-ply, (d) angle-ply and (e) quasi-isotropic laminates.

Symmetric laminates are laminates that have a symmetric stacking sequence with respect to the laminate mid-plane (see Figure 3.1). This means that the material, thickness and orientation of each pair of plies located symmetrically with respect to the laminate mid-plane are the same. A symmetric stacking sequence is usually denoted by writing half of it and using the subscript s:

$$[35/20/40]_s \text{ is the same as } [35/20/40/40/20/35]$$

This contracted notation has the advantage of simplicity, but requires caution when the total number of plies is odd. In such a case, the center ply, half of which lies on one side of the midplane and half on the other, is denoted with an overbar:

$$[35/20/\overline{40}]_s \text{ is the same as } [35/20/40/20/35]$$

Balanced laminates are laminates in which for each $+\theta$ ply there is a $-\theta$ ply (of the same material and thickness) somewhere in the stacking sequence. Special properties of balanced and/or symmetric laminates related to their structural response will be presented in subsequent sections.

Cross-ply laminates consist only of 0° and 90° plies. Angle-ply laminates do not contain any 0° or 90° plies.

Finally, quasi-isotropic laminates have the same stiffness in any direction in their plane (xy plane in Figure 3.1). One way to create a quasi-isotropic stacking sequence of n plies is to

require that there is no direction that has more fibers than any other direction. A simple procedure to accomplish this, is to divide the range of angles from 0° to 180° in n equal segments and, assign to each ply one angle increment corresponding to these segments.

For example, if there are 8 plies the angle increment is $180/8 = 22.5^\circ$. Then, mixing the following angles in any order creates a quasi-isotropic laminate:

$$0, 22.5, 45, 67.5, 90, 112.5 \text{ (or } -67.5\text{)}, 135 \text{ (or } -45\text{)}, 157.5 \text{ (or } -22.5\text{)}$$

Taking this one step further, for a symmetric laminate, the rule is only applied to half the laminate since the other half is automatically created by symmetry. For the same case of $n = 8$, the angle increment is now $180/(8/2) = 45^\circ$. The following angles, in any order and repeated symmetrically give a quasi-isotropic, symmetric, 8-ply laminate.

$$0^\circ, 45^\circ, 90^\circ, 135^\circ \text{ (or } -45^\circ\text{)}$$

Some possible quasi-isotropic stacking sequences in this case are:

$$[0/45/90/-45]_s, [45/-45/0/90]_s, [45/90/0/-45]_s, \text{ etc.}$$

To complete the discussion of stacking sequence notation, other shorthand methods include the use of parentheses with subscripts to denote a repeating pattern within the stacking sequence and the use of numerical subscripts or superscripts outside the brackets. Examples of these are:

$[(15/-15)_3/0/30]_s$ is the same as $[15/-15/15/-15/15/-15/0/30/30/0/-15/15/-15/15/-15/15]$

$[15/-15/0/30]_{s2}$ is the same as $[15/-15/0/30/15/-15/0/30/30/0/-15/15/30/0/-15/15]$

$[15/-15/0/30]_{s^2}$ is the same as $[15/-15/0/30/30/0/-15/15/15/-15/0/30/30/0/-15/15]$

3.2 Constitutive Equations in Three Dimensions

Composite materials are, by their nature, anisotropic. In three dimensions, the engineering stresses and strains describing completely the state of deformation in a composite are denoted in matrix form respectively:

$$\begin{bmatrix} \sigma_x & \sigma_y & \sigma_z & \tau_{yz} & \tau_{xz} & \tau_{xy} \\ \varepsilon_x & \varepsilon_y & \varepsilon_z & \gamma_{yz} & \gamma_{xz} & \gamma_{xy} \end{bmatrix}$$

The first three are the normal stresses (strains) and the last three are the shear stresses (strains). It is customary, for two-dimensional problems to use x and y as the in-plane coordinates (see Figure 3.1) and z as the out-of-plane coordinate (perpendicular to the plane of Figure 3.1).

Stresses and strains are related through the generalized stress-strain relations (Hooke's law) [1–5]:

$$\begin{Bmatrix} \sigma_x \\ \sigma_y \\ \sigma_z \\ \tau_{yz} \\ \tau_{xz} \\ \tau_{xy} \end{Bmatrix} = \begin{bmatrix} E_{11} & E_{12} & E_{13} & E_{14} & E_{15} & E_{16} \\ E_{21} & E_{22} & E_{23} & E_{24} & E_{25} & E_{26} \\ E_{31} & E_{32} & E_{33} & E_{34} & E_{35} & E_{36} \\ E_{41} & E_{42} & E_{43} & E_{44} & E_{45} & E_{46} \\ E_{51} & E_{52} & E_{53} & E_{54} & E_{55} & E_{56} \\ E_{61} & E_{62} & E_{63} & E_{64} & E_{65} & E_{66} \end{bmatrix} \begin{Bmatrix} \varepsilon_x \\ \varepsilon_y \\ \varepsilon_z \\ \gamma_{yz} \\ \gamma_{xz} \\ \gamma_{xy} \end{Bmatrix} \quad (3.1)$$

Note that there is an apparent mix-up of subscripts in Equation (3.1) where the stiffness components E_{ij} have numerical indices while the stress and strain components have letter indices. This is done on purpose to keep the engineering notations for stresses and strains and the usual (contracted tensor) notation for the stiffness terms, which uses numbers instead of letters.

Equation (3.1) relates the strains to stresses through the fourth order elasticity tensor E . It can be shown, based on energy considerations [6] that the elasticity tensor is symmetric, i.e. $E_{ij} = E_{ji}$. Thus, for a general anisotropic body, there are 21 independent elastic constants, as highlighted by the dashed line in Equation (3.1a).

$$\begin{Bmatrix} \sigma_x \\ \sigma_y \\ \sigma_z \\ \tau_{yz} \\ \tau_{xz} \\ \tau_{xy} \end{Bmatrix} = \underbrace{\begin{bmatrix} E_{11} & E_{12} & E_{13} & E_{14} & E_{15} & E_{16} \\ E_{12} & E_{22} & E_{23} & E_{24} & E_{25} & E_{26} \\ E_{13} & E_{23} & E_{33} & E_{34} & E_{35} & E_{36} \\ E_{14} & E_{24} & E_{34} & E_{44} & E_{45} & E_{46} \\ E_{15} & E_{25} & E_{35} & E_{45} & E_{55} & E_{56} \\ E_{16} & E_{26} & E_{36} & E_{46} & E_{56} & E_{66} \end{bmatrix}}_{\text{independent elastic constants}} \begin{Bmatrix} \varepsilon_x \\ \varepsilon_y \\ \varepsilon_z \\ \gamma_{yz} \\ \gamma_{xz} \\ \gamma_{xy} \end{Bmatrix} \quad (3.1a)$$

The discussion in this book is further confined to orthotropic materials. These are materials that possess two planes of symmetry. In such a case, some of the coupling terms in Equation (3.1a) are zero:

$$E_{14} = E_{15} = E_{16} = E_{24} = E_{25} = E_{26} = E_{34} = E_{35} = E_{36} = 0 \quad (3.2)$$

In addition, for an orthotropic body, shear stresses in one plane do not cause shear strains in another. Thus,

$$E_{45} = E_{46} = E_{56} = 0 \quad (3.3)$$

With these simplifications, the stress-strain relations for an orthotropic material have the form:

$$\begin{Bmatrix} \sigma_x \\ \sigma_y \\ \sigma_z \\ \tau_{yz} \\ \tau_{xz} \\ \tau_{xy} \end{Bmatrix} = \begin{bmatrix} E_{11} & E_{12} & E_{13} & 0 & 0 & 0 \\ E_{12} & E_{22} & E_{23} & 0 & 0 & 0 \\ E_{13} & E_{23} & E_{33} & 0 & 0 & 0 \\ 0 & 0 & 0 & E_{44} & 0 & 0 \\ 0 & 0 & 0 & 0 & E_{55} & 0 \\ 0 & 0 & 0 & 0 & 0 & E_{66} \end{bmatrix} \begin{Bmatrix} \varepsilon_x \\ \varepsilon_y \\ \varepsilon_z \\ \gamma_{yz} \\ \gamma_{xz} \\ \gamma_{xy} \end{Bmatrix} \quad (3.4)$$

A ply of unidirectional composite material, with the x axis of Figure 3.1 aligned with the fiber direction and the y axis transverse to it, possesses two planes of symmetry and is thus described by Equation (3.4). The same holds true for a fabric ply with the x axis aligned with one fiber direction and the y axis aligned with the other. Such plies form the building blocks for composite parts discussed in this book. Note that, in the laminate coordinate system, different plies stacked together, which are not 0, 90, or (0/90) will no longer possess two planes of symmetry and some of the coupling terms in Equation (3.1a) are nonzero. However, it is always possible to find an axis system (principal axes), in general not coinciding with the laminate axes, in which the laminate is orthotropic. In general, the entire laminate can be described by a stress-strain relation of the form:

$$\begin{Bmatrix} \sigma_x \\ \sigma_y \\ \sigma_z \\ \tau_{yz} \\ \tau_{xz} \\ \tau_{xy} \end{Bmatrix} = \begin{bmatrix} E_{11} & E_{12} & E_{13} & 0 & 0 & E_{16} \\ E_{12} & E_{22} & E_{23} & 0 & 0 & E_{26} \\ E_{13} & E_{23} & E_{33} & 0 & 0 & E_{36} \\ 0 & 0 & 0 & E_{44} & E_{45} & 0 \\ 0 & 0 & 0 & E_{45} & E_{55} & 0 \\ E_{16} & E_{26} & E_{36} & 0 & 0 & E_{66} \end{bmatrix} \begin{Bmatrix} \varepsilon_x \\ \varepsilon_y \\ \varepsilon_z \\ \gamma_{yz} \\ \gamma_{xz} \\ \gamma_{xy} \end{Bmatrix} \quad (3.5)$$

where E_{ij} are now laminate and not ply quantities.

The inverse of Equation (3.5), expressing the strains in terms of the stresses via the compliance tensor S_{ij} is also often used:

$$\begin{Bmatrix} \varepsilon_x \\ \varepsilon_y \\ \varepsilon_z \\ \gamma_{yz} \\ \gamma_{xz} \\ \gamma_{xy} \end{Bmatrix} = \begin{bmatrix} S_{11} & S_{12} & S_{13} & 0 & 0 & S_{16} \\ S_{12} & S_{22} & S_{23} & 0 & 0 & S_{26} \\ S_{13} & S_{23} & S_{33} & 0 & 0 & S_{36} \\ 0 & 0 & 0 & S_{44} & S_{45} & 0 \\ 0 & 0 & 0 & S_{45} & S_{55} & 0 \\ S_{16} & S_{26} & S_{36} & 0 & 0 & S_{66} \end{bmatrix} \begin{Bmatrix} \sigma_x \\ \sigma_y \\ \sigma_z \\ \tau_{yz} \\ \tau_{xz} \\ \tau_{xy} \end{Bmatrix} \quad (3.6)$$

where the compliance matrix is the inverse of the stiffness matrix:

$$[S] = [E]^{-1} \quad (3.7)$$

Note that Equations (3.5)–(3.7) refer to laminate quantities while Equation (3.4) refers to an orthotropic material such as a ply. The underlying assumptions are that: (a) at the laminate and, often, the ply scales, the fiber/matrix combination can be treated as a homogeneous material with smeared properties; (b) plane sections remain plane during deformation; (c) there is a perfect bond between fibers and matrix; and (d) there is a perfect bond between plies.

3.2.1 Tensor Transformations

If the stiffness (or compliance) properties are known in one coordinate system they can be obtained in any other coordinate system through standard tensor transformations. These can be expressed concisely if the tensor notation is used (each index ranges from 1 to 3 and repeating indices sum). Defining ℓ_{ij} to be the (direction) cosine of the angle between axes i and j , the compliance tensor S_{mnpq} in one coordinate system is obtained in terms of the compliance tensor

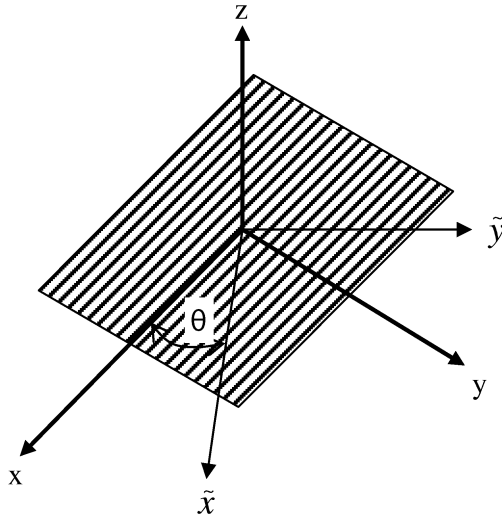


Figure 3.2 Coordinate system transformation

S_{ijkl} in another via the relation:

$$S_{mnpq} = \ell_{mi}\ell_{nj}\ell_{pk}\ell_{qr}S_{ijkl} \quad (3.8)$$

with an analogous relation for the stiffness E_{mnpq} .

If the two coordinate systems have the z axis (out-of-plane in the case of a laminate) in common, Equation (3.8) simplifies and can be expanded relatively easily. If the original coordinate system coincides with the ply axis system (x along fibers, y perpendicular to the fibers, as shown in Figure 3.2), then the compliance matrix in a coordinate system whose axis \tilde{x} forms an angle θ with the x axis of the original coordinate system, can be shown to be given by Equations (3.9).

$$\begin{aligned}
 S_{11} &= S_{11}^0 \cos^4 \theta + (2S_{12}^0 + S_{66}^0) \sin^2 \theta \cos^2 \theta + S_{22}^0 \sin^4 \theta \\
 S_{12} &= (S_{11}^0 + S_{22}^0 - S_{66}^0) \sin^2 \theta \cos^2 \theta + S_{12}^0 (\sin^4 \theta + \cos^4 \theta) \\
 S_{13} &= S_{13}^0 \cos^2 \theta + S_{23}^0 \sin^2 \theta \\
 S_{22} &= S_{11}^0 \sin^4 \theta + (2S_{12}^0 + S_{66}^0) \sin^2 \theta \cos^2 \theta + S_{22}^0 \cos^4 \theta \\
 S_{23} &= S_{13}^0 \sin^2 \theta + S_{23}^0 \cos^2 \theta \\
 S_{33} &= S_{33}^0 \\
 S_{16} &= 2S_{11}^0 \cos^3 \theta \sin \theta - 2S_{22}^0 \cos \theta \sin^3 \theta + (2S_{22}^0 + S_{66}^0) (\cos \theta \sin^3 \theta - \cos^3 \theta \sin \theta) \\
 S_{26} &= 2S_{11}^0 \cos \theta \sin^3 \theta - 2S_{22}^0 \cos^3 \theta \sin \theta + (2S_{22}^0 + S_{66}^0) (\cos^3 \theta \sin \theta - \cos \theta \sin^3 \theta) \\
 S_{36} &= 2(S_{13}^0 - S_{23}^0) \cos \theta \sin \theta \\
 S_{44} &= S_{55}^0 \sin^2 \theta + S_{44}^0 \cos^2 \theta \\
 S_{45} &= (S_{55}^0 - S_{44}^0) \sin \theta \cos \theta \\
 S_{55} &= S_{55}^0 \cos^2 \theta + S_{44}^0 \sin^2 \theta \\
 S_{66} &= 4(S_{11}^0 + S_{22}^0 - 2S_{12}^0) \sin^2 \theta \cos^2 \theta + S_{66}^0 (\sin^4 \theta + \cos^4 \theta - 2\sin^2 \theta \cos^2 \theta)
 \end{aligned} \quad (3.9)$$

where the quantities in the xyz coordinate system (basic ply) have a superscript 0 and are given in terms of the corresponding stiffnesses of the basic ply by:

$$\begin{aligned}
 S_{11}^0 &= \frac{1}{E_{11}} \\
 S_{12}^0 &= -\frac{v_{12}}{E_{11}} \\
 S_{66}^0 &= \frac{1}{G_{12}} \\
 S_{22}^0 &= \frac{1}{E_{22}} \\
 S_{13}^0 &= -\frac{v_{13}}{E_{11}} \\
 S_{23}^0 &= -\frac{v_{23}}{E_{22}} \\
 S_{33}^0 &= \frac{1}{E_{33}} \\
 S_{44}^0 &= \frac{1}{G_{23}} \\
 S_{55}^0 &= \frac{1}{G_{13}}
 \end{aligned} \tag{3.10}$$

where E_{ij} are stiffnesses of the basic (0°) ply with subscripts 1, 2, and 3 corresponding to the coordinates x , y , and z .

3.3 Constitutive Equations in Two Dimensions: Plane Stress

When dealing with thin composites, where the thickness of the laminate is much smaller than the other dimensions of the structure, the laminate is often assumed to be in a state of plane stress. This is usually the case of a composite plate that is thin compared with its in-plane dimensions. Then, the out-of-plane stresses σ_z , τ_{yz} , and τ_{xz} are negligible compared to the in-plane stresses:

$$\sigma_z \approx \tau_{yz} \approx \tau_{xz} \approx 0 \tag{3.11}$$

For an orthotropic material such as a single ply in the ply axes or a symmetric and balanced laminate in the laminate axes, placing Equation (3.11) in Equation (3.5) gives:

$$\begin{aligned}
 \sigma_x &= E_{11}\epsilon_x + E_{12}\epsilon_y + E_{13}\epsilon_z \\
 \sigma_y &= E_{12}\epsilon_x + E_{22}\epsilon_y + E_{23}\epsilon_z \\
 0 &= E_{13}\epsilon_x + E_{23}\epsilon_y + E_{33}\epsilon_z \\
 0 &= E_{44}\gamma_{yz} \\
 0 &= E_{55}\gamma_{xz} \\
 \tau_{xy} &= E_{66}\gamma_{xy}
 \end{aligned} \tag{3.12a-f}$$

From equations (3.12d) and (3.12e),

$$\gamma_{yz} = \gamma_{xz} = 0 \quad (3.13)$$

Equation (3.12c) can be solved for ε_z and the result substituted in Equations (3.12a) and (3.12b). This gives the equations

$$\begin{aligned}\sigma_x &= E_{11}\varepsilon_x + E_{12}\varepsilon_y + E_{13}\left(-\frac{E_{13}}{E_{33}}\varepsilon_x - \frac{E_{23}}{E_{33}}\varepsilon_y\right) \\ \sigma_y &= E_{12}\varepsilon_x + E_{22}\varepsilon_y + E_{23}\left(-\frac{E_{13}}{E_{33}}\varepsilon_x - \frac{E_{23}}{E_{33}}\varepsilon_y\right)\end{aligned} \quad (3.14)$$

which, upon collecting terms can be rewritten as:

$$\begin{aligned}\sigma_x &= \left(E_{11} - \frac{E_{13}^2}{E_{33}}\right)\varepsilon_x + \left(E_{12} - \frac{E_{13}E_{23}}{E_{33}}\right)\varepsilon_y \\ \sigma_y &= \left(E_{12} - \frac{E_{13}E_{23}}{E_{33}}\right)\varepsilon_x + \left(E_{22} - \frac{E_{23}^2}{E_{33}}\right)\varepsilon_y\end{aligned} \quad (3.15)$$

Equations (3.14) and (3.15) along with Equation (3.12f) form the constitutive relations (stress-strain equation) for composite materials undergoing plane stress. Redefining

$$\begin{aligned}Q_{xx} &= E_{11} - \frac{E_{13}^2}{E_{33}} \\ Q_{xy} &= E_{12} - \frac{E_{13}E_{23}}{E_{33}} \\ Q_{yy} &= E_{22} - \frac{E_{23}^2}{E_{33}} \\ Q_{ss} &= E_{66}\end{aligned} \quad (3.16)$$

the equations for plane stress can be rewritten in matrix form:

$$\begin{Bmatrix} \sigma_x \\ \sigma_y \\ \tau_{xy} \end{Bmatrix} = \begin{bmatrix} Q_{xx} & Q_{xy} & 0 \\ Q_{xy} & Q_{yy} & 0 \\ 0 & 0 & Q_{ss} \end{bmatrix} \begin{Bmatrix} \varepsilon_x \\ \varepsilon_y \\ \gamma_{xy} \end{Bmatrix} \quad (3.17)$$

It should be emphasized that the form of Equations (3.17) is the same irrespective of whether one deals with a single ply or a laminate, provided that the coordinate system is such that both the ply and the laminate are orthotropic. However, the values of the stiffnesses Q_{xx} , Q_{xy} , etc., differ between ply and laminate.

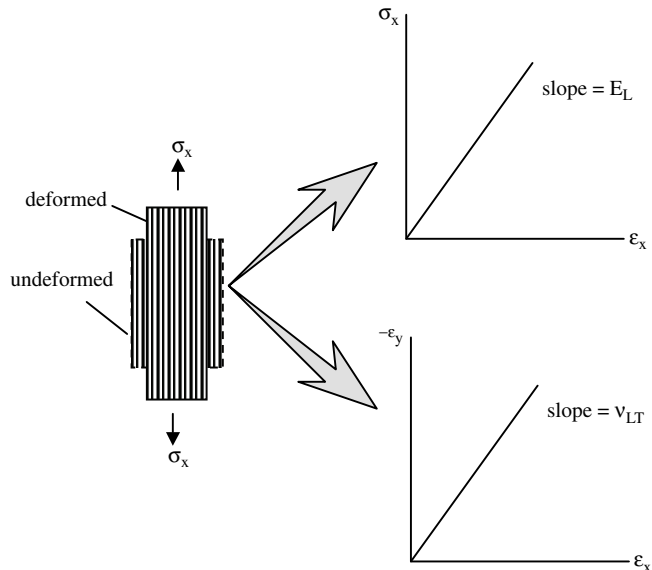


Figure 3.3 Quantities measured in a uniaxial tension test of a single unidirectional ply

The easiest way to use Equations (3.17) is to start from basic ply properties as measured from simple coupon tests, calculate the values for Q_{xx} , Q_{xy} , etc., then determine the corresponding values for any (rotated) ply and, finally, an entire laminate.

Let E_L , E_T , G_{LT} , and v_{LT} be the Young's modulus along the fibers (longitudinal direction), Young's modulus transverse to the fibers, shear modulus, and (major) Poisson's ratio respectively. These values can all be obtained from standard coupon tests.

Now in a uniaxial tension test (see Figure 3.3), where the applied load is parallel to the fibers of a unidirectional ply (which define the x direction), the slope of the applied stress σ_x versus longitudinal strain ε_x is the Young's modulus E_L and the slope of the transverse strain $-\varepsilon_y$ versus longitudinal strain ε_x is the Poisson's ratio v_{LT} :

$$v_{LT} = - \frac{\varepsilon_y}{\varepsilon_x} \quad (3.18)$$

Using this to substitute for ε_y in the first of Equations (3.17) gives:

$$\sigma_x = Q_{xx}\varepsilon_x - Q_{xy}v_{LT}\varepsilon_x \quad (3.19)$$

For the same uniaxial tension test, $\sigma_y = 0$ and the second of Equations (3.17) gives

$$0 = Q_{xy}\varepsilon_x + Q_{yy}\varepsilon_y \Rightarrow \frac{Q_{xy}}{Q_{yy}} = - \frac{\varepsilon_y}{\varepsilon_x} \quad (3.20)$$

Comparing, Equations (3.18) and (3.20)

$$v_{LT} = \frac{Q_{xy}}{Q_{yy}} \quad (3.21)$$

and substituting in Equation (3.19),

$$\sigma_x = \left(Q_{xx} - \frac{Q_{xy}^2}{Q_{yy}} \right) \epsilon_x \quad (3.22)$$

Equation (3.22) implies that the slope E_L of the σ_x versus ϵ_x curve (see Figure 3.3) is given by:

$$E_L = Q_{xx} - \frac{Q_{xy}^2}{Q_{yy}} \quad (3.23)$$

In a completely analogous fashion, but now considering a uniaxial tension test transverse to the fibers, and noticing that v_{TL} is the Poisson's ratio that describes contraction in the x direction when a tension load is applied in the y direction, Equations (3.24) and (3.25) are obtained as analogues to Equations (3.21) and (3.23):

$$v_{TL} = \frac{Q_{xy}}{Q_{xx}} \quad (3.24)$$

$$E_T = Q_{yy} - \frac{Q_{xy}^2}{Q_{xx}} \quad (3.25)$$

Note that Equations (3.21) and (3.24) imply that

$$v_{LT} Q_{yy} = v_{TL} Q_{xx} \quad (3.26)$$

Equations (3.23), (3.25) and (3.26) form a system of three equations in the three unknowns Q_{xx} , Q_{xy} , and Q_{yy} . Solving gives,

$$Q_{xx} = \frac{E_L}{1 - v_{LT} v_{TL}} \quad (3.27)$$

$$Q_{yy} = \frac{E_T}{1 - v_{LT} v_{TL}} \quad (3.28)$$

$$Q_{xy} = \frac{v_{LT} E_T}{1 - v_{LT} v_{TL}} = \frac{v_{TL} E_L}{1 - v_{LT} v_{TL}} \quad (3.29)$$

Considering now a pure shear test of a unidirectional ply where G_{LT} is the slope of the shear stress (τ_{xy}) versus the shear strain (γ_{xy}) curve, the last of equations (3.17) implies that

$$Q_{ss} = G_{LT} \quad (3.30)$$

Equations (3.27)–(3.30) can be used to substitute in Equations (3.17) to obtain the final form of the stress–strain equations for an orthotropic ply under plane stress:

$$\begin{Bmatrix} \sigma_x \\ \sigma_y \\ \tau_{xy} \end{Bmatrix} = \begin{bmatrix} \frac{E_L}{1 - v_{LT}v_{TL}} & \frac{v_{LT}E_T}{1 - v_{LT}v_{TL}} & 0 \\ \frac{v_{LT}E_T}{1 - v_{LT}v_{TL}} & \frac{E_T}{1 - v_{LT}v_{TL}} & 0 \\ 0 & 0 & G_{LT} \end{bmatrix} \begin{Bmatrix} \epsilon_x \\ \epsilon_y \\ \gamma_{xy} \end{Bmatrix} \quad (3.31)$$

The next step is to obtain the stress–strain relations for any ply rotated by an angle θ . In general the stress strain Equations (3.17) now become:

$$\begin{Bmatrix} \sigma_1 \\ \sigma_2 \\ \tau_{12} \end{Bmatrix} = \begin{bmatrix} Q_{11} & Q_{12} & Q_{16} \\ Q_{12} & Q_{22} & Q_{26} \\ Q_{16} & Q_{26} & Q_{66} \end{bmatrix} \begin{Bmatrix} \epsilon_1 \\ \epsilon_2 \\ \gamma_{12} \end{Bmatrix} \quad (3.32)$$

To relate these quantities to the corresponding ones for an orthotropic ply requires transforming stresses, strains, and stiffnesses by the angle θ .

The stiffness transformation follows the standard tensor transformation (Equations (3.8)), which, for a ply rotated in its plane, as is the case of interest here, are simplified to the equations analogous to Equations (3.9) that were obtained for the compliances. For the plane stress case, Equations (3.8) or (3.9) applied to the stiffness tensor give the stiffnesses in the 1–2 coordinate system of Figure 3.4 as:

$$\begin{aligned} Q_{11}^{(\theta)} &= m^4 Q_{xx} + n^4 Q_{yy} + 2m^2n^2 Q_{xy} + 4m^2n^2 Q_{ss} \\ Q_{22}^{(\theta)} &= n^4 Q_{xx} + m^4 Q_{yy} + 2m^2n^2 Q_{xy} + 4m^2n^2 Q_{ss} \\ Q_{12}^{(\theta)} &= m^2n^2 Q_{xx} + m^2n^2 Q_{yy} + (m^4 + n^4)Q_{xy} - 4m^2n^2 Q_{ss} \\ Q_{66}^{(\theta)} &= m^2n^2 Q_{xx} + m^2n^2 Q_{yy} - 2m^2n^2 Q_{xy} + (m^2 - n^2)^2 Q_{ss} \\ Q_{16}^{(\theta)} &= m^3n Q_{xx} - mn^3 Q_{yy} + (mn^3 - m^3n)Q_{xy} + 2(mn^3 - m^3n)Q_{ss} \\ Q_{26}^{(\theta)} &= mn^3 Q_{xx} - m^3n Q_{yy} + (m^3n - mn^3)Q_{xy} + 2(m^3n - mn^3)Q_{ss} \end{aligned} \quad (3.33)$$

where $m = \cos \theta$ and $n = \sin \theta$

The stresses and strains transform using second-order tensor transformation equations instead of the fourth-order tensor transformation for stiffnesses and compliances given by Equation (3.8). Using ℓ_{ij} to denote the direction cosines between axes i and j , the stress transformation equations can be written as:

$$\sigma_{mn} = \ell_{mp}\ell_{nq}\sigma_{pq} \quad (3.34)$$

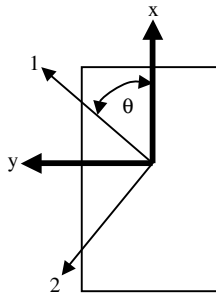


Figure 3.4 Coordinate system for ply rotated by an angle θ

which, expanded out for the case shown in Figure 3.4 reads:

$$\begin{Bmatrix} \sigma_1 \\ \sigma_2 \\ \tau_{12} \end{Bmatrix} = \begin{bmatrix} \cos^2\theta & \sin^2\theta & 2\sin\theta\cos\theta \\ \sin^2\theta & \cos^2\theta & -2\sin\theta\cos\theta \\ -\sin\theta\cos\theta & \sin\theta\cos\theta & (\cos^2\theta - \sin^2\theta) \end{bmatrix} \begin{Bmatrix} \sigma_x \\ \sigma_y \\ \tau_{xy} \end{Bmatrix} \quad (3.35)$$

An analogous expression is obtained for the strain transformation. However, since here engineering notation is used (instead of tensor notation) the form of Equation (3.35) for the (engineering) strains is:

$$\begin{Bmatrix} \varepsilon_1 \\ \varepsilon_2 \\ \gamma_{12} \end{Bmatrix} = \begin{bmatrix} \cos^2\theta & \sin^2\theta & \sin\theta\cos\theta \\ \sin^2\theta & \cos^2\theta & -\sin\theta\cos\theta \\ -2\sin\theta\cos\theta & 2\sin\theta\cos\theta & (\cos^2\theta - \sin^2\theta) \end{bmatrix} \begin{Bmatrix} \varepsilon_x \\ \varepsilon_y \\ \gamma_{xy} \end{Bmatrix} \quad (3.36)$$

Note the changes in the factors of 2 in the last row and column of the transformation matrix. These come from the fact that the engineering shear strain is twice the tensor strain: $\gamma_{xy} = 2\varepsilon_{12}$.

While the equations in terms of stresses and strains can be (and often are) used, in practice it is convenient to define force and moment resultants by integrating through the thickness of a laminate. For a laminate of thickness h as shown in Figure 3.5, the following quantities are defined:

$$\begin{aligned} N_x &= \int_{-\frac{h}{2}}^{\frac{h}{2}} \sigma_x dz \\ N_y &= \int_{-\frac{h}{2}}^{\frac{h}{2}} \sigma_y dz \\ N_{xy} &= \int_{-\frac{h}{2}}^{\frac{h}{2}} \tau_{xy} dz \end{aligned} \quad (3.37)$$

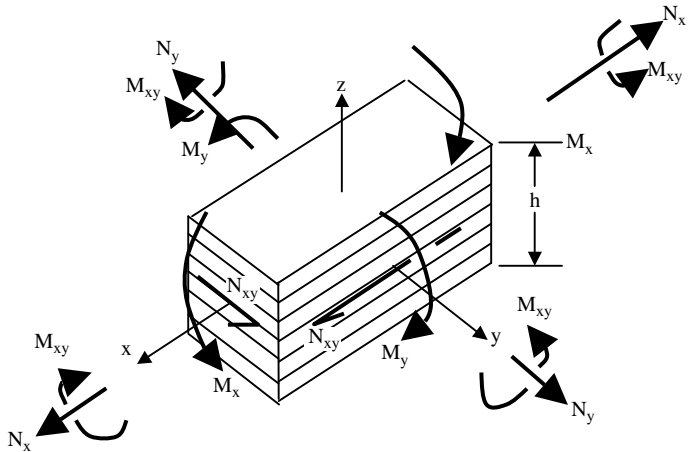


Figure 3.5 Force and moment resultants applied to a laminate (arrows indicate sign convention for positive values)

which are the force resultants and

$$\begin{aligned}
 M_x &= \int_{-\frac{h}{2}}^{\frac{h}{2}} \sigma_x z dz \\
 M_y &= \int_{-\frac{h}{2}}^{\frac{h}{2}} \sigma_y z dz \\
 M_{xy} &= \int_{-\frac{h}{2}}^{\frac{h}{2}} \tau_{xy} z dz
 \end{aligned} \tag{3.38}$$

which are the moment resultants.

Note that the units of force and moment resultants are force per unit width and moment per unit width respectively.

Using the force resultants in Equation (3.37), average laminate stresses can be defined as follows:

$$\sigma_{xav} = \frac{1}{h} \int_{-\frac{h}{2}}^{\frac{h}{2}} \sigma_x dz = \frac{N_x}{h}$$

$$\begin{aligned}\sigma_{yav} &= \frac{N_y}{h} \\ \tau_{xyav} &= \frac{N_{xy}}{h}\end{aligned}\quad (3.39)$$

where Equations (3.37) are used to substitute for the integrals involved.

The relation between force resultants and laminate strains can be obtained by using Equation (3.32) and integrating through the laminate thickness. Since the stiffnesses are constant in each ply (but not necessarily the same from one ply to the next), the z integrations become summations over all the plies in the laminate. In the laminate coordinate system xy , Equation (3.32) integrated with respect to z gives

$$\begin{Bmatrix} N_x \\ N_y \\ N_{zy} \end{Bmatrix} = \begin{bmatrix} A_{11} & A_{12} & A_{16} \\ A_{12} & A_{22} & A_{26} \\ A_{16} & A_{26} & A_{66} \end{bmatrix} \begin{Bmatrix} \varepsilon_x \\ \varepsilon_y \\ \gamma_{xy} \end{Bmatrix} \quad (3.40)$$

where

$$A_{ij} = \sum_{k=1}^n Q_{ij}(z_k - z_{k-1}) \quad (3.41)$$

where $i,j = 1,2,6$, the summation is carried over all n plies of the laminate and z_k, z_{k-1} are the upper and lower z coordinates of the k th ply, as shown in Figure 3.6.

Equations (3.40) and (3.41) describe the membrane deformations of a laminate under in-plane loads. For a laminate under bending loads, the standard Kirchhoff plate theory assumptions are used: Plane sections remain plane and perpendicular to the neutral axis. Denoting the out-of-plane displacement by w , the curvatures κ_x , κ_y , and κ_{xy} are defined as:

$$\begin{aligned}\kappa_x &= -\frac{\partial^2 w}{\partial x^2} \\ \kappa_y &= -\frac{\partial^2 w}{\partial y^2} \\ \kappa_{xy} &= -2 \frac{\partial^2 w}{\partial x \partial y}\end{aligned}\quad (3.42)$$

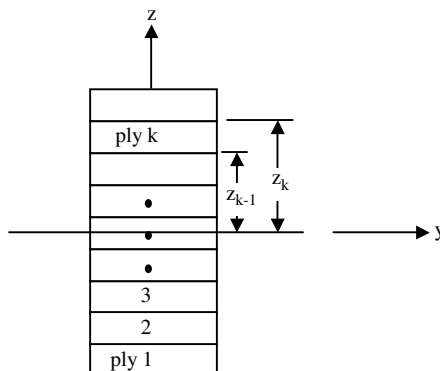


Figure 3.6 Ply numbering system

It can be shown that κ_x and κ_y are inversely proportional to the local radii of curvature in the x and y directions respectively. Note that w is only a function of the in-plane coordinates x and y and is not a function of the out-of-plane coordinate z .

In a pure bending situation with small deflections, the strains are proportional to the curvatures and are assumed to vary linearly through the laminate thickness (see also Section 5.2.2). They are then given by

$$\begin{aligned}\varepsilon_x &= z\kappa_x \\ \varepsilon_y &= z\kappa_y \\ \gamma_{xy} &= z\kappa_{xy}\end{aligned}\quad (3.43)$$

Now writing the first of Equations (3.32) in the laminate coordinate system xy , multiplying both sides by z and integrating through the thickness of the laminate, gives:

$$\int_{-\frac{h}{2}}^{\frac{h}{2}} \sigma_x z dz = \int_{-\frac{h}{2}}^{\frac{h}{2}} Q_{11} z^2 \kappa_x dz + \int_{-\frac{h}{2}}^{\frac{h}{2}} Q_{12} z^2 \kappa_y dz + \int_{-\frac{h}{2}}^{\frac{h}{2}} Q_{16} z^2 \kappa_{xy} dz \quad (3.44)$$

According to the first of Equations (3.38), the left-hand side of Equation (3.44) is M_x . Denoting

$$D_{11} = \int_{-\frac{h}{2}}^{\frac{h}{2}} Q_{11} z^2 dz, \quad D_{12} = \int_{-\frac{h}{2}}^{\frac{h}{2}} Q_{12} z^2 dz, \quad \text{and} \quad D_{16} = \int_{-\frac{h}{2}}^{\frac{h}{2}} Q_{16} z^2 dz$$

Equation (3.44) can be rewritten in the form:

$$M_x = D_{11} \kappa_x + D_{12} \kappa_y + D_{16} \kappa_{xy} = -D_{11} \frac{\partial^2 w}{\partial x^2} - D_{12} \frac{\partial^2 w}{\partial y^2} - 2D_{16} \frac{\partial^2 w}{\partial x \partial y} \quad (3.45)$$

where D_{11} , D_{12} , and D_{16} are laminate bending stiffnesses.

Operating on the second and third of Equations (3.32) in an analogous fashion, the following constitutive equations for pure bending of a laminate can be obtained:

$$\begin{Bmatrix} M_x \\ M_y \\ M_{zy} \end{Bmatrix} = \begin{bmatrix} D_{11} & D_{12} & D_{16} \\ D_{12} & D_{22} & D_{26} \\ D_{16} & D_{26} & D_{66} \end{bmatrix} \begin{Bmatrix} \kappa_x \\ \kappa_y \\ \kappa_{xy} \end{Bmatrix} \quad (3.46)$$

where

$$D_{ij} = \sum_{k=1}^n \frac{Q_{ij}}{3} (z_k^3 - z_{k-1}^3) \quad (3.47)$$

with $i,j = 1,2,6$, the summation carried over all plies n of the laminate, and z_k, z_{k-1} the upper and lower z coordinates of the k th ply, as shown in Figure 3.6.

Equations (3.40) describe the pure membrane deformations of a laminate and Equations (3.46) the pure bending deformations. In this decoupled form, in-plane strains ε_x , ε_y , and γ_{xy} can only be caused by in-plane loads N_x , N_y , and N_{xy} while curvatures κ_x , κ_y , and κ_{xy} can only be caused by bending moments M_x , M_y , and M_{xy} . However, for a general laminate, it is possible to have coupling between the membrane and bending behaviors, with strains caused by bending moments and/or curvatures caused by in-plane loads. In such a case the strains are given by a superposition of the membrane strains and the curvatures. The membrane strains are constant through the thickness of the laminate and equal to the mid-plane strains ε_{xo} , ε_{yo} , and γ_{xyo} . Therefore,

$$\begin{aligned}\varepsilon_x &= \varepsilon_{xo} + z\kappa_x \\ \varepsilon_y &= \varepsilon_{yo} + z\kappa_y \\ \gamma_{xy} &= \gamma_{xyo} + z\kappa_{xy}\end{aligned}\quad (3.48)$$

Reducing Equations (3.32) to a format in terms of force and moment resultants and combining Equations (3.40), (3.46), and (3.48) the generalized constitutive relations for any laminate (including membrane-bending coupling) have the form:

$$\left\{ \begin{array}{l} N_x \\ N_y \\ N_{xy} \\ M_x \\ M_y \\ M_{xy} \end{array} \right\} = \left[\begin{array}{cccccc} A_{11} & A_{12} & A_{16} & B_{11} & B_{12} & B_{16} \\ A_{12} & A_{22} & A_{26} & B_{12} & B_{22} & B_{26} \\ A_{16} & A_{26} & A_{66} & B_{16} & B_{26} & B_{66} \\ B_{11} & B_{12} & B_{16} & D_{11} & D_{12} & D_{16} \\ B_{12} & B_{22} & B_{26} & D_{12} & D_{22} & D_{26} \\ B_{16} & B_{26} & B_{66} & D_{16} & D_{26} & D_{66} \end{array} \right] \left\{ \begin{array}{l} \varepsilon_{xo} \\ \varepsilon_{yo} \\ \gamma_{xyo} \\ \kappa_x \\ \kappa_y \\ \kappa_{xy} \end{array} \right\} \quad (3.49)$$

where A_{ij} and D_{ij} were defined by Equations (3.41), and (3.47) and

$$B_{ij} = \sum_{k=1}^n \frac{Q_{ij}}{2} (z_k^2 - z_{k-1}^2) \quad (3.50)$$

with $i,j = 1,2,6$, the summation carried over all plies n of the laminate, and z_k, z_{k-1} the upper and lower z coordinates of the k th ply, as shown in Figure 3.6.

It is important to note that if the order of plies in a stacking sequence is changed the A matrix remains unaffected but the B and D matrices change. This can be of particular importance for buckling-critical designs and provides an option of optimizing a layup without increasing its weight by reordering the plies.

If the midplane strains and curvatures of a laminate are known, direct substitution in Equations (3.49) will give the applied forces and moments. Usually, however, the forces and moments are known and the strains and curvatures are sought for. They can be obtained by inverting relations (3.49). The result is [4, 5]:

$$\begin{Bmatrix} \varepsilon_{xo} \\ \varepsilon_{yo} \\ \gamma_{xyo} \\ \kappa_x \\ \kappa_y \\ \kappa_{xy} \end{Bmatrix} = \begin{Bmatrix} \alpha_{11} & \alpha_{12} & \alpha_{16} & \beta_{11} & \beta_{12} & \beta_{16} \\ \alpha_{12} & \alpha_{22} & \alpha_{26} & \beta_{21} & \beta_{22} & \beta_{26} \\ \alpha_{16} & \alpha_{26} & \alpha_{66} & \beta_{61} & \beta_{62} & \beta_{66} \\ \beta_{11} & \beta_{21} & \beta_{61} & \delta_{11} & \delta_{12} & \delta_{16} \\ \beta_{12} & \beta_{22} & \beta_{62} & \delta_{12} & \delta_{22} & \delta_{26} \\ \beta_{16} & \beta_{26} & \beta_{66} & \delta_{16} & \delta_{26} & \delta_{66} \end{Bmatrix} \begin{Bmatrix} N_x \\ N_y \\ N_{xy} \\ M_x \\ M_y \\ M_{xy} \end{Bmatrix} \quad (3.51)$$

where

$$[\alpha] = [A]^{-1} + [A]^{-1}[B]\left[D - [B][A]^{-1}[B]\right]^{-1}[B][A]^{-1} \quad (3.52)$$

$$[\beta] = -[A][B]\left[D - [B][A]^{-1}[B]\right]^{-1} \quad (3.53)$$

$$[\delta] = \left[D - [B][A]^{-1}[B]\right]^{-1} \quad (3.54)$$

with square brackets denoting a matrix and the exponent -1 denoting the inverse of a matrix. Note that the β matrix at the top right of Equation (3.51) need not be symmetric. Its transpose appears at the lower left of the matrix in the right-hand side of Equation (3.51).

The most important laminate layup is that of a symmetric laminate (see also Section 3.1). For such a laminate, the coupling matrix B is zero. This can be seen from Equation (3.50) where the contributions to each entry of the matrix coming from two plies located symmetrically with respect to the midplane subtract each other (Q_{ij} are the same because the laminate is symmetric and the coefficients $z_k^2 - z_{k-1}^2$ are equal and opposite). With the B matrix zero, there is no membrane-stretching coupling in the laminate behavior. Also, Equations (3.52), (3.53), (3.54) simplify. Denoting the inverse of the A matrix by a and the inverse of the D matrix by d , Equations (3.52)–(3.54) become:

$$[\alpha] = [A]^{-1} = [a] \quad (3.52a)$$

$$[\beta] = 0 \quad (3.53a)$$

$$[\delta] = [D]^{-1} = [d] \quad (3.54a)$$

and substituting in Equation (3.51)

$$\begin{Bmatrix} \varepsilon_{xo} \\ \varepsilon_{yo} \\ \gamma_{xyo} \\ \kappa_x \\ \kappa_y \\ \kappa_{xy} \end{Bmatrix} = \begin{Bmatrix} a_{11} & a_{12} & a_{16} & 0 & 0 & 0 \\ a_{12} & a_{22} & a_{26} & 0 & 0 & 0 \\ a_{16} & a_{26} & a_{66} & 0 & 0 & 0 \\ 0 & 0 & 0 & d_{11} & d_{12} & d_{16} \\ 0 & 0 & 0 & d_{12} & d_{22} & d_{26} \\ 0 & 0 & 0 & d_{16} & d_{26} & d_{66} \end{Bmatrix} \begin{Bmatrix} N_x \\ N_y \\ N_{xy} \\ M_x \\ M_y \\ M_{xy} \end{Bmatrix} \quad (3.51a)$$

valid for a symmetric laminate.

Laminate symmetry will be invoked often in subsequent chapters. It should be emphasized here that, in designing composite structures, symmetric and balanced laminates are preferred. They decouple membrane from bending behavior and stretching from shearing deformations, thus avoiding unwanted failure modes that may occur under some loading conditions.

Very often used in design, are the so-called engineering constants. These are stiffness properties that can be measured in the laboratory using simple tests. For example, a uniaxial test of a symmetric and balanced laminate would provide a value for the membrane stiffness E_{xm}^L (or E_{1m} if 1–2 are the laminate axes) of the laminate. For such a laminate under uniaxial loading N_x (with $N_y = 0$), the first two of Equations (3.49) read

$$\begin{aligned} N_x &= A_{11}\varepsilon_{xo} + A_{12}\varepsilon_{yo} \\ 0 &= A_{12}\varepsilon_{xo} + A_{22}\varepsilon_{yo} \end{aligned}$$

The second equation can be used to solve for ε_{yo} :

$$\varepsilon_{yo} = -\frac{A_{12}}{A_{22}}\varepsilon_{xo} \quad (3.55)$$

which, substituted in the first equation, gives

$$N_x = \left(A_{11} - \frac{A_{12}^2}{A_{22}} \right) \varepsilon_{xo} \quad (3.56)$$

Now using the first of Equations (3.39) to substitute for the stress σ_{xav} measured in a uniaxial test, the following relation is obtained

$$\sigma_{xav} = \frac{1}{h} \left(A_{11} - \frac{A_{12}^2}{A_{22}} \right) \varepsilon_{xo} \quad (3.57)$$

It can also be shown that the 11 entry of the inverse of the A matrix for a symmetric and balanced laminate is

$$a_{11} = \frac{A_{22}}{A_{11}A_{22} - A_{12}^2} \quad (3.58)$$

Equations (3.57) and (3.58) imply that the laminate Young's modulus for membrane deformations of a symmetric and balanced laminate is given by:

$$E_{1m} = \frac{1}{h} \frac{A_{11}A_{22} - A_{12}^2}{A_{22}} = \frac{1}{ha_{11}} \quad (3.59)$$

Also, from Equations (3.18) and (3.55), the Poisson's ratio for a symmetric and balanced laminate undergoing membrane deformations is

$$\nu_{12m} = \frac{A_{12}}{A_{22}} \quad (3.60)$$

An analogous expression can be derived for the bending modulus E_{1b} of a laminate. For the special case of a laminate with B matrix zero and $D_{16} = D_{26} = 0$, the fourth and fifth equations of relations (3.49) and (3.51) can be used to eliminate κ_y and obtain the relation

$$M_x = \left(D_{11} - \frac{D_{12}^2}{D_{22}} \right) \kappa_x \quad (3.61)$$

In a pure bending test, such as a four-point bending test, the moment curvature relation has the form:

$$M_x = \frac{M}{b} = \frac{1}{b} E_{1b} I \kappa_x \quad (3.62)$$

where I is the moment of inertia $bh^3/12$.

Comparing Equations (3.61) and (3.62) it can be seen that

$$E_{1b} = \frac{12}{h^3} \left(D_{11} - \frac{D_{12}^2}{D_{22}} \right) \quad (3.63)$$

which, using d_{11} , can be shown to be

$$E_{1b} = \frac{12 D_{11} D_{22} - D_{12}^2}{h^3 D_{22}} = \frac{12}{h^3 d_{11}} \quad (3.64)$$

In general, the stiffness calculated by Equation (3.59), corresponding to stretching of a laminate, is not the same as that calculated by Equation (3.64), which corresponds to bending of a laminate. This will be shown later on to cause some problems on the selection of the stiffness value to be used for certain problems (see, for example, Section 8.2). In general, for bending problems the bending stiffnesses are used and for stretching problems the membrane stiffnesses are used. However, in situations where both behaviors occur simultaneously it is not always clear what values should be used and it is not uncommon to use the values that give the most conservative results.

Relations (3.59) and (3.64) were derived for special laminates to avoid algebraic complexity and to emphasize the underlying physical models. In general, the laminate stiffness properties in all directions for symmetric laminates can be found to be [5]:

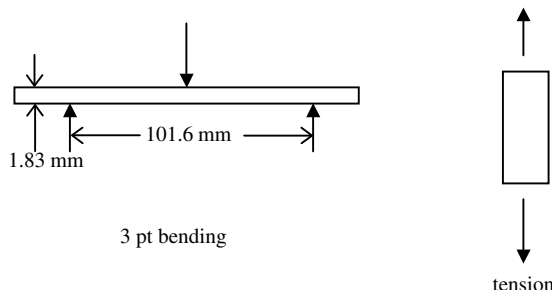
$$\begin{aligned} E_{1m} &= \frac{1}{ha_{11}} & E_{1b} &= \frac{12}{h^3 d_{11}} \\ E_{2m} &= \frac{1}{ha_{22}} & E_{2b} &= \frac{12}{h^3 d_{22}} \\ G_{12m} &= \frac{1}{ha_{66}} & G_{12b} &= \frac{12}{h^3 d_{66}} \\ v_{12m} &= -\frac{a_{12}}{a_{22}} & v_{12b} &= -\frac{d_{12}}{d_{22}} \\ v_{21m} &= -\frac{a_{12}}{a_{11}} & v_{21b} &= -\frac{d_{12}}{d_{11}} \end{aligned} \quad (3.65)$$

Exercises

- 3.1 Assume a layup consists of n plies of the same material, all at the same orientation (not necessarily 0°). Let E be the Young's modulus of a single ply at that orientation, G the corresponding shear modulus, and v_{12} , v_{21} the two Poisson's ratios. Derive analytical expressions for $A_{11}, A_{12}, A_{22}, A_{66}, D_{11}, D_{12}, D_{22}, D_{66}$ as functions of E , G , v_{12} , v_{21} , and the thickness h of the laminate (still having all plies with the same fiber orientation).
- 3.2 By mistake, the layup of a specific laminate fabricated in the factory was not labelled and the stacking sequence is unknown. The laminate was fabricated using a graphite/epoxy material with the following basic ply properties:

$$\begin{aligned}E_x &= 131 \text{ GPa} \\E_y &= 11.7 \text{ GPa} \\G_{xy} &= 4.82 \text{ GPa} \\v_{xy} &= 0.29 \\t_{\text{ply}} &= 0.3048 \text{ mm}\end{aligned}$$

To avoid throwing the expensive laminate away an engineer cuts a small strip of material from the edge. The strip is 152.4 mm long by 25.4 mm wide and has a thickness of 1.83 mm. First he/she tests this in a three-point bending configuration and then in tension as shown in the Figure below:



In the three-point bending test he/she notices that the specimen undergoes pure bending and in the tension test the specimen only elongates (and contracts by a small amount transversely to the load).

Using the results of the three-point bending test, the engineer notices that when plotting the center deflection as a function of the applied load at the center, he/she obtains (for low loads) an (almost) straight line with slope 0.03826 mm/N. Unfortunately, this information is not sufficient to determine the stacking sequence conclusively. Part of the problem is that it is hard to measure the center deflection of the three-point bending test accurately. During the uniaxial tension test the engineer notices that a maximum load of 2225 N results in a specimen elongation of 0.0941 mm. Now the engineer is confident he/she knows the stacking sequence. What is the stacking sequence? (In this factory only laminates with 0,45,−45, and 90 plies are used)

References

1. Tsai, S.W., Mechanics of Composite Materials Part I — Introduction, *Report AFML-TR-66-149, Part I Air Force Materials Laboratory Research and Technology Division*, Wright-Patterson Air Force Base, Ohio, June 1966.
2. Tsai, S.W., Mechanics of Composite Materials, Part II — Theoretical Aspects, *Report AFML-TR-66-149, Part II, Air Force Materials Laboratory Research and Technology Division*, Wright-Patterson Air Force Base, Ohio, November, 1966.
3. Ashton, J.E., Halpin, J.C. and Petit, P.H., *Primer on Composite Materials: Analysis*, Technomic, 1969.
4. Jones, R.M, *Mechanics of Composite Materials*, McGraw-Hill, Washington DC, 1975.
5. Tsai, S.W. and Hahn, H.T., *Introduction to Composite Materials*, Technomic Publishing Co, Westport CT, 1980.
6. Love, A.E.H., *A Treatise on the Mathematical Theory of Elasticity*, 4th edn, Dover Publications, NY, 1944, Article 66.

4

Review of Laminate Strength and Failure Criteria

If the loads applied to a laminate are sufficiently high then the strength of the material is exceeded and the laminate fails. It is, therefore, very important to be able to use the stresses and/or strains calculated in the previous chapter to predict failure. This, however, is complicated by the fact that final failure of a laminate does not always coincide with onset of damage. Depending on the laminate layup and loading, damage may start at a load significantly lower than the load at which final failure occurs. Being able to predict when damage starts and how it evolves requires individual modeling of the matrix and fibers. Usually, damage starts in the form of matrix cracks between fibers in plies transverse to the primary load direction. As the load increases the crack density increases and the cracks may coalesce into delaminations (where plies locally separate from one another) or branch out to adjacent plies [1]. In addition, local stress concentrations may lead to failure of the fiber–matrix interphase. Further increase of the load accumulates this type of damage and causes some fibers to fail until the laminate can no longer sustain the applied load and fails catastrophically. The detailed analysis of damage creation and evolution accounting for the individual constituents of a ply is the subject of micromechanics [2, 3].

In an alternate simplified approach, each ply is modeled as homogeneous, having specific failure modes which are characterized by tests. For a unidirectional ply the following failure modes are usually recognized:

Tension failure along the fibers with strength symbol X^t

Compression failure along the fibers with strength symbol X^c

Tension failure transverse to the fibers with strength symbol Y^t

Compression failure transverse to the fibers with strength symbol Y^c

Pure shear failure of a ply with strength symbol S

These strength values, obtained experimentally, are already one step away from the individual failures of fiber and matrix and their interphase. The details of damage onset,

such as matrix cracks leading to fiber failure or failure of the fiber–matrix interphase leading to fiber failure, are lumped into a single experimentally measured value. This value is a macroscopic value that describes when a single ply will fail catastrophically given a specific loading.

In parallel to, or instead of, the five strength values just mentioned, ultimate strain values can be used for the same loading situations, again obtained experimentally. Using ultimate stress values is interchangeable with ultimate strain values (in terms of obtaining the same failure load at which the ply fails) only for loading situations for which the stress–strain curve is linear to failure or very nearly so. This means that for tension and compression along the fibers, going from predictions obtained with a strength-based model to predictions from a strain model requires only the use of a constant of proportionality which is the Young’s modulus (in the direction of the load) divided by a Poisson’s ratio term. For shear loading and transverse tension or compression, where the stress–strain curves are, usually, nonlinear, simply multiplying strain-based predictions with a constant of proportionality does not give the correct strength failure values. A model that accounts for nonlinearities in the stress–strain curve must be used.

Consider now the case of a laminate in which all the plies are the same with the same arbitrary orientation θ . An arbitrary in-plane loading applied to this laminate, results in the same combined state of stress (and strain) in each ply. This state of stress or strain must be transformed to the principal axes for the ply, which are the ply axes (one axis parallel to the fibers and one transverse to them). The resulting principal stresses (or strains) are compared with their respective maximum values (strength or ultimate strain). Obviously, in this special case, all plies fail simultaneously. The approach where the principal stresses in a ply are compared with the ultimate strength values in the respective directions is the maximum stress theory. The approach where principal strains in a ply are compared with the ultimate strain values in the respective directions is the maximum strain theory. Note that, for generalized loading, even if all stress–strain curves are linear, the predictions from the two methods will differ slightly due to a Poisson’s ratio effect.

The situation becomes more complicated when the plies in a laminate do not all have the same ply orientation. The procedure is as follows:

1. Given the applied loads, the corresponding laminate midplane strains and curvatures are computed using Equations (3.51).
2. These are then used along with Equations (3.48) to determine the individual strains within each ply in the laminate axes (see Figure 4.1).
3. Ply strains in the laminate axes can be translated to ply stresses in the laminate axes using Equations (3.32).
4. Depending on the type of failure criterion used (stress- or strain-based) the ply stresses and/or strains in the laminate axes are transformed to ply stresses and/or strains in the ply axes (see Figure 4.1) using Equations (3.35) and/or (3.36). For each ply, the ply axis system has one axis parallel to the fibers and the other perpendicular to them.
5. Using the results of the previous step, a failure criterion is applied to determine which ply fails. This determines first-ply failure.
6. If desired, post-first-ply failure analysis can follow. The stiffness and strength properties of the failed ply are adjusted accounting for the type of failure that occurred and steps 1–5 are repeated until the next ply fails.
7. Step 6 is repeated until all plies in the laminate have failed.

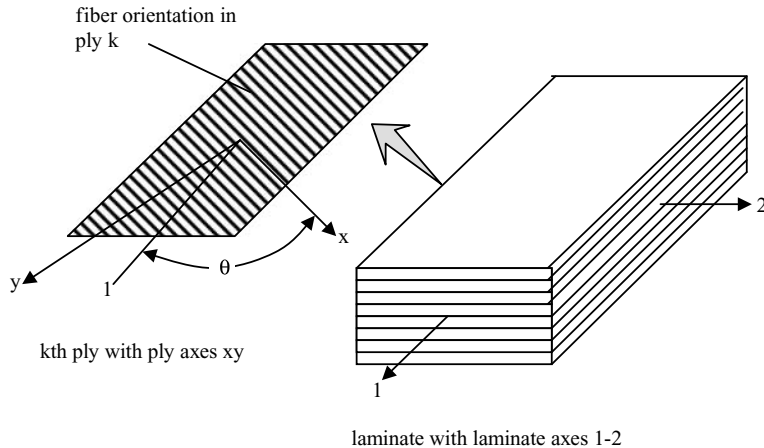


Figure 4.1 Laminate and ply axes systems

The failure predictions obtained with the procedure just described may vary significantly depending on the failure criterion used. There is a large number of failure criteria, stress-based, strain-based, or energy-based. A few representative ones are briefly discussed in subsequent sections.

4.1 Maximum Stress Failure Theory

In this case, the principal stresses in each ply are compared with their corresponding strength values X^t , X^c , Y^t , Y^c , and S . In a design situation these strength values are adjusted through statistical analysis (see Sections 5.1.3–5.1.6) to obtain reduced values that account for material scatter and adverse environmental effects. In some cases, the effect of damage is also included in these reduced strength values. These reduced values are also termed allowables. The maximum stress failure criterion can be expressed as:

$$\begin{aligned} \sigma_x &< X^t \text{ or } X^c \text{ depending on whether } \sigma_x \text{ is tensile or compressive} \\ \sigma_y &< Y^t \text{ or } Y^c \text{ depending on whether } \sigma_y \text{ is tensile or compressive} \\ |\tau_{xy}| &< S \end{aligned} \quad (4.1)$$

where σ_x , σ_y , and τ_{xy} are ply stresses in the ply coordinate system (x parallel to fibers and y perpendicular to fibers). Note that the sign of the shear stress is immaterial as its magnitude is compared with the shear allowable S . If all left-hand sides of Equation (4.1) are less than the right-hand sides there is no failure. Failure occurs as soon as one (or more) of the left-hand sides equals the right-hand side. The failure mode is the one for which Equation (4.1) is met. For example, if σ_x is compressive and the first of Equations (4.1) is met, then the failure mode is compressive failure along the fibers.

4.2 Maximum Strain Failure Theory

In a manner analogous to the maximum stress failure theory, the maximum strain failure criterion can be stated as:

$$\begin{aligned} \varepsilon_x < \varepsilon_{xu}^t \text{ or } \varepsilon_{xu}^c &\quad \text{depending on whether } \varepsilon_x \text{ is tensile or compressive} \\ \varepsilon_y < \varepsilon_{yu}^t \text{ or } \varepsilon_{yu}^c &\quad \text{depending on whether } \varepsilon_y \text{ is tensile or compressive} \end{aligned} \quad (4.2)$$

$$|\gamma_{xy}| < \gamma_{xyu}$$

where ε_x , ε_y , and γ_{xy} are ply strains in the ply coordinate system (x parallel to fibers and y perpendicular to fibers). Also, ε_{xu}^t , ε_{xu}^c , ε_{yu}^t , ε_{yu}^c , and γ_{xyu} are allowable strains in the corresponding direction and loading (tensile or compressive). Note that the sign of the shear strain is immaterial as its magnitude is compared to the shear allowable γ_{xyu} . If all left-hand sides of Equation (4.2) are less than the right-hand sides there is no failure. Failure occurs, in a specific failure mode, as soon as one (or more) of the left-hand sides equals the right-hand side.

4.3 Tsai–Hill Failure Theory

In the two previous failure criteria, each stress or strain is individually compared with its respective allowable. In general, however, stresses (or strains) may interact with each other and lead to failure, even if each compared individually with its respective allowable suggests that there is no failure. Hill [4] was among the first to propose a combined failure criterion for composite materials. For a single ply under plane stress, with ply axes xy as shown in Figure 4.1, the criterion has the form:

$$F_x \sigma_x^2 + F_y \sigma_y^2 + F_{xy} \sigma_x \sigma_y + F_s \tau_{xy}^2 = 1 \quad (4.3)$$

The form of Equation (4.3) is exactly analogous to the von Mises yield criterion in isotropic materials:

$$\frac{\sigma_x^2}{\sigma_{yield}^2} + \frac{\sigma_y^2}{\sigma_{yield}^2} - \frac{\sigma_x \sigma_y}{\sigma_{yield}^2} + \frac{3\tau_{xy}^2}{\sigma_{yield}^2} = 1 \quad (4.4)$$

with σ_{yield} the yield stress of the material. In fact, Equation (4.3) was proposed by Hill (for a three-dimensional state of stress) as a model of yielding in anisotropic materials. For composite materials, where the concept of macroscopic yielding (at the laminate or the ply level) is not really valid, failure replaces yielding.

Equation (4.3) recognizes the fact that the failure strengths of a composite ply are different in different directions. Tsai [5] determined the stress coefficients in Equation (4.3) by considering three simple loading situations: (a) only σ_x acts on a ply with corresponding strength X ; (b) only σ_y acts with corresponding strength Y ; and (c) only τ_{xy} acts with corresponding strength S . For example, if only σ_x acts, Equation (4.3) reads:

$$F_x \sigma_x^2 = 1 \quad (4.5)$$

It is also known that if only σ_x acts, which is parallel to the fibers, failure will occur when σ_x equals X or

$$\sigma_x^2 = X^2 \quad (4.6)$$

Comparing Equations (4.5) and (4.6) it can be seen that:

$$F_x = \frac{1}{X^2} \quad (4.7)$$

Considering the remaining two load cases would give another two conditions to determine two of the three remaining unknowns F_y , F_{xy} , and F_s . One more condition is obtained by considering the original three-dimensional form of the Hill yield criterion [4] in which F_x, F_y , and F_{xy} are interdependent through distortional deformations of a representative volume of material. This gives one additional equation. The final form of the Tsai–Hill failure criterion is:

$$\frac{\sigma_x^2}{X^2} - \frac{\sigma_x \sigma_y}{X^2} + \frac{\sigma_y^2}{Y^2} + \frac{\tau_{xy}^2}{S^2} = 1 \quad (4.8)$$

4.4 Tsai–Wu Failure Theory

The Tsai–Wu failure criterion [6] was a result of an attempt to mathematically generalize the Tsai–Hill failure criterion creating a curve fit based on tensor theory and accounting for the fact that composites have different strengths in tension and compression. This means that the Tsai–Wu failure theory is not entirely based on physical phenomena, but includes a curve-fitting aspect. In fact, one of the unknown coefficients in the criterion is obtained by requiring that the von Mises yield criterion be recovered if the material were isotropic. As was mentioned in the previous section, yielding and, more so, distortional energy theory on which the von Mises criterion is based, are not applicable to composites so the Tsai–Wu criterion should be viewed as a convenient (and useful) curve fit more than a physics-based model of failure. The form of the criterion is:

$$\frac{\sigma_y^2}{X^t X^c} + \frac{\sigma_y^2}{Y^t Y^c} - \sqrt{\frac{1}{X^t X^c} \frac{1}{Y^t Y^c}} \sigma_x \sigma_y + \left(\frac{1}{X^t} - \frac{1}{X^c} \right) \sigma_x + \left(\frac{1}{Y^t} - \frac{1}{Y^c} \right) \sigma_y + \frac{\tau_{xy}^2}{S^2} = 1 \quad (4.9)$$

Note that tensile and compressive strengths are input as positive values (magnitudes) in the above equation. With the exception of biaxial compression situations where the predictions are, at best, unrealistic, the Tsai–Wu criterion gives predictions that range from acceptable to excellent when compared with test results.

4.5 Other Failure Theories

In the discussion of some of the failure criteria presented in the previous sections some of the shortfalls of these failure theories were mentioned. Many attempts have been made in the past to propose improved failure criteria [7–9] that do not suffer from the shortfalls mentioned and are in closer agreement with experimental results. This is still an open subject of research and the sometimes heated discussion [10, 11] has yet to reach definitive conclusions.

One of the major problems of interaction failure criteria such as the Tsai–Wu and Tsai–Hill is the physical meaning of interaction terms (in addition to difficulty of experimentally obtaining them). Related to that, but more generic as a problem of some of the failure criteria already presented, is the smearing of properties and treating each ply as homogeneous with single values to represent failure strengths in different directions [10]. Failure theories [12] that account for the individual failure modes of fiber and matrix are more promising in that respect. Specifically, the Hashin–Rotem failure criterion has the form [12]:

$$\left. \begin{array}{l} \frac{\sigma_x}{X^t} = 1 \quad \text{when } \sigma_x \text{ is tensile} \\ \frac{\sigma_x}{X^c} = 1 \quad \text{when } \sigma_x \text{ is compressive} \\ \\ \frac{\sigma_y^2}{(Y^t)^2} + \frac{\tau_{xy}^2}{S^2} = 1 \quad \text{when } \sigma_y \text{ is tensile} \\ \frac{\sigma_y^2}{(Y^c)^2} + \frac{\tau_{xy}^2}{S^2} = 1 \quad \text{when } \sigma_y \text{ is compressive} \end{array} \right\} \begin{array}{l} \text{fiber failure} \\ \text{matrix failure} \end{array} \quad (4.10)$$

More recently (see for example [13]), failure criteria based on micromechanics analysis of the composite constituents under different loading situations have emerged and appear to be the most promising, but at a significant increase in complexity and computational cost.

In view of the difficulties of failure theories to accurately predict first-ply failure, extending to subsequent ply failure and final laminate collapse is even harder. In fact, other than disregarding very early failures of plies with fibers transverse to the main tensile load in a laminate, there is no reliable method for performing post-first-ply failure analysis other than the approach by Dávila *et al.* [13] implemented in a finite element environment. Several attempts have been made [14, 15] with varying degrees of success.

In the general case where a laminate is under a three-dimensional state of stress, modified criteria accounting for out-of-plane stresses and their interaction with in-plane stresses have to be used, or, in some cases, individual criteria for in-plane and out-of-plane loads are used [16].

Which failure criterion or criteria will be used in a specific application is very much a matter of preference, available resources, and test data. The simpler failure criteria such as maximum strain or Tsai–Hill and Tsai–Wu (despite their shortcomings) can be very useful for preliminary design if supported by test data covering the load situations of interest. In other cases, emphasis is placed on test data, and laminate strength is obtained from test rather than failure criteria. In what follows in this book, wherever laminate strength is needed (for example for crippling calculations in Section 8.5) it is assumed that the reader will use whichever method to predict laminate strength that he/she considers more reliable and accurate.

References

1. Williams, J.G., Fracture Mechanics of Composites Failure, *Proceedings of the Institution of Mechanical Engineers C: Journal of Mechanical Engineering Sciences*, **204**, 209–218 (1990).

2. Gotsis, P.K., Chamis, C. and Minnetyan, L., Prediction of Composite Laminate Fracture Micromechanics and Progressive Failure, *Composites Science and Technology*, **58**, 1137–1149 (1998).
3. Aboudi, J., Micromechanical Analysis of the Strength of Unidirectional Fiber Composites, *Composites Science and Technology*, **33**, 79–46 (1988).
4. Hill, R., *The Mathematical Theory of Plasticity*, Oxford University Press, London, 1950.
5. Tsai, S.W. *Strength Theories of Filamentary Structures*, in *Fundamental Aspects of Fiber Reinforced Plastic Composites*, Wiley, New York, 1968, pp 3–11.
6. Tsai, S.W. and Wu, E.M., A General Theory of Strength for Anisotropic Materials, *Journal of Composite Materials*, 1971, 58–80.
7. Nahas, M.N., Survey of Failure and Post-Failure Theories of Laminated Fiber-Reinforced Composites, *Journal of Composites Technology and Research*, **8**, 138–153 (1986).
8. Quinn, B.J. and Sun, C.T., A Critical Evaluation of Failure Analysis Methods for Composite Laminates, *Proc. 10th DoD/NASA/FAA Conf. on Fibrous Composites in Structural Design*, vol. V, 1994, pp V21–V37.
9. Hart-Smith, L.J., A Re-examination of the Analysis of In-plane Matrix Failures in Fibrous Composite Laminates, *Composites Science and Technology*, **56**, 107–121 (1996).
10. Hart-Smith, L.J., The role of biaxial stresses in discriminating between meaningful and illusory composite failure theories, *Composite Structures*, **25** (1993) 3–20.
11. Hart-Smith, L.J., An inherent fallacy in composite interaction failure criteria, *Composites*, **24** (1993) 523–524.
12. Hashin, Z. and Rotem, A., A Fatigue Failure Criterion for Fiber Reinforced Materials, *Journal of Composite Materials*, **7**, 448–464 (1973).
13. Dávila, C., Camanho, P.P. and Rose, C.A., Failure Criteria for FRP Laminates, *Journal of Composite Materials*, **39**, 323–345 (2005).
14. Nuismer, R.J., Continuum Modeling of Damage Accumulation and Ultimate Failure in Fiber Reinforced Laminated Composite Materials, *Research Workshop, Mechanics of Composite Materials*, Duke University, Durham NC, 1978, pp 55–77.
15. Reddy, Y.S. and Reddy, J.N., Three-Dimensional Finite Element Progressive Failure Analysis of Composite Laminates Under Axial Extension, *Journal of Composites Technology and Research*, **15**, 73–87 (1993).
16. Brewer, J.C. and Lagace, P.A., Quadratic Stress Criterion for Initiation of Delamination, *Journal of Composite Materials*, **22**, 1141–1155 (1988).

5

Composite Structural Components and Mathematical Formulation

5.1 Overview of Composite Airframe

A section of a fuselage structure, showing some of the typical parts that make it up, is shown in Figure 5.1. Similar part types are used to make up a wing structure.

The types of parts that make up an airframe (fuselage and/or wing) are the same for metal and composite structure. In fact, it is possible to replace, part for part, an aluminum airframe by an equivalent composite airframe. This would typically be a skin-stiffened built-up structure with fasteners connecting the different parts. In general, such a one-for-one replacement does not make full use of composite capabilities and results in minor weight reductions (<15%) with relatively high fabrication cost because the different parts are made separately and assembled together with fasteners. Such a construction, especially when the skin layup is quasi-isotropic is referred to as ‘black aluminum’ to emphasize the fact that the design imitates or closely matches the aluminum design, and little or no attempt is made to use composites to their fullest potential.

Each part or component in an airframe structure serves a specific purpose (or, sometimes, multiple purposes) so that the ensemble is as efficient as possible. Efficiency typically refers to the lowest weight, given a set of applied loads, but it can be any combination of desired attributes such as weight, cost, natural frequency, etc. With reference to Figure 5.1, the parts used in a composite (also metal) airframe can be broken into the part families or types shown in Table 5.1. Note that a less detailed breakdown was given in chapter 2, Table 2.1 for the purposes of the cost discussion.

Each part must be designed so that it does not fail under the applied loads and it meets all other design requirements (see Section 5.1.1). Usually, the main objective is to keep the weight as low as possible but, as already mentioned, additional objectives such as minimum cost (see Chapter 2) are also incorporated in the design process.

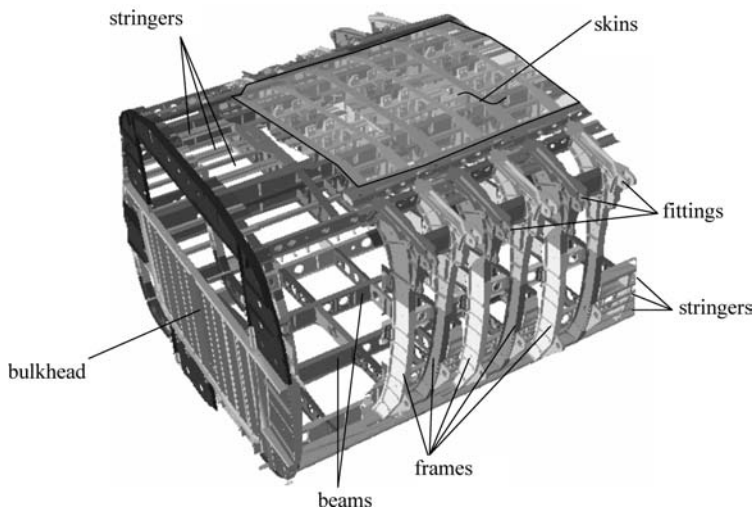


Figure 5.1 Typical fuselage part break-down

5.1.1 The Structural Design Process: The Analyst's Perspective

The objective of the structural design process is to create a structure that meets specific requirements and has certain desirable attributes. The typical design requirements can be summarized into: (1) fit, form, and function; (2) applied loads; (3) corrosion resistance and

Table 5.1 Part families in a composite airframe

Part family	Description	Usage	
Skins	Two-dimensional thin structures covering the outside of fuselage or wing; usually single curvature	Fuselage	Wing
Stringers, stiffeners, panel breakers	One dimensional beam-like structures	Fuselage	Wing
Frames, bulkheads	Two-dimensional ring-like structures at specific intervals along fuselage	Fuselage	
Beams	Two-dimensional plate-like structures	Fuselage	Wing
Spars	Two-dimensional plate-like structures along the length of wing		Wing
Ribs	Two dimensional plate-like structures at specific intervals along wingspan		Wing
Intercostals	Two-dimensional plate-like structures acting as supports	Fuselage	
Fittings	Three-dimensional structures connecting adjacent parts	Fuselage	Wing
Decks, floors	Two-dimensional flat structures	Fuselage	
Doors, fairings	Two-dimensional structures usually with compound curvature	Fuselage	Wing

resistance to fluids; (4) thermal expansion coefficient placement; (5) frequency placement. Briefly, each of these is discussed below.

Fit, form, and function. The structure to be designed must fit within the allowable envelope, i.e. avoid interference with adjacent structure, must have the appropriate material and generic shape so it performs optimally and must perform the assigned function without flaws. The latter includes providing attachment points for other structure as needed and access (through-paths for example) for intersecting parts such as electrical and hydraulic equipment or ducts.

Applied loads. The structure to be designed must not fail under the applied static loads and must have the desired life under the applied fatigue loads. In addition, the structure must be able to withstand certain static and fatigue loads in the presence of damage without jeopardizing the operation of the remainder of the structure (e.g. if the structure is damaged and load is transferred to the adjacent structure the adjacent structure should still be able to perform without failure).

Corrosion resistance, resistance to fluids (jet fuel, etc). Exposure to water vapors or water or other fluids such as fuel and hydraulic fluids is unavoidable during the service life of many parts. The amount of corrosion and/or the associated reduction of strength or stiffness must be minimized.

Thermal expansion coefficient placement. Airframe structures are exposed to wide variations in ambient temperature, either due to their location on the airframe (e.g. parts near the exhaust of an engine) or due to the environment (e.g. satellites). Such structures must be designed to have low thermal expansion coefficients so that any deformations resulting from temperature changes do not compromise the performance of the structure and do not lead to premature failure.

Frequency placement. Airframe structures operate in a vibration environment with specific driving frequencies (from the engines) or random vibrations (gusts, etc). The natural frequencies of the main structural modes such as the first few bending and torsional modes must be sufficiently far from the driving frequencies to avoid large deflections and premature failure.

Depending on the application, some or all of these design requirements must be met. In some cases additional requirements may be imposed. What makes the problem more challenging is that these requirements must be met while specific desirable attributes are also achieved. The most common desirable attributes are: (1) minimum weight; (2) minimum cost; (3) low maintenance; (4) replaceability across assemblies, etc. These are discussed briefly below.

Minimum weight. Minimizing the structural weight increases the amount of payload or weight of fuel that can be carried (for a given gross weight). Or, if the weight reduction is not translated to payload or fuel increase, it translates to overall size reductions (engines are smaller, wings are smaller, etc.), which, in turn, reduces fuel consumption and acquisition and maintenance cost.

Minimum cost. This can be: (a) the recurring fabrication cost (labor and materials to build each part or aircraft); (b) the nonrecurring cost which is the cost incurred once in each program and includes development/research cost, tooling cost, cost for testing and certification, cost for developing drawings and doing analysis, etc.; (c) acquisition cost (cost incurred by the customer in purchasing the part or aircraft); (d) operating cost, etc. See also Chapter 2 for a brief discussion on cost of composite airframe structures.

Low maintenance. This is related to the minimum cost described above, but merits special mention. Over the long life of an aircraft, maintenance cost (including inspection, disposition

of problems found and associated repair) can become a very significant portion of the life-cycle cost of the aircraft. Designing structure that minimizes this cost is very desirable and attractive to customers.

Replaceability across assemblies. This is also (indirectly) related to the cost and low maintenance items mentioned earlier. Depending on the part geometry, adjacent structure, and fabrication and assembly methods selected, the accuracy of the part geometry and how closely it mates with adjacent structure can vary widely, to the point that exchanging nominally the same parts between two different assemblies can be almost impossible without significant rework to eliminate interferences or fill in gaps (shimming). If, however, the design and fabrication process yield parts of acceptable cost and high accuracy, then replacing a part will only require simple disassembly of the part to be replaced and assembly of the replacement part. This drastically reduces repair and maintenance costs and minimizes turn-around times so that aircraft grounded for inspection and repairs can be returned to service very quickly.

The design process applied to a specific geometry is shown schematically in Figure 5.2.

Given the applied loads and the available space (the shaded area on the left of Figure 5.2), the structural analyst/designer has to come up with a shape that fits the given space, provides hard points for load applications and attachments, and includes cutouts for any equipment that passes through. Some of the cutouts may be included as ‘lightening holes’ to reduce weight. In addition, the designer uses local reinforcements, doublers or flanges, around the cutouts and the attachment points for better load transfer across the part and for increased stability. The geometry (thicknesses, widths, heights, etc.) are selected so that the weight is minimized (for most cases minimum weight is one of the desirable attributes). This results in the structure shown on the right of the figure.

In terms of the sequence of steps and decision flow, the design process can be summarized in the chart of Figure 5.3. The analyst obtains the applied loads and local design requirements and uses the available materials to select the preliminary design. Use of simple analysis methods and experience (if available) with similar parts in the past firms up the geometry, and this becomes the structural configuration. The structural configuration is a combination of geometry, material, and fabrication process. Typically, at this point the requirements are met or are close to being met (for example the applied loads may cause failure, but the reserve factor is close to 1). A series of iterations, as shown by the loops in Figure 5.3, follows in order to fine-tune the design. They consist of more detailed analysis to minimize the weight (or meet other desirable attributes) without failing under the applied loads and, if needed, fabrication or producibility trials to verify that the design is manufacturable at acceptable cost. Tests may also

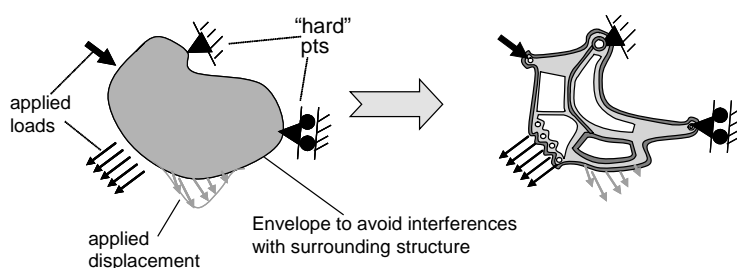


Figure 5.2 Designing a part to meet specific requirements

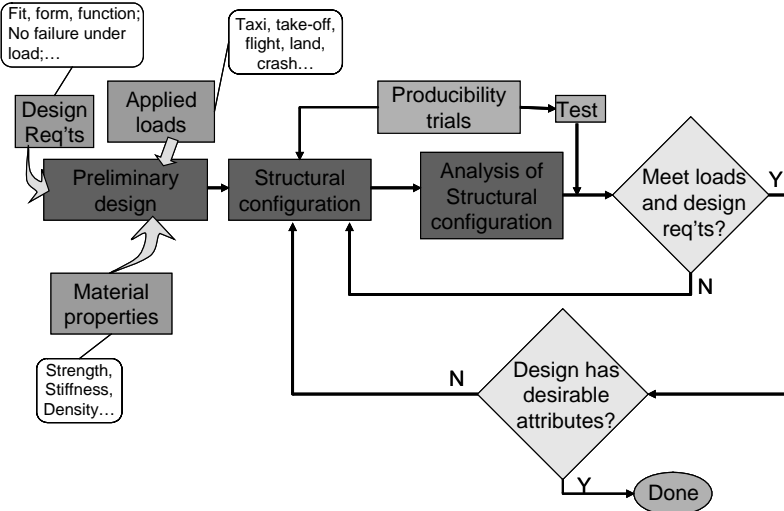


Figure 5.3 Simplified flow diagram of the design/structural analysis process

be used to verify the analysis predictions and to check that there are no issues that were not satisfactorily addressed by the design process.

At this point it is worthwhile to go through some order of magnitude calculations to see what this process implies in terms of time required. A typical aircraft is designed for a series of flight maneuvers (takeoff, climb, turn, approach, land, etc) and taxi maneuvers. These are done for a variety of speeds, accelerations, load factors, etc. and correspond to a large number of static and fatigue load combinations for which each part of the aircraft must be designed. In addition, there are crash load cases that must be included in the design of each part (or at least the parts that see substantial loads during a crash). Nowadays, with the advanced simulation software available and our improved understanding of structural behavior during different maneuvers, the total number of load cases (static and fatigue) that have to be analyzed is of the order of 1000.

Assume now that the structural analyst has, on average, three design concepts to consider for each part to be designed. For example, for a skin structure, the three design concepts can be: (a) stiffened panel; (b) sandwich panel; and (c) isogrid panel as shown in Figure 5.4a. Also assume that for each of the three design concepts there are, on the average, three fabrication processes/material combinations. For the case of the stiffened panel for example, these could be co-cured, fastened, or bonded as shown in Figure 5.4b. Note that all these options, so far, assume one choice of layup for each of the components.

In order to determine the optimum solution, i.e. the solution that meets the design requirements and optimizes the desired attribute(s) such as weight, cost, etc., a certain optimization algorithm must be used. Genetic algorithms are one of the most effective optimization schemes because they are very efficient in dealing with discontinuous variables such as the laminate thickness and multiple optima [1]. A genetic algorithm optimization scheme works by generating a certain number of designs during each iteration (or generation) and evaluating each design against the constraints and objective function. This evaluation

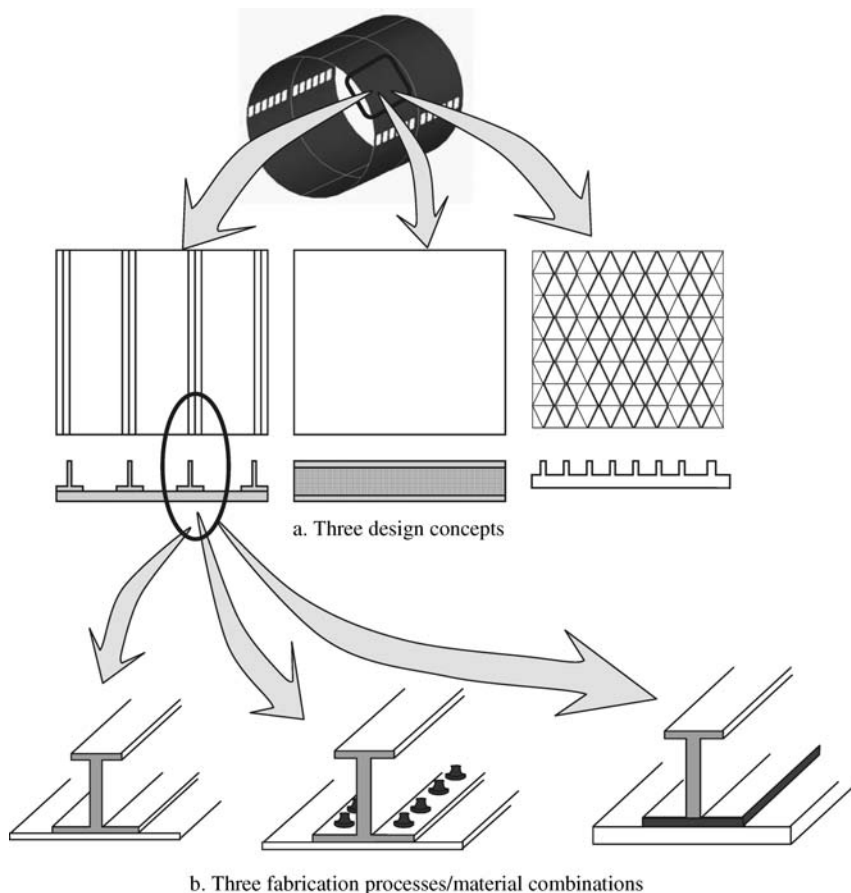


Figure 5.4 Options to be considered during design/analysis of a part (See Plate 13 for the colour figure)

implies detailed analysis of each design to determine if it meets the applied loads. The worst performers are eliminated from the design pool while the best performers are recombined to create new designs for the next generation. Typically, to converge to an optimum solution a genetic algorithm will need approximately 1000 iterations (or generations) with approximately 15 designs per generation. With these assumptions, the number of analyses needed to optimize a single part is of the order of:

$$\begin{aligned}
 & 1000 \text{ (load cases or maneuvers)} \times 3 \text{ design concepts} \times 3 \text{ process/material} \\
 & \text{combinations per concept} \times 1000 \text{ generations} \times 15 \text{ designs analyzed per generation} \\
 & = 135 \text{ million analyses!}
 \end{aligned}$$

Of course there are shortcuts one can use by eliminating less critical load cases for example, but if one considers: (a) additional analyses that are needed for convergence checks if the finite element method is used for each analysis; (b) load redistribution runs to account for the fact that

as the design changes load transfer through the part and around it changes and thus the applied loads change; and (c) applied load changes (mostly increases) that invariably occur during the design effort, the above estimate of 135 million analyses is probably representative of what would be needed.

Clearly, this number of analyses for each part to be designed is prohibitive if the analysis method is time consuming such as the finite element or finite difference method. For example, to finish 135 million analyses in one year working for 365 days 24 hours per day one would have to complete more than 4 analyses per second. In practice the number of analyses is reduced by reducing the design concepts and process/material combinations per part, and limiting the number of parts to be optimized to a subset of the entire structure. But this, in turn, means that the structure is by necessity suboptimal since not all options are considered nor are all parts optimized. Even with those shortcuts, the number of finite element or finite difference analyses required is still prohibitive.

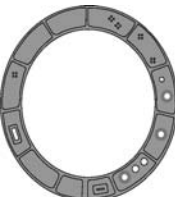
Therefore, until the computation time for the more accurate analysis methods such as finite elements improves by at least a factor of 50, extensive optimization of large quantities of parts or assemblies is not economically feasible. For this reason, simpler, reasonably accurate, and much faster methods of analysis are necessary. In the following chapters, some of these simpler analysis methods are presented. In general, they lend themselves to automation and can be combined with efficient optimization schemes to optimize large quantities of parts. However, it is important to note, and it will be stressed time and again throughout this text, that in order to simplify the analysis approximations have to be made which lead to results that are not as accurate as more detailed methods would generate and do not apply to all cases. If used judiciously, they can help hone in on the final design (or close to it) in terms of finalizing process, material, design concept, and most of the geometry so that more detailed (and more time consuming) methods need only be used once (or few times) per part to firm up the final design.

5.1.2 Basic Design Concept and Process/Material Considerations for Aircraft Parts

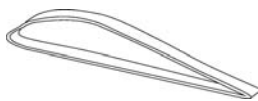
This section gives some of the top-level alternatives a designer/analyst has to consider when designing a composite part. This is summarized in Table 5.2 and is by no means an exhaustive discussion, but helps in understanding the process one has to go through before even analyzing a part. The relation of some of these decisions to the analysis methodology that must be done is highlighted. The different types of analysis are only mentioned here and presented in detail in subsequent chapters. The types of parts discussed here follow the listing of Table 5.1.

As shown in Table 5.2, the different options for design concepts for each type of part make it difficult to know *a priori* the optimum configuration for each application and type of loading. At times, a compromise is necessary in order to better blend the structure to be designed with adjacent structure where some geometry, for example the stiffener spacing, is fixed. Also, knowledge of the fabrication options and corresponding process capabilities is necessary in order to fully exploit the potential of a design concept. For example, maintaining fiber continuity in all three directions in a three-dimensional structure such as a fitting may not be possible, thereby creating interfaces where only resin is available to carry loads if fasteners are not used. This is the case in Figure 5.5 where there are no fibers across planes a-a and b-b.

Table 5.2 Design considerations, alternatives, and implications for analysis

Part	Configuration	Alternatives to be considered	Implications for analysis
Skins	Monolithic with stiffeners 	<ul style="list-style-type: none"> • Stiffeners co-cured, fastened, secondarily bonded? • Cutouts molded in or cut afterwards? Reinforced with doublers or flanged? • Reinforcement co-cured, fastened or secondarily bonded? 	Material strength Notched strength ⁽¹⁾ Buckling Delamination
	Sandwich 	<ul style="list-style-type: none"> • Full-depth core everywhere or with rampdown for attachments? • Assembly via co-curing, fastened or secondarily bonded? 	Material strength (facesheet, core, adhesive), notched strength ⁽¹⁾ Buckling Wrinkling (symmetric, antisymmetric) Shear crimping Intracellular buckling Delamination, disbond
Stringers, Stiffeners panel breakers	Cross-sectional shape: L, C, Z, T, I, J, Hat 	<ul style="list-style-type: none"> • Confine buckling pattern between stiffeners (panel breakers)? 	Material strength Notched strength ⁽¹⁾ Column buckling Crippling Skin/stiffener separation Inter-rivet buckling
Frames and bulkheads		<ul style="list-style-type: none"> • Co-cured with skin, fastened or secondarily bonded? • Single piece or multiple pieces? • Cutouts flanged or with doublers? • Cutouts molded-in or cut afterwards? 	Material strength Notched strength Buckling of webs ⁽¹⁾ Crippling of stiffeners or caps Crippling of reinforcements

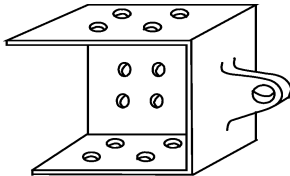
Beams, spars, ribs,
intercostals



- Co-cured with skin, fastened or secondarily bonded?
- Single piece or multiple pieces?
- Cutouts flanged or with doublers?
- Cutouts molded-in or cut afterwards?

Material strength, notched strength⁽¹⁾
Web buckling
Crippling of flanges
Crippling of reinforcements around cutouts

Fittings



- How to mold a 3-D piece with continuous fibers in all directions?

Material strength, notched strength⁽¹⁾
Lug failure⁽²⁾
Bearing failure
Delamination

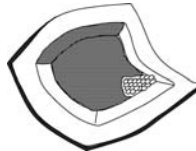
Decks and floors



- Stiffened, grid-stiffened or sandwich?

Material strength, notched strength⁽¹⁾
Stiffened panel failure modes
Sandwich failure modes

Doors and fairings



- Stiffened or sandwich?
- How does compound curvature change fiber orientation locally?

Material strength, notched strength⁽¹⁾
Stiffened panel failure modes
Sandwich failure modes

(1) Notched strength: OHT = open hole tension; OHC = open hole compression; TAI = tension after impact; CAI = compression after impact; SAI = shear after impact

(2) Net section failure, shear-out failure, bearing failure

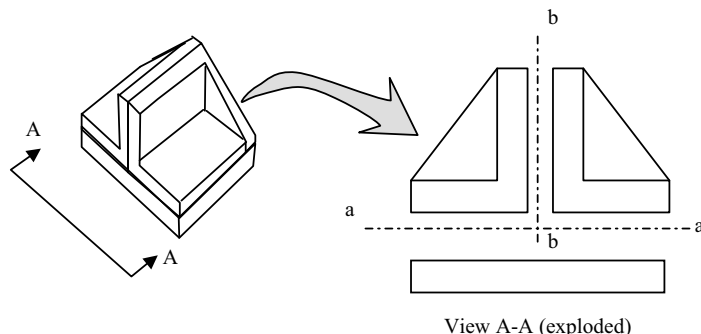


Figure 5.5 Schematic of a three-dimensional connection of parts without fiber continuity in all primary load directions

As summarized in Table 5.2, apart from the basic strength and notched strength failure modes, different parts may have different failure modes that must be analyzed separately. It is important to note that if these failure modes are not anticipated in advance, they cannot be picked up by analysis methods that are not set up to accurately capture them. For example, a finite element method may not pick up failure of a lug if the mesh is not fine enough at the three different locations where net tension, shear-out, or bearing failure may occur (Figure 5.6). Or, without proper mesh size and boundary conditions, long-wave (global) and short-wave (e.g. crippling or wrinkling) buckling modes cannot be accurately quantified.

5.1.3 Sources of Uncertainty: Applied loads, Usage and Material Scatter

It should be recognized that in any large-scale design problem, such as that of an airframe, there are sources of uncertainty. As a result, several input quantities in the design process are not accurately known and the design/analysis process must take these uncertainties into account to make sure that the worst case scenario, however improbable, if it were to occur, would not lead to failure. The three most important sources of uncertainty are: (1) knowledge of applied loads; (2) variability in usage; and (3) material scatter. These are examined briefly below.

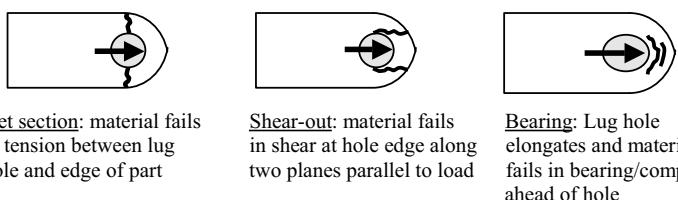


Figure 5.6 Three of the failure modes in a lug

5.1.3.1 Knowledge of Applied Loads

As mentioned in Section 5.1.1 the structure of an aircraft must be designed for a large variety of maneuvers. For each of those maneuvers the externally applied loads (e.g. aerodynamic loads) must be known accurately. However, it is difficult to determine exactly these applied loads because of the complexity of the phenomena involved (e.g. flow separation), the complexity of the structure (e.g. wing–fuselage interaction) and the limitations in computational power available. Typically, some approximations are necessary in the computer simulation and it is not uncommon to introduce safety factors to provide a degree of conservatism in determining the applied loads. This is one of the reasons for the use of the 1.5 multiplicative factor between limit and ultimate load. The structure is not designed to the highest expected load during its service life, which is called the limit load, but to that load multiplied by a safety factor of 1.5, which is the ultimate load.

5.1.3.2 Variability in Usage

Even if the applied loads were accurately known for a certain maneuver, there is uncertainty in practice in performing the maneuver. Nominally the same maneuver (e.g. 3g turn) will have differences in the transient loads exerted on the aircraft from one operator to the next. For this reason, each maneuver is simulated many times while varying different parameters (rate of control action for example) but staying within the parameters defining the maneuver, and the peak load(s) calculated during the simulation are recorded. Then, the loads corresponding to this maneuver are selected so as to cover most loads recorded (for example, the 95th percentile may be selected). This process is shown schematically in Figure 5.7.

Depending on the maneuver, there are, in general more than one load that may be of interest, corresponding to different load types or load directions and different times during the maneuver, such as maximum power, maximum or minimum control stick input, etc. The situation shown in Figure 5.7 is simplified in that it isolates one load type and shows one maximum load of interest, the peak load recorded during the simulation. Each of the peak loads can be plotted in a frequency plot as shown at the bottom of the figure. Standard statistical methods are then used to determine the percentile of interest. Note that the statistical distribution of the peak load is not necessarily a normal distribution and the one shown in Figure 5.7 is just an example.

5.1.3.3 Material Scatter

The strength of the material used in fabricating a specific design is not a single well-defined number. Inherent variability in the microstructure of the material, material variability from one material batch to another, fluctuations in the fabrication method (e.g. curing cycle), variations in geometry within tolerances (e.g. thickness variation within the same specimen) lead to a range of strength values when the same nominal geometry and layup are tested. This variability is shown for typical unidirectional graphite/epoxy in tension and compression in Figure 5.8.

A design must account for this variation and protect against situations where the strength of the material used may be at the low end of the corresponding statistical strength distribution. For this purpose, specific statistically meaningful values are selected that are guaranteed to be

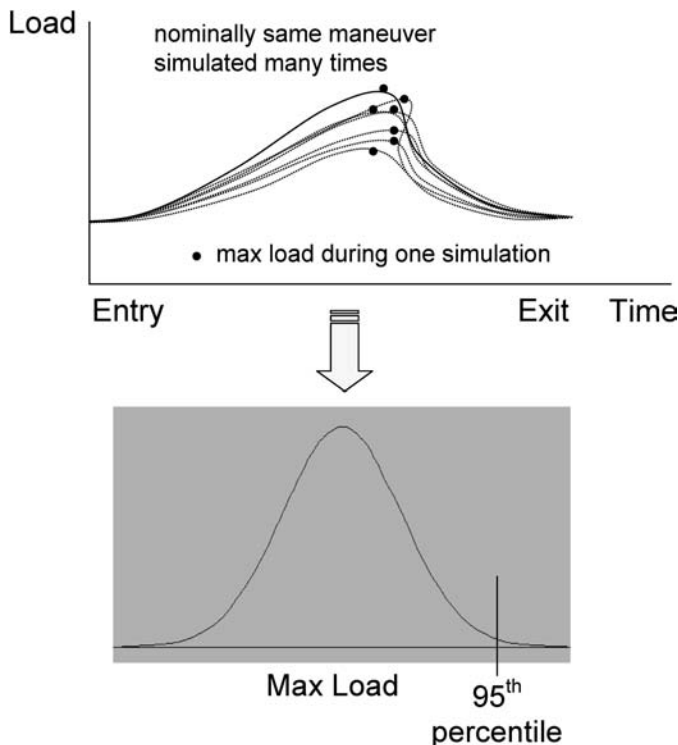


Figure 5.7 Selection of applied load (95th percentile used here as an example) to be used in designing for a specific maneuver

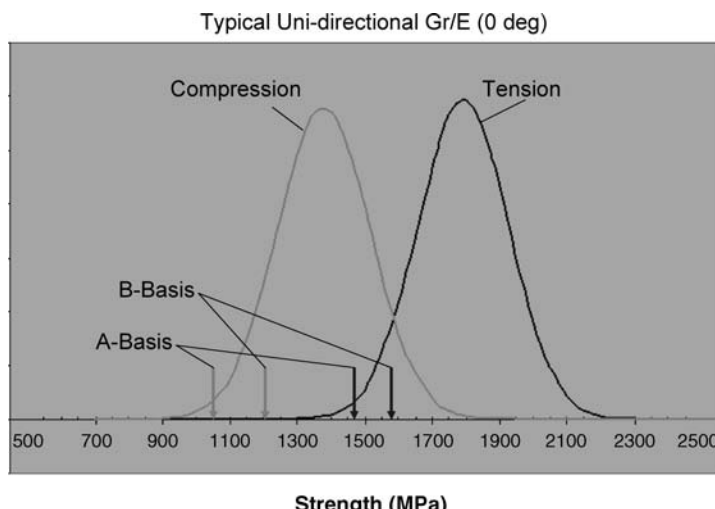


Figure 5.8 Typical ranges for tension and compression strength values for 0° unidirectional graphite/epoxy

lower than most of the strength population. The two most commonly used values are the B-Basis and the A-Basis strength values [2]. The A-Basis value is the one percentile of the population: 99% of the tests performed will have strength greater than or equal to the A-Basis value. The B-Basis value is the tenth percentile of the population: 90% of the tests performed will have strength greater than or equal to the B-Basis value.

In general, the A-Basis value is used with single load path primary structure, where failure may lead to loss of structural integrity of a component. The B-Basis is used with secondary structure or structure with multiple load paths, where loss of one load path does not lead to loss of structural integrity of the component. The A- and B-Basis values are calculated on the basis of statistical methods accounting for batch-to-batch variation, the type of statistical strength distribution, and the number of data points [2, 3].

Stiffness has a similar variability to that of strength. However, one should be careful in using low percentile values for stiffness because they may not represent a conservative scenario. If the material used in a structure has stiffness at the low end of the stiffness statistical distribution, this means that surrounding structure, being stiffer will absorb more load. This would require appropriate adjustment of applied loads and it opens up a series of scenarios that may or may not be realistic. Instead, using the average or mean stiffness everywhere in the structure would not unduly transfer load from one part to its neighbors and is more representative. So stiffness-sensitive calculations such as buckling do not, usually, require the lowest stiffness values (B- or A-Basis) but the mean values.

5.1.4 Environmental Effects

Composites are susceptible to environmental effects. In general, as the temperature and/or the moisture content increase beyond room temperature ambient conditions, the strength and stiffness properties degrade. Also, at temperatures lower than room temperature, most strength properties are also lower than at room temperature. An example for a typical graphite/epoxy material is shown in Figure 5.9.

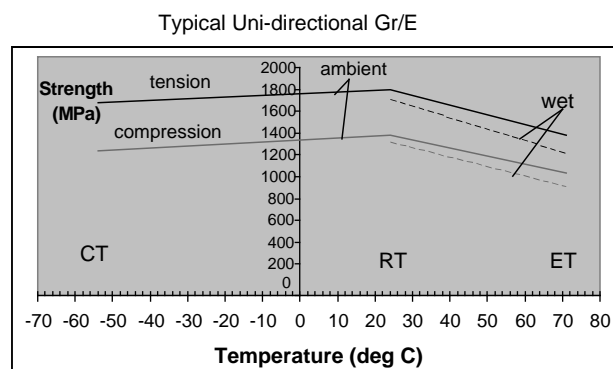


Figure 5.9 Variation of tension and compression strength as a function of temperature and moisture content

Two sets of curves are shown in Figure 5.9. The continuous lines correspond to the ‘dry’ or ambient condition. The exposure of the specimens to moisture has been minimal. The dashed lines correspond to the wet condition where the specimens are fully saturated with moisture. Increasing the moisture level decreases the strength. Increasing the temperature beyond room temperature decreases the strength. Depending on the property and the material, decreasing the temperature below room temperature may increase or decrease the strength. Typically, a decrease is observed, as shown in Figure 5.9.

Given the type of behavior shown in Figure 5.9, complete characterization of a material would require knowledge of its properties over the entire range of anticipated temperature and moisture environments during service. In general this is accomplished by doing tests at representative conditions that identify extreme points of the trends and interpolating in between. The number of such key conditions depends on material loading and application (e.g. civilian versus military application). The minimum number is three. These are: (1) the cold temperature (CT in Figure 5.9) condition (usually CTA for cold temperature ambient); (2) the room temperature (RT) condition which is split into RTA, the room temperature ambient, and RTW, the room temperature wet condition where the specimens are fully saturated; and (3) the elevated temperature (ET) condition which is split into ETA (elevated temperature ambient) and ETW (elevated temperature wet) condition.

For design purposes, the most conservative strength properties across all conditions are used. It is important to keep in mind, however, that when trying to match specific test results, the properties corresponding to the test environment and material condition at the time during test should be used. Stiffness also shows a similar sensitivity to environment, and it is customary to perform preliminary design using the lowest stiffness across environments.

5.1.5 Effect of Damage

Composites exhibit notch sensitivity. A notch can be any form of damage, such as impact or crack or cutout. The strength in the presence of damage is significantly lower and varies with the damage size and type. Typical trends of compression strength in the presence of damage are shown in Figure 5.10, adjusted from reference [4].

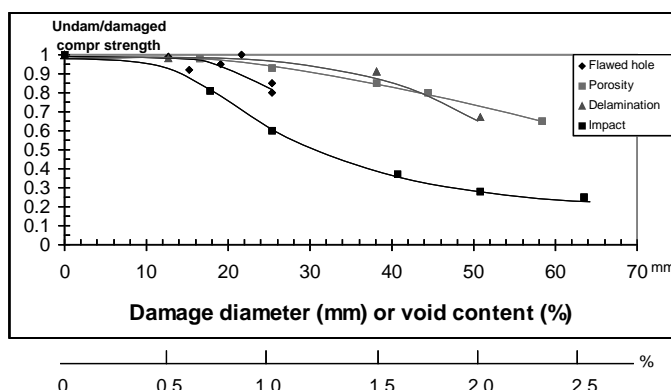


Figure 5.10 Sensitivity of compression strength of composites to various types of damage

While the trends shown in Figure 5.10 are representative of the behavior of most composites, the specific values shown are only applicable to specific layups and materials. For other materials and/or layups, specific analysis supported by tests must be carried out for each type of damage in order to accurately quantify the residual strength in the presence of damage.

The types of damage shown in Figure 5.10 are the most common types encountered in practice. Of those, the most critical is impact damage. Impact damage is caused by a large variety of sources, ranging from tool drops and foot traffic to impact with large objects (e.g. luggage) and hail damage.

This strength reduction in the presence of damage must be taken into account in the design process. The approach is dependent on the inspection method used and its reliability. First, the type and size of damage or flaw that the chosen inspection method can find consistently and reliably must be determined. Then, the threshold of detectability is defined as the damage size above which all damage can be found by the inspection method with a certain confidence (e.g. 99% of the time). This threshold of detectability divides the damage that may occur during manufacturing or service in two categories: (a) nondetectable damage; and (b) detectable damage. These are then tied to specific load levels the structure must withstand. As already mentioned in Section 5.1.3 the two main load levels of interest in structural design of airframe structures are the limit and ultimate load. The limit load is the highest load the structure is ever expected to encounter during service. The ultimate load is the limit load multiplied by 1.5.

A structure with damage below the threshold of detectability of the selected inspection method must be capable of withstanding ultimate load without failure. A structure with damage above the threshold of detectability level of the selected inspection method must be capable of withstanding limit load without failure.

In practice, the most common inspection method used is visual inspection. This is because it combines low cost with ease of implementation. This does not mean that more accurate and more reliable inspection techniques such as ultrasound, X-rays, etc. are not used at different times in the life of an aircraft. Usually, however, these methods are applied during planned detailed inspections at the depot level where an aircraft is taken out of service and specially trained personnel with appropriate equipment conduct a thorough inspection of the structure. On a more regular basis, the structure is inspected visually.

With visual inspection the preferred method of inspection during service today, the structural requirements in the presence of damage become:

- structure with damage up to barely visible impact damage (BVID) must withstand ultimate load without failure
- structure with damage greater than BVID, i.e. structure with visible damage (VD) must withstand limit load without failure

The VD is usually defined as damage that is clearly visible from a distance of 1.5 meters under ambient light conditions. Then BVID is damage just below the VD. It is recognized that the definition of BVID is subjective and dependent on the inspector and his/her experience level. For this reason attempts to more accurately define BVID have been made by tying the BVID to a specific indentation size. Usually, 1 mm deep indentation is considered to correspond to BVID.

It should be emphasized that besides limit and ultimate load, other load levels may be used in practice, albeit less frequently. One example is the ‘safe return to base load’, which is usually a

fraction of the limit load (typically 80%) and limits the structure to loads that will not cause catastrophic failure in the presence of larger damage levels such as those caused by bird or lightning strike, etc.

In view of the experimentally measured strength reductions shown in Figure 5.10, the design/analysis process must use analytical methods that allow determination of the reduced strength in the presence of various types of damage. Usually, a conservative approach is selected and the structure is designed for the worst type of damage (impact) since this will cover all other cases. Due to the complexity of the analysis for determining the amount of damage caused by a specific threat and the subsequent complexity of the analysis for determining the strength of the structure in the presence of damage, simplified methods are commonly used for preliminary design [5–11].

A conservative approach is usually followed that avoids computationally intensive analysis methods that model damage creation and its evolution under load. The method consists of designing the structure to meet (a) limit load in the presence of a 6 mm diameter hole (VD) and (b) ultimate load in the presence of low-speed impact damage (BVID). It is important to note, however, that this approach has its limitations because it is not applicable to all threat scenarios. For example, it can be extremely conservative in cases of thick composite structures. The typical damage scenarios based on common threats during manufacturing and service should not include a 6 mm through hole for example because it is a very unlikely event. Designing for damage must be done with care on a case-by-case basis after careful examination of threats and requirements. And, most importantly, it should be supported by tests that verify the analysis method and its applicability to the loading, layups, and configurations under consideration.

5.1.6 Design Values and Allowables

The discussion in Sections 5.1.3–5.1.55.2.4 indicated that the strength of a composite structure takes a range of values as a result of material variability, environmental effects, and sensitivity to damage. As a result, the strength value used in a design must be such that if the ‘worst of all situations’ is combined in service, the resulting structure will still meet the load requirements without failure. The ‘worst of all situations’ combines material at the low end of the strength distribution (Figure 5.8) operating at the worst environment (Figure 5.9) with the worst type of damage present (Figure 5.10). Therefore, sufficiently conservative strength values must be used. A procedure that leads to such design values for strength is shown schematically in Figure 5.11.

The mean RTA strength at the far right of the figure is reduced by a ‘knockdown’ factor representing the worst environment for the loading and material selected. This is further reduced by another factor that represents the worst type of damage (usually impact damage). This value is treated as the mean with the effect of damage and environment already included. Around this mean value the statistical distribution representing the material scatter for the property in question (tension, compression, shear, etc.) is created. The design value is determined as a value to the left end of the statistical distribution (e.g. A- or B-Basis value as described in Section 5.1.3), which is expected to be lower than a certain high percentage (90% for B-Basis and 99% for A-Basis) of all test results for the property of interest at the most degrading environment and with the highest permissible amount of damage.

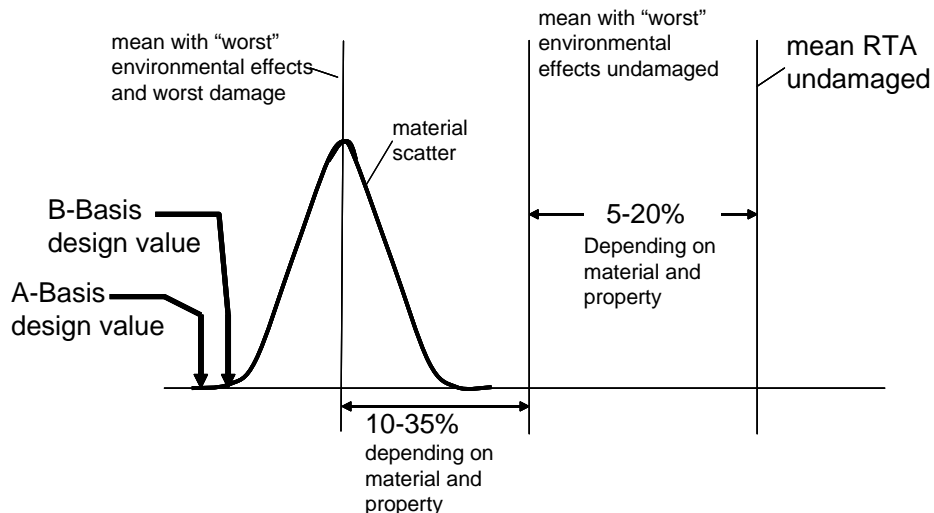


Figure 5.11 Determination of design strength values accounting for effects of damage, environment and material scatter

This approach can be done rigorously by determining the worst type of damage, which usually is BVID, and the worst type of environment, which, usually, is ETW for the strength property of interest. Then, a sufficient number of specimens with this damage is conditioned in that environment and strength tests are carried out. The number of specimens is selected so expected batch-to-batch variation is reproduced and the results give sufficient statistical confidence in the conclusions. Statistical analysis methods [3] are then used to determine the design values which, when they are statistically significant values are called allowables.

To save time and reduce cost during preliminary design it is customary to test a limited number of specimens at various environments to obtain a percentage reduction between mean strengths at various environments. This is done with and without damage to determine the reduction due to the presence of damage at different environments. Finally, a sufficient number of tests (six per batch) from at least three batches in one of the environments gives the material scatter. This gives design values that can be used in preliminary design.

An example follows. Assume that the compression failure strain for undamaged quasi-isotropic layup of a material at RTA environment is 11000 microstrain (μs). And that tests have shown that the environment with the biggest reduction in strength is ETW with a mean failure strain equal to 80% of the RTA mean strain. Also, tests at RTA have shown that the mean failure strain with BVID is 65% of the mean RTA strain. Finally, tests of undamaged specimens at RTA have shown a B-Basis value that is 80% of the mean RTA value (this corresponds to a normal distribution with coefficient of variation, i.e. standard deviation divided by the mean, of about 11%). Following the procedure described above and shown in Figure 5.11, a design value that can be used for preliminary design is

$$\varepsilon_{\text{des}} = \frac{\text{mean RTA}}{0.8} \times \frac{\text{worst envir. (ETW)}}{0.65} \times \frac{\text{BVID effect}}{0.8} = 4576 \mu\text{s} \quad (5.1)$$

mean RTA
 worst envir.
 (ETW)
 BVID effect
 mat'l scatter effect

It should be noted that this corresponds to a B-Basis value with environment and damage effects included and should, therefore, be used in situations where B-Basis is applicable (see Section 5.1.3). It is also of interest that this value of approximately $4500 \mu\text{s}$ is typical of many (first-generation) thermoset materials and layups that do not depart significantly from quasi-isotropic, and has been used widely for preliminary sizing of structure. Of course, once designs are almost finalized and most likely layups have been selected, additional testing for spot-checking the validity of this value and more rigorous statistical analysis are necessary to verify or update this value.

Equation (5.1) demonstrates that the design values for composite materials may be less than half the RTA mean undamaged values. This is an important consideration in anticipating the weight savings that can result from use of composites because the significant reduction in strength offsets a lot of the weight savings one would expect on the basis of density difference alone. A simple comparison between aluminum and graphite/epoxy (Gr/E) composites is shown in Table 5.3. This is a simple comparison to show the relative differences. For aluminum the yield strain is used as the failure strain. The failure stress (yield stress in the case of aluminum) is approximated in Table 5.3 as the product of the Young's modulus times the failure strain. The failure strain and stress for the second Gr/E layup (last column) are approximate.

It can be seen from Table 5.3 that the strength of aluminum can be significantly higher than that of Gr/E. This means that in order to carry the same load with Gr/E, as with aluminum, one has to use higher thickness. For a plate-type application, the weight is calculated as

$$W = \rho t(\text{Area})$$

where ρ is the density, t the thickness and *Area* the planform area of the plate.

If the structure fails exactly when the required applied load is reached, the thickness needed is calculated from

$$\sigma_{fail} = \frac{F_a}{wt} \Rightarrow t = \frac{F_a}{w\sigma_{fail}}$$

where F_a is the applied load, σ_{fail} is the failure strength of the material and w is the width of the cross section over which F_a acts.

Using this expression for the thickness t to substitute in the weight expression,

$$W = \rho \frac{F_a}{w\sigma_{fail}} (\text{Area})$$

Table 5.3 Comparison of compression strength values (aluminum versus Gr/E)

	Aluminum (7075-T6)	Quasi-isotropic Gr/E	Gr/E layup used in compression ⁽¹⁾
Density (kg/m^3)	2777	1611	1611
Young's modulus (GPa)	68.9	48.2	71.7
Compressive (yield) failure strain (μs)	5700	4576	~ 4500
Compressive failure stress (MPa)	392.7	220.8	~ 322.6

(1) [45/-45/0/0/90/0/0/-45/45]

Table 5.4 Weight comparison for plate application based on strength

	Quasi-isotropic design/Al	$[45/-45/0_2/90]_s$ /Al
$\frac{W_{Gr}}{W_{Al}}$	1.03	0.706

Note: The overbar over the 90° ply in the stacking sequence in the third column denotes a ply that does not repeat symmetrically with respect to mid-plane, i.e. 90° is the mid-ply in this case.

Then, the ratio of the weight W_{Gr} of a graphite/epoxy panel to that of aluminum W_{Al} for the same applied load F_a and the same planform area, can be found after some rearranging to be:

$$\frac{W_{Gr}}{W_{Al}} = \frac{\left(\frac{\rho}{\sigma_{fail}}\right)_{Gr}}{\left(\frac{\rho}{\sigma_{fail}}\right)_{Al}}$$

Using the values from Table 5.3 gives the weight ratios in Table 5.4.

As can be seen from Table 5.4, the quasi-isotropic composite design (column 2) is approximately the same weight as the aluminum counterpart, in fact it is 3% heavier. The more tailored $[45/-45/0_2/90]_s$ layup is approximately 30% lighter than the aluminum counterpart. This case serves as an example that shows the advantages of tailoring designs for maximum use of composite capabilities instead of using quasi-isotropic layups that lead to so-called ‘black aluminum’ designs.

5.1.7 Additional Considerations of the Design Process

The analysis methods used are always a tradeoff between accuracy and cost and ease of use. In a preliminary design stage where many candidate designs must be traded quickly, especially if formal optimization is introduced early in the design process, using conservative ‘reasonably accurate’ methods is preferred over very accurate computationally intensive approaches. This allows the examination of many more options than would not be possible with more detailed methods. The term ‘reasonably accurate’ is, of course, subjective and, usually, is tied to how conservative one can afford to be before the design weight starts increasing beyond acceptable levels. Often, approximate analytical methods are modified based on test results, and adjusted accordingly to give accurate predictions over a limited range of applicability. In addition, test methods are often used to circumvent problems with analytical modeling of structural details present in the structure, the detailed modeling of which would make the entire analysis very expensive. Two such examples are: (a) modeling of fasteners in bolted structures; and (b) knowing the exact type of boundary conditions provided by the edge supports or intermediate structure present.

Typical airframe structures have a large variety of failure modes. Which failure mode starts failure and which one eventually leads to catastrophic failure of the structure is a function of the material, layup, and geometry used. Changing any of these can alter the failure mode scenario.

One example is sandwich structure where each of the skins may fail in: (1) material strength, (2) wrinkling (symmetric or unsymmetric), (3) dimpling or intracellular buckling, (4) shear crimping (precipitated by core failure). In addition, the adhesive connecting core and facesheets may fail in (5) adhesive strength (tension, compression, or shear), or the core itself may fail in (6) core strength (tension, compression, or shear), and finally the entire sandwich may fail in (7) sandwich buckling. And these do not include additional failure modes specific to sandwich rampdown if there is one present. See Chapter 10 for a detailed discussion of sandwich structures.

In general, *a priori* knowledge of the possible failure modes is necessary for a good design. Different failure modes may interact, which makes their analytical simulation without the use of extensive very detailed analysis tools, such as finite elements, very difficult. This is a case where tests are used to adjust the simpler analysis methods or suggest how the existing methods must be modified to more accurately match test results.

The most efficient design is the one that just fails when the applied design load (ultimate or limit depending on the requirement) is reached. Trying to implement this during preliminary design may not be advisable since the analysis methods may not be sufficiently accurate, test results with allowables may not be completed, loads may increase, etc. So there may be a difference between the failure load of the design and the applied load. The relative magnitudes of failure load and applied loads are related through the loading index, the reserve factor, or the margin of safety. All three refer to the same thing in a slightly different way. The loading index is the ratio of the applied load to the failure load. If less than one, there is no failure. The reserve factor is the inverse of the loading index and equals the ratio of the failure load to the applied load. If greater than one it implies the structure does not fail and the applied load must be increased by a factor equal to the reserve factor for failure to occur. Finally, the margin of safety is the reserve factor minus one. Expressed in percent, if it is positive it implies no failure and denotes by what percentage the applied load must be increased to cause failure. If negative, it implies failure and denotes by what percentage the applied load must be decreased to prevent failure. It is customary to maintain positive (but not very high) margins of safety during preliminary design and, later on, as the design is finalized, detailed analysis supported by testing increases confidence in the design, and the applied loads are ‘frozen’, can be driven as close to zero as possible by fine-tuning the design to increase its efficiency.

5.2 Governing Equations

The starting point are the governing equations for a composite plate. These are: (a) the equilibrium equations; (b) the stress–strain equations; and (c) the strain–displacement equations. Versions of the stress–strain and strain–displacement equations have been used already in Sections 3.2 and 3.3. The reader is referred to the literature for detailed derivation of these equations [12–14]. Only the final form of these equations is given here.

5.2.1 Equilibrium Equations

With reference to Figure 5.12, the equilibrium equations (no body forces) have the form,

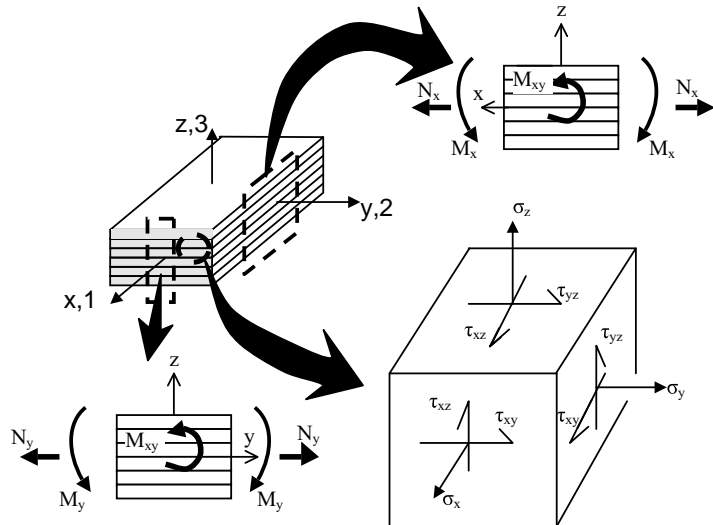


Figure 5.12 Coordinate system and force and moment sign convention

$$\begin{aligned}
 \frac{\partial \sigma_x}{\partial x} + \frac{\partial \tau_{xy}}{\partial y} + \frac{\partial \tau_{xz}}{\partial z} &= 0 \\
 \frac{\partial \tau_{xy}}{\partial x} + \frac{\partial \sigma_y}{\partial y} + \frac{\partial \tau_{yz}}{\partial z} &= 0 \\
 \frac{\partial \tau_{xz}}{\partial x} + \frac{\partial \tau_{yz}}{\partial y} + \frac{\partial \sigma_z}{\partial z} &= 0
 \end{aligned} \tag{5.2}$$

or in terms of force and moment resultants,

$$\begin{aligned}
 \frac{\partial N_x}{\partial x} + \frac{\partial N_{xy}}{\partial y} &= 0 \\
 \frac{\partial N_{xy}}{\partial x} + \frac{\partial N_y}{\partial y} &= 0 \\
 \frac{\partial Q_x}{\partial x} + \frac{\partial Q_y}{\partial y} &= 0
 \end{aligned} \tag{5.3a – c}$$

with

$$\begin{aligned}
 Q_x &= \frac{\partial M_x}{\partial x} + \frac{\partial M_{xy}}{\partial y} \\
 Q_y &= \frac{\partial M_{xy}}{\partial x} + \frac{\partial M_y}{\partial y}
 \end{aligned} \tag{5.3d – e}$$

5.2.2 Stress–Strain Equations

In terms of stresses, the stress–strain equations for an orthotropic material can be written as (see also Equation 3.5),

$$\begin{Bmatrix} \sigma_x \\ \sigma_y \\ \sigma_z \\ \tau_{yz} \\ \tau_{xz} \\ \tau_{xy} \end{Bmatrix} = \begin{bmatrix} E_{11} & E_{12} & E_{13} & 0 & 0 & E_{16} \\ E_{12} & E_{22} & E_{23} & 0 & 0 & E_{26} \\ E_{13} & E_{23} & E_{33} & 0 & 0 & E_{36} \\ 0 & 0 & 0 & E_{44} & E_{45} & 0 \\ 0 & 0 & 0 & E_{45} & E_{55} & 0 \\ E_{16} & E_{26} & E_{36} & 0 & 0 & E_{66} \end{bmatrix} \begin{Bmatrix} \varepsilon_x \\ \varepsilon_y \\ \varepsilon_z \\ \gamma_{yz} \\ \gamma_{xz} \\ \gamma_{xy} \end{Bmatrix} \quad (5.4)$$

Note that, for convenience, the subscripts used with the stiffnesses in Equation (5.4) are 1–6 with 1,2 and 3 coinciding with x , y , and z and 4, 5, and 6 used for the shear moduli as shown in Equation (5.4).

In terms of force and moment resultants, the stress–strain equations can be written as,

$$\begin{Bmatrix} N_x \\ N_y \\ N_{xy} \\ M_x \\ M_y \\ M_{xy} \end{Bmatrix} = \begin{bmatrix} A_{11} & A_{12} & A_{16} & B_{11} & B_{12} & B_{16} \\ A_{12} & A_{22} & A_{26} & B_{12} & B_{22} & B_{26} \\ A_{16} & A_{26} & A_{66} & B_{16} & B_{26} & B_{66} \\ B_{11} & B_{12} & B_{16} & D_{11} & D_{12} & D_{16} \\ B_{12} & B_{22} & B_{26} & D_{12} & D_{22} & D_{26} \\ B_{16} & B_{26} & B_{66} & D_{16} & D_{26} & D_{66} \end{bmatrix} \begin{Bmatrix} \varepsilon_{xo} \\ \varepsilon_{yo} \\ \gamma_{xyo} \\ \kappa_x \\ \kappa_y \\ \kappa_{xy} \end{Bmatrix} \quad (5.5)$$

where A_{ij} are the elements of the membrane stiffness matrix for a laminate, B_{ij} are the elements of the membrane–bending coupling matrix for a laminate, and D_{ij} are the elements of the bending matrix of the laminate (see also Chapter 3).

The vector multiplying the stiffness matrix in the right-hand side of Equation (5.5) consists of the midplane strains and curvatures of the laminate. The curvatures κ_x , κ_y , and κ_{xy} are given by

$$\begin{aligned} \kappa_x &= -\frac{\partial^2 w}{\partial x^2} \\ \kappa_y &= -\frac{\partial^2 w}{\partial y^2} \\ \kappa_{xy} &= -2 \frac{\partial^2 w}{\partial x \partial y} \end{aligned} \quad (5.6)$$

The strains at any through-the-thickness location of a laminate are obtained assuming the standard linear variation with the out-of-plane coordinate z as

$$\begin{aligned} \varepsilon_x &= \varepsilon_{xo} + z \kappa_x \\ \varepsilon_y &= \varepsilon_{yo} + z \kappa_y \\ \gamma_{xy} &= \gamma_{xyo} + z \kappa_{xy} \end{aligned} \quad (5.7)$$

5.2.3 Strain-Displacement Equations

For small displacements and rotations, the equations relating midplane strains to displacements are,

$$\begin{aligned}\varepsilon_{xo} &= \frac{\partial u}{\partial x} \\ \varepsilon_{yo} &= \frac{\partial v}{\partial y} \\ \gamma_{xyo} &= \frac{\partial u}{\partial y} + \frac{\partial v}{\partial x}\end{aligned}\tag{5.8}$$

Similarly, the out-of-plane strains are given by,

$$\begin{aligned}\varepsilon_z &= \frac{\partial w}{\partial z} \\ \gamma_{yz} &= \frac{\partial v}{\partial z} + \frac{\partial w}{\partial y} \\ \gamma_{xz} &= \frac{\partial u}{\partial z} + \frac{\partial w}{\partial x}\end{aligned}\tag{5.9}$$

Since the three midplane strains in Equation (5.8) are expressed in terms of only two displacements, a strain compatibility condition can be derived by eliminating the displacements from Equations (5.8). Differentiate the first of (5.8) twice with respect to y and the second of (5.8) twice with respect to x . Finally differentiate the last of (5.8) once with respect to x and once with respect to y . Combining the results leads to

$$\frac{\partial^2 \varepsilon_{xo}}{\partial y^2} + \frac{\partial^2 \varepsilon_{yo}}{\partial x^2} - \frac{\partial^2 \gamma_{xyo}}{\partial x \partial y} = 0\tag{5.10}$$

Similarly, two more compatibility relations can be obtained by combining corresponding equations from (5.8) and (5.9) or using cyclic symmetry:

$$\frac{\partial^2 \varepsilon_{yo}}{\partial z^2} + \frac{\partial^2 \varepsilon_z}{\partial y^2} - \frac{\partial^2 \gamma_{yz}}{\partial y \partial z} = 0\tag{5.11}$$

$$\frac{\partial^2 \varepsilon_z}{\partial x^2} + \frac{\partial^2 \varepsilon_{xo}}{\partial z^2} - \frac{\partial^2 \gamma_{xz}}{\partial x \partial z} = 0\tag{5.12}$$

Depending on which quantities are used as variables, equations (5.2)–(5.12) form a system of equations in these unknown variables. For example, if stresses, strains, and displacements are used as unknowns, equations (5.2), (5.4), (5.8) and (5.9) form a system of 15 equations in the 15 unknowns: σ_x , σ_y , σ_z , τ_{yz} , τ_{xz} , τ_{xy} , ε_{xo} , ε_{yo} , ε_z , γ_{yz} , γ_{xz} , γ_{xyo} , u , v , and w . Alternatively, for a plate problem, if forces, moments, strains and displacements are used, Equations (5.3), (5.5), (5.6)

and (5.8) form a system of 17 equations in the 17 unknowns, $N_x, N_y, N_{xy}, M_x, M_y, M_{xy}, Q_x, Q_y, \varepsilon_{xo}, \varepsilon_{yo}, \gamma_{xyo}, K_x, K_y, K_{xy}, u, v$, and w .

These systems of equations can be reduced all the way to one equation in some cases, by eliminating appropriate variables according to the needs of specific problems. Some of these reductions will be shown in later chapters.

5.2.4 von Karman Anisotropic Plate Equations for Large Deflections

The case of large deflections merits special attention since they become important in some problems such as post-buckling of composite plates. The von Karman equations for large deflections are derived in this section. Consider the case of a plate undergoing large deflections with distributed loads p_x, p_y , and p_z (units of force/area). The basic assumptions that: (a) the out-of-plane stress σ_z is negligible compared with the in-plane stresses; and (b) plane sections remain plane and normal to the midplane after deformation (leading to zero out of plane shear strains γ_{yz} and γ_{xz}) are still valid. To keep the resulting equations relatively simple (and still covering a wide variety of applications) it is also assumed that: (a) the laminate is symmetric (coupling matrix $B = 0$); (b) the coupling terms D_{16} and D_{26} terms of the bending matrix D are zero; and (c) the laminate is balanced (shearing-stretching coupling terms $A_{16} = A_{26} = 0$). The deformed and undeformed state of a plate element dx in the xz plane is shown in Figure 5.13.

With reference to Figure 5.13 the coordinates of any point A' on the left edge of element dx , are given by:

$$A'_x = x_o + u - \zeta \frac{\partial w}{\partial x}$$

$$A'_z = w + \zeta$$

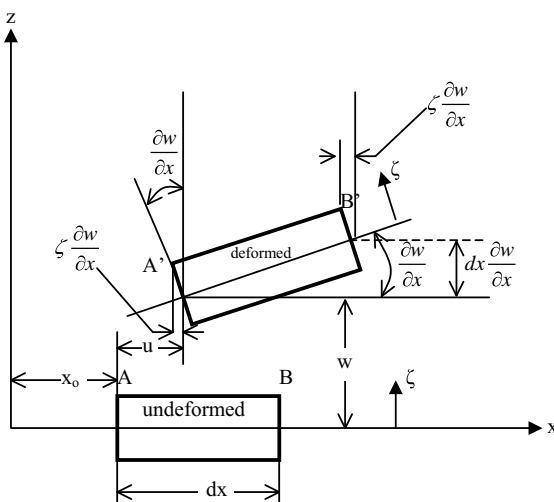


Figure 5.13 Deformation pattern for a plate element dx in the xz plane

The x coordinate of any point B' on the right edge of element dx is given by a Taylor series expansion (truncated after the second term) of the coordinate at the left end shifted by the length of the element dx :

$$B'_x = x_o + u - \zeta \frac{\partial w}{\partial x} + \frac{\partial}{\partial x} \left[x_o + u - \zeta \frac{\partial w}{\partial x} \right] dx + dx = x_o + u - \zeta \frac{\partial w}{\partial x} + \frac{\partial}{\partial x} \left[u - \zeta \frac{\partial w}{\partial x} \right] dx + dx$$

The z coordinate of any point B' on the right edge of element dx is given by

$$B'_z = w + dx \frac{\partial w}{\partial x} + \zeta$$

The x and z components of the deformed element $A'B'$ are then given by

$$\begin{aligned} A'B'_x &= B'_x - A'_x = dx + \frac{\partial}{\partial x} \left[u - \zeta \frac{\partial w}{\partial x} \right] dx \\ A'B'_z &= B'_z - A'_z = \frac{\partial w}{\partial x} dx \end{aligned}$$

Therefore, the length of the deformed element $A'B'$ is given by

$$\begin{aligned} A'B' &= \sqrt{(A'B'_x)^2 + (A'B'_z)^2} = \sqrt{\left(dx + \left(\frac{\partial u}{\partial x} - \zeta \frac{\partial^2 w}{\partial x^2} \right) dx \right)^2 + \left(\frac{\partial w}{\partial x} \right)^2 dx^2} \\ &= dx \sqrt{1 + \left(\frac{\partial u}{\partial x} - \zeta \frac{\partial^2 w}{\partial x^2} \right)^2 + 2 \left(\frac{\partial u}{\partial x} - \zeta \frac{\partial^2 w}{\partial x^2} \right) + \left(\frac{\partial w}{\partial x} \right)^2} \end{aligned}$$

The second term under the square root is small compared with the remaining terms and is neglected. The remaining expression is expanded using the binomial theorem:

$$(a+b)^r = a^r + r a^{r-1} b + \dots$$

and letting $a=1$ in the expression for $A'B'$ and keeping only leading terms:

$$\begin{aligned} A'B' &= \left\{ 1 + \frac{1}{2} \left[2 \left(\frac{\partial u}{\partial x} - \zeta \frac{\partial^2 w}{\partial x^2} \right) + \left(\frac{\partial w}{\partial x} \right)^2 \right] \right\} dx \Rightarrow \\ A'B' &= \left[1 + \frac{\partial u}{\partial x} - \zeta \frac{\partial^2 w}{\partial x^2} + \frac{1}{2} \left(\frac{\partial w}{\partial x} \right)^2 \right] dx \end{aligned}$$

Then, the axial strain ε_x is given by

$$\varepsilon_x = \frac{A'B' - AB}{AB} = \frac{\left[1 + \frac{\partial u}{\partial x} - \zeta \frac{\partial^2 w}{\partial x^2} + \frac{1}{2} \left(\frac{\partial w}{\partial x} \right)^2 \right] dx - dx}{dx} = \frac{\partial u}{\partial x} - \zeta \frac{\partial^2 w}{\partial x^2} + \frac{1}{2} \left(\frac{\partial w}{\partial x} \right)^2$$

Using now the first of Equations (5.7) and (5.6), and noting that in this case $z \rightarrow \zeta$

$$\varepsilon_x = \varepsilon_{xo} + \zeta \left(- \frac{\partial^2 w}{\partial x^2} \right)$$

Comparing the two expressions for ε_x it follows that,

$$\varepsilon_{xo} = \frac{\partial u}{\partial x} + \frac{1}{2} \left(\frac{\partial w}{\partial x} \right)^2 \quad (5.13a)$$

which is a nonlinear strain displacement equation because of the square of the slope $\partial w / \partial x$.

In a similar fashion, it can be shown that the other two midplane strains are given by:

$$\begin{aligned} \varepsilon_{yo} &= \frac{\partial v}{\partial y} + \frac{1}{2} \left(\frac{\partial w}{\partial y} \right)^2 \\ \gamma_{xyo} &= \frac{\partial u}{\partial y} + \frac{\partial v}{\partial x} + \left(\frac{\partial w}{\partial x} \right) \left(\frac{\partial w}{\partial y} \right) \end{aligned} \quad (5.13b, c)$$

The curvatures κ_x , κ_y , and κ_{xy} are still given by Equations (5.6).

Now the first two of Equations (5.3), which represent force equilibrium along the x and y axes, are the same as before, with the addition of the distributed loads p_x and p_y :

$$\begin{aligned} \frac{\partial N_x}{\partial x} + \frac{\partial N_{xy}}{\partial y} + p_x &= 0 \\ \frac{\partial N_{xy}}{\partial x} + \frac{\partial N_y}{\partial y} + p_y &= 0 \end{aligned} \quad (5.3a, b)$$

For force equilibrium along the z axis, the situation is as shown in Figure 5.14. Angles are sufficiently small so that

$$\begin{aligned} \tan \phi &\approx \phi \\ \sin \phi &\approx \phi \\ \cos \phi &\approx 1 \end{aligned}$$

With $\varphi = \partial w / \partial x$ or $\partial w / \partial y$ (respectively), summation of forces in the z direction gives

$$\begin{aligned} -Q_x dy + \left(Q_x + \frac{\partial Q_x}{\partial x} dx \right) dy - Q_y dx + \left(Q_y + \frac{\partial Q_y}{\partial y} dy \right) dx - N_x \frac{\partial w}{\partial x} dy \\ + \left(N_x \frac{\partial w}{\partial x} + \frac{\partial}{\partial x} \left(N_x \frac{\partial w}{\partial x} \right) dx \right) dy - N_y \frac{\partial w}{\partial y} dx \end{aligned}$$

(eq continued in next page)

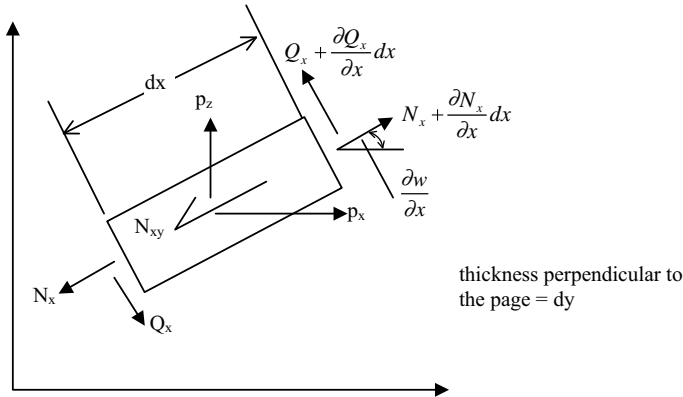


Figure 5.14 Force equilibrium of plate element in x and z directions

$$\begin{aligned}
 & + \left(N_y \frac{\partial w}{\partial y} + \frac{\partial}{\partial y} \left(N_y \frac{\partial w}{\partial y} \right) dy \right) dx - N_{xy} \frac{\partial w}{\partial x} dx \\
 & + \left(N_{xy} \frac{\partial w}{\partial x} + \frac{\partial}{\partial y} \left(N_{xy} \frac{\partial w}{\partial x} \right) dy \right) dx + N_{xy} \frac{\partial w}{\partial y} dy \\
 & + \left(N_{xy} \frac{\partial w}{\partial y} + \frac{\partial}{\partial x} \left(N_{xy} \frac{\partial w}{\partial y} \right) dx \right) dy + p_z dx dy = 0
 \end{aligned}$$

Cancelling and collecting terms,

$$\begin{aligned}
 & \frac{\partial Q_x}{\partial x} + \frac{\partial Q_y}{\partial y} + N_x \frac{\partial^2 w}{\partial x^2} + 2N_{xy} \frac{\partial^2 w}{\partial x \partial y} + N_y \frac{\partial^2 w}{\partial y^2} + \\
 & \frac{\partial w}{\partial x} \left(\frac{\partial N_x}{\partial x} + \frac{\partial N_{xy}}{\partial y} \right) + \frac{\partial w}{\partial y} \left(\frac{\partial N_{xy}}{\partial x} + \frac{\partial N_y}{\partial y} \right) + p_z = 0
 \end{aligned}$$

But, from Equations (5.3a) and (5.3b) the quantities in parentheses in the equation above are equal to $-p_x$ and $-p_y$ respectively. Substituting leads to the nonlinear equation:

$$\frac{\partial Q_x}{\partial x} + \frac{\partial Q_y}{\partial y} + N_x \frac{\partial^2 w}{\partial x^2} + 2N_{xy} \frac{\partial^2 w}{\partial x \partial y} + N_y \frac{\partial^2 w}{\partial y^2} - p_x \frac{\partial w}{\partial x} - p_y \frac{\partial w}{\partial y} + p_z = 0 \quad (5.14)$$

The moment equilibrium equations (5.3d) and (5.3e) are the same as before. Equations (5.3a), (5.3b), (5.3d), (5.3e), (5.14), (5.13a–c), (5.5), and (5.6) form the new nonlinear system of 17 equations in the 17 unknowns N_x , N_y , N_{xy} , M_x , M_y , M_{xy} , Q_x , Q_y , ε_{xo} , ε_{yo} , γ_{xyo} , κ_x , κ_y , κ_{xy} , u , v , and w . The nonlinear equations are the three strain–displacement equations (5.13a–c) and the force equilibrium equation (5.14).

In addition to these equations, following the same procedure as for Equation (5.10), the strain compatibility condition can be shown to give the nonlinear equation:

$$\frac{\partial^2 \varepsilon_{xo}}{\partial y^2} + \frac{\partial^2 \varepsilon_{yo}}{\partial x^2} - \frac{\partial^2 \gamma_{xyo}}{\partial x \partial y} = \left(\frac{\partial^2 w}{\partial x \partial y} \right)^2 - \frac{\partial^2 w}{\partial x^2} \frac{\partial^2 w}{\partial y^2} \quad (5.10a)$$

The 17 equations can be reduced to two equations as follows: first, use Equations (5.3d), (5.3e) to substitute in Equation (5.14). This gives

$$\frac{\partial^2 M_x}{\partial x^2} + 2 \frac{\partial^2 M_{xy}}{\partial x \partial y} + \frac{\partial^2 M_y}{\partial y^2} + N_x \frac{\partial^2 w}{\partial x^2} + 2N_{xy} \frac{\partial^2 w}{\partial x \partial y} + N_y \frac{\partial^2 w}{\partial y^2} - p_x \frac{\partial w}{\partial x} - p_y \frac{\partial w}{\partial y} + p_z = 0 \quad (5.15)$$

Then, use the moment-curvature relations from (5.5) and recall that $B_{ij} = D_{16} = D_{26} = 0$:

$$\begin{aligned} M_x &= -D_{11} \frac{\partial^2 w}{\partial x^2} - D_{12} \frac{\partial^2 w}{\partial y^2} \\ M_y &= -D_{12} \frac{\partial^2 w}{\partial x^2} - D_{22} \frac{\partial^2 w}{\partial y^2} \\ M_{xy} &= -2D_{66} \frac{\partial^2 w}{\partial x \partial y} \end{aligned}$$

to substitute in Equation (5.15):

$$\begin{aligned} D_{11} \frac{\partial^4 w}{\partial x^4} + 2(D_{12} + 2D_{66}) \frac{\partial^4 w}{\partial x^2 \partial y^2} + D_{22} \frac{\partial^4 w}{\partial y^4} \\ = N_x \frac{\partial^2 w}{\partial x^2} + 2N_{xy} \frac{\partial^2 w}{\partial x \partial y} + N_y \frac{\partial^2 w}{\partial y^2} - p_x \frac{\partial w}{\partial x} - p_y \frac{\partial w}{\partial y} + p_z \end{aligned} \quad (5.16)$$

Equation (5.16) is the first von Karman equation, describing the bending behavior of the plate (left-hand side) and how it couples with stretching (right-hand side). As can be seen from the first three terms in the right-hand side, it is nonlinear.

For the second von Karman equation, the Airy stress function F is introduced so that the equilibrium equations (5.3a) and (5.3b) are satisfied:

$$\begin{aligned} N_x &= \frac{\partial^2 F}{\partial y^2} + V \\ N_y &= \frac{\partial^2 F}{\partial x^2} + V \\ N_{xy} &= -\frac{\partial^2 F}{\partial x \partial y} \end{aligned} \quad (5.17)$$

with V the potential function for the distributed loads p_x and p_y ,

$$\begin{aligned} p_x &= -\frac{\partial V}{\partial x} \\ p_y &= -\frac{\partial V}{\partial y} \end{aligned} \quad (5.18)$$

From Equation (5.5), the in-plane portion

$$\begin{aligned} N_x &= A_{11}\varepsilon_{xo} + A_{12}\varepsilon_{yo} \\ N_y &= A_{12}\varepsilon_{xo} + A_{22}\varepsilon_{yo} \\ N_{xy} &= A_{66}\gamma_{xyo} \end{aligned}$$

can be solved for the midplane strains,

$$\begin{aligned} \varepsilon_{xo} &= \frac{A_{22}}{A_{11}A_{22}-A_{12}^2}N_x - \frac{A_{12}}{A_{11}A_{22}-A_{12}^2}N_y \\ \varepsilon_{yo} &= -\frac{A_{12}}{A_{11}A_{22}-A_{12}^2}N_x + \frac{A_{11}}{A_{11}A_{22}-A_{12}^2}N_y \\ \gamma_{xyo} &= \frac{1}{A_{66}}N_{xy} \end{aligned} \quad (5.19)$$

which, in turn, can be substituted in the strain compatibility relation (5.10a) to give,

$$\begin{aligned} \frac{1}{A_{11}A_{22}-A_{12}^2} \left(A_{22} \frac{\partial^2 N_x}{\partial y^2} - A_{12} \frac{\partial^2 N_y}{\partial y^2} + A_{11} \frac{\partial^2 N_y}{\partial x^2} - A_{12} \frac{\partial^2 N_x}{\partial x^2} \right) \\ - \frac{1}{A_{66}} \frac{\partial^2 N_{xy}}{\partial x \partial y} = \left(\frac{\partial^2 w}{\partial x \partial y} \right)^2 - \frac{\partial^2 w}{\partial x^2} \frac{\partial^2 w}{\partial y^2} \end{aligned}$$

Now (5.17) is used to express N_x , N_y , and N_{xy} , in terms of F and V :

$$\begin{aligned} \frac{1}{A_{11}A_{22}-A_{12}^2} \left(A_{22} \frac{\partial^4 F}{\partial y^4} - 2A_{12} \frac{\partial^4 F}{\partial x^2 \partial y^2} + A_{11} \frac{\partial^4 F}{\partial x^4} + (A_{22}-A_{12}) \frac{\partial^2 V}{\partial y^2} + (A_{11}-A_{12}) \frac{\partial^2 V}{\partial x^2} \right) + \\ \frac{1}{A_{66}} \frac{\partial^4 F}{\partial x^2 \partial y^2} = \left(\frac{\partial^2 w}{\partial x \partial y} \right)^2 - \frac{\partial^2 w}{\partial x^2} \frac{\partial^2 w}{\partial y^2} \end{aligned} \quad (5.20)$$

This is the second von Karman equation, relating the membrane behavior of the plate (left-hand side) with the out-of-plane curvatures (right-hand side). The terms in the right-hand side are nonlinear.

5.3 Reductions of Governing Equations: Applications to Specific Problems

This section shows two examples where the governing equations are solved exactly and the results are used in the design of specific applications.

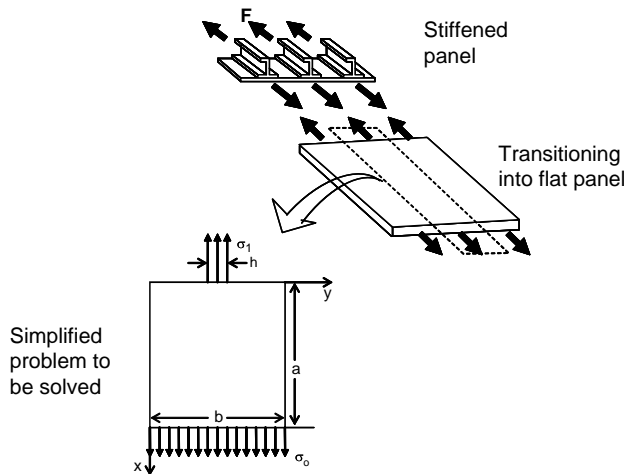


Figure 5.15 Model for a stiffener termination

5.3.1 Composite Plate Under Localized In-Plane Load [15]

The situation is shown in Figure 5.15. In practice, besides the obvious case where an in-plane point load is applied on a plate, this case arises when a stiffener is terminated. This happens when the axial load applied to a stiffened panel is reduced to the point that a monolithic panel may be sufficient to take the load, or in cases with moderate loads where there is not enough room to accommodate the stiffeners.

The situation shown in Figure 5.15 represents the load from a single stiffener introduced in a rectangular panel and reacted by a uniform load at the other end. It is assumed that the stiffener spacing is such that there is no interaction between stiffeners (which covers most cases of realistic stiffener spacing, which is at least 6 cm). Also, to simplify the derivation, the length of the panel a is assumed to be sufficiently long that the details of the concentrated load introduction at one end have died down before the other end is reached. This is also a realistic assumption since the typical panel length, such as that corresponding to the frame spacing in a fuselage, is much longer than the distance required for the transient effects to die out.

It is exactly these transients that the designer is required to design for. In the vicinity of the point of introduction of the concentrated load high normal and shear stresses develop that converge to their far-field (uniform stress) values fairly quickly. The size of this transition region both along the x axis and along the y axis defines the size of reinforcement or doubler that must be added to help transition the local load without failure. Determining the stresses in the vicinity of the load application will help determine the dimensions $\ell \times w$ of the required reinforcement as shown in Figure 5.16.

In addition to the assumptions already mentioned, the following conditions are imposed:

- Plate is homogeneous and orthotropic
- Layup is symmetric (B matrix = 0) and balanced ($A_{16} = A_{26} = 0$)
- No bending/twisting coupling ($D_{16} = D_{26} = 0$)

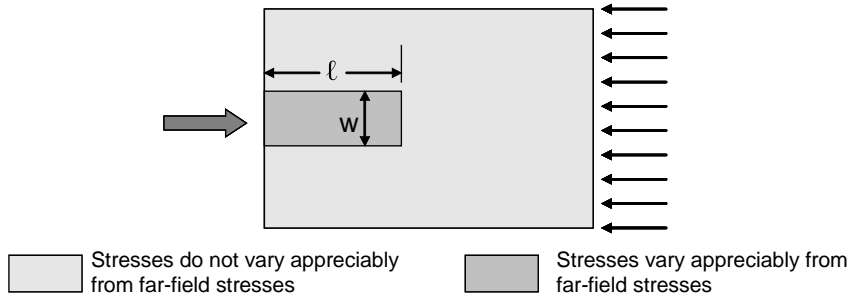


Figure 5.16 Doubler dimensions

Under these assumptions, the stress-strain equations (5.5) can be solved for the midplane strains to give the relations (5.19). The average stresses through the plate thickness are given by

$$\sigma_x = \frac{N_x}{H}$$

$$\sigma_y = \frac{N_y}{H}$$

$$\tau_{xy} = \frac{N_{xy}}{H}$$

where H is the plate thickness.

Placing these into eqs (5.19) and dropping the subscript o for convenience,

$$\begin{aligned} \varepsilon_x &= \frac{HA_{22}\sigma_x - HA_{12}\sigma_y}{A_{11}A_{22} - A_{12}^2} & \gamma_{xy} &= H \frac{\tau_{xy}}{A_{66}} \\ \varepsilon_y &= \frac{HA_{11}\sigma_y - HA_{12}\sigma_x}{A_{11}A_{22} - A_{12}^2} \end{aligned} \quad (5.21)$$

These expressions for the strains can now be placed into the (linear) strain compatibility condition (5.10):

$$\frac{A_{11}A_{22} - A_{12}^2}{A_{66}} \frac{\partial^2 \tau_{xy}}{\partial x \partial y} = A_{22} \frac{\partial^2 \sigma_x}{\partial y^2} - A_{12} \frac{\partial^2 \sigma_y}{\partial y^2} + A_{11} \frac{\partial^2 \sigma_y}{\partial x^2} - A_{12} \frac{\partial^2 \sigma_x}{\partial x^2} \quad (5.22)$$

Now, for a plane stress problem the out-of-plane stresses σ_z , τ_{xz} , and τ_{yz} are zero. Then, the stress equilibrium condition (5.2a) gives,

$$\frac{\partial^2 \tau_{xy}}{\partial x \partial y} = - \frac{\partial^2 \sigma_x}{\partial x^2} \quad (5.23)$$

Similarly, from (5.2b),

$$\frac{\partial^2 \sigma_y}{\partial y^2} = -\frac{\partial^2 \tau_{xy}}{\partial x \partial y} \quad (5.24)$$

which, in view of Equation (5.23), gives

$$\frac{\partial^2 \sigma_y}{\partial y^2} = \frac{\partial^2 \sigma_x}{\partial x^2} \quad (5.25)$$

Substituting in (5.22) gives

$$-\frac{A_{11}A_{22}-A_{12}^2}{A_{66}}\frac{\partial^2 \sigma_x}{\partial x^2} = A_{22}\frac{\partial^2 \sigma_x}{\partial y^2} - A_{12}\frac{\partial^2 \sigma_x}{\partial x^2} + A_{11}\frac{\partial^2 \sigma_y}{\partial x^2} - A_{12}\frac{\partial^2 \sigma_x}{\partial x^2} \quad (5.26)$$

Now differentiate (5.25) twice with respect to x and (5.26) twice with respect to y to obtain

$$\frac{\partial^2 \sigma_y}{\partial x^2 \partial y^2} = \frac{\partial^2 \sigma_x}{\partial x^4} \quad (5.27)$$

and

$$-\frac{A_{11}A_{22}-A_{12}^2}{A_{66}}\frac{\partial^4 \sigma_x}{\partial x^2 \partial y^2} = A_{22}\frac{\partial^4 \sigma_x}{\partial y^4} - A_{12}\frac{\partial^4 \sigma_x}{\partial x^2 \partial y^2} + A_{11}\frac{\partial^4 \sigma_y}{\partial x^2 \partial y^2} - A_{12}\frac{\partial^4 \sigma_x}{\partial x^2 \partial y^2} \quad (5.28)$$

The stress σ_y can be eliminated from Equation (5.28) with the use of Equation (5.27). Then, collecting terms gives the governing equation for σ_x :

$$\frac{\partial^4 \sigma_x}{\partial x^4} + \left[\frac{A_{11}A_{22}-A_{12}^2}{A_{11}A_{66}} - 2\frac{A_{12}}{A_{11}} \right] \frac{\partial^4 \sigma_x}{\partial x^2 \partial y^2} + \frac{A_{22}}{A_{11}} \frac{\partial^4 \sigma_x}{\partial y^4} = 0$$

or defining

$$\begin{aligned} \beta &= \frac{A_{11}A_{22}-A_{12}^2}{A_{11}A_{66}} - 2\frac{A_{12}}{A_{11}} \\ \gamma &= \frac{A_{22}}{A_{11}} \end{aligned} \quad (5.29)$$

$$\frac{\partial^4 \sigma_x}{\partial x^4} + \beta \frac{\partial^4 \sigma_x}{\partial x^2 \partial y^2} + \gamma \frac{\partial^4 \sigma_x}{\partial y^4} = 0$$

Equation (5.29) must be solved subject to the following boundary conditions:

$$\begin{aligned}\sigma_x(x=0) &= 0 \quad 0 \leq y \leq \frac{b-h}{2} \quad \text{and} \quad \frac{b+h}{2} \leq y \leq b \\ \sigma_x(x=0) &= \sigma_1 = \frac{F}{Hh} \quad \text{for} \quad \frac{b-h}{2} \leq y \leq \frac{b+h}{2} \\ \sigma_x(x=a) &= \sigma_o = \frac{F}{bH} \end{aligned}\tag{5.30a-e}$$

$$\begin{aligned}\sigma_y(y=0) &= \sigma_y(y=b) = 0 \\ \tau_{xy}(x=0) &= \tau_{xy}(x=a) = \tau_{xy}(y=0) = \tau_{xy}(y=b) = 0\end{aligned}$$

Conditions (5.30a) and (5.30b) define the applied concentrated load on one end ($x=0$) of the plate. The stress σ_x is zero there except for the narrow region of width h at the center where it equals $F/(Hh)$. Condition (5.30c) defines the uniform stress applied at the other end of the plate (at $x=a$). Finally, conditions (5.30d) and (5.30e) state that the transverse stress σ_y and the shear stress τ_{xy} are zero at the corresponding plate edges.

The solution of Equation (5.29) can be obtained using separation of variables [16]. Following this procedure, it is expedient to assume a solution of the form,

$$\sigma_x \approx f_n(x) \cos \frac{n\pi y}{b}\tag{5.31}$$

Substituting in the governing equation (5.29), the y dependence cancels out and the following ordinary differential equation for f_n is obtained:

$$\frac{d^4 f_n}{dx^4} - \beta \left(\frac{n\pi}{b} \right)^2 \frac{d^2 f_n}{dx^2} + \gamma \left(\frac{n\pi}{b} \right)^4 f_n = 0\tag{5.32}$$

From the theory of linear ordinary differential equations with constant coefficients, the solution to (5.32) is found as

$$f_n = C e^{\phi x}\tag{5.33}$$

with

$$\phi = \pm \frac{1}{\sqrt{2}} \left(\frac{n\pi}{b} \right) \sqrt{\beta \pm \sqrt{\beta^2 - 4\gamma}}\tag{5.34}$$

Note that Equation (5.34) implies four different values of ϕ to be used in Equation (5.33) yielding four different solutions for f_n as should be expected from the fourth order differential equation (5.32). It is also important to note that the quantities under the square roots in Equation (5.34) can be negative, leading to complex values for ϕ . In such a case the four different right-hand sides of Equation (5.34) appear in pairs of complex conjugates leading to a real solution for the stress σ_x .

If the real part of φ given by Equation (5.34) is positive, the stress σ_x will increase with increasing x . And for a long plate (value of a in Fig 5.15 is large) this would lead to unbounded stresses. So, if the plate is long enough for the effect of the load introduction at $x=0$ to have died down, the two solutions for φ with positive real parts must be neglected. The remaining two solutions (with negative real parts) are denoted by φ_1 and φ_2 and can be combined with Equations (5.31) and (5.33)) to give the most general expression for σ_x as a linear combination of all the possible solutions (all possible values of n in Equation (5.31)):

$$\sigma_x = K_o + \sum_{n=1}^{\infty} A_n [e^{\phi_1 x} + C_n e^{\phi_2 x}] \cos \frac{n\pi y}{b} \quad (5.35)$$

A constant K_o , which is also a solution to Equation (5.29) has been added in Equation (5.35) to obtain the most general form of the solution. The right-hand side of Equation (5.35) is a Fourier cosine series.

Now, as mentioned earlier, the out-of-plane stresses σ_z , τ_{xz} , τ_{yz} are assumed to be zero, which eliminates the last term in each of the equilibrium equations (5.2a) and (5.2b) and identically satisfies Equation (5.2c). Then, from Equation (5.2a),

$$\frac{\partial \tau_{xy}}{\partial y} = - \frac{\partial \sigma_x}{\partial x} \quad (5.36)$$

Differentiating Equation (5.35) with respect to x and then integrating the result with respect to y to substitute in Equation (5.36) leads to

$$\tau_{xy} = - \sum_{n=1}^{\infty} A_n [\phi_1 e^{\phi_1 x} + C_n \phi_2 e^{\phi_2 x}] \frac{b}{n\pi} \sin \frac{n\pi y}{b} + G_1(z) \quad (5.37)$$

Applying now the boundary condition (5.30e) at $y=0$ leads to the following condition

$$\tau_{xy}(y=0) = 0 \Rightarrow G_1(z) = 0$$

Then, (5.30e) at $x=0$ leads to

$$\tau_{xy}(x=0) = 0 \Rightarrow \phi_1 + C_n \phi_2 = 0 \Rightarrow C_n = - \frac{\phi_1}{\phi_2}$$

Note that the condition (5.30e) at $x=a$ is satisfied as long as a is large enough and the exponentials in Equation (5.37) have died out. Incorporating these results in Equation (5.37), τ_{xy} is obtained as:

$$\tau_{xy} = - \sum_{n=1}^{\infty} \phi_1 A_n [e^{\phi_1 x} - e^{\phi_2 x}] \frac{b}{n\pi} \sin \frac{n\pi y}{b}$$

The last of the conditions (5.30e) is at $y=b$ and it leads to

$$\tau_{xy}(y=b) = 0 \Rightarrow \sin n\pi = 0 \Rightarrow \text{satisfied for any } n$$

The final expression for τ_{xy} is, therefore,

$$\tau_{xy} = - \sum_{n=1}^{\infty} \phi_1 A_n [e^{\phi_1 x} - e^{\phi_2 x}] \frac{b}{2n\pi} \sin \frac{2n\pi y}{b} \quad (5.38)$$

Note that $2n$ is substituted for n ; this is needed in order to satisfy (5.30d).

This, in turn implies that Equation (5.35) for σ_x has the form,

$$\sigma_x = K_o + \sum_{n=1}^{\infty} A_n [e^{\phi_1 x} + C_n e^{\phi_2 x}] \cos \frac{2n\pi y}{b} \quad (5.35a)$$

In an analogous manner, σ_y is determined from (5.2b), with $\tau_{yz} = 0$

$$\frac{\partial \sigma_y}{\partial y} = - \frac{\partial \tau_{xy}}{\partial x} \quad (5.39)$$

which, combined with (5.38) and condition (5.30d) leads to

$$\sigma_y = \sum_{n=1}^{\infty} \left(\frac{b}{2n\pi} \right)^2 \phi_1 A_n (\phi_1 e^{\phi_1 x} - \phi_2 e^{\phi_2 x}) \left(1 - \cos \frac{2n\pi y}{b} \right) \quad (5.40)$$

At this point all unknowns in the stress expressions (5.35a), (5.38), and (5.40) have been determined except for K_o and A_n . These are determined as Fourier cosine series coefficients using conditions (5.30a) and (5.30b). The constant K_o is the average of stress σ_x at any x value,

$$K_o = \frac{F}{bH} \quad (5.41)$$

For the A_n coefficients, multiplying both sides of (5.30a) by $\cos 2q\pi y/b$ and integrating from 0 to b leads to

$$\int_0^b \sigma_x(x=0) \cos \frac{2q\pi y}{b} dy = \int_0^b \left(K_o + \sum A_n \left(e^{\phi_1 x} - \frac{\phi_1}{\phi_2} e^{\phi_2 x} \right) \Big|_{x=0} \cos \frac{2n\pi y}{b} \right) \cos \frac{2q\pi y}{b} dy \quad (5.42)$$

Now $\sigma_x(x=0)$ is zero everywhere except at the center of the plate where it equals the applied load F divided by the area over which F acts. This is shown in Figure 5.17.

Substituting in Equation (5.42) and carrying out the integrations leads to the final expression for A_n :

$$A_n = \frac{F}{hH} \frac{\phi_2}{\phi_2 - \phi_1} \frac{2}{n\pi} \cos n\pi \sin \frac{n\pi h}{b} \quad (5.43)$$

This completes the determination of the stresses in the plate. It is in closed form and exact within the assumptions made during the derivation. Since the solution is in terms of infinite

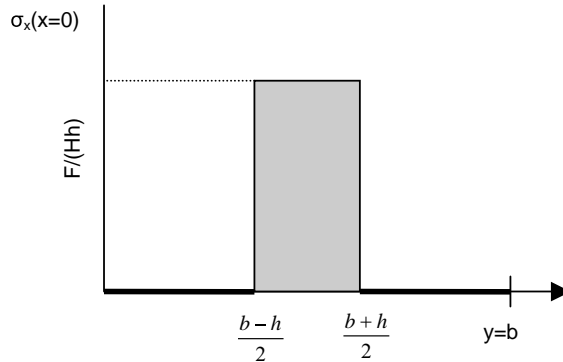


Figure 5.17 Applied normal stress σ_x at one end of the plate

series, see Equations (5.35), (5.37) and (5.40), some guidelines on selecting the number of terms after which they can be truncated and still give sufficient accuracy in the results is needed. One way to do that is to evaluate Equation (5.35) at $x = 0$ and compare it with the applied load. This is shown in Figure 5.18.

The laminate selected in Figure 5.18 has the layup $(\pm 45)_4$ consisting of four plies of plain weave fabric material each at 45° with the load direction. The geometry and applied loading information are shown in Figure 5.18. The basic material properties are as follows:

$$\begin{aligned} E_x &= E_y = 73 \text{ GPa} \\ G_{xy} &= 5.3 \text{ GPa} \\ v_{xy} &= 0.05 \\ \text{ply thickness } (t_{\text{ply}}) &= 0.19 \text{ mm} \end{aligned}$$

It can be seen from Figure 5.18 that, even with 160 terms in the series in Equation (5.35a), the step function behavior of the applied load is not exactly reproduced. In addition, outside the region of the applied load, i.e. $(b - h)/2 < y < (b + h)/2$, the σ_x stress at $x = 0$ is very small, but not exactly zero as it should be. More terms would be necessary for even better accuracy. In what follows, predictions of the method are compared with finite element results (obtained with ANSYS) using $n = 80$.

The axial stress σ_x as a function of x obtained from Equation (5.35a) is compared with the finite element prediction in Figure 5.19. Very good agreement between the two methods is observed. The shear stress τ_{xy} as a function of y is compared with the finite element results at $x/a = 0.0075$ in Figure 5.20. Excellent agreement between the two methods is observed. Finally the transverse stress σ_y is compared with the finite element predictions in Figure 5.21 where the stress is plotted as a function of y at $x/a = 0.0075$. Again, very good agreement is observed.

It appears from the results in Figures 5.19–5.21 that, even though the applied σ_x is not exactly reproduced at $x = 0$ (see Figure 5.18), $n = 80$ gives sufficient accuracy for predicting the in-plane stresses in this problem. The good agreement of the method with the finite element results gives confidence in its use for the design of reinforcements in composite plates with localized loads, such as those coming from stiffener terminations shown in Figure 5.15.

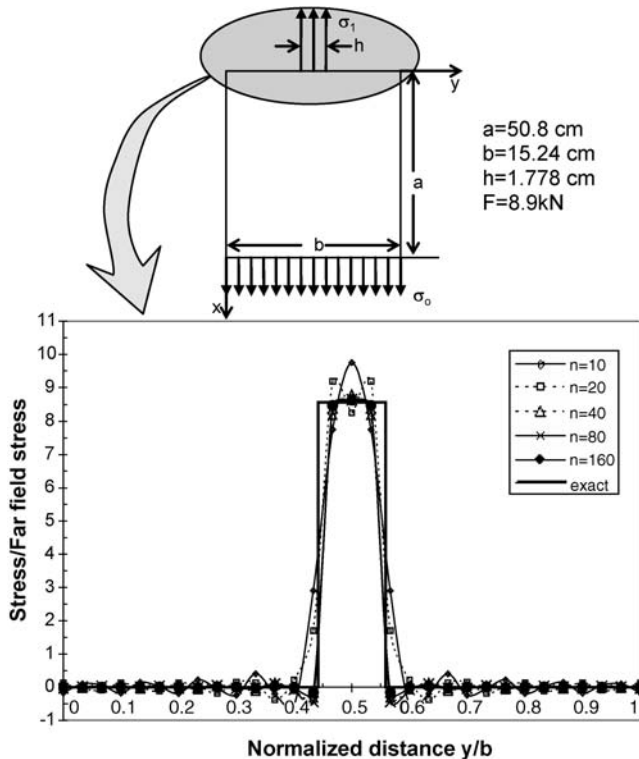


Figure 5.18 Applied stress at panel edge ($x = 0$) and approximation as a function of the number of terms in the series

There are two main issues that need to be addressed. The first is which layup minimizes the peak stresses that develop in the vicinity of the point-load introduction. It should be noted that the peak σ_x stress is $F/(Hh)$ where F is the applied load, H is the laminate thickness and h is the width over which the concentrated load is applied.

The peak σ_y and τ_{xy} stresses are not as obvious and only through methods like the one presented here can they be calculated and their potentially deleterious effect on panel performance be mitigated. The second issue is the size (in terms of length ℓ and width w) (Figure 5.16) of the reinforcement needed to transition the applied concentrated load to the far-field uniform load without failure. Some results showing how the method can be applied to specific problems are shown in Figures 5.22–5.24.

The effect of layup on the peak stress σ_y is shown in Figure 5.22. Only a few representative layups are used here to show trends. The material used is the same plain weave fabric mentioned earlier. The geometry is the same as that shown in Figure 5.18.

Of the three layups shown in Figure 5.22, the softest, $(\pm 45)_4$ has the highest peak stress and is, therefore, to be avoided in such applications. The remaining two layups, the quasi-isotropic $[(\pm 45)/(0/90)]_s$ and the orthotropic $(0/90)_4$ have much lower peak stresses. Also of interest is the fact that the region over which the σ_y stress is appreciable in the y direction is much narrower for the $(\pm 45)_4$ layup than for the $[(\pm 45)/(0/90)]_s$ or the $(0/90)_4$ layup. This means that the width

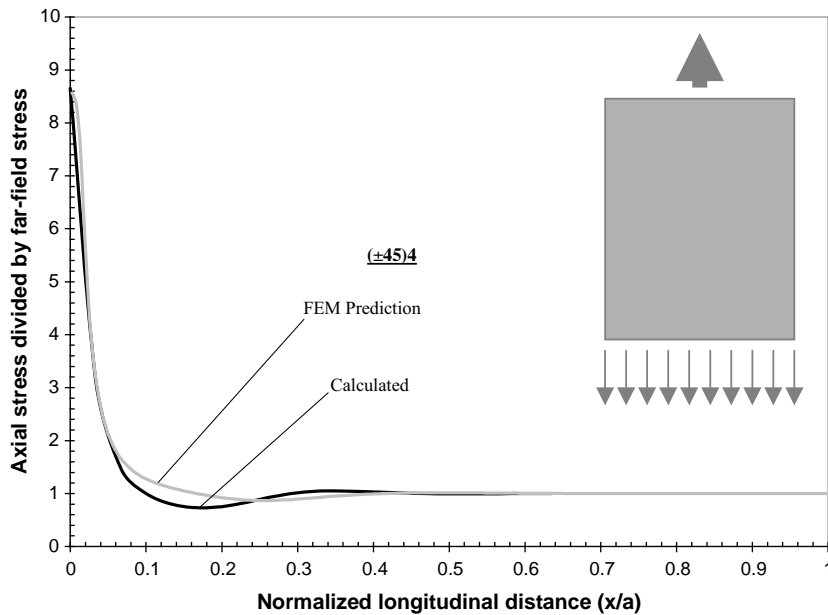


Figure 5.19 Axial stress at the center of the panel ($y = b/2$) compared with finite element results (FEM)

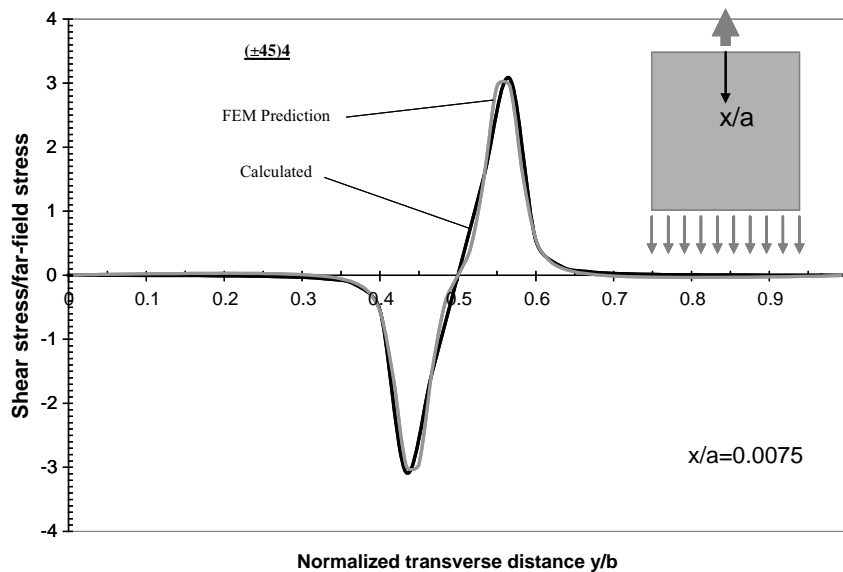


Figure 5.20 Shear stress as a function of the transverse coordinate y at $x/a = 0.0075$

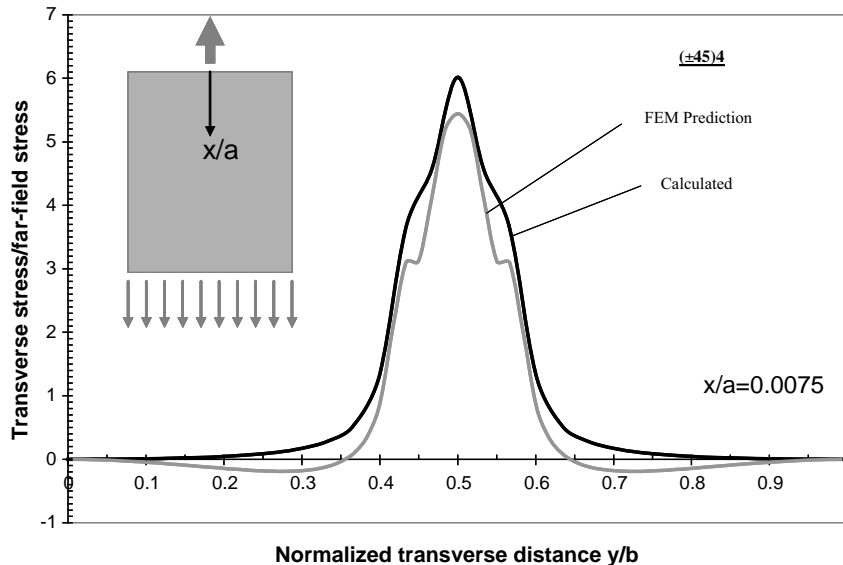


Figure 5.21 Transverse stress as a function of y at $x/a = 0.0075$

w of the reinforcement or doubler needed (see Figure 5.16) must be wider for the last two layups, extending possibly from $y/b = 0.3$ to $y/b = 0.7$ than for the $(\pm 45)_4$ layup where it can be confined in the region $0.4 < y/b < 0.6$.

The axial stress σ_x is shown in Figure 5.23 as a function of distance from the load introduction point for the three layups $(\pm 45)_4$, $[(\pm 45)/(0/90)]_s$, and $(0/90)_4$. All three layups start with the same peak value at $x = 0$ which is the applied load F divided by the area (Hh) over

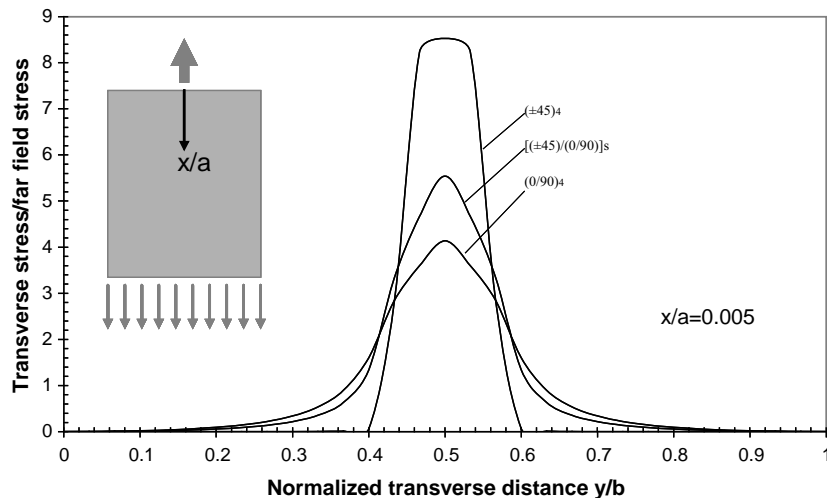


Figure 5.22 Transverse stress σ_y as a function of y for different layups ($x/a = 0.005$)

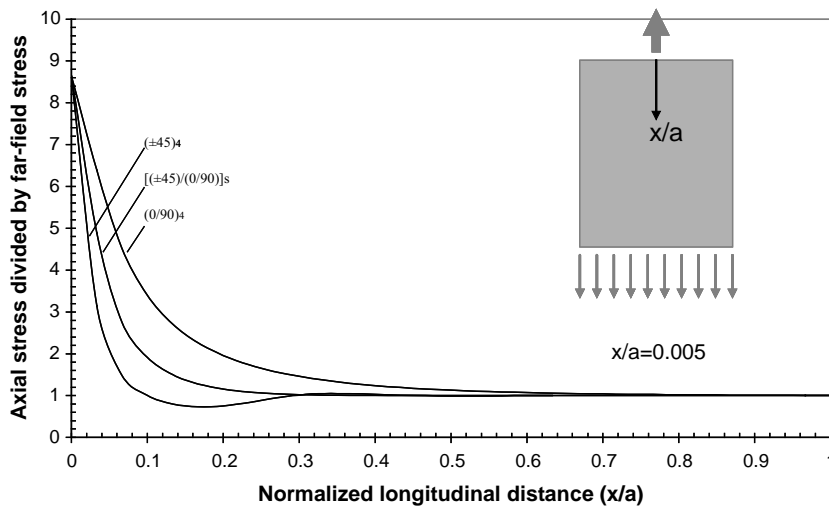


Figure 5.23 Axial stress as a function of distance from load introduction for three different layups

which it acts. However, the rate of decay to the far-field value is different for each layup. The $(0/90)_4$ layup has the slowest rate of decay suggesting a longer doubler (length ℓ in Figure 5.16) is needed with $\ell \approx 0.5a$ compared with the other two layups for which a length $\ell \approx 0.3a$ would suffice.

Finally, the shear stress τ_{xy} is shown in Figure 5.24 for the same three layups. The stress is shown as a function of the transverse coordinate y at a specific x/a value. Of the three layups, $(\pm 45)_4$ shows the highest peaks followed by $[(\pm 45)/(0/90)]_s$. For all three layups, the range of y values over which τ_{xy} is significant is $0.35 < y/b < 0.65$. This range gives an idea of the width w

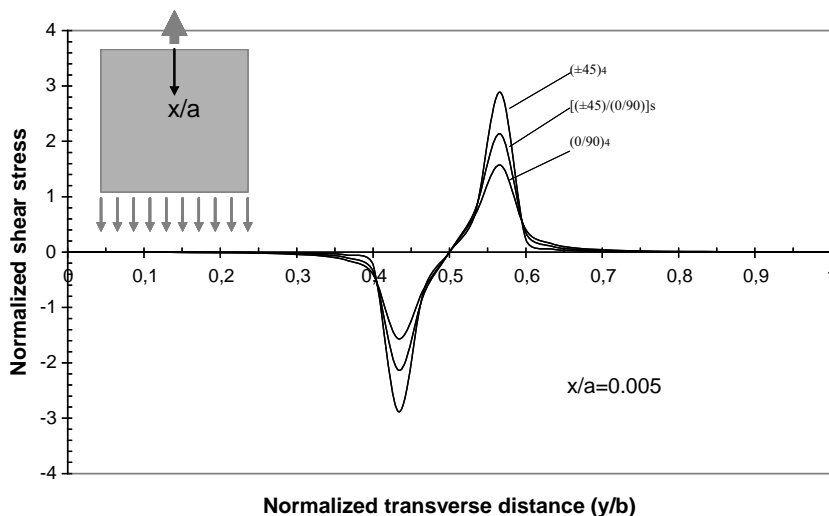


Figure 5.24 Shear stress versus y for three different layups

needed for the doubler. Note that this value is less than the value found by examining the σ_y stress in Figure 5.22. This means that the value found in examining Figure 5.22 should be used as it covers both cases.

The results presented in Figure 5.22–5.24 are only a subset of the cases that should be examined for a complete assessment of the doubler requirements. Other locations in the panel should also be checked so that the extreme values and locations of all three stresses σ_x , σ_y , and τ_{xy} can be determined so the doubler characteristics can be defined. The results in Figures 5.22–5.24 give a good idea of the basic trends. Based on these results, the basic characteristics of the doubler needed from the analysis so far are as follows:

- Axial stresses in $(0/90)_4$ panels decay more slowly (require longer doublers) than $(\pm 45)_4$ or $[(\pm 45)/(0/90)]_s$ panels
- On the other hand, transverse and shear stresses in $(\pm 45)_4$ or $[(\pm 45)/(0/90)]_s$ panels are more critical than in $(0/90)_4$ panels
- Preliminary doubler (reinforcement dimensions): $\ell = 0.5a$ for $(0/90)_4$ and $0.3a$ for $(\pm 45)_4$ or $[(\pm 45)/(0/90)]_s$ panels and $w = 0.3b$ for all panels

While the analysis so far is very helpful in giving basic design guidelines, it is by no means complete. It should be borne in mind that once a doubler is added to the panel, the load distribution changes and additional iterations are necessary. The previous discussion is a good starting point for a robust design. Finally, for the specific case of a stiffener termination, the analysis presented assumed that the concentrated load acts at the midplane of the plate. For a terminating stiffener, the load in the stiffener acts at the stiffener neutral axis and is, therefore, offset from the center of the plate. This means that, in addition to the axial load examined here, a moment equal to the axial load times the offset from the stiffener neutral axis to the plate midplane should be added.

5.3.2 Composite Plate Under Out-of-Plane Point Load

The situation is shown in Figure 5.25. The plate of dimensions $a \times b$ is loaded by a vertical force F . The coordinates of the point where the load is applied are x_o and y_o . Besides the obvious application of a point load on a plate, this problem can be used to obtain the basic trends in structural response of a plate under low-speed impact damage (Figure 5.26).

The plate is assumed to have zero out-of-plane deflection w all around its boundary (simply supported). It is also assumed that the plate is symmetric (B matrix = 0) and there is no bending twisting coupling ($D_{16} = D_{26} = 0$). Finally, the out-of-plane stresses σ_z , τ_{xz} , and τ_{yz} are neglected.

The goal is to determine the out-of-plane displacement w of the plate as a function of location. Since the B matrix of the layup of the plate is zero, the out-of-plain behavior of the plate decouples from the in-plane behavior. Then, the governing equation is (5.16) with $p_x = p_y = 0$ and the nonlinear terms neglected since we are interested in a linear (small deflections) solution:

$$D_{11} \frac{\partial^4 w}{\partial x^4} + 2(D_{12} + 2D_{66}) \frac{\partial^4 w}{\partial x^2 \partial y^2} + D_{22} \frac{\partial^4 w}{\partial y^4} = p_z \quad (5.16a)$$

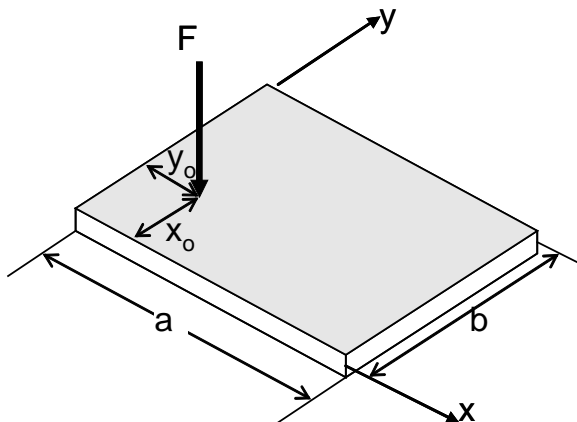


Figure 5.25 Composite plate under point load

The out-of-plane applied load p_z in this case can be expressed with the use of delta functions as

$$p_z = F\delta(x - x_o)\delta(y - y_o) \quad (5.44)$$

where

$$\begin{aligned} \delta(x - x_o) &= 1 && \text{when } x = x_o \\ &= 0 && \text{otherwise} \end{aligned}$$

Then, the governing equation is

$$D_{11}\frac{\partial^4 w}{\partial x^4} + 2(D_{12} + 2D_{66})\frac{\partial^4 w}{\partial x^2 \partial y^2} + D_{22}\frac{\partial^4 w}{\partial y^4} = F\delta(x - x_o)\delta(y - y_o) \quad (5.45)$$

with D_{ij} the bending stiffness terms for the plate layup.

Since $w = 0$ at the plate boundary, a solution to Equation (5.45) is sought in the form

$$w = \sum \sum A_{mn} \sin \frac{m\pi x}{a} \sin \frac{n\pi y}{b} \quad (5.46)$$

with A_{mn} unknown coefficients.

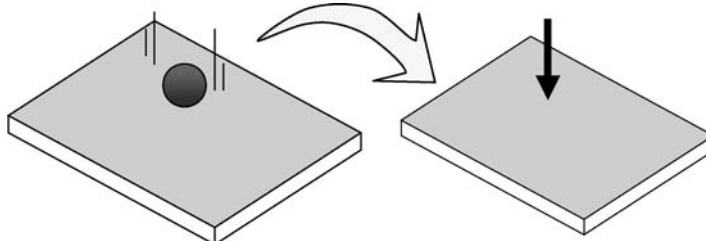


Figure 5.26 Low-speed impact modeled as point load

It can be seen that if Equation (5.46) is placed in ((5.45) the left-hand side will contain terms multiplied by $\sin(m\pi x/a)\sin(n\pi y/b)$. In order to proceed, the right-hand side of Equation (5.45) must also be expanded in a double Fourier series in order to be able to match terms in the left- and right-hand side. Setting,

$$F\delta(x - x_o)\delta(y - y_o) = \sum \sum B_{mn} \sin \frac{m\pi x}{a} \sin \frac{n\pi y}{b} \quad (5.47)$$

where B_{mn} are unknown coefficients, one can multiply both sides of (5.47) by $\sin(p\pi x/a)\sin(q\pi y/b)$ and integrate over the plate domain (x from 0 to a and y from 0 to b) to obtain,

$$\begin{aligned} & \iint F\delta(x - x_o)\delta(y - y_o) \sin \frac{p\pi x}{a} \sin \frac{q\pi y}{b} dx dy \\ &= \iint \sum \sum B_{mn} \sin \frac{m\pi x}{a} \sin \frac{p\pi x}{a} \sin \frac{n\pi y}{b} \sin \frac{q\pi y}{b} dx dy \end{aligned} \quad (5.48)$$

Now the integral of a function multiplied by the delta function is equal to the function evaluated at the location where the delta function is nonzero. So, carrying out the integrations in (5.48),

$$F \sin \frac{m\pi x_o}{a} \sin \frac{n\pi y_o}{b} = B_{mn} \frac{ab}{4} \quad (5.49)$$

from which

$$B_{mn} = \frac{4F}{ab} \sin \frac{m\pi x_o}{a} \sin \frac{n\pi y_o}{b} \quad (5.50)$$

Equation (5.50) can be placed in (5.47) which, along with (5.46), can be placed in (5.45) to give

$$\begin{aligned} & \sum_{m=1}^{\infty} \sum_{n=1}^{\infty} A_{mn} \left[D_{11} \left(\frac{m\pi}{a} \right)^4 + 2(D_{12} + 2D_{66}) \frac{m^2 n^2 \pi^4}{a^2 b^2} + D_{22} \left(\frac{n\pi}{b} \right)^4 \right] \sin \frac{m\pi x}{a} \sin \frac{n\pi y}{b} = \\ & \sum_{m=1}^{\infty} \sum_{n=1}^{\infty} \frac{4F}{ab} \sin \frac{m\pi x_o}{a} \sin \frac{n\pi y_o}{b} \sin \frac{m\pi x}{a} \sin \frac{n\pi y}{b} \end{aligned} \quad (5.51)$$

and matching coefficients of $\sin(m\pi x/a)\sin(n\pi y/b)$ the coefficients A_{mn} are determined as

$$A_{mn} = \frac{\frac{4F}{ab} \sin \frac{m\pi x_o}{a} \sin \frac{n\pi y_o}{b}}{D_{11} \left(\frac{m\pi}{a} \right)^4 + 2(D_{12} + 2D_{66}) \frac{m^2 n^2 \pi^4}{a^2 b^2} + D_{22} \left(\frac{n\pi}{b} \right)^4} \quad (5.52)$$

Combining Equation (5.52) with (5.46) gives the complete expression for w for this case:

$$w = \sum \sum \frac{\frac{4F}{ab} \sin \frac{m\pi x_o}{a} \sin \frac{n\pi y_o}{b} \sin \frac{m\pi x}{a} \sin \frac{n\pi y}{b}}{D_{11} \left(\frac{m\pi}{a} \right)^4 + 2(D_{12} + 2D_{66}) \frac{m^2 n^2 \pi^4}{a^2 b^2} + D_{22} \left(\frac{n\pi}{b} \right)^4} \quad (5.53)$$

For the case where F acts at the center of the plate, the maximum out-of-plane deflection δ at the plate center is obtained by substituting $x = x_o/2$ and $y = y_o/2$ in Equation (5.53),

$$\delta = w_{\max} = \sum \sum \frac{\frac{4F}{ab} \sin^2 \frac{m\pi}{2} \sin^2 \frac{n\pi}{2}}{D_{11} \left(\frac{m\pi}{a} \right)^4 + 2(D_{12} + 2D_{66}) \frac{m^2 n^2 \pi^4}{a^2 b^2} + D_{22} \left(\frac{n\pi}{b} \right)^4} \quad (5.54)$$

Once the deflections are determined, classical laminated-plate theory can be used to obtain bending moments and, in turn, strains and stresses to check the plate for failure.

As in the previous section, this is an exact solution to the problem within the context of the assumptions made. It should also be kept in mind that because of the linearization in Equation (5.16a), the solution is only valid for small out-of-plane deflections w .

5.4 Energy Methods

For most practical problems, the governing equations described in the previous section cannot be solved exactly and, in some cases, approximate solutions are hard to obtain. As a powerful alternative, energy methods can be used. Minimizing the energy stored in the system or structure can yield useful, approximate, and reasonably accurate solutions.

Two energy minimization principles are of interest here: (1) minimum potential energy; and (2) minimum complementary energy. In both cases, some of the governing equations are satisfied exactly and some approximately through energy minimization. They both derive from the following two theorems [17]:

Minimum potential energy: Of all *geometrically compatible displacement states*, those which also satisfy the *force balance conditions* give stationary values to the potential energy.

Minimum complementary energy: Of all *self-balancing force states*, those which also satisfy the requirements of *geometric compatibility* give stationary values to the *complementary energy*".

The governing equations, given in the previous section can be split into: (a) equilibrium equations; (b) compatibility equations (which are the strain compatibility equations obtained once the displacements are eliminated from the strain-displacement equations); and (c) the constitutive law or stress-strain equations.

In the case of the principle of minimum potential energy, if the strain compatibility relations and displacement boundary conditions are exactly satisfied, then minimization of the potential energy results in a solution that satisfies the equilibrium equations in an average sense. In the case of the principle of minimum complementary energy, if the stress equilibrium equations and force boundary conditions are exactly satisfied, then minimization of the complementary

Table 5.5 Approximate and exact evaluations of field equations during energy minimization

Equilibrium equations	Strain compatibility condition	Force boundary conditions	Displacement boundary conditions	Energy	Solution is
Exactly	Exactly	Exactly	Exactly	Minimized	Exact
Approximately	Exactly	(In an average sense)	Exactly	Minimize potential (displacement-based)	Approximate
Exactly	Approximately	Exactly	(In an average sense)	Minimize complementary	Approximate

energy results in a solution that satisfies strain compatibility in an average sense. Both approaches yield approximate solutions whose accuracy depends on the number of terms assumed in the displacement (minimum potential energy) or stress expressions (minimum complementary energy) and how well the assumed functions approximate the sought-for response.

The two situations as well as the situation corresponding to the exact solution are shown in Table 5.5.

The energy methods are not limited to the two approaches just described. Hybrid approaches where combinations of some stresses and displacements are assumed are also possible [18].

5.4.1 Energy Expressions for Composite Plates

According to the principle of virtual work for linear elasticity, the incremental internal energy stored in a body equals the incremental work done by external forces:

$$\delta U = \delta W_s + \delta W_b$$

where W_s is the work done by surface forces and W_b is the work done by body forces.

Then, if we define the total incremental energy $\delta\Pi$ as the difference between internal energy and external work,

$$\delta\Pi = \delta U - \delta W_s - \delta W_b \quad (5.55)$$

the exact solution would make the energy variation $\delta\Pi$ zero or would minimize the total energy Π :

$$\Pi = U - W_s - W_b = U - W \quad (5.56)$$

5.4.1.1 Internal Strain Energy \mathbf{U}

The increment in the internal potential energy δU is obtained by integrating all contributions of products of stresses and incremental strains

$$\delta U = \iiint_V \{ \sigma_x \delta \varepsilon_x + \sigma_y \delta \varepsilon_y + \sigma_z \delta \varepsilon_z + \tau_{yz} \delta \gamma_{yz} + \tau_{xz} \delta \gamma_{xz} + \tau_{xy} \delta \gamma_{xy} \} dx dy dz \quad (5.57)$$

where the integration is over the entire volume V of the body in question.

For a plate, Equation (5.57) reduces to

$$\delta U = \iiint_V \{ \sigma_x \delta \varepsilon_x + \sigma_y \delta \varepsilon_y + \tau_{xy} \delta \gamma_{xy} \} dx dy dz \quad (5.58)$$

Using equations (5.7) to substitute for the strains in terms of curvatures and midplane strains gives

$$\delta U = \iiint_V \{ \sigma_x (\delta \varepsilon_{xo} + z \delta \kappa_x) + \sigma_y (\delta \varepsilon_{yo} + z \delta \kappa_y) + \tau_{xy} (\delta \gamma_{xyo} + z \delta \kappa_{xy}) \} dx dy dz \quad (5.59)$$

For a plate of constant thickness h , the z integration in Equation (5.59) can be carried out using

$$\int_{-\frac{h}{2}}^{\frac{h}{2}} \begin{bmatrix} \sigma_x \\ \sigma_y \\ \tau_{xy} \end{bmatrix} dz = \begin{bmatrix} N_x \\ N_y \\ N_{xy} \end{bmatrix} \text{ and } \int_{-\frac{h}{2}}^{\frac{h}{2}} \begin{bmatrix} z \sigma_x \\ z \sigma_y \\ z \tau_{xy} \end{bmatrix} dz = \begin{bmatrix} M_x \\ M_y \\ M_{xy} \end{bmatrix}$$

to give

$$\delta U = \iint_A \{ N_x \delta \varepsilon_{xo} + N_y \delta \varepsilon_{yo} + N_{xy} \delta \gamma_{xyo} + M_x \delta \kappa_x + M_y \delta \kappa_y + M_{xy} \delta \kappa_{xy} \} dx dy \quad (5.60)$$

where A is the area of the plate.

At this point, several options are available depending on which version of energy minimization principle (e.g. displacement-based or stress-based) is to be used.

For a displacement-based formulation, Equations (5.5) can be used to express

$$\begin{aligned} \delta U = & \iint_A \{ (A_{11} \varepsilon_{xo} + A_{12} \varepsilon_{yo} + A_{16} \gamma_{xyo} + B_{11} \kappa_x + \dots) \delta \varepsilon_{xo} \\ & + (A_{12} \varepsilon_{xo} + A_{22} \varepsilon_{yo} + A_{26} \gamma_{xyo} + B_{12} \kappa_x + \dots) \delta \varepsilon_y \\ & + (A_{16} \varepsilon_{xo} + A_{26} \varepsilon_{yo} + A_{66} \gamma_{xyo} + B_{16} \kappa_x + \dots) \delta \gamma_{xyo} \\ & + (B_{11} \varepsilon_{xo} + B_{12} \varepsilon_{yo} + B_{16} \gamma_{xyo} + D_{11} \kappa_x + \dots) \delta \kappa_x \\ & + (B_{12} \varepsilon_{xo} + B_{22} \varepsilon_{yo} + B_{26} \gamma_{xyo} + D_{12} \kappa_x + \dots) \delta \kappa_y \\ & + (B_{16} \varepsilon_{xo} + B_{26} \varepsilon_{yo} + B_{66} \gamma_{xyo} + D_{16} \kappa_x + \dots) \delta \kappa_{xy} \} dx dy \end{aligned} \quad (5.61)$$

forces and moments in terms of midplane strains and curvatures.

It is now observed that

$$\varepsilon_{xo}\delta\varepsilon_{xo} = \frac{1}{2}\delta(\varepsilon_{xo})^2$$

$$\varepsilon_{xo}\delta\varepsilon_{yo} + \varepsilon_{yo}\delta\varepsilon_{xo} = \delta(\varepsilon_{xo}\varepsilon_{yo})$$

$$\varepsilon_{xo}\delta\kappa_x + \kappa_x\delta\varepsilon_{xo} = \delta(\varepsilon_{xo}\kappa_x)$$

with analogous expressions for the other midplane strains and curvatures.

These expressions are substituted in Equation (5.61) and integrated term by term. For example, the first term of (5.61) becomes

$$\iint_A A_{11}(\varepsilon_{xo})\delta\varepsilon_{xo}dxdy = \frac{1}{2}\iint_A A_{11}\delta(\varepsilon_{xo})^2dxdy \rightarrow \frac{1}{2}\iint_A A_{11}(\varepsilon_{xo})^2dxdy$$

This substitution leads to the following expression for the internal strain energy U :

$$\begin{aligned} U = & \frac{1}{2}\iint_A \left\{ A_{11}(\varepsilon_{xo})^2 + 2A_{12}(\varepsilon_{xo})(\varepsilon_{yo}) + 2A_{16}(\varepsilon_{xo})(\gamma_{xyo}) + A_{22}(\varepsilon_{yo})^2 + 2A_{26}(\varepsilon_{yo})(\gamma_{xyo}) + A_{66}(\gamma_{xyo})^2 \right\} dxdy \\ & + \iint_A \left\{ B_{11}(\varepsilon_{xo})\kappa_x + B_{12}((\varepsilon_{yo})\kappa_x + (\varepsilon_{xo})\kappa_y) + B_{16}((\gamma_{xyo})\kappa_x + (\varepsilon_{xo})\kappa_{xy}) + B_{22}(\varepsilon_{yo})\kappa_y + B_{26}((\gamma_{xyo})\kappa_y + (\varepsilon_{yo})\kappa_{xy}) + B_{66}(\gamma_{xyo})\kappa_{xy} \right\} dxdy \\ & + \frac{1}{2}\iint_A \left\{ D_{11}\kappa_x^2 + 2D_{12}\kappa_x\kappa_y + 2D_{16}\kappa_x\kappa_{xy} + D_{22}\kappa_y^2 + 2D_{26}\kappa_y\kappa_{xy} + D_{66}\kappa_{xy}^2 \right\} dxdy \end{aligned} \quad (5.62)$$

Finally, to express the internal strain energy in terms of displacements u , v , and w , the strain–displacement equations (5.6) and (5.8) are used to obtain:

$$\begin{aligned} U = & \frac{1}{2}\iint_A \left\{ A_{11}\left(\frac{\partial u}{\partial x}\right)^2 + 2A_{12}\frac{\partial u}{\partial x}\frac{\partial v}{\partial y} + 2A_{16}\frac{\partial u}{\partial x}\left(\frac{\partial u}{\partial y} + \frac{\partial v}{\partial x}\right) + A_{22}\left(\frac{\partial v}{\partial y}\right)^2 \right. \\ & \left. + 2A_{26}\frac{\partial v}{\partial y}\left(\frac{\partial u}{\partial y} + \frac{\partial v}{\partial x}\right) + A_{66}\left(\frac{\partial u}{\partial y} + \frac{\partial v}{\partial x}\right)^2 \right\} dxdy \\ & - \iint_A \left\{ B_{11}\frac{\partial u}{\partial x}\frac{\partial^2 w}{\partial x^2} + B_{12}\left(\frac{\partial v}{\partial y}\frac{\partial^2 w}{\partial x^2} + \frac{\partial u}{\partial x}\frac{\partial^2 w}{\partial y^2}\right) + B_{16}\left[\left(\frac{\partial u}{\partial y} + \frac{\partial v}{\partial x}\right)\frac{\partial^2 w}{\partial x^2} + 2\frac{\partial u}{\partial x}\frac{\partial^2 w}{\partial x\partial y}\right] \right. \\ & \left. + B_{22}\frac{\partial v}{\partial y}\frac{\partial^2 w}{\partial y^2} + B_{26}\left[\left(\frac{\partial u}{\partial y} + \frac{\partial v}{\partial x}\right)\frac{\partial^2 w}{\partial y^2} + 2\frac{\partial v}{\partial y}\frac{\partial^2 w}{\partial x\partial y}\right] + 2B_{66}\left(\frac{\partial u}{\partial y} + \frac{\partial v}{\partial x}\right)\frac{\partial^2 w}{\partial x\partial y} \right\} dxdy \\ & + \frac{1}{2}\iint_A \left\{ D_{11}\left(\frac{\partial^2 w}{\partial x^2}\right)^2 + 2D_{12}\frac{\partial^2 w}{\partial x^2}\frac{\partial^2 w}{\partial y^2} + 4D_{16}\frac{\partial^2 w}{\partial x^2}\frac{\partial^2 w}{\partial x\partial y} + D_{22}\left(\frac{\partial^2 w}{\partial y^2}\right)^2 \right. \\ & \left. + 4D_{26}\frac{\partial^2 w}{\partial y^2}\frac{\partial^2 w}{\partial x\partial y} + 4D_{66}\left(\frac{\partial^2 w}{\partial x\partial y}\right)^2 \right\} dxdy \end{aligned} \quad (5.63)$$

The first set of terms in Equation (5.63) involves the membrane stiffnesses A_{ij} ($i,j = 1,2,6$) and represents stretching (or membrane) energy. The last set, involving bending stiffnesses D_{ij} ($i,j = 1,2,6$) represents energy stored in bending of the plate. The remaining terms, involving B_{ij} ($i,j = 1,2,6$) represent energy stored through bending–membrane coupling. If the plate has symmetric layup, $B_{ij} = 0$ and Equation (5.63) decouples in two parts, the membrane (involving the A matrix) and the bending (involving the D matrix) portion.

At the other extreme, a stress-based energy formulation starts with Equation (5.60) and uses the inverse of the stress–strain equations (5.5) to substitute for the strains. For simplicity, only the case of a symmetric layup is shown here. The inverted stress–strain equations,

$$\begin{Bmatrix} \varepsilon_x^o \\ \varepsilon_y^o \\ \gamma_{xy}^o \\ \kappa_x \\ \kappa_y \\ \kappa_{xy} \end{Bmatrix} = \begin{Bmatrix} a_{11} & a_{12} & a_{16} & 0 & 0 & 0 \\ a_{12} & a_{22} & a_{26} & 0 & 0 & 0 \\ a_{16} & a_{26} & a_{66} & 0 & 0 & 0 \\ 0 & 0 & 0 & d_{11} & d_{12} & d_{16} \\ 0 & 0 & 0 & d_{12} & d_{22} & d_{26} \\ 0 & 0 & 0 & d_{16} & d_{26} & d_{66} \end{Bmatrix} \begin{Bmatrix} N_x \\ N_y \\ N_{xy} \\ M_x \\ M_y \\ M_{xy} \end{Bmatrix} \quad (5.64)$$

where $[a]$ and $[d]$ are the inverses of the laminate $[A]$ and $[D]$ matrices, can be used to substitute in Equation (5.60):

$$\begin{aligned} \delta U = & \iint_A \{N_x \delta(a_{11}N_x + a_{12}N_y + a_{16}N_{xy}) + N_y \delta(a_{12}N_x + a_{22}N_y + a_{26}N_{xy}) \\ & + N_{xy} \delta(a_{16}N_x + a_{26}N_y + a_{66}N_{xy}) + M_x \delta(d_{11}M_x + d_{12}M_y + d_{16}M_{xy}) \\ & + M_y \delta(d_{12}M_x + d_{22}M_y + d_{26}M_{xy}) + M_{xy} \delta(d_{16}M_x + d_{26}M_y + d_{66}M_{xy})\} dx dy \end{aligned} \quad (5.65)$$

A completely analogous procedure as in deriving Equation (5.63) from (5.61) leads to the final expression for the stress-based (complementary) energy:

$$\begin{aligned} U = & \frac{1}{2} \iint_A \left\{ a_{11}N_x^2 + 2a_{12}N_xN_y + 2a_{16}N_xN_{xy} + a_{22}N_y^2 + 2a_{26}N_yN_{xy} + a_{66}N_{xy}^2 \right\} dx dy \\ & + \frac{1}{2} \iint_A \left\{ d_{11}M_x^2 + 2d_{12}M_xM_y + 2d_{16}M_xM_{xy} + d_{22}M_y^2 + 2d_{26}M_yM_{xy} + d_{66}M_{xy}^2 \right\} dx dy \end{aligned} \quad (5.66)$$

Equation (5.66) has the stretching and bending portions already decoupled because the laminate was assumed symmetric.

5.4.1.2 External Work \mathbf{W}

The derivation for the external work does not have any difference between composite and noncomposite plates. It is derived for a general plate and included here for completeness. With

reference to Equation (5.55), the incremental work δW_b done by applied body forces on a body is given by

$$\delta W_b = \iiint V \{f_x \delta u + f_y \delta v + f_z \delta w\} dx dy dz$$

where V is the volume of the body, f_x, f_y, f_z are forces per unit volume in the x, y and z directions respectively, and $\delta u, \delta v$, and δw are incremental displacements in the x, y and z directions.

For a plate, the body forces can be integrated through the thickness

$$\begin{aligned}\int f_x dz &= p_{xb} \\ \int f_y dz &= p_{yb} \\ \int f_z dz &= p_{zb}\end{aligned}$$

with the subscript b denoting that these contributions to surface forces come from integrating the body forces.

Combining these with any surface forces applied over the plate surface and the contribution from any forces or moments applied on the plate edges, gives

$$\begin{aligned}\delta W = \delta W_b + \delta W_s &= \iint_{Ap} \{p_x \delta u + p_y \delta v + p_z \delta w\} dx dy + \\ &\int_0^a \left[N_x \delta u + N_{xy} \delta v + Q_x \delta w - M_x \delta \left(\frac{\partial w}{\partial x} \right) \right]_{x=0}^{x=a} dy + \\ &\int_0^a \left[N_{xy} \delta u + N_y \delta v + Q_y \delta w - M_y \delta \left(\frac{\partial w}{\partial y} \right) \right]_{y=0}^{y=b} dx\end{aligned}$$

where a and b are the plate dimensions and A_p is the plate area. The contributions from p_{xb}, p_{yb} , and p_{zb} are included in the first term within p_x, p_y , and p_z respectively. The second and third terms in the right-hand side of the above expression include contributions from applied forces N_x, N_y , and N_{xy} (in-plane) or (transverse shear) forces Q_x and Q_y (out-of-plane) or bending moments M_x and M_y at the plate edges ($x = 0, a$ and/or $y = 0, b$).

Integrating the incremental contributions on left- and right-hand sides gives

$$\begin{aligned}W = \iint_{Ap} \{p_x u + p_y v + p_z w\} dx dy + \int_0^b \left[N_x u + N_{xy} v + Q_x w - M_x \frac{\partial w}{\partial x} \right]_{x=0}^{x=a} dy + \\ \int_0^a \left[N_{xy} u + N_y v + Q_y w - M_y \frac{\partial w}{\partial y} \right]_{y=0}^{y=b} dx\end{aligned}\tag{5.67}$$

For the case of plate buckling problems, p_x and p_y in Equation (5.67) can be evaluated further. Assuming there is no stretching or shearing of the plate midplane during buckling, the

mid-plane strains ε_{xo} , ε_{yo} and γ_{xyo} are zero. Then, for large deflections, Equations (5.13a–c) imply

$$\frac{\partial u}{\partial x} + \frac{1}{2} \left(\frac{\partial w}{\partial x} \right)^2 = 0$$

$$\frac{\partial v}{\partial y} + \frac{1}{2} \left(\frac{\partial w}{\partial y} \right)^2 = 0$$

$$\frac{\partial u}{\partial y} + \frac{\partial v}{\partial x} + \left(\frac{\partial w}{\partial x} \right) \left(\frac{\partial w}{\partial y} \right) = 0$$

Consider now the first term of Equation (5.67) with $p_z = 0$ for a buckling problem. Using Equations (5.3a,b) to substitute for p_x and p_y ,

$$\iint_A (p_x u + p_y v) dx dy = \iint_A \left\{ \left(-\frac{\partial N_x}{\partial x} - \frac{\partial N_{xy}}{\partial y} \right) u + \left(-\frac{\partial N_{xy}}{\partial x} - \frac{\partial N_y}{\partial y} \right) v \right\} dx dy$$

Integrating by parts, for a rectangular plate of dimensions a and b , gives

$$\begin{aligned} \iint_A (p_x u + p_y v) dx dy &= \int_0^b \left\{ \left[-N_x u - N_{xy} v \right]_{x=0}^{x=a} + \int_0^a \left[N_x \frac{\partial u}{\partial x} + N_{xy} \frac{\partial v}{\partial x} \right] dx \right\} dy \\ &\quad + \int_0^a \left\{ \left[-N_{xy} u - N_y v \right]_{y=0}^{y=b} + \int_0^b \left[N_{xy} \frac{\partial u}{\partial y} + N_y \frac{\partial v}{\partial y} \right] dy \right\} dx \\ &= \int_0^a \left[-N_{xy} u - N_y v \right]_{y=0}^{y=b} dx + \int_0^b \left[-N_x u - N_{xy} v \right]_{x=0}^{x=a} dy \\ &\quad + \iint_{0,0}^{a,b} \left[N_x \frac{\partial u}{\partial x} + N_{xy} \frac{\partial v}{\partial x} + N_{xy} \frac{\partial u}{\partial y} + N_y \frac{\partial v}{\partial y} \right] dx dy \end{aligned}$$

The derivatives $\partial u / \partial x$, $\partial v / \partial y$, and the sum $\partial u / \partial y + \partial v / \partial x$ can be substituted for derivatives of w , as shown in the large deflection equations above. Then, combining everything in Equation (5.67), canceling terms and noting that for a typical buckling problem $Q_x = Q_y = M_x = M_y = 0$ leads to

$$W = \iint_{0,0}^{a,b} \left\{ -\frac{1}{2} N_x \left(\frac{\partial w}{\partial x} \right)^2 - \frac{1}{2} N_y \left(\frac{\partial w}{\partial y} \right)^2 - N_{xy} \left(\frac{\partial w}{\partial x} \right) \left(\frac{\partial w}{\partial y} \right) \right\} dx dy$$

or

$$W = -\frac{1}{2} \int_0^a \int_0^b \left\{ N_x \left(\frac{\partial w}{\partial x} \right)^2 + N_y \left(\frac{\partial w}{\partial y} \right)^2 + 2N_{xy} \left(\frac{\partial w}{\partial x} \right) \left(\frac{\partial w}{\partial y} \right) \right\} dx dy \quad (5.68)$$

valid for plate buckling problems.

Exercises

5.1 A certain composite material is proposed for use at two different locations of the same application. Location 1 is designed by tension with a design (ultimate) load of 1750 N/mm. Location 2 is designed by shear with a design (ultimate) load of 2450 N/mm. The proposed material has been tested in tension and shear with the results shown in Table E5.1.

Table E5.1 Test data for proposed composite material

Specimen	Tension (Pa)	Shear (Pa)
1		3.0918E + 08
2	6.7217E + 08	4.0789E + 08
3	6.1025E + 08	3.2922E + 08
4	6.3263E + 08	2.9084E + 08
5	6.5498E + 08	3.6868E + 08
6	5.3391E + 08	3.3140E + 08
7	6.5647E + 08	3.6039E + 08
Mean	6.2673E + 08	3.4251E + 08

Originally, the two parts at the locations of interest were made with aluminum with the following properties:

Table E5.2 Aluminum properties (7075 Al from [19])

	Tension (Pa)	Shear (Pa)
Mean	5.1016E + 08	3.2815E + 08
B-Basis	4.9637E + 08	3.2402E + 08
A-Basis	4.7569E + 08	3.1712E + 08

An aspiring engineer looks at the two tables of properties, in particular the mean values, and claims that he/she can save at least 30% of the weight at both locations by switching from aluminum to composite. You are to check if the engineer is right in his/her claim for both locations considering: (a) a single load path application and (b) a multiple load path application.

You are to assume that the test data in Table E5.1 follows a normal distribution for both tension and shear. Note that for a normal distribution the B- and A-Basis values are given by

$$B = \text{Mean} - k_B \sigma$$

$$A = \text{Mean} - k_A \sigma$$

where σ is the standard deviation of the test results and k_A, k_B are the so-called one-sided tolerance limit factors given by (see for example [2] chapter 9).

Table E5.3 One-sided tolerance limit factors for normal distribution

Number of specimens	$k_{90}^{(1)}$	$k_{99}^{(1)}$
6	3.006	5.741
7	2.755	4.642

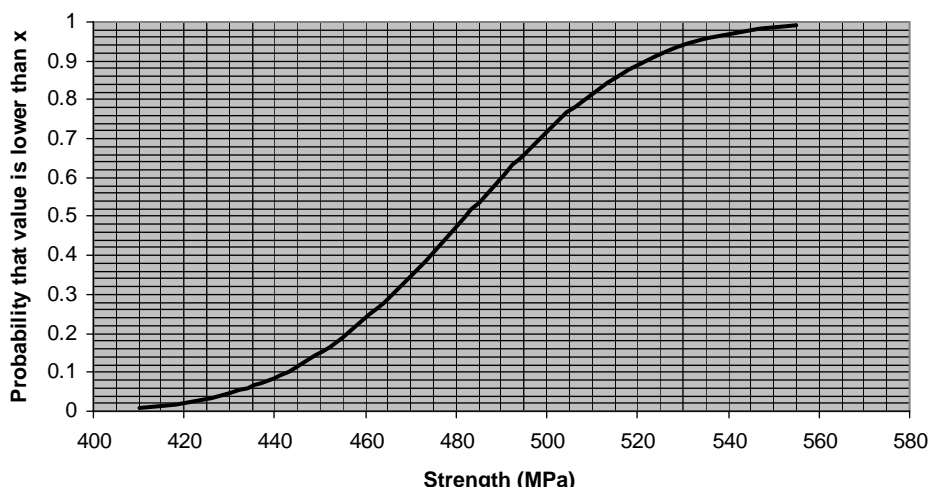
⁽¹⁾ 90 and 99 refer to the % of tests that will be stronger than the corresponding Basis value

In your calculations consider ONLY the material scatter. Do not include effects of damage and environment.

- 5.2 The tension strength data for a specific composite material and layup at RTA conditions is given in the table below:

Specimen	Value (MPa)
1	538.8
2	475.6
3	447.9
4	461.7
5	495.4
6	483
7	479.3
8	442.5
9	471.6
10	525.5

Assuming that the experimental data are normally distributed, it can be shown that the fraction of the population with strength less than any given value (cumulative probability) is given by the following graph:



Assume that at any other environmental condition, the tension strength is given as a fraction of its corresponding value at RTA condition and that fraction can be obtained from the material covered in this chapter.

This composite material and layup are to be used in a wing-box (single load path primary structure). The best available aluminum is 7075-T6 with the following properties (from reference [19]):

	RTA	ETW
Mean (MPa)	586.0	562.5
B-Basis (MPa)	551.5	529.4
A-Basis (MPa)	537.7	516.2
Density (kg/m^3)	2773.8	2773.8

Determine the weight savings of using the composite instead of aluminum if: (a) the design is based on RTA properties and (b) the design is based on ETW properties. Looking at your results, are the weight savings resulting from using composites in this application worth the extra material and processing cost associated with composites?

- 5.3 A simply-supported rectangular composite plate (Figure E5.1) with dimensions 152.4×508 mm is loaded at $x = 127$ mm and $y = 38.1$ mm by a force F perpendicular to the plate. The layup of the plate is $(\pm 45)/(0/90)_3/(\pm 45)$ and the basic material properties are as shown in Figure E5.1.

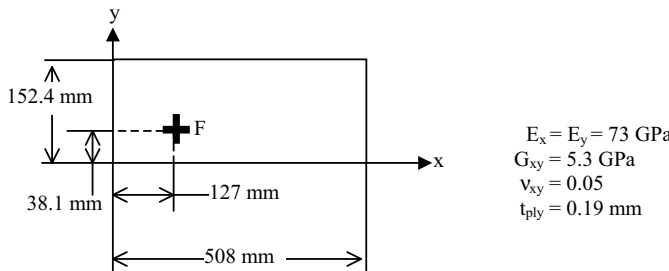


Figure E5.1

- (a) Determine the location in the plate where each of the three stresses σ_x , σ_y , and τ_{xy} is maximized.
- (b) Since the three stresses do not reach their peak values at the same location, discuss how one would go about predicting the load F at which the plate would fail (assume that the ultimate strength values such as X^t , X^c , Y^t , Y^c , and S with X strength along fibers or warp direction for a plain weave fabric and Y strength perpendicular to the fibers or fill direction for a plain weave fabric, and superscripts t and c tension and compression respectively, are known).
- (c) Determine the maximum values of the through the thickness averaged out-of-plane shear stresses τ_{xz} , and τ_{yz} and their locations for a unit load $F = 1 \text{ N}$. Compare these

values with the maximum values for σ_x , σ_y , and τ_{xy} from part (a) and comment on whether the assumption made in section 5.3.2 that τ_{xz} , and τ_{yz} can be neglected is valid.

- 5.4 For a composite rectangular panel simply supported all around under pressure loading, determine if the linear solution for the out-of-plane deflections is sufficient to use in design. The applied pressure corresponds to an overload pressure case of a pressurized composite fuselage of almost 1.4 atmospheres or 20 psi. (Note: the units are British (Imperial) in this problem because you are to use the ESDU data sheets which have charts in these units). The situation is shown in Figure E5.2.

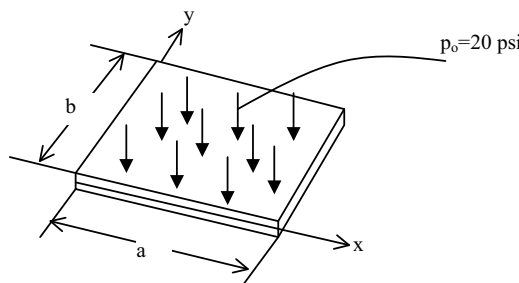


Figure E5.2

- Derive an expression for the deflection at the center of the plate δ .
- For the case $a = b = 50$ in, $D_{11} = D_{22} = 347\ 000$ in lb, $D_{12} = 110\ 000$ in lb, $D_{66} = 120\ 000$ in lb and $t = 0.5$ in, the solution for δ as a function of p_o can be found in the ESDU data sheets. The ESDU solution is a large-deflection, moderate-rotation solution that will be more accurate as the applied pressure increases. Find the ESDU solution and plot δ versus applied pressure for pressures from 0 to 20 psi for your solution and the ESDU solution. Compare the two solutions and determine when your (linear) solution departs significantly from the ESDU (nonlinear) solution. Can your linear solution be used for the overpressure case of 20 psi? Before you give your final answer on this, keep in mind that this is a design problem so you do not always have to be accurate as long as you are conservative (and can afford the associated increase in weight).
- In view of your comparison in Exercise 5.4, and the ESDU curves you found, what exactly does ‘simply supported plate’ mean in this case? (discuss in-plane and out-of plane boundary conditions that your linear solution satisfies versus the cases that ESDU provides)

References

- Gürdal, Z., Haftka, R.T., and Hajela, P. *Design and Optimization of Laminated Composite Materials*, John Wiley and Sons, Inc, 1999, Chapter 5.4.
- Metallic Materials and Elements for Aerospace Vehicle Structures*, Military Handbook 5H, US Department of Defense, December 1998, Chapter 9.

3. *Composite Materials Handbook*, Mil-Hdbk-17-1F, US Department of Defense, vol. 1, 2002, Chapter 8.3.
4. Whitehead, R.S., Lessons Learned for Composite Structures, *Proc 1st NASA Advanced Composites Technology Conf., Seattle WA*, 1990, pp 399–415.
5. Williams, J.C., Effect of Impact Damage and Open Holes on the Compression Strength of tough resin/high strength fiber laminates, *NASA-TM-85756*, 1984.
6. Puhui, C., Zhen, S. and Junyang, W., A New Method for Compression After Impact Strength Prediction of Composite Laminates, *Journal of Composite Materials*, **36**, 589–610 (2002).
7. Kassapoglou, C., Jonas, P.J. and Abbott, R., Compressive Strength of Composite Sandwich Panels after Impact Damage: An Experimental and Analytical Study, *Journal of Composites Technology and Research*, **10**, 65–73 (1988).
8. Nyman, T., Bredberg, A. and Schoen, J., Equivalent Damage and Residual Strength of Impact Damaged Composite Structures, *Journal of Reinforced Plastics and Composites*, **19**, 428–448 (2000).
9. Dost, E.F., Ilcewicz, L.B., Avery, W.B., and Coxon, B.R., Effect of Stacking Sequence on Impact Damage Resistance and Residual Strength for Quasi-isotropic Laminates, *ASTM STP 1110*, 1991, pp 476–500.
10. Xiong, Y., Poon, C., Straznicky, P.V., and Vietinghoff, H., A Prediction Method for the Compressive Strength of Impact Damaged Composite Laminates, *Composite Structures*, **30**, 357–367 (1993).
11. Kassapoglou, C., Compression Strength of Composite Sandwich Structures After Barely Visible Impact Damage, *Journal of Composites Technology and Research*, 1996, 274–284.
12. Rivello, R.M., *Theory and Analysis of Flight Structures*, McGraw-Hill Book Co., 1969, Chapter 2.
13. Whitney, J.M., *Structural Analysis of Laminated Anisotropic Plates*, Technomic Publishing Co., Lancaster PA, 1987, Chapters 1 and 2.
14. Herakovich, C.T., *Mechanics of Fibrous Composites*, John Wiley and Sons, Inc, 1998, Chapter 5.
15. Kassapoglou, C. and Bauer, G., Composite Plates Under Concentrated Load on One End and Distributed Load on the Opposite End, *Mechanics of Advanced Materials and Structures*, **17**, 196–203 (2010).
16. Hildebrand, F.B., *Advanced Calculus for Applications*, Prentice Hall, Englewood Cliffs, New Jersey, 1976, Chapter 9.
17. Crandall, S.H. *Engineering Analysis*, McGraw-Hill, 1956, Section 4.4.
18. Pian, T.H.H., Variational principles for incremental finite element methods, *Journal of the Franklin Institute*, **302**, 473–488 (1976).
19. *Metallic Materials and Elements for Aerospace Vehicle Structures*, Military Handbook 5H, US Department of Defense, December 1998, Chapter 3.

6

Buckling of Composite Plates

Composite plates under compression and/or shear loading are sensitive to buckling failures. A typical situation where a stiffened composite plate has buckled between the stiffeners is shown in Figure 6.1.

Unlike beams, where buckling is, typically, very close to final failure, plates may have significant post-buckling ability (see Chapter 7). However, post-buckling of composite plates requires accurate knowledge of the possible failure modes and their potential interaction. For example, in a stiffened panel such as that of Figure 6.1, the portion of the skin buckling away from the reader tends to peel off the stiffeners. The skin–stiffener separation mode is fairly common in post-buckled stiffened panels and may lead to premature failure. Depending on the application, designing for buckling and using any post-buckling capability as an extra degree of conservatism is one of the possible approaches. Even in post-buckled panels, accurate calculation of the buckling load for different loading combinations and boundary conditions is paramount in the design.

6.1 Buckling of Rectangular Composite Plate under Biaxial Loading

The derivation of the buckling equation follows the approach described by Whitney [1]. A rectangular composite plate under biaxial loading is shown in Figure 6.2.

The governing equation is obtained from Equation (5.16) by setting $N_{xy} = p_x = p_y = p_z = 0$:

$$D_{11} \frac{\partial^4 w}{\partial x^4} + 2(D_{12} + 2D_{66}) \frac{\partial^4 w}{\partial x^2 \partial y^2} + D_{22} \frac{\partial^4 w}{\partial y^4} = N_x \frac{\partial^2 w}{\partial x^2} + N_y \frac{\partial^2 w}{\partial y^2} \quad (6.1)$$

where w is the out-of-plane displacement of the plate.

Note that the governing equation (6.1) assumes that the bending–twisting coupling terms D_{16} and D_{26} are negligible compared with the remaining terms D_{11} , D_{12} , D_{22} , and D_{66} . The plate is assumed simply supported all around its boundary and the only loads applied are N_x and N_y as shown in Figure 6.2. Then, the boundary conditions are,

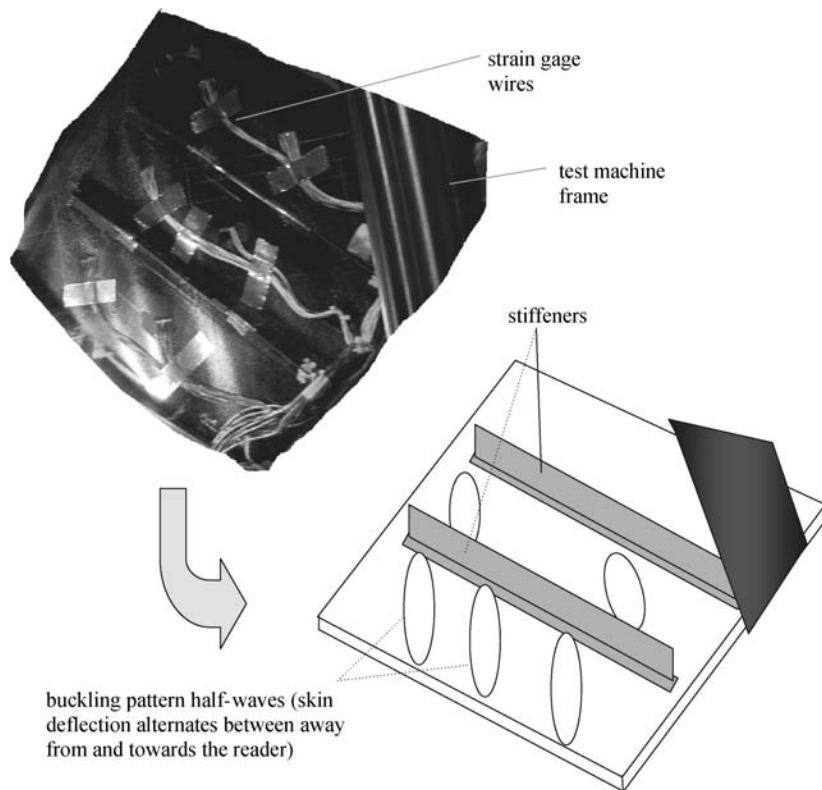


Figure 6.1 Composite stiffened panel buckling under shear (See Plate 14 for the colour figure)

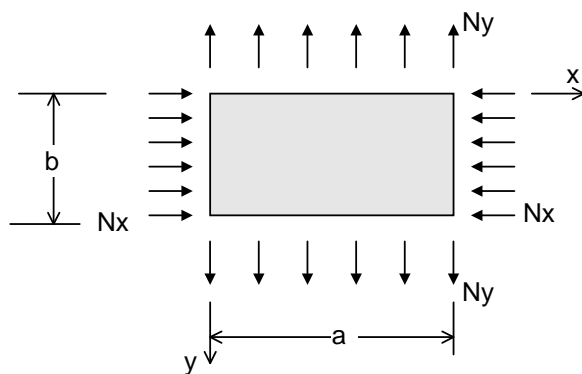


Figure 6.2 Rectangular composite panel under biaxial loading

$$\begin{aligned} w = M_x &= -D_{11} \frac{\partial^2 w}{dx^2} - D_{12} \frac{\partial^2 w}{dy^2} = 0 \quad \text{at } x = 0 \text{ and } x = a \\ w = M_y &= -D_{12} \frac{\partial^2 w}{dx^2} - D_{22} \frac{\partial^2 w}{dy^2} = 0 \quad \text{at } y = 0 \text{ and } y = b \end{aligned} \quad (6.2)$$

An expression for w that satisfies all boundary conditions (Equations (6.2)) is,

$$w = \sum \sum A_{mn} \sin \frac{m\pi x}{a} \sin \frac{n\pi y}{b} \quad (6.3)$$

Substituting in Equation (6.1) and rearranging and defining the plate aspect ratio $AR = a/b$ gives,

$$\pi^2 A_{mn} [D_{11} m^4 + 2(D_{12} + 2D_{66}) m^2 n^2 (AR)^2 + D_{22} n^4 (AR)^4] = -A_{mn} a^2 [N_x m^2 + N_y n^2 (AR)^2] \quad (6.4)$$

When buckling occurs, the out-of-plane deflection w of the plate is nonzero. This means that the coefficients A_{mn} of Equation (6.3) are nonzero and cancel out in Equation (6.4). It is convenient to let $k = N_y/N_x$ and to let the buckling load N_x be denoted by $-N_o$ (minus sign to indicate compression). Then, from Equation (6.4),

$$N_o = \frac{\pi^2 [D_{11} m^4 + 2(D_{12} + 2D_{66}) m^2 n^2 (AR)^2 + D_{22} n^4 (AR)^4]}{a^2 (m^2 + kn^2 (AR)^2)} \quad (6.5)$$

The buckling load N_o is a function of the number of half-waves m in the x direction and n in the y direction and thus, changes as m and n , which define the buckling mode, change. The sought-for buckling load is the lowest value of Equation (6.5) so the right-hand side of (6.5) must be minimized with respect to m and n .

As an application of Equation (6.5), consider a square plate with quasi-isotropic layup $[(45/-45)_2/0_2/90_2]_s$ with basic ply properties (x parallel to fibers):

$$E_x = 137.9 \text{ GPa}$$

$$E_y = 11.7 \text{ GPa}$$

$$v_{xy} = 0.31$$

$$G_{xy} = 4.82 \text{ GPa}$$

$$t_{\text{ply}} = 0.1524 \text{ mm}$$

where t_{ply} is the (cured) ply thickness.

Determine the compressive buckling load N_o for various values of k .

Using classical laminated-plate theory (CLPT) the bending stiffness terms are found to be:

$$D_{11} = 65.4 \text{ kN/mm}$$

$$D_{12} = 37.2 \text{ kN/mm}$$

$$D_{22} = 51.1 \text{ kN/mm}$$

$$D_{66} = 38.6 \text{ kN/mm}$$

$$D_{16} = 5.40 \text{ kN/mm}$$

$$D_{26} = 5.40 \text{ kN/mm}$$

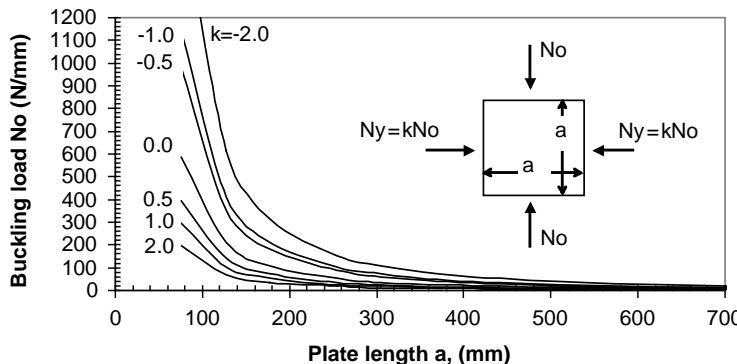


Figure 6.3 Buckling load of a square quasi-isotropic plate as a function of plate size and biaxial loading ratio N_y/N_x

The bending-twisting coupling terms D_{16} and D_{26} are less than 15% of the next larger term so using Equation (6.1) will give accurate trends and reasonable buckling predictions.

For a given value of k , Equation (6.5) is evaluated for successive values of n and m until the combination that minimizes the buckling load N_o is obtained. This load is shown in Figure 6.3 as a function of the plate size and different ratios k .

As expected, increasing the plate size decreases the buckling load, which varies with the inverse of the square of the plate size. Both positive and negative values of k are shown in Figure 6.3. Positive values mean that the sign of N_y is the same as N_o . And since N_o is compressive, $k > 0$ implies biaxial compression. Then, negative values of k correspond to tensile N_y values. As is seen from Figure 6.3, a tensile N_y ($k < 0$) tends to stabilize the plate and increase its buckling load. Compressive N_y ($k > 0$) tends to precipitate buckling earlier (material is pushed from both x and y directions) and decreases the buckling load. The case of $k = 0$ corresponds to uniaxial compression (see below).

It is interesting to note that the minimum buckling load was obtained for $n = 1$ in all cases. It can be shown [2, 3] that for a rectangular plate under biaxial loading the number of half-waves n in one of the two directions will always be 1.

Finally, Equation (6.5) also gives negative values of N_o when $k < 0$. This means that N_o is tensile and, since $k < 0$, N_y is compressive. So the plate still buckles, but now the compressive load is in the y direction while the load in the x direction is tensile.

6.2 Buckling of Rectangular Composite Plate under Uniaxial Compression

This case was derived as a special case in the previous section when $k = 0$. The buckling load when the plate is under compression is given by Equation (6.5) with k set to zero:

$$N_o = \frac{\pi^2 [D_{11}m^4 + 2(D_{12} + 2D_{66})m^2n^2(AR)^2 + D_{22}n^4(AR)^4]}{a^2m^2} \quad (6.6)$$

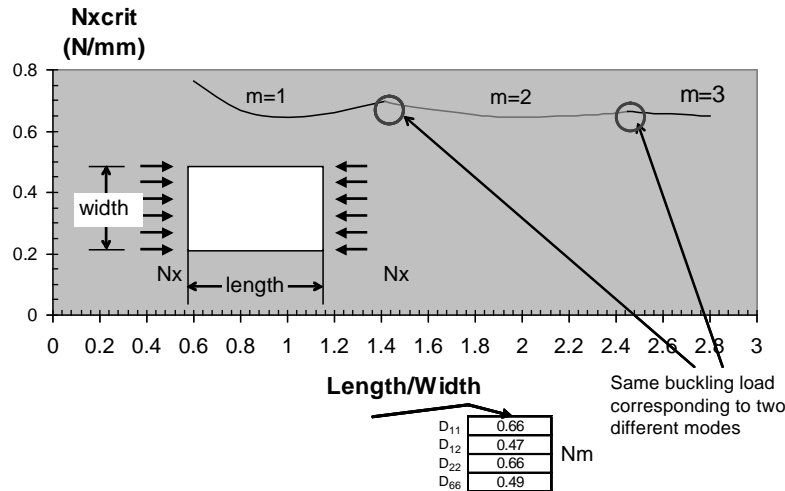


Figure 6.4 Dependence of buckling load on plate aspect ratio

The right-hand side is minimized when $n = 1$, i.e. only one half-wave is present in the direction transverse to the applied load. Setting $n = 1$ and rearranging,

$$N_o = \frac{\pi^2}{a^2} \left[D_{11}m^2 + 2(D_{12} + 2D_{66})(AR)^2 + D_{22} \frac{(AR)^4}{m^2} \right] \quad (6.7)$$

The value of m that minimizes the right-hand side of Equation (6.7) gives the buckling load of a simply supported rectangular composite plate under compression.

As can be seen from Equation (6.7), in addition to the bending stiffnesses D_{11} , D_{12} , D_{22} , and D_{66} , the buckling load is also dependent on the aspect ratio ($AR = \text{length}/\text{width}$) of the plate. This dependence is shown in Figure 6.4 for a plate with fixed length 508 mm.

As is seen from Figure 6.4, as the aspect ratio increases, the number of half-waves m in the direction of the load increases. Typically, for each m value, there is a value of AR that minimizes the buckling load. Points of intersection of curves corresponding to successive m values indicate that the plate may buckle in either of the two modes (differing by one half-wave) and have the same buckling load. In practice, due to eccentricities and inaccuracies due to fabrication, these cusps cannot be reproduced. The plate will tend to buckle in one of the two modes and will not switch to the other.

The results in Figure 6.4 correspond to a quasi-isotropic layup (± 45)/(0/90)/(± 45) with D matrix values as shown in the same figure. The laminate thickness for this laminate is 0.5715 mm. It is of interest to compare with an aluminum plate of the same thickness, length and aspect ratio. This is done in Figure 6.5. Note that the buckling loads for aluminum can be obtained using the same Equation (6.7) with proper redefinition of the D matrix terms.

As is seen from Figure 6.5, the buckling load of an aluminum plate of the same thickness can be as much as 20% higher (for $AR \approx 0.5$) than that of an equal thickness quasi-isotropic composite plate. Based on this result, to match the buckling load of the aluminum plate at the worst case ($AR = 0.5$) the quasi-isotropic plate thickness must be increased by a factor of $(1.2)^{1/3}$. The one-third power is because the D matrix terms are proportional to thickness to the

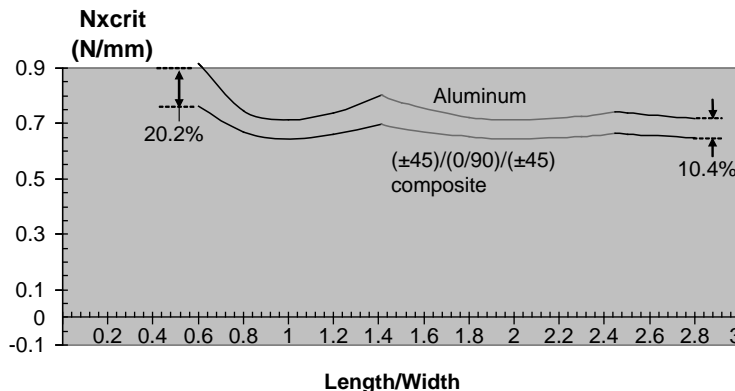


Figure 6.5 Comparison of buckling loads for equal thickness aluminum and quasi-isotropic composite plates (length = 508 mm)

third power (see also Equation 3.47). It is recognized here that typical composite materials are not available at any desired thickness, but only in multiples of specific ply thicknesses. Therefore, this calculation would have to be rounded up to the next integral multiple of ply thicknesses. Assuming, for now, continuity of thickness for the composite plate so that preliminary comparisons can be obtained, the required increase in thickness for the composite plate would be

$$\text{thickness increase} = 1.2^{1/3} = 1.063$$

Therefore, for the same size plate, the weight ratio between a composite (graphite/epoxy) and an aluminum panel is

$$\frac{W_{Gr/E}}{W_{Al}} = 0.58 \frac{1.063}{1} = 0.616 \quad (6.8)$$

↓ ↓ ↓
 density 1 thickness
 ratio ratio

Equation (6.8) implies that a quasi-isotropic composite with the same buckling load under compression as an aluminum plate, is approximately 62% of the aluminum weight or results in, approximately, 38% weight savings. It is important to keep in mind that this result assumes that any thickness is achievable with a composite material (which is not true, as mentioned above) and that there are no other factors that may affect the design such as material scatter, environmental effects, and sensitivity to damage. Accounting for these effects tends to decrease the weight savings.

6.2.1 Uniaxial Compression, Three Sides Simply Supported, One Side Free

The discussion so far in this section has been confined to a simply supported plate. The effect of the boundary conditions can be very important. As a special case, of interest in future discussion (Section 8.5 on stiffener crippling) the case of a rectangular composite plate under compression with three sides simply supported and one (not loaded) side free, is discussed here. The situation is shown in Figure 6.6.

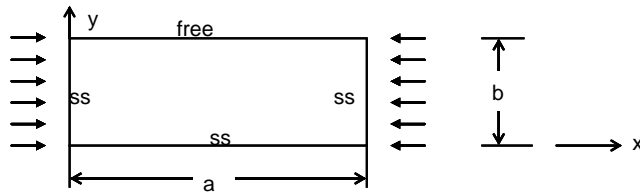


Figure 6.6 Plate under compression with one (unloaded) edge free and three edges simply-supported

An approximate solution is obtained following the same steps as for the plate simply supported all around. Analogous to Equation (6.3) an expression for w is assumed in the form,

$$w = \sum \sum A_{mn} \sin \frac{m\pi x}{a} \sin \frac{\lambda n\pi y}{b} \quad (6.9)$$

where λ is a parameter appropriately selected to satisfy the boundary conditions of the problem.

The governing equation is the same as (6.1) with $N_y = 0$:

$$D_{11} \frac{\partial^4 w}{\partial x^4} + 2(D_{12} + 2D_{66}) \frac{\partial^4 w}{\partial x^2 \partial y^2} + D_{22} \frac{\partial^4 w}{\partial y^4} = N_x \frac{\partial^2 w}{\partial x^2} \quad (6.10)$$

The boundary conditions for Equation (6.10) are

$$w(x = 0) = w(x = a) = 0$$

$$w(y = 0) = 0$$

$$M_x = -D_{11} \frac{\partial^2 w}{\partial x^2} - D_{12} \frac{\partial^2 w}{\partial y^2} = 0 \quad \text{at } x = 0, a \quad (6.11)$$

$$M_y = -D_{12} \frac{\partial^2 w}{\partial x^2} - D_{22} \frac{\partial^2 w}{\partial y^2} = 0 \quad \text{at } y = 0, b$$

The value of λ must be chosen such that w given by Equation (6.9) is free to attain any value at the free edge $y = b$. For example, if $\lambda = 1$, w at $y = b$ is zero and the simply supported case discussed earlier is recovered. A plot of w as a function of y for different λ values is shown in Figure 6.7.

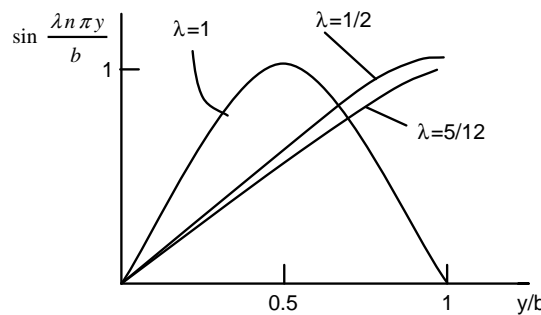


Figure 6.7 Shape of w deflection for various values of the parameter λ

It appears from Figure 6.7, that λ values in the vicinity of 1/2 would give a reasonable representation of w . It should be noted that $\lambda = 1/2$ gives a slope of w at $y = b$ that equals zero which is unlikely to be the case since w is arbitrary at $y = b$ and there is no reason for its slope to be equal to zero all along the edge $y = b$.

The results obtained with this expression for w are approximate for another reason: The last of the boundary conditions (Equation 6.11), is not satisfied. The moment M_y at $y = b$ will not be zero and its value will depend on λ .

Following the same procedure as for the simply supported case above, the expression for the buckling load corresponding to Equation (6.7) is,

$$N_o = \frac{\pi^2}{a^2} \left[D_{11}m^2 + 2(D_{12} + 2D_{66})\lambda^2(AR)^2 + D_{22} \frac{(AR)^4}{m^2} \lambda^4 \right] \quad (6.12)$$

The exact solution to this problem is [4]

$$N_o = 12 \frac{D_{66}}{b^2} + \frac{1}{(AR)^2} \sqrt{\frac{D_{11}}{D_{22}}} \quad (6.13)$$

The approximation of Equation (6.12) and the exact solution (6.13) are compared in Figure 6.8 for the same quasi-isotropic layup (± 45)/(0/90)/(± 45) of Figure 6.4.

The approximate solution is very close to the exact answer especially for $\lambda = 5/12$. In particular, for infinitely long plate, the exact solution (6.13) becomes

$$N_{xcrit} = \frac{12D_{66}}{b^2} \quad (6.13a)$$

and the approximate solution becomes

$$N_{xcrit} = \frac{4\pi^2}{b^2} \lambda^2 D_{66} + \frac{2\pi^2}{b^2} D_{12} \quad (6.12a)$$

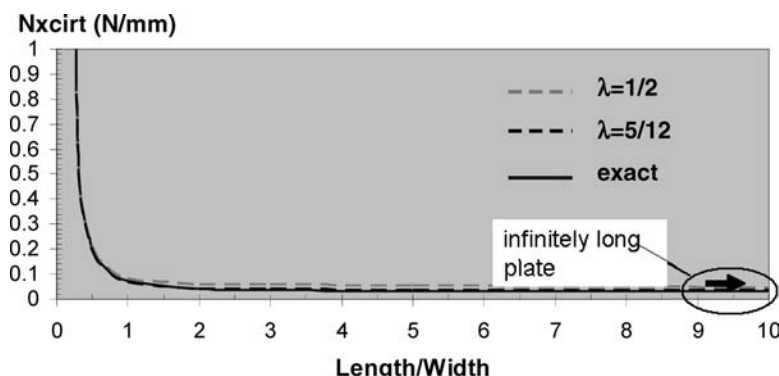


Figure 6.8 Comparison of approximate (two λ values) and exact solutions for buckling load of a rectangular composite panel under compression with three simply supported edges and one (unloaded) edge free

Note that since the plate is infinitely long, the two expressions are only dependent on the plate width b now.

Setting $b = 508$ mm, for $\lambda = 1/2$ the two answers differ by 46.9%, but for $\lambda = 5/12$ the two differ by only 12.5%. Obviously, if an exact solution to a problem such as the one under discussion exists and does not require expensive computation (e.g. solution of a large eigenvalue problem), it will be preferred over an approximate solution. Unfortunately, in most cases, approximate solutions may be all that is available during design and preliminary analysis. The example given is meant to show the potential and the drawbacks of approximate methods.

6.3 Buckling of Rectangular Composite Plate under Shear

A rectangular composite plate under shear is shown in Figure 6.9. As before, the layup of the plate is assumed symmetric (B matrix = 0) and with negligible bending-twisting coupling ($D_{16} \approx D_{26} \approx 0$). The approach to determine the buckling load parallels the Galerkin solution given in [5].

The governing equation is again derived from Equation (5.16) with $N_x = N_y = p_x = p_y = p_z = 0$:

$$D_{11} \frac{\partial^4 w}{\partial x^4} + 2(D_{12} + 2D_{66}) \frac{\partial^4 w}{\partial x^2 \partial y^2} + D_{22} \frac{\partial^4 w}{\partial y^4} = 2N_{xy} \frac{\partial^2 w}{\partial x \partial y} \quad (6.14)$$

In the Galerkin approach, an assumed expression of the solution is substituted in the governing equation which, in turn, is multiplied by characteristic (usually orthogonal) functions and then integrated over the domain of the problem. This results in algebraic equations for the unknown coefficients in the assumed expression for the solution and, at the same time, minimizes the error [6].

To solve Equation (6.14) by the Galerkin method, the following expression for w is used which is the same as Equation (6.3):

$$w = \sum \sum A_{mn} \sin \frac{m\pi x}{a} \sin \frac{n\pi y}{b} \quad (6.3)$$

where A_{mn} are unknowns to be determined.

As the terms in Equation (6.3) comprise orthogonal sine functions, the same characteristic functions are used. Multiplying Equation (6.14) by the characteristic functions $\sin(m\pi x/a)\sin(n\pi y/b)$ and integrating gives

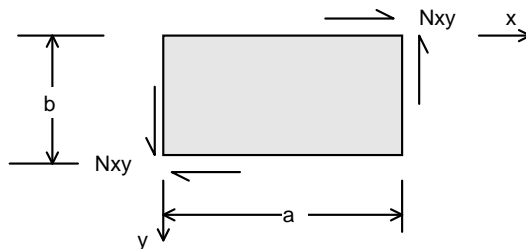


Figure 6.9 Rectangular composite plate under shear

$$\iint \left[D_{11} \frac{\partial^4 w}{\partial x^4} + 2(D_{12} + 2D_{66}) \frac{\partial^4 w}{\partial x^2 \partial y^2} + D_{22} \frac{\partial^4 w}{\partial y^4} - 2N_{xy} \frac{\partial^2 w}{\partial x \partial y} \right] \sin \frac{m\pi x}{a} \sin \frac{n\pi y}{b} dx dy = 0 \quad (6.15)$$

where the integrations are carried over the entire plate ($0 \leq x \leq a$ and $0 \leq y \leq b$)

Note that each set of m, n values gives a different equation to be solved where all unknowns A_{mn} appear. Substituting for w from Equation (6.3) and carrying out the integrations gives

$$\begin{aligned} \pi^4 \left[D_{11} m^4 + 2(D_{12} + 2D_{66}) m^2 n^2 (AR)^2 + D_{22} n^4 (AR)^4 \right] A_{mn} - 32mn(AR)^3 b^2 N_{xy} \sum \sum T_{ij} A_{ij} &= 0 \\ T_{ij} = \frac{ij}{(m^2 - i^2)(n^2 - j^2)} &\text{ for } m \pm j \text{ odd and } n \pm j \text{ odd} \\ T_{ij} = 0 &\text{ otherwise} \end{aligned} \quad (6.16)$$

with $AR = a/b$ the aspect ratio of the plate

Equation (6.16) uncouples to two independent sets of homogeneous equations, one for $m + n$ odd and one for $m + n$ even. The form of each set of equations is:

$$[E]\{A_{mn}\} = 0 \quad (6.17)$$

with $[E]$ a coefficient matrix with ij th entry given by

$$\begin{aligned} E_{ij} = -32mn(AR)^2 b^2 N_{xy} T_{ij} + \\ \pi^4 \left[D_{11} m^4 + 2(D_{12} + 2D_{66}) m^2 n^2 (AR)^2 + D_{22} n^4 (AR)^4 \right] \delta(m-i)\delta(n-j) \end{aligned} \quad (6.18)$$

where $\delta(m-i)=1$ when $m=i$ and 0 otherwise, and $\delta(n-j)=1$ when $n=j$ and zero otherwise.

Equations (6.17) have coefficients A_{mn} that are a function of the shear load N_{xy} as shown in Equation (6.18). For each of the independent sets of Equations (6.17), a nontrivial solution ($A_{mn} \neq 0$) is obtained when the determinant of the coefficient matrix is set equal to zero,

$$\begin{aligned} \det[E]_{m+n=\text{odd}} &= 0 \\ \det[E]_{m+n=\text{even}} &= 0 \end{aligned}$$

Each of these two equations results in an eigenvalue problem where the eigenvalue is the buckling load N_{xy} and the eigenvector gives the buckling mode. The lowest eigenvalue across both problems is the sought-for buckling load. For symmetric and balanced (specielly orthotropic) plates, the eigenvalues appear in pairs of positive and negative values, indicating that if the load direction changes the plate will buckle when the applied load reaches the same magnitude.

The approach just described gives very accurate buckling loads, provided sufficient terms in Equation (6.3) are used and an accurate eigenvalue solver is available. The following is a less involved, approximate method to obtain the buckling load under shear.

For $0.5 \leq a/b < 1$, the buckling load is given by

$$N_{xyEcr} = \frac{\frac{\pi^4 b}{a^3}}{\sqrt{\frac{14.28}{D1^2} + \frac{40.96}{D1D2} + \frac{40.96}{D1D3}}} \quad \text{with} \quad (6.19)$$

$$D1 = D_{11} + D_{22} \left(\frac{a}{b} \right)^4 + 2(D_{12} + 2D_{66}) \left(\frac{a}{b} \right)^2$$

$$D2 = D_{11} + 81D_{22} \left(\frac{a}{b} \right)^4 + 18(D_{12} + 2D_{66}) \left(\frac{a}{b} \right)^2$$

$$D3 = 81D_{11} + D_{22} \left(\frac{a}{b} \right)^4 + 18(D_{12} + 2D_{66}) \left(\frac{a}{b} \right)^2$$

For $a/b = 0$, use the results of the next section for long plates. Finally, for $0 \leq a/b < 0.5$, interpolate linearly between the result for $a/b = 0$ and $a/b = 0.5$. The accuracy of this approach depends on the bending stiffnesses of the plate and its aspect ratio a/b , and ranges from less than one percent to 20% for typical layups used in practice.

6.4 Buckling of Long Rectangular Composite Plates under Shear

The Galerkin-based derivation of the previous section can be simplified significantly if one of the plate dimensions is long compared with the other. In such a case, the long dimension does not affect the buckling load and the buckling pattern is confined over a length L , which is significantly lower than the panel long dimension. The situation is shown in Figure 6.10.

Following Thielemann [7], and assuming a simply supported plate, an expression for the out-of-plane displacement w can be assumed in the form:

$$w = w_o \sin \frac{\pi x}{a} \sin \frac{\pi(y - x \tan \alpha)}{L} \quad (6.20)$$

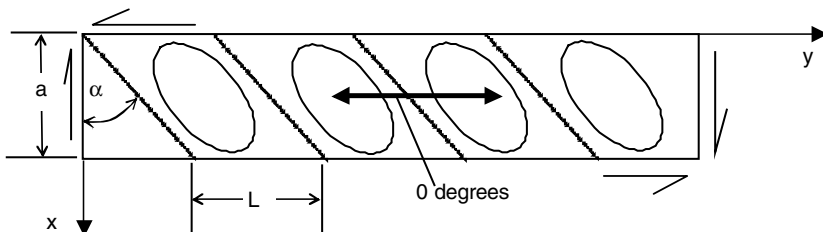


Figure 6.10 Buckling pattern in a long rectangular plate under shear

This expression satisfies the conditions that w is zero along the long sides ($x=0$ and $x=a$) and along lines inclined by an angle α to the x axis separated by distance L , as shown in Figure 6.10. It should be noted that in the actual buckling pattern these inclined lines of zero w are not perfectly straight as Equation (6.20) implies, but the error in assuming perfectly straight lines is small.

The buckling load is obtained by minimizing the energy stored in the plate. It is assumed that the laminate is symmetric so the internal potential energy (Equation 5.63) decouples in a membrane (in-plane) portion (the terms involving the A matrix) and a bending (out-of-plane) portion (the terms involving the D matrix). For the buckling problem under consideration, only w is of interest and, therefore, only the terms involving the D matrix are used. In addition, it is assumed that $D_{16}=D_{26}=0$. Then, the internal potential energy has the form:

$$U = \frac{1}{2} \iint_A \left\{ D_{11} \left(\frac{\partial^2 w}{\partial x^2} \right)^2 + 2D_{12} \frac{\partial^2 w}{\partial x^2} \frac{\partial^2 w}{\partial y^2} + 4D_{66} \left(\frac{\partial^2 w}{\partial x \partial y} \right)^2 + D_{22} \left(\frac{\partial^2 w}{\partial y^2} \right)^2 \right\} dx dy \quad (6.21)$$

Using Equation (6.20) to substitute for w in Equation (6.21) and carrying out the integrations gives:

$$U = \frac{aL}{2} \left\{ \begin{aligned} & D_{11} \left[\frac{w_o^2 \pi^4}{4} \left(\frac{1}{a^2} + \frac{\tan^2 \alpha}{L^2} \right)^2 + \frac{w_o^2 \pi^4}{a^2 L^2} \tan^2 \alpha \right] + 2D_{12} \frac{w_o^2 \pi^4}{4L^2} \left(\frac{1}{a^2} + \frac{\tan^2 \alpha}{L^2} \right) + \\ & D_{22} \frac{w_o^2 \pi^4}{4L^4} + 4D_{66} \left(\frac{w_o^2 \pi^4}{4a^2 L^2} + \frac{w_o^2 \pi^4}{4L^4} \tan^2 \alpha \right) \end{aligned} \right\}$$

which, after rearranging and simplifying, becomes:

$$U = \frac{w_o^2 \pi^4 L}{8a^3} \left[\begin{aligned} & D_{11} (1 + 6 \tan^2 \alpha AR^2 + \tan^4 \alpha AR^4) + 2(D_{12} + 2D_{66})(AR^2 + AR^4 \tan^2 \alpha) + \\ & D_{22} AR^4 \end{aligned} \right] \quad (6.22)$$

where $AR = a/L$

Now the work done by the applied load N_{xy} is given by Equation (5.68) with $N_x = N_y = 0$

$$W = -\frac{1}{2} \iint_0^a \int_0^b \left\{ 2N_{xy} \left(\frac{\partial w}{\partial x} \right) \left(\frac{\partial w}{\partial y} \right) \right\} dx dy \quad (6.23)$$

Using Equation (6.20) to substitute for w and carrying out the integrations gives:

$$W = \frac{w_o^2 AR \pi^2}{4} \tan \alpha N_{xy} \quad (6.24)$$

Minimizing the total potential energy

$$\Pi = U - W \quad (6.25)$$

with respect to the unknown coefficient w_o implies,

$$\frac{\partial \Pi}{\partial w_o} = 0 \quad (6.26)$$

which, using Equations (6.22) and (6.24) results in:

$$\begin{aligned} & \frac{2w_o\pi^4 L}{8a^3} \left[D_{11}(1 + 6\tan^2 \alpha AR^2 + \tan^4 \alpha AR^4) + 2(D_{12} + 2D_{66})(AR^2 + AR^4 \tan^2 \alpha) + \right. \\ & \left. D_{22}AR^4 \right] \\ & - \frac{2w_o AR \pi^2 \tan \alpha}{4} N_{xy} = 0 \end{aligned} \quad (6.27)$$

The obvious (trivial) solution to Equation (6.27) is $w_o = 0$ which corresponds to the in-plane pre-buckling situation (out-of-plane displacement w is zero). For $w_o \neq 0$, N_{xy} must attain a critical value which corresponds to the buckling load. Therefore, solving Equation (6.27) for $N_{xy} = N_{xycrit}$ gives the buckling load:

$$N_{xycrit} = \frac{\pi^2}{2AR^2 a^2 \tan \alpha} \left[\frac{D_{11}(1 + 6\tan^2 \alpha AR^2 + \tan^4 \alpha AR^4) + 2(D_{12} + 2D_{66})(AR^2 + AR^4 \tan^2 \alpha) + D_{22}AR^4}{2(D_{12} + 2D_{66})(AR^2 + AR^4 \tan^2 \alpha) + D_{22}AR^4} \right] \quad (6.28)$$

Equation (6.28) shows that the buckling load is a function of the angle α and the length L through the aspect ratio AR . Since the buckling load is the lowest load at which out-of-plane displacements w are permissible, the values of $\tan \alpha$ and AR must be determined for which the right-hand side of Equation (6.28) is minimized. This is done by differentiating with respect to the two parameters $\tan \alpha$ and AR and setting the result equal to zero. Then,

$$\frac{\partial N_{xycrit}}{\partial (AR)} = 0 \Rightarrow AR = \left[\frac{D_{11}}{D_{11} \tan^4 \alpha + 2(D_{12} + 2D_{66}) \tan^2 \alpha + D_{22}} \right]^{1/4} \quad (6.29)$$

and

$$\begin{aligned} \frac{\partial N_{xycrit}}{\partial (\tan \alpha)} = 0 \Rightarrow & 3D_{11}AR^4 \tan^4 \alpha + (6D_{11}AR^2 + 2(D_{12} + 2D_{66})AR^4) \tan^2 \alpha \\ & -(D_{11}2(D_{12} + 2D_{66})AR^2 + D_{22}AR^4) = 0 \end{aligned} \quad (6.30)$$

Equations (6.29) and (6.30) are solved simultaneously for AR and $\tan \alpha$. The results are substituted in Equation (6.28) to obtain the buckling load N_{xycrit} .

The accuracy of this approach is compared with a solution obtained by Seydel [8] where the governing differential equation (6.14) is solved as a product of an exponential function in y and an unknown function of x . For the comparison, a $(0/90)_8$ laminate with basic ply properties: $E_x = E_y = 68.9$ GPa, $v_{xy} = 0.05$, $G_{xy} = 4.83$ GPa, and ply thickness = 0.1905 mm is selected. The result is shown in Figure 6.11 where the two methods are shown to be in excellent agreement (largest difference is less than 7%).

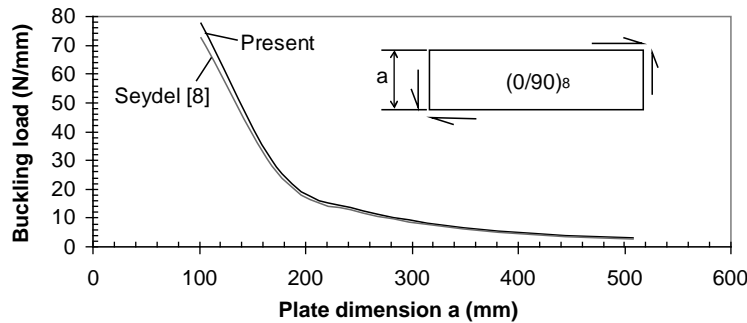


Figure 6.11 Buckling load of a long simply supported plate under shear: comparison of two approaches

6.5 Buckling of Rectangular Composite Plates under Combined Loads

A composite plate under compression and shear is shown in Figure 6.12. Its edges are assumed to be simply supported.

The out-of-plane displacement w is assumed to be of the form

$$w = w_1 \sin \frac{\pi x}{a} \sin \frac{\pi y}{b} + w_2 \sin \frac{2\pi x}{a} \sin \frac{2\pi y}{b} \quad (6.31)$$

The two terms in the right-hand side of Equation (6.31) are two of the terms in the w expressions in previous sections (see Equation 6.3). Equation (6.31) satisfies the simply supported boundary conditions on w ,

$$\begin{aligned} w(x = 0) &= w(x = a) = 0 \\ w(y = 0) &= w(y = b) = 0 \end{aligned}$$

and the fact that the bending moments at the plate boundary are also zero

$$M_x = -D_{11} \frac{\partial^2 w}{\partial x^2} - D_{12} \frac{\partial^2 w}{\partial y^2} = 0$$

$$M_y = -D_{12} \frac{\partial^2 w}{\partial x^2} - D_{22} \frac{\partial^2 w}{\partial y^2} = 0$$

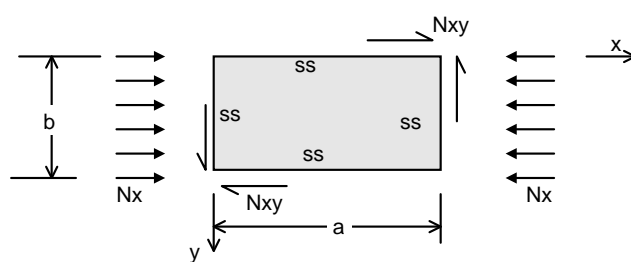


Figure 6.12 Simply supported plate under compression and shear

However, substituting in the last two of Equations (5.3) shows that Equation (6.31) results in nonzero transverse shear forces $V (= Q_z - \partial M_{xy}/\partial x)$ and $Q_y - \partial M_{xy}/\partial y)$ at the plate boundary. This solution is, therefore, an approximation since there are no transverse shear forces applied on the plate boundaries. In an energy minimization approach, which is the method that will be used in this case, it is not necessary to satisfy the force boundary conditions when the problem is formulated in terms of displacements. This was discussed in Section 5.4. The more terms are used in the w expression (6.31) the higher the accuracy and the force boundary conditions will, in the limit, be satisfied in an average sense.

Minimization of the total potential energy of the plate will lead to two equations for the two unknowns w_1 and w_2 in the assumed expression for w . It is important to note that for shear loading cases, assuming a single term for w will not work (see Exercise 6.5). The assumed shape using one term is quite different from the plate deformations caused by the shear loading when the plate buckles. At least two terms are necessary to begin capturing the buckling mode.

For a displacement-based approach, Equations (5.63) and (5.68) can be used. Since the plate is symmetric (B matrix terms are equal to zero) the in-plane and out-of-plane contributions to the energy decouple. To determine the out-of-plane displacement w , therefore, the total energy to be minimized, strain energy minus work done, has the form:

$$\Pi_c = \frac{1}{2} \iint \left\{ D_{11} \left(\frac{\partial^2 w}{\partial x^2} \right)^2 + 2D_{12} \frac{\partial^2 w}{\partial x^2} \frac{\partial^2 w}{\partial y^2} + D_{22} \left(\frac{\partial^2 w}{\partial y^2} \right)^2 + 4D_{66} \left(\frac{\partial^2 w}{\partial x \partial y} \right)^2 + \right. \\ \left. 4D_{16} \frac{\partial^2 w}{\partial x^2} \frac{\partial^2 w}{\partial x \partial y} + 4D_{26} \frac{\partial^2 w}{\partial y^2} \frac{\partial^2 w}{\partial x \partial y} \right\} dx dy \\ - \frac{1}{2} \iint N_x \left(\frac{\partial w}{\partial x} \right)^2 dx dy - \iint N_{xy} \frac{\partial w}{\partial x} \frac{\partial w}{\partial y} dx dy \quad (6.32)$$

It is further assumed that the bending-twisting coupling terms $D_{16} \approx D_{26} \approx 0$.

Equation (6.31) is substituted in the expression (6.32) for Π_c . As an example, the first term is shown below:

$$\left(\frac{\partial^2 w}{\partial x^2} \right)^2 = w_1^2 \frac{\pi^4}{4b^4} \left(1 - \cos \frac{2\pi x}{a} \right) \left(1 - \cos \frac{2\pi y}{b} \right) + w_2^2 \frac{16\pi^4}{4b^4} \left(1 - \cos \frac{4\pi x}{a} \right) \left(1 - \cos \frac{4\pi y}{b} \right) \\ + 2w_1 w_2 \frac{4\pi^4}{b^4} \frac{1}{4} \left(\cos \frac{\pi x}{a} - \cos \frac{3\pi x}{a} \right) \left(\cos \frac{\pi y}{b} - \cos \frac{3\pi y}{b} \right)$$

with similar expressions for the remaining derivatives present in Equation (6.32).

Carrying out the integrations gives

$$\int_0^a \int_0^b \left(\frac{\partial^2 w}{\partial x^2} \right)^2 dx dy = w_1^2 \frac{\pi^4}{4a^4} ab + w_2^2 \frac{4\pi^4}{a^4} ab$$

$$\int_0^a \int_0^b \left(\frac{\partial^2 w}{\partial y^2} \right)^2 dx dy = w_1^2 \frac{\pi^4}{4b^4} ab + w_2^2 \frac{4\pi^4}{b^4} ab$$

$$\int_0^a \int_0^b \left(\frac{\partial^2 w}{\partial x^2} \frac{\partial^2 w}{\partial y^2} \right) dx dy = w_1^2 \frac{\pi^4}{4a^2 b^2} ab + w_2^2 \frac{4\pi^4}{a^2 b^2} ab$$

$$\int_0^a \int_0^b \left(\frac{\partial^2 w}{\partial x \partial y} \right)^2 dx dy = w_1^2 \frac{\pi^4}{4a^2 b^2} ab + w_2^2 \frac{4\pi^4}{a^2 b^2} ab$$

$$\int_0^a \int_0^b \left(\frac{\partial w}{\partial x} \right)^2 dx dy = w_1^2 \frac{\pi^2}{4a^2} ab + w_2^2 \frac{\pi^2}{a^2} ab$$

$$\int_0^a \int_0^b \left(\frac{\partial w}{\partial x} \frac{\partial w}{\partial y} \right) dx dy = \frac{w_1 w_2 \pi^2}{2ab} \left(\frac{2a}{3\pi} + \frac{2a}{\pi} \right) \left(\frac{2b}{3\pi} - \frac{2b}{\pi} \right) + \frac{w_1 w_2 \pi^2}{2ab} \left(\frac{2a}{3\pi} - \frac{2a}{\pi} \right) \left(\frac{2b}{3\pi} + \frac{2b}{\pi} \right)$$

So the final form for Π_c is

$$\Pi_c = \frac{1}{2} \left\{ \begin{array}{l} D_{11} \left[w_1^2 \frac{\pi^4}{4a^3} b + w_2^2 \frac{4\pi^4}{a^3} b \right] + 2(D_{12} + 2D_{66}) \left[w_1^2 \frac{\pi^4}{4ab} + w_2^2 \frac{4\pi^4}{ab} \right] + \\ D_{22} \left[w_1^2 \frac{\pi^4}{4b^3} a + w_2^2 \frac{4\pi^4}{b^3} a \right] \\ - \frac{N_o}{2} \left[w_1^2 \frac{\pi^2}{4a} b + w_2^2 \frac{\pi^2}{a} b \right] - kN_o w_1 w_2 \left(-\frac{16}{9} \right) \left(-\frac{16}{9} \right) \end{array} \right\} \quad (6.32a)$$

where, for simplicity,

$$\frac{N_{xy}}{N_x} = k$$

and $N_o = N_{x\text{crit}}$ the value of N_x which, simultaneously with $N_{xy} = kN_x$ causes buckling of the plate.

The energy expression (6.32a) is minimized with respect to the unknown coefficients w_1 and w_2 . This leads to,

$$\frac{\partial \Pi_c}{\partial w_1} = 0$$

$$\frac{\partial \Pi_c}{\partial w_2} = 0$$

and substituting,

$$\begin{aligned} \frac{1}{2} \left\{ D_{11} \frac{w_1 \pi^4 b}{2a^3} + 2(D_{12} + 2D_{66}) \frac{\pi^4 w_1}{2ab} + D_{22} \frac{w_1 \pi^4 a}{2b^3} \right\} - N_o \frac{w_1 \pi^2 b}{4a} + \frac{32}{9} k N_o w_2 &= 0 \\ \frac{1}{2} \left\{ D_{11} \frac{8w_2 \pi^4 b}{a^3} + 2(D_{12} + 2D_{66}) \frac{8\pi^4 w_2}{ab} + D_{22} \frac{8w_2 \pi^4 a}{b^3} \right\} - N_o \frac{w_2 \pi^2 b}{a} + \frac{32}{9} k N_o w_1 &= 0 \end{aligned} \quad (6.33)$$

Setting, for simplicity,

$$K_1 = \frac{1}{4} \left[D_{11} \frac{\pi^4 b}{a^3} + 2(D_{12} + 2D_{66}) \frac{\pi^4}{ab} + D_{22} \frac{\pi^4 a}{b^3} \right]$$

Equations (6.33) can be recast in the following generalized eigenvalue problem:

$$\begin{bmatrix} K_1 & 0 \\ 0 & 16K_1 \end{bmatrix} \begin{Bmatrix} w_1 \\ w_2 \end{Bmatrix} = N_o \begin{bmatrix} \frac{\pi^2 b}{4a} & -\frac{32}{9} k \\ -\frac{32}{9} k & \frac{\pi^2 b}{a} \end{bmatrix} \begin{Bmatrix} w_1 \\ w_2 \end{Bmatrix} \quad (6.33a)$$

which, with terms appropriately defined, is of the form

$$\underline{A} \underline{x} = \alpha \underline{B} \underline{x}$$

The solution is obtained by premultiplying both sides of the equation by \underline{B}^{-1} the inverse of \underline{B} to obtain the standard eigenvalue problem,

$$\underline{B}^{-1} \underline{A} \underline{x} = \alpha \underline{I} \underline{x}$$

where \underline{I} is the identity matrix.

With

$$\underline{B}^{-1} = \frac{1}{\frac{\pi^4 b^2}{4a^2} - \left(\frac{32}{9} k \right)^2} \begin{bmatrix} \frac{\pi^2 b}{a} & \frac{32}{9} k \\ \frac{32}{9} k & \frac{\pi^2 b}{4a} \end{bmatrix}$$

the standard eigenvalue problem has the form:

$$\begin{bmatrix} \frac{\pi^2 b}{a} & 16 \frac{32}{9} k \\ \frac{32}{9} k & \frac{\pi^2 b}{4a} 16 \end{bmatrix} \begin{Bmatrix} w_1 \\ w_2 \end{Bmatrix} = \underbrace{N_o \left(\frac{\pi^4 b^2}{4a^2} - \left(\frac{32}{9} k \right)^2 \right)}_{\alpha} \frac{1}{K_1} \begin{Bmatrix} w_1 \\ w_2 \end{Bmatrix}$$

where the quantity premultiplying the vector $\{w_1 \ w_2\}^T$ on the right-hand side is the eigenvalue α .

By bringing the right-hand side to the left of the above equation, a system of homogeneous equations is obtained. For a nontrivial solution, the determinant of the resulting left-hand side must be set equal to zero. Then, the eigenvalues are obtained as solutions to

$$\det \left[\tilde{B}^{-1} A - \alpha I \right] = 0$$

which leads to the following equation for the eigenvalue α :

$$\left(\frac{\pi^2 b}{a} - \alpha \right) \left(\frac{4\pi^2 b}{a} - \alpha \right) - \frac{512(32)}{81} k^2 = 0$$

Solving for α and recovering N_o , leads to

$$N_o = \frac{\pi^2}{a^2} \frac{\left(D_{11} + 2(D_{12} + 2D_{66}) \frac{a^2}{b^2} + D_{22} \frac{a^4}{b^4} \right)}{2 - \frac{8192}{81} \frac{a^2}{b^2 \pi^4} k^2} \left[5 \pm \sqrt{9 + \frac{65536}{81} \frac{a^2}{\pi^4 b^2} k^2} \right] \quad (6.34)$$

Of the two solutions given by Equation (6.34) the one giving the lowest buckling load (in absolute value) is selected.

Before proceeding with the general case where both N_x and N_{xy} are nonzero, two special cases, those of pure compression and pure shear, are examined. This will give insight to how accurate or inaccurate this two-term solution is.

For pure compression, $N_{xy} = 0$ and, therefore, $k = 0$. Substituting in Equation (6.34), the buckling load under compression is given by

$$N_o = \frac{\pi^2}{a^2} \left(D_{11} + 2(D_{12} + 2D_{66}) \frac{a^2}{b^2} + D_{22} \frac{a^4}{b^4} \right) \quad (6.35)$$

Comparison of this expression with the general expression (6.7) for buckling under compression shows that the current expression coincides with the exact solution given by that equation when the number of half-waves m parallel to the loading direction equals 1. If the panel aspect ratio is large and/or the difference in bending stiffnesses D_{11} and D_{22} is large, the present approximate solution will depart from the exact solution. The approximate expression just derived and the exact solution are compared in Figure 6.13. In this comparison, the bending stiffness values were taken to be $D_{11} = D_{22} = 0.66$ N m, $D_{12} = 0.47$ N m, $D_{66} = 0.49$ N m, and $D_{16} = D_{26} = 0$. As is seen from Figure 6.13, the two solutions are identical up to aspect ratios of approximately 1.5. For greater aspect ratios, the approximate solution gives higher buckling loads than the exact solution.

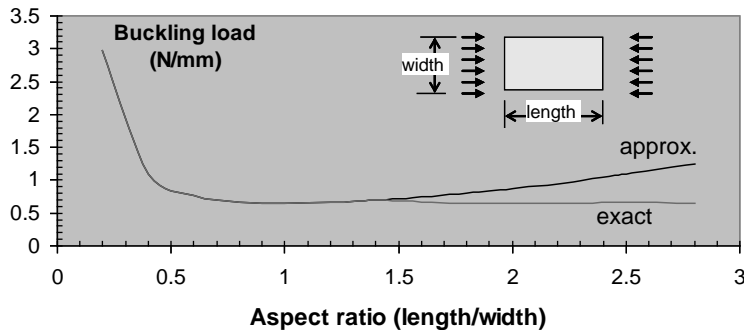


Figure 6.13 Approximate and exact buckling loads as a function of panel aspect ratio

For pure shear, the ratio $k = N_{xy}/N_x$ is allowed to become large (implying N_x is negligible compared with N_{xy}). Then, Equation (6.34) simplifies to

$$N_o k = \pm \frac{\pi^2}{a^2} \frac{\left(D_{11} + 2(D_{12} + 2D_{66}) \frac{a^2}{b^2} + D_{22} \frac{a^4}{b^4} \right)}{\frac{32}{9} \frac{a}{b\pi^2}} \quad (6.36)$$

By recognizing that $N_o k = N_{xy}$ and rearranging,

$$N_{xycrit} = \pm \frac{9\pi^4 b}{32a^3} \left(D_{11} + 2(D_{12} + 2D_{66}) \frac{a^2}{b^2} + D_{22} \frac{a^4}{b^4} \right) \quad (6.37)$$

Equation (6.37) gives an approximate expression for the buckling load of a rectangular composite panel under shear. The \pm sign indicates that buckling can be caused by either positive or negative shear loads. This expression is, typically, 27–30% higher than the exact solution one can obtain using the procedure in Section 6.3. The accuracy of Equation (6.37) can be improved if more terms are included in Equation (6.31) at considerable increase in algebraic complexity [9].

For the combined load case, Equation (6.34) will provide an approximation to the buckling load. However, for combined loading, the accuracy of this equation is higher than what was obtained for the compression and shear acting alone, as was seen in Equations (6.35) and (6.37). The reason is that, even though the individual buckling loads may be approximate, the interaction between the two loading types is accurately captured by Equation (6.34). A comparison of Equation (6.34) with the interaction curve [10] that has been found to be very accurate for this type of load combination,

$$\frac{N_x}{N_{xcrit}} + \left(\frac{N_{xy}}{N_{xycrit}} \right)^2 = 1 \quad (6.38)$$

is shown in Figure 6.14. The approximate and ‘exact’ solutions are very close to each other.

Interaction curves such as the one shown in Figure 6.14 can be very useful in design. They provide a means for determining: (a) if a panel fails under combined loads N_x and N_{xy} ; or (b) the

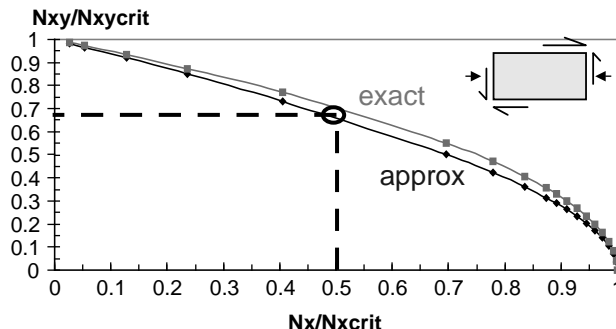


Figure 6.14 Interaction curve for buckling of composite rectangular plate under combined compression and shear

maximum allowable in one direction (compression or shear) given the applied load in the other. Load combinations inside the interaction curve imply that the panel does not buckle. Load combinations corresponding to points outside the interaction curve correspond to a panel that has buckled already. As an example, consider a case where the applied compressive load is half the buckling load of the panel when only compression is applied ($N_x/N_{xcrit} = 0.5$). This point gives the x coordinate in Figure 6.14. The corresponding y coordinate is (approximately) 0.67. This means that if the applied shear load is less than 67% of the shear buckling load when shear acts alone, the panel will not buckle under this load combination.

6.6 Design Equations for Different Boundary Conditions and Load Combinations

Approaches similar to those presented in the three previous sections can be used to obtain expressions for the buckling loads of rectangular composite panels with different boundary conditions and/or applied loads. A brief summary for the most common cases [4, 10–12] is given in Table 6.1. Note that, in all cases, in Table 6.1, the panel is assumed to have no bending-twisting coupling ($D_{16} = D_{26} = 0$).

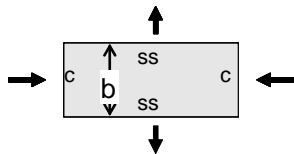
As an example of using Table 6.1, examine the effect of various boundary conditions on a square composite plate under uniaxial compression. The side of the plate is a and the bending stiffnesses are $D_{11} = D_{22} = 660.5 \text{ N mm}$, $D_{12} = 467.4 \text{ N mm}$, and $D_{66} = 494.5 \text{ N mm}$. Normalizing the results to the case of a plate simply supported all around, the results shown in Figure 6.15 are obtained. The notation CCL implies the loaded sides are clamped. The notation CCU implies the unloaded sides are clamped. An analogous notation scheme is used for the simply supported boundary condition.

As is seen from Figure 6.15, the clamped-all-around plate has the highest buckling load. As expected, the simply supported all-around plate has the lowest buckling load and the clamped/simply supported combinations lie in between the two extremes. It should be noted that, unlike beams where the ratio of clamped to simply supported buckling load is 4, for plates, the corresponding ratio is significantly less (less than 2.5 for the case of Figure 6.15).

Table 6.1 Buckling loads for various boundary conditions and load combinations

	$N_o = \frac{\pi^2 [D_{11}m^4 + 2(D_{12} + 2D_{66})m^2(AR)^2 + D_{22}(AR)^4]}{a^2 m^2}$
	$\lambda = \frac{a}{b} \left(\frac{D_{22}}{D_{11}} \right)^{1/4}$ $N_o = \frac{\pi^2}{b^2} \sqrt{D_{11}D_{22}}(K) \quad K = \frac{4}{\lambda^2} + \frac{2(D_{12} + 2D_{66})}{\sqrt{D_{11}D_{22}}} + \frac{3}{4}\lambda^2 \quad 0 < \lambda < 1.662$ $K = \frac{m^4 + 8m^2 + 1}{\lambda^2(m+1)} + \frac{2(D_{12} + 2D_{66})}{\sqrt{D_{11}D_{22}}} + \frac{\lambda^2}{m^2 + 1} \quad \lambda > 1.662$
	$\lambda = \frac{a}{b} \left(\frac{D_{22}}{D_{11}} \right)^{1/4}$ $N_o = \frac{\pi^2}{b^2} \sqrt{D_{11}D_{22}}(K) \quad K = \frac{m^2}{\lambda^2} + \frac{2(D_{12} + 2D_{66})}{\sqrt{D_{11}D_{22}}} + \frac{16}{3} \frac{\lambda^2}{m^2}$
	$\lambda = \frac{a}{b} \left(\frac{D_{22}}{D_{11}} \right)^{1/4}$ $N_o = \frac{\pi^2}{b^2} \sqrt{D_{11}D_{22}}(K) \quad K = \frac{4}{\lambda^2} + \frac{8(D_{12} + 2D_{66})}{3\sqrt{D_{11}D_{22}}} + 4\lambda^2 \quad 0 < \lambda < 1.094$ $K = \frac{m^4 + 8m^2 + 1}{\lambda^2(m^2 + 1)} + \frac{2(D_{12} + 2D_{66})}{\sqrt{D_{11}D_{22}}} + \frac{\lambda^2}{m^2 + 1} \quad \lambda > 1.094$
	$\lambda = \frac{a}{b} \left(\frac{D_{22}}{D_{11}} \right)^{1/4}$ $N_o = \frac{\pi^2}{b^2} \sqrt{D_{11}D_{22}}(K) \quad K = \frac{12}{\pi^2} \frac{D_{66}}{\sqrt{D_{11}D_{22}}} + \frac{1}{\lambda^2}$ $M_o = \frac{\pi^2}{b^2} \sqrt{D_{11}D_{22}}(K)$
	$\lambda = \frac{a}{b} \left(\frac{D_{22}}{D_{11}} \right)^{1/4}$ $K = 0.047\pi^2 b^2 \sqrt{\left(\frac{m^2}{\lambda^2} + \frac{2(D_{12} + 2D_{66})}{\sqrt{D_{11}D_{22}}} + \frac{\lambda^2}{m^2} \right) \left(\frac{m^2}{\lambda^2} + \frac{8(D_{12} + 2D_{66})}{\sqrt{D_{11}D_{22}}} + 16 \frac{\lambda^2}{m^2} \right)}$

(continued)

Table 6.1 (continued)

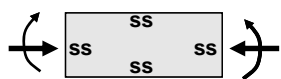
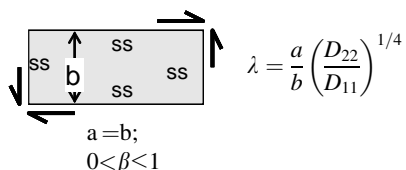
$$N_o = \frac{\pi^2 [D_{11}m^4 + 2(D_{12} + 2D_{66})m^2n^2(AR)^2 + D_{22}n^4(AR)^4]}{a^2(m^2 + kn^2(AR)^2)}$$

$$N_{xycrit} = \frac{4}{b^2} (D_{11}D_{22})^{1/4} (K)$$

$$K = 8.2 + 5 \frac{(D_{12} + 2D_{66})}{\sqrt{D_{11}D_{22}}} \frac{1}{10^{(\frac{A}{\beta} + B\beta)}} \quad \beta = \left(\frac{D_{11}}{D_{22}} \right)^{1/4}$$

$$A = -0.27 + 0.185 \frac{(D_{12} + 2D_{66})}{\sqrt{D_{11}D_{22}}}$$

$$B = 0.82 + 0.46 \frac{(D_{12} + 2D_{66})}{\sqrt{D_{11}D_{22}}} - 0.2 \left(\frac{(D_{12} + 2D_{66})}{\sqrt{D_{11}D_{22}}} \right)^2$$

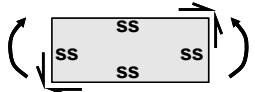


$$R_b^{1.76} + R_c = 1$$

$$R_b = \frac{M}{M_{crit}}, \quad R_c = \frac{N_x}{N_{xcrit}}$$

$$R_b^2 + R_s^2 = 1$$

$$R_b = \frac{M}{M_{crit}}, \quad R_s = \frac{N_{xy}}{N_{xycrit}}$$



$$R_c + R_s^2 = 1$$

$$R_c = \frac{N}{N_{xrit}}, \quad R_s = \frac{N_{xy}}{N_{xycrit}}$$

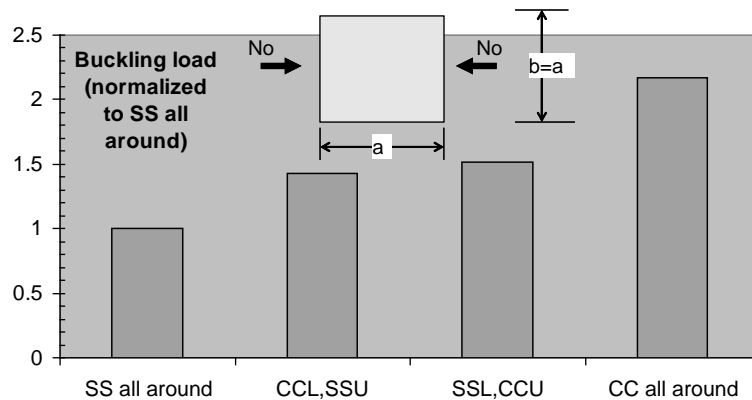


Figure 6.15 Effect of boundary conditions on buckling load of a square composite plate under compression

Exercises

- 6.1 Consider a composite plate with bending stiffnesses D_{11} , D_{12} , D_{22} , and D_{66} ($D_{16} = D_{26} = 0$) and dimensions a , b as shown below (Figure E6.1). Use the derivation shown in Section 6.5 and assume the compression load $N_x = 0$. Verify the approximate expression for the buckling load under shear shown in that section by deriving the new 2×2 eigenvalue problem and solving for all the eigenvalues. What does the sign of the eigenvalue mean? (Hint: start either from the energy expression or from the two equations obtained after differentiation, and set $N_x = 0$).
- 6.2 One of the spars of a wing is 101.6 cm deep. A bending moment $M = 11290.3$ N m is acting on the spar web (Figure E6.2).

The manufacturer of the spar has automated the process of laying up the following stacking sequence: [45/-45/0/90/0/-45/45] with the intent of simply stacking up multiples of this base laminate everywhere to keep the fabrication costs low. The basic material properties are:

$$\begin{aligned}E_{11} &= 131 \text{ GPa} \\E_{22} &= 11.37 \text{ GPa} \\G_{12} &= 4.82 \text{ GPa} \\i_{12} &= 0.29 \\t_{\text{ply}} &= 0.1524 \text{ mm}\end{aligned}$$

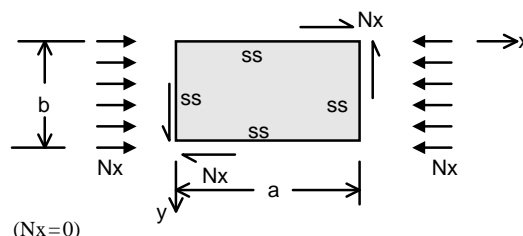


Figure E6.1 Composite plate under shear

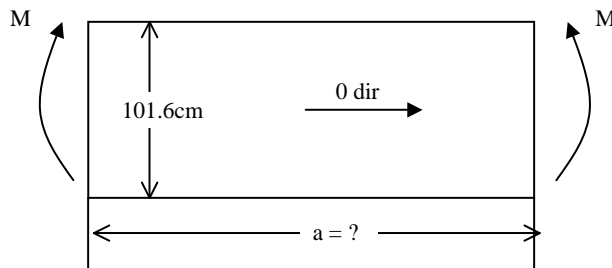
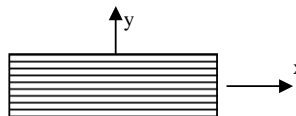


Figure E6.2 Spar web under in-plane bending moment M

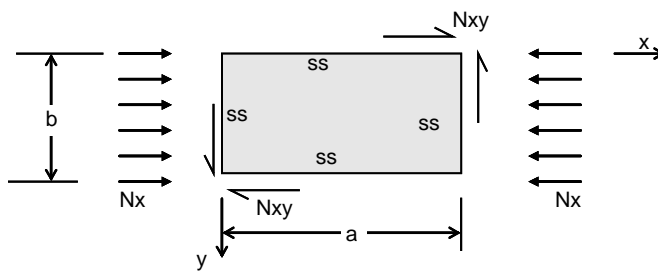
To keep the number of basic laminates stacked together in the spar web low, the manufacturer/designer intends to use ribs to break up the spar. The rib spacing is a .

Create a graph that shows how the maximum allowable rib spacing a varies with the number n of basic laminates used for the spar not to buckle. What is the value of a when $n = 3$, i.e. when the web layup is: $[45/-45/0/90/0/-45/45]_3$?

- 6.3 Prove that for a simply supported square composite panel for which $D_{11} = D_{22}$, the number of half-waves m into which the panel buckles under compression is always 1. What should the condition be between D_{11} and D_{22} for the square panel to buckle in two half-waves? (Assume $D_{16} = D_{26} = 0$.)
- 6.4 A rectangular composite plate with simply supported sides all around is under compression and shear. A Gr/E unidirectional composite material is available with basic (single ply) properties:



$$\begin{aligned}E_x &= 137.9 \text{ GPa} \\E_y &= 11.72 \text{ GPa} \\v_{xy} &= 0.29 \\G_{xy} &= 5.171 \text{ GPa} \\t_{\text{ply}} &= 0.1524 \text{ mm}\end{aligned}$$



$$a = 558.8 \text{ mm}; b = 304.8 \text{ mm}$$

Figure E6.3 Composite plate under combined loading

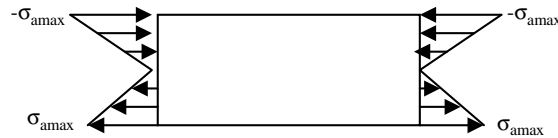


Figure E6.4 Composite plate with linearly distributed edge stress

The application is a wing skin (bending upwards as shown in Figure E6.4) with the following four loading conditions (note that here, $N_x > 0$ means compression):

Load case	1	2	3	4
N_x (N/mm)	4.99	31.54	23.84	34.34
N_{xy} (N/mm)	0.50	25.23	35.76	171.69

For ease of manufacture you want to only use layups of the form $[45_n/-45_n/0_n/90_n]_s$.

- (a) If the D_{ij} terms of the D matrix for the basic layup $[45/-45/0/90]_s$ are known and denoted by D_{ijb} , determine the D_{ij} for any value of n as a function of D_{ijb} .
 - (b) Use your result in (a) to determine the lowest value of n such that all load conditions are met without buckling of the plate. Do not use any knockdowns for environment, material scatter or damage.
 - (c) For your final answer in (b), determine the maximum applied stress σ_{amax} for a linearly distributed applied normal stress as shown in Figure E6.4 that causes buckling of the plate.
- 6.5 Use only the first term of Equation (6.31) to determine the buckling load of a composite rectangular plate of dimensions $a \times b$ under shear. Do this by: (a) energy minimization and (b) solution of the governing equation. Discuss the merits of this approach and its disadvantages.

References

- Whitney, J.M., *Structural Analysis of Laminated Anisotropic Plates*, Technomic Publishing 1987, Section 5.5
- Tung, T.K. and Surdenas, J., Buckling of Rectangular Orthotropic Plates Under Biaxial Loading, *Journal of Composite Materials*, **21**, 124–128 (1987).
- Libove, C., Buckle Pattern of Biaxially Compressed Simply Supported Orthotropic Rectangular Plates, *Journal of Composite Materials*, **17**, 45–48 (1983).
- Barbero, E.J., *Introduction to Composite Material Design*, Taylor & Francis Inc, Philadelphia, PA, 1999, Chapter 9.
- Whitney, J.M., *Structural Analysis of Laminated Anisotropic Plates*, Technomic Publishing, 1987, Section 5.7
- Mura, T., and Koya, T., *Variational Methods in Mechanics*, Oxford University Press, 1992, Chapter 8.
- Thielemann, W., Contribution to the Problem of Buckling of Orthotropic Plates With Special Reference to Plywood, *NACA TM 1263*, 1950.
- Seydel, E., On the Buckling of Rectangular Isotropic or Orthogonal Isotropic Plates by Tangential Stresses, *Ing. Archiv*, **4**, 169 (1933).
- Kassapoglu, C., Simultaneous Cost and Weight Minimization of Composite Stiffened Panels Under Compression and Shear, *Composites Part A: Applied Science and Manufacturing*, **28**, 419–435 (1997).

10. Sullins, R.T., Smith, G.W. and Spier, E.E.*Manual for Structural Stability Analysis of Sandwich Plates and Shells*, NASA CR-1457, December 1969.
11. *Composite Materials Handbook, Mil-Hdbk-17-3F*, vol. 3, Polymer matrix composites materials usage, design and analysis, January 1997, Chapter 5.7.
12. Roberts, J.C., Analytic Techniques for Sizing the Walls of Advanced Composite Electronics Enclosure, *Composites Part B: Engineering*, **30**, 177–187 (1999).

7

Post-Buckling

Post-buckling is the load regime a structure enters after buckling (Figure 7.1). In several situations, dictated by robust design practices, externally imposed requirements, or even the degree of comfort a designer is willing to accept, especially for single load path critical structures, buckling may be taken to coincide with final failure. However, in general, there may be considerable load capacity beyond buckling before final failure occurs. This is true in particular for plates, which, in contrast with beams (Figure 7.2) may have significant load-carrying ability beyond buckling. This ability is often capitalized on to generate designs of lighter weight.

As is seen from Figure 7.2, after buckling ($P/P_{cr} > 1$) the center deflections of a beam increase rapidly compared with those of a plate. This means that, in a beam, high bending moments develop early in the post-buckling regime and will lead to failure. In a plate on the other hand, the deflections increase more slowly with increasing load and the panel can withstand significant excursion in the post-buckling regime before the resulting bending moments become critical.

This ability of plates to withstand load in the post-buckling regime without failing makes such configurations very attractive for design. Thinner skins can be used in wings and fuselages, resulting in lighter structure. However, designing in the post-buckling regime requires knowledge and accurate quantification of failure modes that are not present below the buckling load. One such failure mode is the skin–stiffener separation in stiffened panels shown schematically in Figure 7.3.

The buckled pattern consists of a number of half-waves as shown in Figure 7.3. Depending on which way the skin deforms locally, there will be locations such as the one shown in Figure 7.3 where the skin tends to peel away from the stiffeners. Out-of-plane normal and shear stresses develop which may exceed the material strength and lead to separation and final failure.

Even if the out-of-plane stresses that develop during post-buckling do not lead to skin–stiffener separation under static loading, they may lead to the creation of delaminations under repeated loading. Designing post-buckled panels that perform well under fatigue loading requires accurate knowledge of internal loads and the use of geometries and layups that delay the creation and growth of delaminations.



Figure 7.1 Post-buckled curved composite stiffened panel (See Plate 15 for the colour figure)

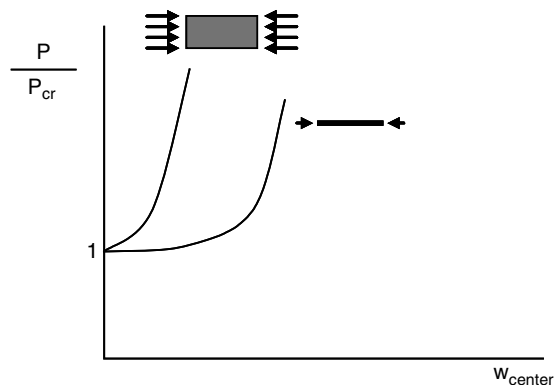


Figure 7.2 In-plane load versus center deflection for plates and beams

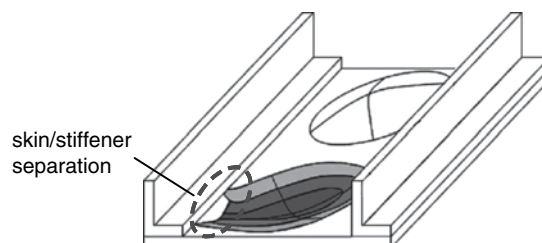


Figure 7.3 Post-buckled skin between stiffeners in a stiffened panel

The tendency for the stiffeners to separate from the skin or, more generally, for delaminations to form, is higher for higher values of the ratio of the applied load to the buckling load. This ratio is referred to as the post-buckling ratio (PB) and, for post-buckled structures, is greater than 1. The PB ratio to be used in a design must be carefully selected, especially for load situations that include shear. Note that the post-buckling ratio should not be confused with the post-buckling factor defined later in Section 7.2.

At the conservative end of the design spectrum, PB is not allowed to exceed 1.5. This means that the structure would buckle at limit load and fail at ultimate load. This protects against fatigue loading as the fatigue loads are lower than the limit load and, therefore, the structure does not buckle repeatedly during service. At the other end of the design spectrum, PB values greater than 5 are very challenging because the loads in the post-buckling regime, both static and fatigue, are significant and it is hard to design efficient structure that will not fail after a relatively low number of cycles.

In a typical structure, such as a stiffened panel, a number of components or structural details may buckle. Selecting the sequence in which the various components of a structure will buckle is crucial for creating a lightweight design. For example, for the stiffened panel of Figure 7.4 the following buckling modes can be identified: (a) panel buckles as a whole, the stiffeners serve to mainly increase the bending stiffness of the panel; (b) skin between stiffeners buckles and stiffeners remain straight, stiffeners carry significant axial loads; (c) stiffeners buckle as columns; and (d) stiffener flanges buckle locally (crippling).

The panel in Figure 7.4 is loaded under compression, but the buckling modes mentioned are valid, with minor changes for any load situation that may induce buckling. For a panel under compression, it is usually more efficient to carry most of the compressive load by the stiffeners. The stiffener cross-sectional area required to carry compressive load is a smaller fraction of the total weight than the skin cross-section required to carry significant amounts of compressive load. This means that the stiffeners must remain straight (no column buckling and no crippling see Sections 8.3 and 8.5) and the panel should not buckle as a whole which would force the

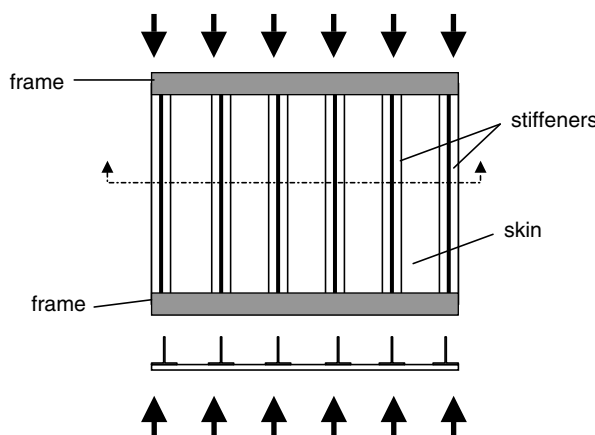


Figure 7.4 Stiffened panel under compressive load

stiffeners to bend out-of-plane and lose axial load capability. Therefore, usually, the buckling scenario for a post-buckled panel under compression requires that buckling of the skin between stiffeners happens first.

For a panel buckling under shear load, forcing the skin between stiffeners to buckle first is also desirable. For judiciously chosen stiffener spacing and with sufficient bending stiffness in the stiffeners, the buckling load of the skin between stiffeners can be increased or, more importantly, the amount of skin thickness required to have the skin between stiffeners buckle at a required PB ratio can be decreased. This decrease in skin thickness decreases the panel weight.

After the skin between stiffeners buckles the load can be increased until the desired PB value is reached. At that point the next failure mode occurs which can be any of the buckling and failure modes mentioned above, or material failure of any of the constituents. The preferred failure mode is skin material failure and/or crippling of the stiffeners. (Global) buckling of the panel as a whole or column buckling of the stiffeners is avoided because this would overload adjacent panels in the structure and might lead to catastrophic failure. Local skin or stiffener failures still leave some load-carrying ability in the panel and the load redistributed in adjacent panels is less. This results in a more damage tolerant overall structure.

In addition to the failure modes and their sequence, the boundary conditions of the panel as a whole, but also of the skin between stiffeners, can be very important and, at least for the skin, is directly related to when skin buckling occurs. As was shown in Section 6.6, the boundary conditions can increase the buckling load by more than a factor of 2 (clamped versus simply supported conditions in Figure 6.15). This is directly related to the stiffener cross-section selected. A schematic of the two extreme behaviors is shown in Figure 7.5.

In both cases in Figure 7.5 it is assumed that the stiffeners have sufficient bending stiffness to stay straight and force the panel to buckle between them. This means that they act as panel breakers (see Section 9.2.1 for related discussion). In Figure 7.5a the torsional rigidity of the stiffeners is negligible (open cross-section stiffeners). As a result, they rotate with the skin locally and the corresponding boundary condition they impose is that of a simple support (zero deflection but nonzero rotation). In Figure 7.5b, the closed-cross-section stiffeners have very high torsional rigidity and they locally force the skin to remain nearly horizontal. In such a case, the imposed boundary condition approaches that of a fixed support (zero deflection and slope).

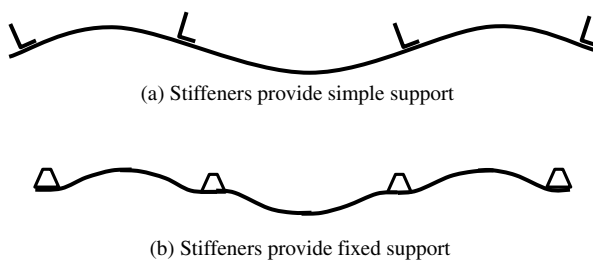


Figure 7.5 Skin buckling between stiffeners – effect of stiffener support

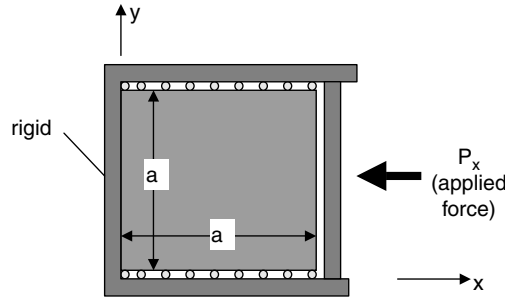


Figure 7.6 Square composite panel under compression

7.1 Post-buckling Analysis of Composite Panels under Compression

The specific case of a square simply supported plate with three edges immovable and one loaded in compression (Figure 7.6) will be used as the example to bring out the most important characteristics of the behavior.

The in-plane deflections u and v of the panel at the three edges $y = 0$, $x = 0$, $y = a$ are zero (immovable edges). This means that an in-plane transverse force P_y must develop at $y = 0$ and $y = a$ in order to keep the panel edges from moving. The out-of-plane deflection w of the panel is zero all around its boundary (simple-support condition). The applied load P_x (units of force) at $x = a$ is a result of a uniformly applied deflection $-C$ at that location. The boundary conditions of the problem can then be written as:

$$\begin{aligned} w &= 0 \text{ at } x = y = 0 \text{ and } x = y = a \\ u &= 0 \text{ at } x = 0 \\ v &= 0 \text{ at } y = 0 \text{ and } y = a \\ u &= -C \text{ at } x = a \end{aligned} \tag{7.1}$$

As the plate may undergo moderate to large deflections once it buckles, the governing equations are the two von Karman large-deflection equations (5.16) and (5.20) repeated here for convenience:

$$\begin{aligned} D_{11} \frac{\partial^4 w}{\partial x^4} + 2(D_{12} + 2D_{66}) \frac{\partial^4 w}{\partial x^2 \partial y^2} + D_{22} \frac{\partial^4 w}{\partial y^4} &= N_x \frac{\partial^2 w}{\partial x^2} + 2N_{xy} \frac{\partial^2 w}{\partial x \partial y} + N_y \frac{\partial^2 w}{\partial y^2} \\ -p_x \frac{\partial w}{\partial x} - p_y \frac{\partial w}{\partial y} + p_z & \end{aligned} \tag{5.16}$$

$$\begin{aligned} \frac{1}{A_{11}A_{22}-A_{12}^2} \left(A_{22} \frac{\partial^4 F}{\partial y^4} - 2A_{12} \frac{\partial^4 F}{\partial x^2 \partial y^2} + A_{11} \frac{\partial^4 F}{\partial x^4} + (A_{22}-A_{12}) \frac{\partial^2 V}{\partial y^2} + (A_{11}-A_{12}) \frac{\partial^2 V}{\partial x^2} \right) + \\ \frac{1}{A_{66}} \frac{\partial^4 F}{\partial x^2 \partial y^2} &= \left(\frac{\partial^2 w}{\partial x \partial y} \right)^2 - \frac{\partial^2 w}{\partial x^2} \frac{\partial^2 w}{\partial y^2} \end{aligned} \tag{5.20}$$

For the present case where the distributed loads p_x , p_y , and p_z are zero (and the potential V is zero), these equations simplify to:

$$D_{11} \frac{\partial^4 w}{\partial x^4} + 2(D_{12} + 2D_{66}) \frac{\partial^4 w}{\partial x^2 \partial y^2} + D_{22} \frac{\partial^4 w}{\partial y^4} = N_x \frac{\partial^2 w}{\partial x^2} + 2N_{xy} \frac{\partial^2 w}{\partial x \partial y} + N_y \frac{\partial^2 w}{\partial y^2} \quad (5.16a)$$

and

$$\frac{1}{A_{11}A_{22}-A_{12}^2} \left(A_{22} \frac{\partial^4 F}{\partial y^4} - 2A_{12} \frac{\partial^4 F}{\partial x^2 \partial y^2} + A_{11} \frac{\partial^4 F}{\partial x^4} \right) - \frac{1}{A_{66}} \frac{\partial^4 F}{\partial x^2 \partial y^2} = \left(\frac{\partial^2 w}{\partial x \partial y} \right)^2 - \frac{\partial^2 w}{\partial x^2} \frac{\partial^2 w}{\partial y^2} \quad (5.20a)$$

The solution to equations (5.16a) and (5.20a) can be obtained using infinite series. Here, for simplicity, the series are truncated after the first few terms. The results will be of sufficient accuracy to show the basic trends.

The following expressions are assumed for w and F :

$$w = w_{11} \sin \frac{\pi x}{a} \sin \frac{\pi y}{a} \quad (7.2)$$

$$F = -\frac{P_x}{a} \frac{y^2}{2} - \frac{P_y}{a} \frac{x^2}{2} + K_{20} \cos \frac{2\pi x}{a} + K_{02} \cos \frac{2\pi y}{a} \quad (7.3)$$

with w_{11} , K_{20} , K_{02} , and P_y unknowns.

It is readily seen that the expression for w satisfies the first of boundary conditions (Equations (7.1)). The expression for the Airy stress function F is constructed such that the average loads P_x , at any station x , and P_y , at any station y , are recovered. This can be seen by integrating the first two of equations (5.17) with $V = 0$. The first is integrated with respect to y and the second with respect to x .

Using Equations (7.2) and (7.3) to substitute in Equation (5.20a) gives,

$$\begin{aligned} & \frac{A_{22}}{A_{11}A_{22}-A_{12}^2} K_{02} \frac{16\pi^4}{a^4} \cos \frac{2\pi y}{a} + \frac{A_{11}}{A_{11}A_{22}-A_{12}^2} K_{20} \frac{16\pi^4}{a^4} \cos \frac{2\pi x}{a} \\ &= w_{11}^2 \frac{\pi^4}{2a^4} \cos \frac{2\pi y}{a} + w_{11}^2 \frac{\pi^4}{2a^4} \cos \frac{2\pi x}{a} \end{aligned} \quad (7.4)$$

Matching coefficients of $\cos 2\pi x/a$ and $\cos 2\pi y/a$ gives

$$K_{02} = \frac{A_{11}A_{22}-A_{12}^2}{A_{22}} \frac{w_{11}^2}{32} \quad (7.5)$$

$$K_{20} = \frac{A_{11}A_{22}-A_{12}^2}{A_{11}} \frac{w_{11}^2}{32} \quad (7.6)$$

With these expressions for the coefficients K_{20} and K_{02} , the second von Karman equation (5.20a) is satisfied exactly.

Before proceeding to the first von Karman equation (5.16a), the transverse load P_y and the displacement $-C$ at $x = a$ corresponding to the applied load P_x are determined. The nonlinear strain displacement equation (5.13a) is rearranged:

$$\frac{\partial u}{\partial x} = \varepsilon_{xo} - \frac{1}{2} \left(\frac{\partial w}{\partial x} \right)^2$$

and the first of the inverted strain–stress equations (5.19) is used to substitute for the midplane strain ε_{xo} . This gives

$$\frac{\partial u}{\partial x} = \frac{A_{22}}{A_{11}A_{22}-A_{12}^2} N_x - \frac{A_{12}}{A_{11}A_{22}-A_{12}^2} N_y - \frac{1}{2} \left(\frac{\partial w}{\partial x} \right)^2$$

Now the first two equations of (5.17) can be used to substitute for N_x and N_y in terms of F (with $V=0$ as mentioned earlier):

$$\frac{\partial u}{\partial x} = \frac{A_{22}}{A_{11}A_{22}-A_{12}^2} \frac{\partial^2 F}{\partial y^2} - \frac{A_{12}}{A_{11}A_{22}-A_{12}^2} \frac{\partial^2 F}{\partial y^2} - \frac{1}{2} \left(\frac{\partial w}{\partial x} \right)^2 \quad (7.7)$$

Integrating over the entire plate,

$$\int_0^a \int_0^a \frac{\partial u}{\partial x} dx dy = \frac{A_{22}}{A_{11}A_{22}-A_{12}^2} \int_0^a \int_0^a \frac{\partial^2 F}{\partial y^2} dx dy - \frac{A_{12}}{A_{11}A_{22}-A_{12}^2} \int_0^a \int_0^a \frac{\partial^2 F}{\partial x^2} dx dy - \frac{1}{2} \int_0^a \int_0^a \left(\frac{\partial w}{\partial x} \right)^2 dx dy$$

Equations (7.2) and (7.3) can be used to substitute for F and w . This leads to

$$\begin{aligned} a(u(a,y)-u(0,y)) &= \frac{A_{22}a^2}{A_{11}A_{22}-A_{12}^2} \left(-\frac{P_x}{a} \right) - \frac{A_{12}a^2}{A_{11}A_{22}-A_{12}^2} \left(-\frac{P_y}{a} \right) \\ &\quad - \frac{1}{2} \iint \left((w_{11} \frac{\pi}{a} \cos \frac{\pi x}{a} \sin \frac{\pi y}{a})^2 \right) dx dy \end{aligned} \quad (7.8)$$

But $u(a,y) = -C$ and $u(0,y) = 0$ from (7.1). Substituting, performing the integration on the right-hand side, and rearranging,

$$C = \frac{aA_{22}}{A_{11}A_{22}-A_{12}^2} \frac{P_x}{a} - \frac{aA_{12}}{A_{11}A_{22}-A_{12}^2} \frac{P_y}{a} + w_{11}^2 \frac{\pi^2}{8a} \quad (7.9)$$

In an exactly analogous fashion, but starting this time from (5.13b):

$$\varepsilon_{yo} = \frac{\partial v}{\partial y} + \frac{1}{2} \left(\frac{\partial w}{\partial y} \right)^2$$

and using the third of Equations (7.1), the transverse load P_y is obtained as:

$$P_y = P_x \frac{A_{12}}{A_{11}} - w_{11}^2 \frac{\pi^2}{8a} \frac{A_{11}A_{22}-A_{12}^2}{A_{11}} \quad (7.10)$$

It is interesting to note that for in-plane problems, where $w_{11}=0$, Equation (7.10) gives

$$P_y = P_x \frac{A_{12}}{A_{11}}$$

Also, for isotropic plates, it can be shown that A_{12}/A_{11} equals the Poisson's ratio ν and thus,

$$P_y = \nu P_x$$

as expected.

At this point, P_y is known from Equation (7.10) and one can substitute in the first von Karman equation (5.20a). To do this, the following intermediate results are used:

$$\begin{aligned}\frac{\partial^4 w}{\partial x^4} &= \frac{\partial^4 w}{\partial x^2 \partial y^2} = \frac{\partial^4 w}{\partial y^4} = w_{11} \left(\frac{\pi}{a} \right)^4 \sin \frac{\pi x}{a} \sin \frac{\pi y}{a} \\ \frac{\partial^2 w}{\partial x^2} &= \frac{\partial^2 w}{\partial y^2} = -w_{11} \left(\frac{\pi}{a} \right)^2 \sin \frac{\pi x}{a} \sin \frac{\pi y}{a} \\ \frac{\partial^2 F}{\partial x^2} &= -\frac{P_y}{a} - \left(\frac{2\pi}{a} \right)^2 \frac{A_{11}A_{22}-A_{12}^2}{A_{11}} \frac{w_{11}^2}{32} \cos \frac{2\pi x}{a} \\ \frac{\partial^2 F}{\partial y^2} &= -\frac{P_x}{a} - \left(\frac{2\pi}{a} \right)^2 \frac{A_{11}A_{22}-A_{12}^2}{A_{22}} \frac{w_{11}^2}{32} \cos \frac{2\pi y}{a}\end{aligned}$$

In addition, the following trigonometric identities are used:

$$\begin{aligned}\sin \frac{\pi x}{a} \cos \frac{2\pi x}{a} &= \frac{1}{2} \left(\sin \frac{3\pi x}{a} - \sin \frac{\pi x}{a} \right) \\ \sin \frac{\pi y}{a} \cos \frac{2\pi y}{a} &= \frac{1}{2} \left(\sin \frac{3\pi y}{a} - \sin \frac{\pi y}{a} \right)\end{aligned}$$

Upon substituting in Equation (5.20a) there will be terms multiplying $\sin(\pi x/a)\sin(\pi y/a)$ and terms multiplying $\sin(3\pi x/a)\sin(\pi y/a)$ or $\sin(\pi x/a)\sin(3\pi y/a)$. The terms involving $3\pi x/a$ or $3\pi y/a$ are higher-order terms that would lead to additional equations if additional terms in the w expression (7.2) had been included. For the current expression for w with only one term, only coefficients of $\sin(\pi x/a)\sin(\pi y/a)$ are matched giving the following equation:

$$\frac{\pi^2 (A_{11}A_{22}-A_{12}^2)A_{11}+3A_{22}}{16A_{11}A_{22}} w_{11}^3 + \left(\frac{\pi^2}{a} (D_{11}+2(D_{12}+2D_{66})+D_{22}) - P_x \left(1 + \frac{A_{12}}{A_{22}} \right) \right) w_{11} = 0$$

which can be solved for w_{11} to give:

$$w_{11} = \sqrt{\frac{16A_{11}A_{22}(D_{11}+2(D_{12}+2D_{66})+D_{22})}{(A_{11}A_{22}-A_{12}^2)(A_{11}+3A_{22})} \left[\frac{P_x}{\frac{\pi^2 (D_{11}+2(D_{12}+2D_{66})+D_{22})}{a} - 1} \right]} \quad (7.11)$$

With w_{11} known from Equation (7.11), P_y can be obtained from (7.10) and K_{02}, K_{20} can be obtained from (7.5) and (7.6). This completely determines the displacement w and the Airy stress function F from Equations (7.2) and (7.3).

Equation (7.11) has certain important implications. The denominator in the quantity in brackets under the square root is the buckling load (units of force) for a square plate with simply supported and immovable edges. This expression is exact for a square plate. By denoting this buckling load by P_{cr} :

$$P_{cr} = \frac{\pi^2}{a} \frac{(D_{11} + 2(D_{12} + 2D_{66}) + D_{22})}{\left(1 + \frac{A_{12}}{A_{11}}\right)} \quad (7.12)$$

Equation (7.11) can be rewritten as:

$$w_{11} = \sqrt{\frac{16A_{11}A_{22}(D_{11} + 2(D_{12} + 2D_{66}) + D_{22})}{(A_{11}A_{22} - A_{12}^2)(A_{11} + 3A_{22})} \left[\frac{P_x}{P_{cr}} - 1 \right]} \quad (7.11a)$$

It can be seen from Equation (7.11a) that the quantity under the square root is negative if the applied load P_x is less than the buckling load P_{cr} . In such a case, w_{11} does not exist. Out-of-plane deflections, corresponding to a positive value of w_{11} are possible only after the plate has buckled and the applied load P_x is greater than the buckling load P_{cr} .

Additional implications are better understood through an example. Consider a square plate with layup $(\pm 45^\circ)/(0/90^\circ)/(\pm 45^\circ)$ made of plain weave fabric plies. Note that for such a symmetric layup D_{16} and D_{26} are always zero. The basic material properties are given below:

$$\begin{aligned} E_x &= E_y = 68.94 \text{ GPa} \\ v_{xy} &= 0.05 \\ G_{xy} &= 5.17 \text{ GPa} \\ t_{\text{ply}} &= 0.19 \text{ mm} \end{aligned}$$

With these properties the pertinent quantities in Equation (7.11) can be calculated:

D_{11}	659.7	N mm	A_{11}	28912.44	N/mm
D_{12}	466.9	N mm	A_{12}	12491.43	N/mm
D_{22}	659.7	N mm	A_{22}	28912.44	N/mm
D_{66}	494.0	N mm	A_{66}	13468.58	N/mm

and a plot of applied (normalized) load versus (normalized) center deflection is given in Figure 7.7. The plate thickness is denoted by h .

As already discussed, the center deflection w_{11} is zero for applied loads P_x lower than the buckling load P_{cr} . Once the applied load P_x exceeds the buckling load P_{cr} , the plate deflects out-of-plane and $w_{11} > 0$. As already suggested by the qualitative discussion of Figure 7.2, the load versus deflection curve is nonlinear and, for a plate, starts relatively flat and increases rapidly only after the center deflection becomes significantly larger than the plate thickness ($w_{11}/h > 1$).

The distribution of the in-plane load N_x is also very interesting. N_x can be obtained from the first of equations (5.17) with $V=0$ after substituting into (7.3) with P_y , K_{02} , and K_{20} given by Equations (7.10), (7.5), and (7.6) respectively. A plot of N_x as a function of the transverse coordinate y is shown in Figure 7.8. N_x is normalized by the average N_x value which equals P_x/a , and the y coordinate is normalized by the plate dimension a . The peak value of N_x occurs at the panel edge, suggesting that failure of a post-buckled plate under compression will initiate there.

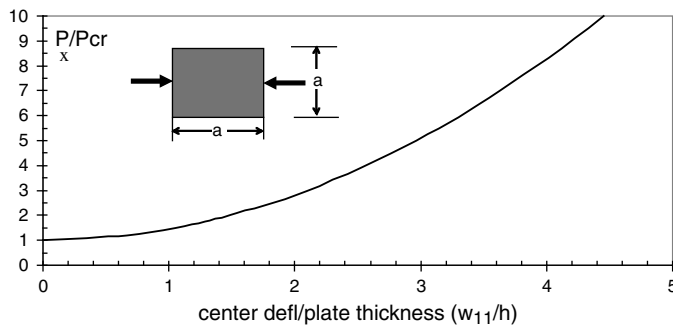


Figure 7.7 Load versus deflection for a square plate with layup $(\pm 45)/(0/90)/(\pm 45)$

The variation of N_x is shown for different load ratios P_x/P_{cr} , starting with $P_x = P_{cr}$, which is the case when the plate just buckles under compression. In that case, the in-plane force N_x is constant across the plate, as indicated by the vertical line in Figure 7.8. As the applied load increases beyond the buckling load ($P_x/P_{cr} > 1$) the N_x distribution is no longer uniform. More load concentrates at the edges of the panel while the load at the center is much lower. Already at $P_x/P_{cr} = 2$ the load at the panel edge is approximately twice the value at the center as can be seen from Figure 7.8. At $P_x/P_{cr} = 5$, the load at the edge is, approximately, four times the load at the panel center.

The reason for this nonuniform distribution is that once the plate buckles, its center is softer than the edges where the supports are. So load is diverted from the center to the edge of the panel. This difference between the load at the center and the edges of the panel becomes more and more pronounced as the load ratio P_x/P_{cr} increases.

This load redistribution can be used in design to generate simpler (conservative) design equations. The approach is based on approximating the actual N_x distribution by a step function that is zero at the panel center and generates the same total applied force. This is shown schematically in Figure 7.9. At each of the loaded edges of the panel, the load N_x is localized at the two edges, is constant, and is acting over an effective width b_{eff} . The magnitude of N_x equals the maximum magnitude of N_x shown in Figure 7.8 for the respective P_x/P_{cr} .

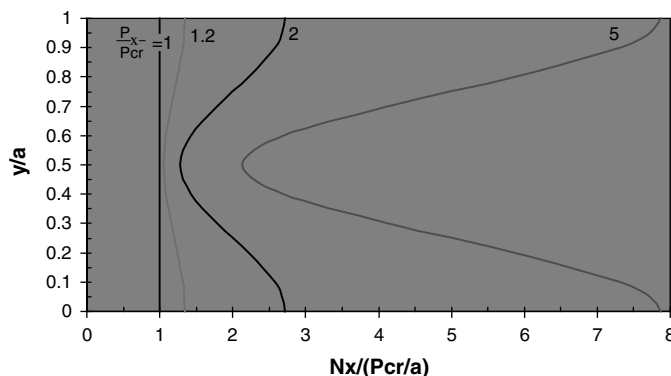


Figure 7.8 In-plane axial load N_x as a function of location and post-buckling ratio

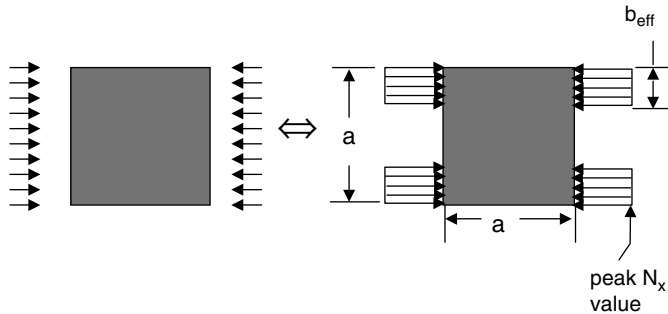


Figure 7.9 Equivalent in-plane compression in the post-buckling regime

The total force applied by this step-wise distribution must equal the applied load P_x . In terms of the force per unit width N_x this requirement can be expressed as:

$$\int N_x dy = 2(N_{x \max}) b_{eff} \quad (7.13)$$

Now from equation (5.17),

$$N_x = \frac{\partial^2 F}{\partial y^2} = -\frac{P_x}{a} - \frac{A_{11}A_{22} - A_{12}^2}{A_{22}} \frac{w_{11}^2}{32} \left(\frac{2\pi}{a}\right)^2 \cos \frac{2\pi y}{a}$$

which is maximized when $y = a/2$, i.e. at the edge of the panel. Then,

$$N_{x \max} = -\frac{P_x}{a} - \frac{A_{11}A_{22} - A_{12}^2}{A_{22}} \frac{w_{11}^2}{32} \left(\frac{2\pi}{a}\right)^2 \quad (7.14)$$

Also, by the definition of P_x ,

$$\int N_x dy = -P_x$$

Using this result and Equation (7.14) to substitute in (7.13), with w_{11} given by (7.11a), gives an equation for b_{eff} . Solving for b_{eff} gives:

$$b_{eff} = a \frac{1}{2 \left(1 + 2 \left(1 + \frac{A_{12}}{A_{11}} \right) \left(1 - \frac{P_{cr}}{P_x} \right) \frac{A_{11}}{A_{11} + 3A_{22}} \right)} \quad (7.15)$$

This b_{eff} can be viewed as the effective portion of the skin over which applying the maximum N_x value given by Equation (7.14) gives a loading that is equivalent to the applied load P_x , but also conservative. It is conservative because a larger portion of the plate is exposed to the maximum value $N_{x \max}$ than the exact N_x distribution suggests. As a result, designing a compressive panel in the post-buckling regime is equivalent to checking if the stress $N_{x \max}/h$ (where h the plate thickness) exceeds the allowable compression stress for the layup used and if so, reinforcing the panel edges over a distance given by Equation (7.15) so that there is no failure.

It should be noted that for a quasi-isotropic layup,

$$\frac{A_{12}}{A_{11}} = \nu_{12}$$

$$\frac{A_{11}}{A_{11} + 3A_{22}} = \frac{1}{4}$$

$$\nu_{12} \approx 0.3$$

and substituting in Equation (7.15) gives

$$b_{eff} = a \frac{1}{2 + 1.3 \left(1 - \frac{P_{cr}}{P_x} \right)} \quad (\text{for quasi-isotropic layup}) \quad (7.15a)$$

For cases with large loading ratios where $P_x \gg P_{cr}$ Equation (7.15a) becomes

$$b_{eff} = 0.303a \quad (\text{for quasi-isotropic layup with } P_x/P_{cr} \gg 1)$$

Equation (7.15) suggests a dependence of b_{eff} on the ratios A_{12}/A_{11} and A_{22}/A_{11} . The first ratio, is a measure of Poisson's ratio and the second a measure of degree of orthotropy. While these ratios are independent, for typical composite materials they lie within a range (for example a 0° ply of unidirectional material has a high degree of orthotropy, and A_{22}/A_{11} can be as low as 0.1, but the corresponding Poisson's ratio A_{12}/A_{11} is typically between 0.25 and 0.35). Based on typical composite material values, the three curves shown in Figure 7.10 can be constructed. The upper and lower curves correspond to extreme cases of high degree of orthotropy and the middle curve corresponds to a quasi-isotropic laminate. The two extreme curves give an idea of the range of variation of b_{eff} for typical composite materials. Note that as expected, all curves go through $b_{eff}/a = 0.5$ when $P_{cr}/P_x = 1$. This means that at buckling the entire skin is effective so the strip on each edge equals half the plate thickness.

It should be emphasized that the preceding discussion and derivation were based on single- or two-term expansions of the deflection w and Airy stress function F . The resulting post-buckled shape has a single half-wave across the entire plate. As such, while the basic

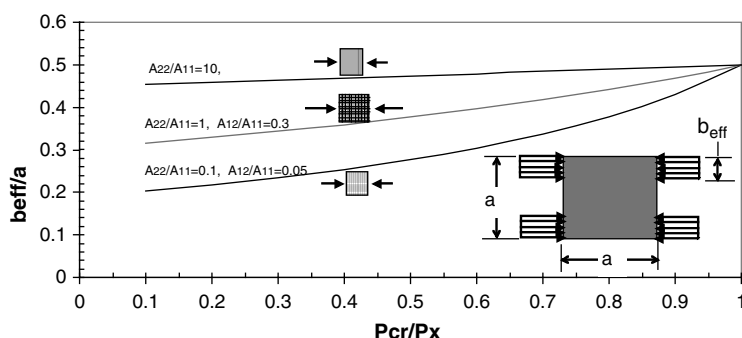


Figure 7.10 Variation of b_{eff} as a function of loading fraction and material properties

conclusions of the present analysis are valid, the absolute numbers may not be sufficiently accurate for detailed analysis (but they are for preliminary design). This is particularly true for plates with aspect ratios different from 1, where the post-buckled shape involves more than the one half-wave assumed here. In such a case, more terms should be included in the analysis (see also Exercise 7.3).

Once w and F are known the internal forces (N_x , N_y , and N_{xy}) and moments (M_x , M_y and M_{xy}) can be determined. Based on these, ply strains and stresses can be calculated and a failure criterion invoked. This can be a first-ply failure criterion (see Chapter 4) or a semi-empirically derived criterion based on test results.

7.1.1 Application: Post-Buckled Panel Under Compression

Consider a square plate simply supported all around ($w = 0$) with three edges immovable (no displacement perpendicular to them in the plane of the plate) and one edge loaded by a force of 2152 N, as shown in Figure 7.11.

Two candidate layups are proposed using plain weave fabric material: Layup A with stacking sequence $(\pm 45)/(0/90)_3/(\pm 45)$ and Layup B with stacking sequence $(0/90)/(\pm 45)/(0/90)/(\pm 45)/(0/90)$. Note that the two layups have exactly the same thickness and plies used. Only the ordering of the plies is different.

The basic material (ply) properties are given by:

Property	Value
E_x	69 GPa
E_y	69 GPa
v_{xy}	0.05
G_{xy}	5.1 GPa
t_{ply}	0.19 mm

It is required to determine the location and magnitude of the highest N_x value and which of the two proposed layups is better for this application.

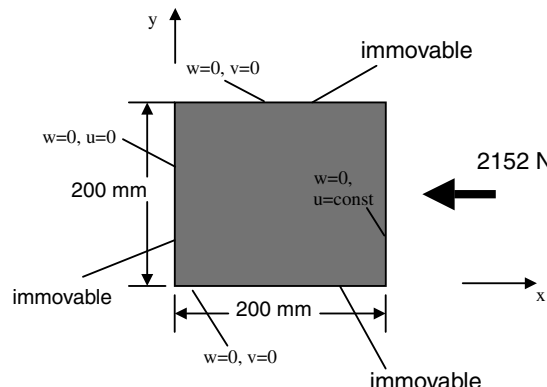


Figure 7.11 Square plate under compression

The boundary conditions and loading are the same as the post-buckling under compression situation analyzed earlier in this section and the solution just derived applies. From classical laminated-plate theory the following properties are obtained for each of the two layups:

	Layup A	Layup B	
a	200	200	mm
b	200	200	mm
A_{11}	55265	55265	N/mm
A_{12}	13821.5	13821.5	N/mm
A_{22}	55265	55265	N/mm
A_{66}	15452.5	15452.5	N/mm
D_{11}	3412.967	4560.031	N mm
D_{12}	1809.787	662.723	N mm
D_{22}	3412.967	4560.031	N mm
D_{66}	1932.848	785.784	N mm
t	0.9525	0.9525	mm
E10	5.44E + 10	5.44E + 10	N/m ²
E20	5.44E + 10	5.44E + 10	N/m ²
E60	1.62E + 10	1.62E + 10	N/m ²

Applying Equation (7.12), the buckling load for Layup A is found to be 718 N and for Layup B 536 N, which is 25% smaller than Layup A. This is due to the rearranging of the stacking sequence. It is interesting to note that placing ($\pm 45^\circ$) plies on the outside as in Layup A increases the buckling load. This can be seen from Equation (7.12) where the coefficient of D_{66} , which is 4, is higher than the coefficients of the remaining D_{ij} terms in the buckling load expression. Thus, increasing D_{66} increases the buckling load more than does the same percentage increase in other D_{ij} terms. And placing $\pm 45^\circ$ plies on the outside of a layup maximizes D_{66} .

Since the applied load is 2152 N, both layups have buckled and the post-buckling ratio PB for Layup A is $2152/718 = 3.0$ and for Layup B is $2152/536 = 4.0$. Using Equation (7.11a) the corresponding maximum center deflections w_{11} for the two layups are found to be:

$$w_{11A} = 1.67 \text{ mm}$$

$$w_{11B} = 1.78 \text{ mm}$$

These deflections are about twice the plate thickness and justify the use of large deflection theory. Even though Layup B has 25% lower buckling load, its center deflection is only 6.5% higher than Layup B, showing that increased bending stiffness has less of an effect in the post-buckling regime.

Using Equations (7.5) and (7.6), the constants K_{02} and K_{20} are found to be:

	Layup A	Layup B
$K_{02} = K_{20} =$	4538.78	5112.312

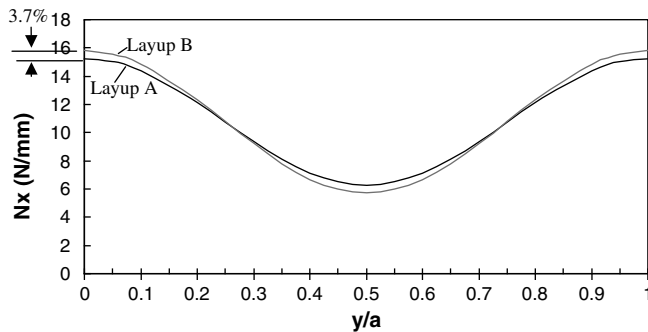


Figure 7.12 Axial force as a function of location

The in-plane force N_x now be determined from Equations (5.17) and (7.3) as:

$$N_x = - \left[\frac{P_x}{a} + \frac{4\pi^2}{a^2} K_{02} \cos \frac{2\pi y}{a} \right]$$

where P_x is the applied load 2152 N and a is the side of the plate, 200 mm.

The expression for N_x is independent of x so it is the same for any x location along the plate. Substituting values, the plot of N_x as a function of y can be obtained and it is shown for both layups in Figure 7.12.

As can be seen from Figure 7.12 and as expected from the expression for N_x above and the earlier discussion, N_x reaches its maximum compressive values at the edges of the panel. It is also evident from Figure 7.12 that the maximum N_x values for the two layups differ only by 3.7%. Thus, a significant difference (25%) in the buckling load leads to a negligible difference in the maximum in-plane force in the plate. This suggests that the failure loads in the post-buckling regime for the two layups will be close to each other. Thus, significant differences in buckling performance do not translate to analogous differences in post-buckling performance.

7.2 Post-buckling Analysis of Composite Plates under Shear

A post-buckled stiffened composite plate under shear is shown in Figure 7.13. The buckling pattern consists of half-waves confined between the stiffeners. These half-waves make an angle α with the stiffener axis.



Figure 7.13 Stiffened composite panel in the post-buckling regime (See Plate 16 for the colour figure)

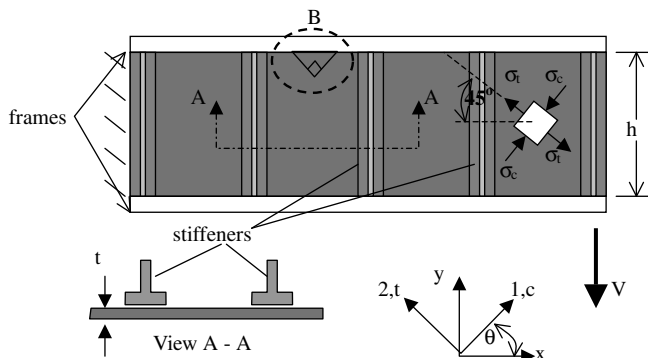


Figure 7.14 Stiffened skin under shear

The situation of Figure 7.13 is idealized in Figure 7.14.

Assuming that the bending loads are taken by the two frames, the skin between stiffeners is under pure shear. The constant (applied) shear in each skin bay is then given by:

$$\tau_a = \frac{V}{ht} \quad (7.16)$$

When the applied shear load V is low, the skin does not buckle and the shear stress τ_a can be resolved into a biaxial state of stress consisting of tension stress σ_t along a 45° line (see last bay in Figure 7.14) and a compression stress σ_c . It can be shown that the magnitudes of σ_t and σ_c are equal. This can be derived from the standard stress transformation equations (3.35):

$$\begin{Bmatrix} -\sigma_c \\ \sigma_t \\ \tau_{12} \end{Bmatrix} = \begin{bmatrix} \cos^2\theta & \sin^2\theta & 2\sin\theta\cos\theta \\ \sin^2\theta & \cos^2\theta & -2\sin\theta\cos\theta \\ -\sin\theta\cos\theta & \sin\theta\cos\theta & \cos^2\theta-\sin^2\theta \end{bmatrix} \begin{Bmatrix} \sigma_x \\ \sigma_y \\ \tau_{xy} \end{Bmatrix} \quad (7.17)$$

In Equation (7.17), the original coordinate system x,y (see Figure 7.14) is rotated through the angle θ to the new $1,2$ (or c,t) coordinate system. A minus sign appears in front of σ_c on the left hand side to stay consistent with the orientation of σ_c in Figure 7.14 (the sign convention requires tensile normal stresses to be positive; σ_c is compressive). Given the sign convention in the xy coordinate system, $\tau_{xy} = -\tau_a$.

Also, in the same coordinate system, $\sigma_x = \sigma_y = 0$. And for $\theta = 45^\circ$, Equation (7.17) simplifies to:

$$\begin{aligned} \sigma_c &= \tau_a \\ \sigma_t &= \tau_a \\ \tau_{12} &= 0 \end{aligned} \quad (7.18)$$

The fact that the shear stress τ_{12} is zero in the $1-2$ coordinate system implies that the $1-2$ axes are principal axes. This is expected from the fact that the skin is under pure shear, which translates to pure biaxial loading (tension and compression) in a coordinate system rotated by 45° with respect to the original.

Equation (7.18) describes the situation until the skin buckles. Once the skin buckles, it is assumed that, the compression direction of the skin cannot support any higher stress. So as the applied load is increased beyond the load that causes skin buckling, the compressive stress σ_c stays constant and equal to its value at buckling. Letting τ_{cr} be the value of τ_a when the skin buckles, the compressive skin stress after the skin buckles is given by

$$\sigma_c = \tau_{cr} \text{ for } \tau_a > \tau_{cr} \text{ or } V > V_{cr} \quad (7.19)$$

where V_{cr} is the applied shear load at which the skin buckles.

The stresses in the skin after it buckles can be determined by considering equilibrium of the triangular piece of skin with base length dx shown in detail B in Figure 7.14. The free-body diagram of that detail is shown in Figure 7.15.

With reference to Figure 7.15, if the length of segment AC is dx , then, by Pythagoras' theorem, the two segments AB and BC are:

$$AB = BC = \frac{dx}{\sqrt{2}} \quad (7.20)$$

As already mentioned, sides AB and BC are under pure compression and pure tension respectively (x and y axes are principal axes). On the other hand, both a shear stress τ_a and a normal stress σ are applied on side AC. Considering force equilibrium in the x direction,

$$\begin{aligned} \sigma_t \left(\frac{tdx}{\sqrt{2}} \right) \sin 45 + \sigma_c \left(\frac{tdx}{\sqrt{2}} \right) \sin 45 - \tau_a t dx &= 0 \Rightarrow \\ \frac{\sigma_t + \sigma_c}{2} &= \tau_a \end{aligned} \quad (7.21)$$

Similarly, considering force equilibrium in the y direction,

$$\begin{aligned} -\sigma_t \left(\frac{tdx}{\sqrt{2}} \right) \cos 45 + \sigma_c \left(\frac{tdx}{\sqrt{2}} \right) \cos 45 + \sigma t dx &= 0 \Rightarrow \\ \frac{\sigma_t - \sigma_c}{2} &= \sigma \end{aligned} \quad (7.22)$$

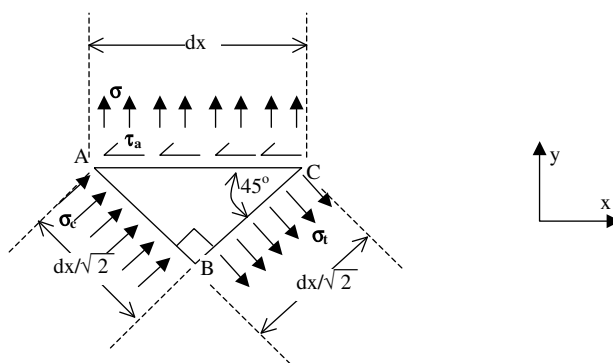


Figure 7.15 Free-body diagram of triangular skin element after buckling

Now σ_c is constant and given by Equation (7.19) while τ_a is proportional to the applied load V and given by Equation (7.16). Therefore, Equations (7.21) and (7.22) form a system of two equations in the two unknowns σ_t and σ . Solving:

$$\begin{aligned}\sigma_t &= 2\tau_a - \sigma_c \\ \sigma &= \tau_a - \sigma_c\end{aligned}$$

and using Equations (7.16) and (7.19),

$$\sigma_t = \frac{2V}{ht} - \tau_{cr} \quad (7.23)$$

$$\sigma = \frac{V}{ht} - \tau_{cr} \quad (7.24)$$

As mentioned earlier, τ_{cr} is the shear stress at which the skin buckles. This can be determined following the procedures of Sections 6.3–6.5 (for example Equation 6.28 for long plates or 6.37 with appropriate adjustment to improve its accuracy).

Designing a composite skin under shear in the post-buckling regime would then require the determination of a layup that will not fail when stresses σ_t and σ_c are applied. Note that these are along the axes 1,2 in Figure 7.14 and, therefore, the resulting layup would be in that coordinate system and would have to be rotated in order to express it in the original xy coordinate system. In addition to the skin, the stiffeners and flanges would have to be designed taking into account the stresses σ and τ_a (for stiffener and flange design see Sections 8.3–8.7).

It is important to note that the preceding derivation only gives the average stresses in the skin and assumes that the angle of the principal axes remains constant and equal to 45° after buckling. In reality, the angle changes as the applied load increases. The solution given above is conservative and mainly underlines the fact that the skin is under increasing tension along diagonal lines (hence the term ‘diagonal tension’ for such situations) and constant compression perpendicular to these diagonal lines. For sufficiently high applied loads the effect of the compression stress σ_c is very small and can be neglected.

An improved analytical approach for post-buckled panels under shear was proposed by Wagner for isotropic materials [1, 2]. In this analysis the effect of stiffener spacing, flange geometry, and skin dimensions is taken into account and an iterative set of equations is derived for the post-buckling angle α (Figure 7.16) and the stresses in the skin, stiffeners and flanges.

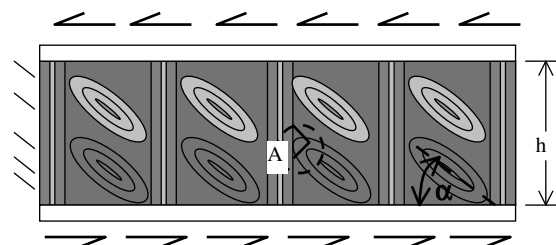


Figure 7.16 Post-buckled skin under shear showing post-buckling angle α

The analysis by Wagner was further improved by Kuhn *et al.* [3, 4] who accounted more accurately for the relative stiffnesses of skin, stiffeners and flanges and used test results to derive some of their semi-empirical equations. In fact, the analysis by Kuhn *et al.* forms even today, with minor modifications, the basis for designing isotropic post-buckled panels under shear.

For the case of composite materials, the analysis by Kuhn *et al.* was modified by Deo *et al.* [5, 6]. The basic results from their work form the starting point for the discussion in Section 7.2.1. In what follows, the mathematical aspects of their method are improved upon in order to minimize or eliminate the need for iterations.

7.2.1 Post-buckling of Stiffened Composite Panels under Shear

The situation is shown in Figure 7.16.

Before going into the equations that describe the state of stress in the panel of Figure 7.16, a qualitative discussion of how loads are shared between the different components might help visualize what happens. Consider that the panel of Figure 7.16 is a portion of a fuselage, with the two flanges (above and below) being frames and the vertical stiffeners being stringers.

It is simpler to visualize what happens if only a shear load is applied as in Figure 7.16. This could be the result of torsion in the fuselage. Combined load cases are briefly discussed in the next section. If the load is low enough and the skin does not buckle, the skin is under pure shear and there is no load in the stringers or the frames.

After the skin buckles in shear, it resists the applied load in diagonal tension along lines forming an angle α with the frames. A small amount of compression (see Equation (7.19)) is also present. As the skin pulls away from the stiffeners it exerts both a tension load along each stiffener and a transverse load that would bend the stiffener in the plane of Figure 7.16. This is shown in Figure 7.17 where detail A from Figure 7.16 is put in equilibrium.

At the interface between skin and stringer a normal stress σ_s and a shear stress τ_s must develop to put the skin in equilibrium. These, in turn, are exerted on the stringer. In order for the stringer to be in equilibrium axial loads P_{st1} and P_{st2} and bending moments must develop. In an

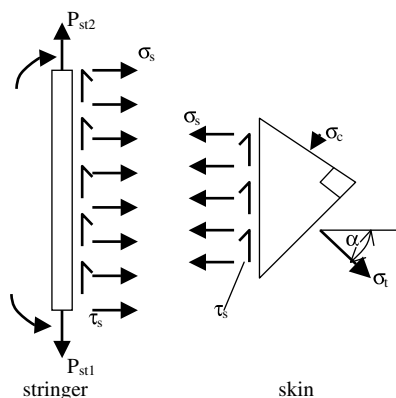


Figure 7.17 Equilibrium of detail A from Figure 7.16

analogous fashion, axial and bending loads develop in the frames. Therefore, determining the stresses or strains not only in the skins, but also in the stringers and frames becomes crucial for designing such structures in the post-buckling regime.

The best analytical solution for composite panels in the post-buckling regime was developed by Deo, Agarwal and Madenci [5] and Deo, Kan and Bhatia, [6]. In that work, the original methodology for metal panels developed by Kuhn, Peterson and Levin [3, 4] was modified to account for the anisotropy of composite panels and the additional failure mode of skin/stiffener separation, typically not present in metal structures.

This work relates the strains in the skin, stiffener and frame to the post-buckling angle α , which is the angle formed by the buckled shape of the skin and the stiffener axis (see Figures 7.16 and 7.17). The equations are transcendental, and iterations are needed to eliminate α in order to obtain strains as a function of geometry and stiffness. An approach to simplify the algebra and solve the equations presented in [5] and [6] is presented below.

The governing equations are as follows:

Post-Buckling Factor k

$$k = \tanh \left[\frac{1}{2} \ln \left(\frac{N_{xy}}{N_{xycr}} \right) \right] \quad (7.25)$$

The post-buckling factor (not to be confused with the post-buckling ratio PB introduced at the start of this chapter) ranges between 0 and 1 and gives a measure of how much of the applied shear load is taken by in-plane shear and how much by diagonal tension. A value of $k = 0$ denotes pure shear. A value of $k = 1$ denotes all the applied load is taken by diagonal tension.

Post-Buckling Angle α

$$\alpha = \tan^{-1} \sqrt{\frac{\varepsilon - \varepsilon_s}{\varepsilon - \varepsilon_f}} \quad (7.26)$$

Skin Strain ε in Diagonal Tension Direction:

$$\varepsilon = \frac{N_{xy}}{E_{wa}} \left[\frac{2k}{\sin 2\alpha} + \frac{E_{wa}}{2G_{sk}} (1-k) \sin 2\alpha \right] \quad (7.27)$$

Stiffener Strain ε_s

$$\varepsilon_s = \frac{-kN_{xy} \cot \alpha}{\left[\frac{EA_s}{h_s t_{sk}} + \frac{1}{2} (1-k) E_{ws} \right]} \quad (7.28)$$

Frame strain ε_f

$$\varepsilon_f = \frac{-kN_{xy} \tan \alpha}{\left[\frac{EA_f}{h_r t_{sk}} + \frac{1}{2}(1-k)E_{wf} \right]} \quad (7.29)$$

where:

N_{xy} = applied shear load (force/length)

N_{xycr} = buckling load under shear of skin between adjacent stiffeners and frames

ε = skin strain in diagonal tension direction

ε_s = strain in the stringer averaged over its length

ε_f = strain in the frame averaged over its length

t_{sk} = skin thickness

h_s = stiffener spacing

h_f = frame spacing

$E_{w\alpha}$ = skin (or web) modulus in diagonal tension direction

E_{ws} = skin (or web) modulus along stiffener direction

E_{wf} = skin (or web) modulus along frame direction

G_{sk} = skin shear modulus

\overline{EA}_s = axial stiffness of stiffener ($= EA_s(EI_s)/\overline{EI}_s$)

\overline{EA}_f = axial stiffness of frame ($= EA_f(EI_f)/\overline{EI}_f$)

EI_s, EI_f = bending stiffness about stiffener, frame neutral axis

$\overline{EI}_s, \overline{EI}_f$ = corresponding bending stiffnesses about skin midsurface

It is important to note that the axial stiffnesses \overline{EA} (= Young's modulus E multiplied by area A) are corrected by the bending stiffnesses EI (= Young's modulus E multiplied by moment of inertia I). This is done to account for the fact that, in general, for a composite beam, the membrane stiffness and the bending stiffnesses are different (see Sections 3.3 and 8.2).

It can be seen from Equations (7.26)–(7.29) that trigonometric functions of α and the strains ε , ε_s , and ε_f all appear in the governing equations. Traditionally, the approach to solving them is to assume a value of α (about 40° is a good starting value), and substitute in Equations (7.27), (7.28) and (7.29) to get the strains ε , ε_s , and ε_f . These strains are then substituted in Equation (7.26) to obtain an updated value for α . The procedure is repeated until two successive values of α are equal to within some preset tolerance value.

This approach is not very efficient because it involves iterations. These iterations would be repeated for each candidate design during an optimization run and would slow the process tremendously. It would be advantageous if these iterations were minimized and another way to solve Equations (7.26)–(7.29) were found.

It turns out that if $E_{w\alpha}$, the skin modulus in the direction of the diagonal tension angle α is assumed constant, Equations (7.26)–(7.29) can be solved exactly without iterations. First, the trigonometric expressions involving α are expressed in terms of $\tan \alpha$:

$$\sin^2 \alpha = \frac{\tan^2 \alpha}{1 + \tan^2 \alpha}$$

$$\cos^2 \alpha = \frac{1}{1 + \tan^2 \alpha}$$

$$\sin 2\alpha = 2 \frac{\tan \alpha}{1 + \tan^2 \alpha}$$

Then, using these expressions, the three strains from Equations (7.27)–(7.29) are written as:

$$\varepsilon = A \frac{1 + \tan^2 \alpha}{2 \tan \alpha} + B \frac{2 \tan \alpha}{1 + \tan^2 \alpha} \quad (7.27a)$$

$$\varepsilon_s = \frac{C}{\tan \alpha} \quad (7.28a)$$

$$\varepsilon_f = D \tan \alpha \quad (7.29a)$$

where

$$A = \frac{N_{xy} 2k}{t_{sk} E_{w\alpha}} \quad (7.30)$$

$$B = \frac{N_{xy} (1-k)}{t_{sk} G_{sk}} \quad (7.31)$$

$$C = \frac{-k N_{xy}}{t_{sk} \left(\frac{\overline{E} A_s}{h_s t_{sk}} + \frac{1}{2} (1-k) E_{ws} \right)} \quad (7.32)$$

$$D = \frac{-k N_{xy}}{t_{sk} \left(\frac{\overline{E} A_r}{h_r t_{sk}} + \frac{1}{2} (1-k) E_{wf} \right)} \quad (7.33)$$

If Equation (7.26) is now used to solve for $\tan \alpha$ and substitute in (7.27a)–(7.29a), the angle α is eliminated and three equations in the three unknowns ε , ε_r , and ε_f are obtained. After some manipulation, ε and ε_s can be eliminated and a single equation in

$$z = \left(\frac{\varepsilon_f}{D} \right)^2 \quad (7.34)$$

is obtained as follows:

$$z^3 + z^2 \frac{2D - A - 4B}{2D - A} + z \frac{A - 2C + 4B}{2D - A} + \frac{A - 2C}{2D - A} = 0 \quad (7.35)$$

From the theory of cubic equations, (see for example [7]), it can be shown that since A and B have the same sign as N_{xy} and C and D have sign opposite to that of N_{xy} , Equation (7.35) has three real and unequal solutions. The solutions are given by

$$\begin{aligned}
 z_1 &= 2\sqrt{-Q}\cos\frac{\theta}{3} - \frac{a_2}{3} \\
 z_2 &= 2\sqrt{-Q}\cos\left(\frac{\theta + 2\pi}{3}\right) - \frac{a_2}{3} \\
 z_3 &= 2\sqrt{-Q}\cos\left(\frac{\theta + 4\pi}{3}\right) - \frac{a_2}{3}
 \end{aligned} \tag{7.36}$$

with

$$\begin{aligned}
 \theta &= \cos^{-1}\left(\frac{R}{\sqrt{-Q^3}}\right) \\
 R &= \frac{9a_1a_2 - 27a_o - 2a_2^3}{54} \\
 Q &= \frac{3a_1 - a_2^2}{9}
 \end{aligned} \tag{7.37}$$

and

$$\begin{aligned}
 a_o &= \frac{A - 2C}{2D - A} \\
 a_1 &= \frac{A - 2C + 4B}{2D - A} \\
 a_2 &= \frac{2D - A - 4B}{2D - A}
 \end{aligned} \tag{7.38}$$

Of the three solutions in Equation (7.36), only the positive ones are acceptable because, otherwise, the right-hand side of Equation (7.34), which is positive, would be a negative number. If there are more than one positive solutions, the lowest one should be selected.

As was mentioned earlier, the solution of Equation (7.36)–(7.38) assumes that the stiffness of the skin in the direction of α , $E_{w\alpha}$, is constant. However, without knowing α a priori $E_{w\alpha}$ is not known exactly. A small number of iterations (typically significantly fewer than those required with the traditional approach mentioned earlier) is required after all. To determine the skin stiffness along any direction α , it is assumed that a tension load is applied in that direction and the stress-strain equations are solved for. This parallels the derivation of Equations (5.19) in chapter 5. For a symmetric and balanced skin, the normal stresses σ_{11} and σ_{22} in a

coordinate system with the 1 axis aligned with α are given by the following expressions (see Equation 3.32):

$$\begin{aligned}\sigma_{11} &= Q_{11}\varepsilon_{11} + Q_{12}\varepsilon_{22} \\ \sigma_{22} &= Q_{12}\varepsilon_{11} + Q_{22}\varepsilon_{22}\end{aligned}$$

But $\sigma_{22} = 0$ since only a tension load is applied in the 1 (or α) direction. Therefore, solving for ε_{22} :

$$\varepsilon_{22} = -\frac{Q_{12}}{Q_{22}}$$

and substituting in the equation for σ_{11} :

$$\sigma_{11} = \underbrace{\left(Q_{11} - \frac{Q_{12}^2}{Q_{22}} \right)}_{E_{w\alpha}} \varepsilon_{11}$$

from which,

$$E_{w\alpha} = Q_{11} - \frac{Q_{12}^2}{Q_{22}} \quad (7.39)$$

with the standard transformation giving the stiffnesses Q_{11} , Q_{12} , and Q_{22} (see Equations 3.33):

$$\begin{aligned}Q_{11} &= Q_{xx}\cos^4\alpha + Q_{yy}\sin^4\alpha + 2\sin^2\alpha\cos^2\alpha(Q_{xy} + 2Q_{ss}) \\ Q_{22} &= Q_{xx}\sin^4\alpha + Q_{yy}\cos^4\alpha + 2\sin^2\alpha\cos^2\alpha(Q_{xy} + 2Q_{ss}) \\ Q_{12} &= \sin^2\alpha\cos^2\alpha(Q_{xx} + Q_{yy} - 4Q_{ss}) + (\sin^4\alpha + \cos^4\alpha)Q_{xy}\end{aligned} \quad (7.40)$$

and, from Equations (3.27)–(3.29):

$$\begin{aligned}Q_{xx} &= \frac{E_{xx}}{1 - v_{xy}v_{yx}} \\ Q_{yy} &= \frac{E_{yy}}{1 - v_{xy}v_{yx}} \\ Q_{xy} &= \frac{v_{yx}E_{xx}}{1 - v_{xy}v_{yx}} \\ Q_{ss} &= G_{sk}\end{aligned} \quad (7.41)$$

where E_{xx} , E_{yy} , G_{sk} , v_{xy} , v_{yx} are engineering constants for the entire skin laminate with x coinciding with the stiffener direction and y coinciding with the frame direction.

The solution procedure is then as follows:

1. Select a value of $E_{w\alpha}$. Typically, since $\alpha \approx 45^\circ$ select E_{wa} corresponding to the 45° direction.
2. Calculate the coefficients in Equation (7.35) using Equations (7.37) and (7.38).
3. Calculate z_1 , z_2 , z_3 from Equation (7.36).
4. Pick the positive z value from step 3. If there are more than one positive values, use the lowest one.
5. Calculate a new value of $E_{w\alpha}$ using Equations (7.39)–(7.41). If it is equal to the previous value of $E_{w\alpha}$ within a preset tolerance, the diagonal tension analysis is complete. If not, go to step 2 above and repeat the process.

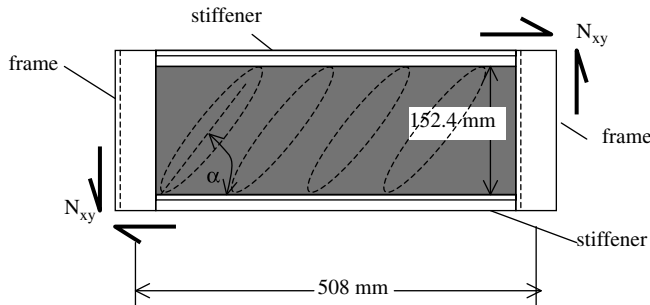


Figure 7.18 Stiffened skin under shear load

7.2.1.1 Application: Post-Buckled Stiffened Fuselage Skin under Shear

Consider the portion of fuselage skin enclosed by two adjacent stiffeners and frames as shown in Figure 7.18. The skin is under pure shear N_{xy} .

A notional sketch of the post-buckling shape with the half-waves inclined at an angle α to the stiffener axis is also included in Figure 7.18. The length of the stiffeners and frames are set at typical values of 508×152.4 mm respectively. Two different skin layups of the same thickness are used: (a) $(\pm 45)_5$ and (b) $(\pm 45)/(0/90)_3/(\pm 45)$. The material used for the skin is plain weave fabric with properties:

$$\begin{aligned} E_x &= E_y = 68.9 \text{ GPa} \\ G_{xy} &= 4.82 \text{ GPa} \\ v_{xy} &= 0.05 \\ t_{\text{ply}} &= 0.1905 \text{ mm} \end{aligned}$$

The details of the stiffener and frame layups are of no interest at this point other than the fact that, for both skin layups, EA for the stiffener is 6953 kN and for the frame is 75 828 kN. The buckling load for the skin of case (a) is determined to be 10.82 N/mm and for the skin of case (b) 10.88 N/mm. Note that the buckling loads are essentially the same for the two cases.

The results for the post-buckling behavior for both cases are shown in Figures 7.19–7.21. The post-buckling angle α (see Figure 7.18) for the two different skin layups is given in Figure 7.19 as a function of the applied load normalized by the buckling load.

For both cases, the post-buckling angle starts at 45° when the applied load N_{xy} equals the buckling load $N_{xy,\text{crit}}$ and decreases towards an asymptote around 25° for high values of $N_{xy}/N_{xy,\text{crit}}$. The post-buckling angle for the $(\pm 45)/(0/90)_3/(\pm 45)$ skin is slightly higher.

The strains in the skin, stiffener and frame for the $(\pm 45)_5$ skin layup are shown as a function of the applied load in Figure 7.20. It is seen that the stiffener and frame are always in compression. While the skin strains are relatively linear, the stiffener and frame strains are nonlinear and they increase more rapidly than the skin strains. If now the cutoff strain of $4500 \mu\epsilon$ calculated in Section 5.1.6 is used for the stiffener and frame, which are in compression, and a corresponding value of $6000 \mu\epsilon$ is used for the skin, which is in tension, (tension allowable is higher than compression allowable for most layups used in practice) it can

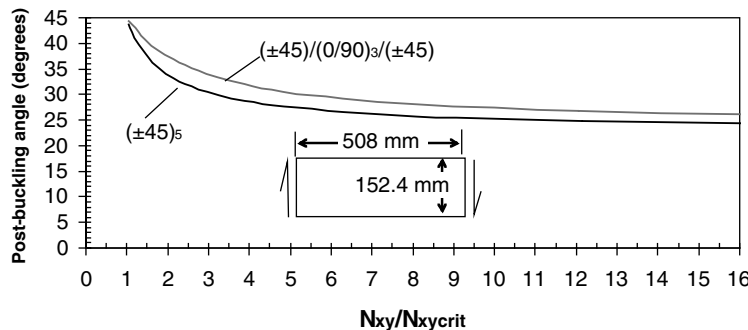


Figure 7.19 Postbuckling angle as a function of applied shear load

be seen from Figure 7.20 that the stiffener will fail first at a value of N_{xy}/N_{xycrit} , slightly higher than 11. This is interesting because at lower loads the skin has higher strains than the stiffener, but they are increasing more slowly as the load increases.

It is important to note that the use of cutoff strains does not explicitly account for the layup. This is a conservative approach for generating or evaluating a preliminary design. A more detailed analysis would require knowledge of the specific layups and geometries for the skin and stiffener. Also, additional failure modes such as crippling of the stiffener or frame (see Section 8.5) and skin–stiffener separation (see Section 9.2.2) would have to be included in the evaluation. The present discussion gives a good starting point for generating a viable design.

The corresponding strains for the second case with skin layup $(\pm 45)/(0/90)_3/(\pm 45)$ are shown in Figure 7.21. Again, the stiffener and frame are in compression while the skin is in tension. Unlike the case of the $(\pm 45)_5$ skin where the stiffener strains rapidly

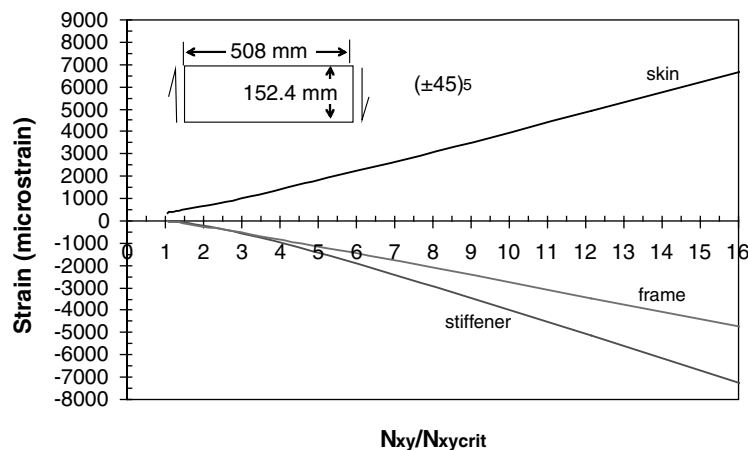


Figure 7.20 Strains in the post-buckling regime for $(\pm 45)_5$ skin

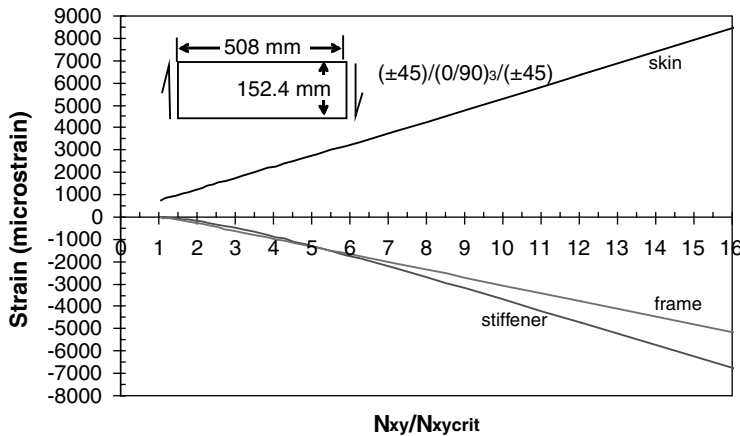


Figure 7.21 Strains in the post-buckling regime for $(\pm 45)/(0/90)_3/(\pm 45)$ skin

exceeded in magnitude the skin strains, here the skin strains are always higher in magnitude. This is due to the fact that the skin in this case is significantly stiffer and absorbs more load, thus unloading the stiffeners to some extent. However, the stiffeners are still critical as the cutoff value of $4500 \mu\text{s}$ for the stiffeners is reached before the cutoff value of $6000 \mu\text{s}$ is reached for the skin.

Comparing the results in Figures 7.20 and 7.21 it is seen that, even though the dimensions, the stiffeners, and the frames are identical and the skin buckling loads are the same, the post-buckling behavior in the second case is significantly different. For example, at low applied loads the skin strains are twice as high for the second case. This difference decreases as the applied load increases, but is still at least 25% at high applied loads.

7.2.2 Post-buckling of Stiffened Composite Panels under Combined Uniaxial and Shear Loading

When both shear and an axial load (tension or compression) act on a stiffened panel, the state of stress developing in the post-buckling skin is quite complicated and very hard to obtain without a good computational model, usually based on finite elements. Also, the situation changes if the axial load is tension instead of compression.

A stiffened composite panel under combined shear and compression is shown in Figure 7.22. A typical half-wave of the buckled pattern is also shown. Note that, unlike the pure shear case where the post-buckling angle α starts at 45° at buckling and decreases slowly with increasing load (see example in previous section) the presence of a compressive load keeps the half wave closer to the 90° orientation, i.e. the post-buckling angle α starts higher than 45° at buckling.

The load combination that leads to buckling can be obtained following the procedures of Sections 6.5 and 6.6. The conservative approach for designing in the post-buckling regime is to assume that all the compressive load beyond the buckling load is absorbed by the stiffeners.

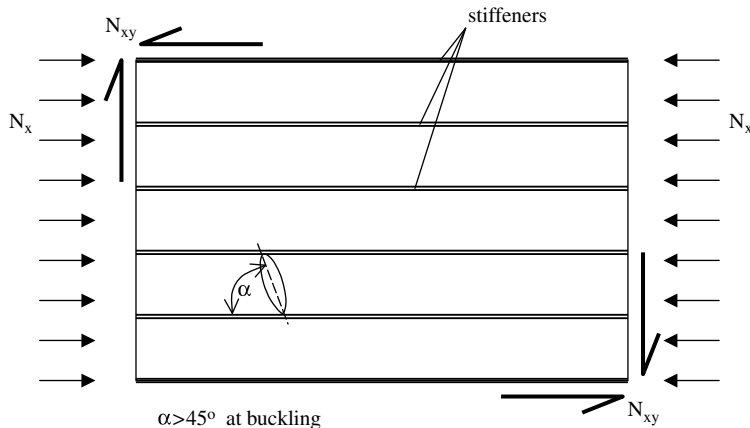


Figure 7.22 Post-buckled panel under compression and shear

This extra compressive load would increase the stiffener strains and make them more critical than in the case where no compressive load is applied. The load in the skin would be a combination of the strains obtained when only the shear is applied, and the (constant) compressive strains corresponding to the buckling load. That is, beyond buckling, the compression load in the skin is constant and equal to its buckling value, but the shear is increasing according to the post-buckling analysis given in the previous section. The fact that the skin is loaded by the compressive strains that were exerted at the buckling load in addition to the diagonal tension strains resulting from the shear load, is more critical than in the case where only shear load was applied.

In contrast to the combined compression and shear case, a tension and shear case is, usually, less critical. First, the magnitude of the buckling load under tension and shear is lower. Then, in the post-buckling regime, the tension strains caused by the applied tensile load are split between skin and stiffeners according, roughly, to their respective EA ratios. This means that the compression strains in the stiffeners caused by the shear load are relieved and the stiffeners are less critical. In the skin, the diagonal compression strains are relieved while the diagonal tension strains are increased. However, since in most designs the stiffeners are much stiffer than the skin (have much higher EA) the amount of tension left in the skin is small and most of it is taken by the stiffeners.

The procedure for preliminary design and analysis of a composite stiffened panel under combined uniaxial load and shear is summarized in Figure 7.23. Note that in this figure $N_x > 0$ corresponds to tension. This procedure should be viewed as approximate because it requires combining skin strains caused by shear load applied alone and a portion of strains from compression applied alone. This implies some kind of superposition is being used. However, linear superposition is not valid in the post-buckling regime because the deflections are large and the problem is nonlinear. Only for applied loads that do not exceed the buckling loads significantly, is superposition (approximately) valid. Therefore, the results of this process are approximate. They can be very useful in determining a good starting design for further more detailed analysis.

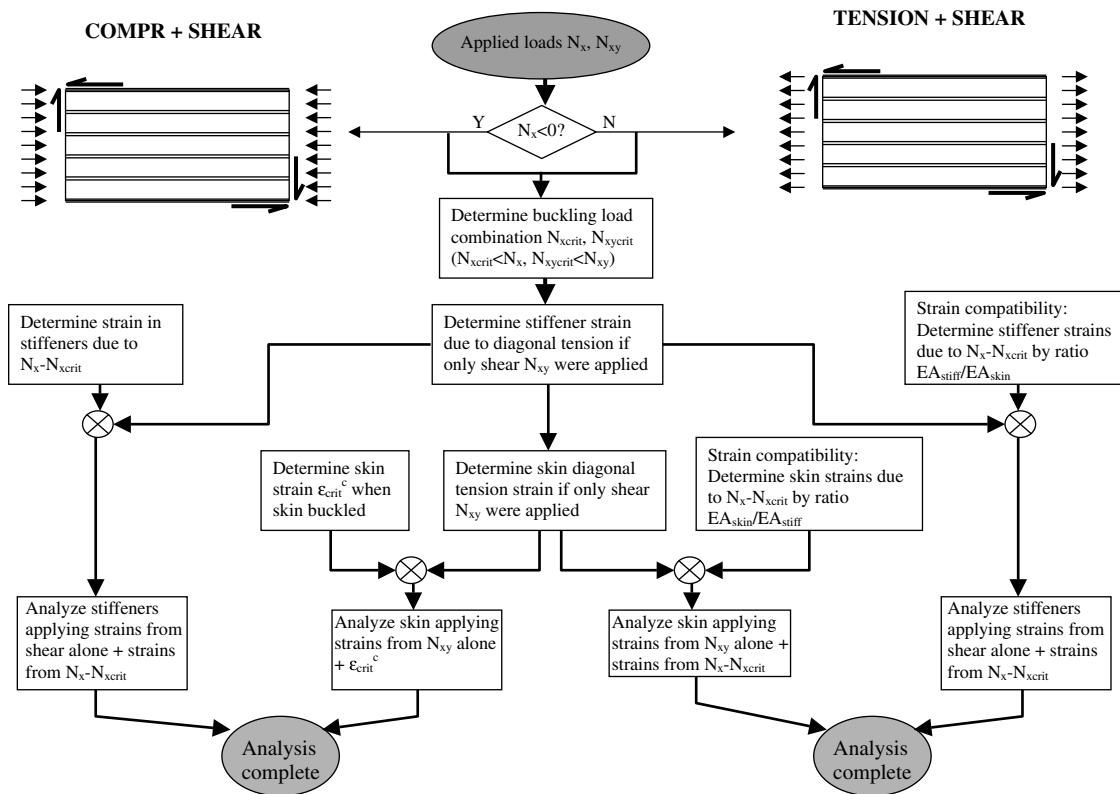


Figure 7.23 Design/analysis procedure for stiffened panels under combined uniaxial load and shear

Exercises

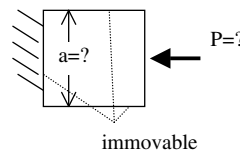
- 7.1 Refer to the application discussed in Section 7.1. A fabric material is made available that has the basic properties given in the following table:

Property	Value
E_x	69 GPa
E_y	69 GPa
v_{xy}	0.05
G_{xy}	5.1 GPa
t_{ply}	0.19 mm

The material is to be used in a skin application. The skin panel of interest is square of dimensions 200×200 mm and the applied ultimate load is 2152 N. The following two skin layups are proposed for this application: (a) $(\pm 45)/(0/90)_3/(\pm 45)$ and (b) $(0/90)/(\pm 45)/(0/90)/(\pm 45)/(0/90)$. Given the highest value of N_x determined in Section 7.1 and its location, comment on or discuss the following. Based on the highest N_x value, which of the two layups is stronger and why? What is better, placing plies with fibers aligned with the load away from the laminate midplane, or placing plies with fibers at 45° to the load away from the laminate midplane?

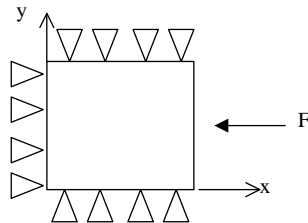
- 7.2 The layup for the skin in a certain application is dictated to be: $[(45/-45)_2/0/90]_s$ (total of 11 plies). The basic material properties are given below:

$$\begin{aligned} E_{11} &= 131 \text{ GPa} \\ E_{22} &= 11.37 \text{ GPa} \\ G_{12} &= 4.82 \text{ GPa} \\ v_{12} &= 0.29 \\ t_{ply} &= 0.1524 \text{ mm} \end{aligned}$$



This skin is square and under compression and is allowed to post-buckle. Three of the edges of the skin are immovable and the fourth one is under load P (N). If the maximum deflection of the skin is not allowed to exceed 6.35 mm (to avoid interference with adjacent structure) determine: (a) the largest dimension a the skin can have and (b) the corresponding maximum allowable load P if the axial strain in the plate is not to exceed 5000 microstrain (this includes scatter, environmental effects and damage). In order to correlate load to strain, use the effective width concept and assume that $\sigma = E\varepsilon$ is the constitutive relation (Hooke's law) with E the engineering membrane stiffness of the laminate at hand.

- 7.3 Using the same assumed expressions for w and F (Equations (7.2) and (7.3)) re-derive the post-buckling solution for a non-square plate, i.e. determine w_{11} and b_{eff} for a rectangular plate of dimensions $a \times b$. Once you derive the expression for the center deflection, verify that it coincides with the expression (7.11) for the case $a = b$. Determine the range of aspect ratios a/b for which the buckling mode has only one half wave ($m = 1$). Use this result to suggest over what range your post-buckling solution in this problem is accurate.
- 7.4 A square composite plate of side 254 mm simply supported all around is loaded on one side by a force F . The remaining three edges are fixed so they do not move in-plane. Determine the location and magnitude of the maximum strains ε_{xo} and ε_{yo} .



7.5 For the case of Exercise 7.4, a composite material with properties

$$E_x = 137.9 \text{ GPa}$$

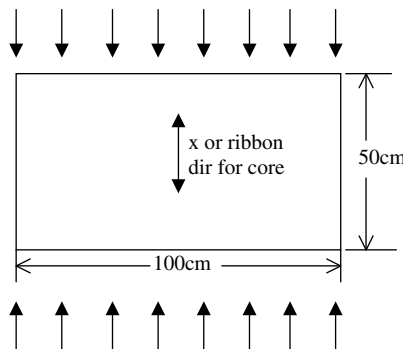
$$E_y = 11.72 \text{ GPa}$$

$$\nu_{xy} = 0.29$$

$$G_{xy} = 5.171 \text{ GPa}$$

$$t_{\text{ply}} = 0.1524 \text{ mm}$$

is made available. If the applied load is $F = 31.1 \text{ kN}$ determine the 10-ply symmetric and balanced laminate consisting of only 45° , -45° , 0° , and 90° plies that has the lowest value of maximum ε_{xz} found in Exercise 7.4. Do not use more than two 0° or two 90° plies per half-laminate. You do not have to use all four ply orientations. Accounting for damage, material scatter, and environmental effects, determine either the margin of safety, or the loading factor, or the reserve factor.



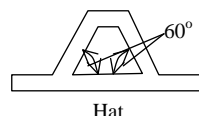
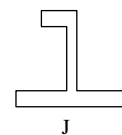
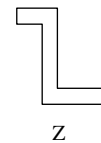
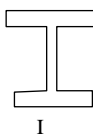
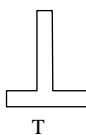
7.6 (May be done in conjunction with Exercise 10.5). You are to design a composite panel under compressive load using a skin-stiffener configuration. The panel dimensions are $100 \times 50 \text{ cm}$ and the applied load is 1750 N/mm acting parallel to the 50 cm dimension.

Two composite materials are available, with properties as follows:

Unidirectional tape graphite/epoxy	Plain weave fabric graphite/epoxy
$E_x = 131 \text{ GPa}$	68.9 GPa
$E_y = 11.4 \text{ GPa}$	68.9 GPa
$v_{xy} = 0.31$	0.05
$G_{xy} = 5.17 \text{ GPa}$	5.31 GPa
$t_{\text{ply}} = 0.1524 \text{ mm}$	0.1905 mm
$X_t = 2068 \text{ MPa}$	1378.8 MPa
$X_c = 1723 \text{ MPa}$	1378.8 MPa
$Y_t = 68.9 \text{ MPa}$	1378.8 MPa
$Y_c = 303.3 \text{ MPa}$	1378.8 MPa
$S = 124.1 \text{ MPa}$	119.0 MPa
$\rho = 1611 \text{ kg/m}^3$	1611 kg/m ³

Once you determine any strength values needed for any of the layups selected you are to assume the same knockdowns mentioned in Section 5.1.6 for environment, material scatter and damage.

Of the seven shapes below select one for the stiffeners.



You are to select the layup for the skin and each member of the stiffener cross-section for a post-buckling factor of 2.5 and a post-buckling factor of 5. You may use one of the two composite materials or a combination of both. You will need to decide on a stiffener spacing and use the solution to Exercise 7.3. It is up to you to decide if you want to reinforce the skin at the edges (near the stiffeners) over the effective width in order to get a lighter design or simply use the same layup for the skin everywhere. Note that the stiffener height cannot exceed 10 cm and no horizontal flange of the stiffener can exceed 5.5 cm. The skin or any member of the stiffener cannot be thinner than 0.57 mm. Make sure that

you account for all failure modes that apply in this case. Assume that the stiffeners are co-cured with the skin.

Determine the layup of each member of each stiffener and its dimensions observing the following design rules: (a) laminates are symmetric and balanced; (b) at least 10% of the fibers are in each of the four principal directions 0, 45, -45, and 90°; (c) no more than four unidirectional plies of the same orientation may be next to each other; (d) use only 0, 45, -45, and 90° plies. Provide a simple sketch of the cross-section of stiffeners that shows the plies, layup, dimensions, etc. Calculate the corresponding weights for skin/stiffened panel with PB = 2.5, skin/stiffened panel with PB = 5.0 and, if available, compare with the results from Exercise 10.5.

References

1. Wagner, H., Structures of Thin Sheet Metal, Their Design and Construction, *NACA Memo 490*.
2. Wagner, H., Flat Sheet Girder With Thin Metal Web, Part I (*NACA TM 604*), Part II (*NACA TM 605*), and Part III, (*NACA TM 606*).
3. Kuhn, P., Peterson, J.P. and Levin, L.R., A Summary of Diagonal Tension Part 1 – Methods of Analysis, *NACA TN 2661*, 1952.
4. Kuhn, P., Peterson, J.P. and Levin, L.R., A Summary of Diagonal Tension Part 2 – Experimental Evidence, *NACA TN 2662*, 1952.
5. Deo R.B., Agarwal, B.L. and Madenci, E., Design Methodology and Life Analysis of Postbuckled Metal and Composite Panels, *AFWAL-TR-85-3096*, vol. I, December 1985.
6. Deo, R.B., Kan, H.P. and Bhatia, N.M., Design Development and Durability Validation of Postbuckled Composite and Metal Panels, Volume III – Analysis and Test Results, *Northrop Corp., WRDC-TR-89-3030*, vol. III, November 1989.
7. <http://mathworld.wolfram.com/CubicEquations.html>

8

Design and Analysis of Composite Beams

The term beams is used here as a generic term referring to all one-dimensional parts that may be used in a structure. These include stiffeners, stringers, panel breakers, etc. There are many cross-sectional shapes that are used in practice. Of those, the ones used most frequently are (Figure 8.1): L or angle, C or channel, Z, T or blade, I, J, and Hat or omega.

8.1 Cross-section Definition Based on Design Guidelines

For a composite beam such as the one shown in Figure 8.2, each member may have a different layup. This would result in different stiffnesses and strengths for each of the flanges and web, and would allow more efficient usage of composite materials through tailoring. Typically, the letter b with appropriate subscript is used to denote the longer dimension of each member and the letter t the shortest (the thickness).

As beams tend to be used in stability-critical situations, cross-sections with high moments of inertia are preferred. Besides the obvious implications for the beam geometry (high b_2 value for example in Figure 8.2), there are certain guidelines that relate to the layup, which, when implemented, also contribute to robust performance.

With reference to Figure 8.2, stiff material must be located as far from the neutral axis as possible. Defining the 0 direction to be aligned with the beam axis (perpendicular to the plane of Figure 8.2), this stiffness requirement would result in the two flanges, the one next to the skin and the one away from the skin, being made up of mostly 0° plies.

Another clue can be deduced from the theory of joints (see for example [1, 2]). It has been demonstrated that as the thickness of the adherends decreases, the strength of the joint increases because the peak stresses at the end of each adherend, where the load transfer to the adhesive is completed, are lower. This implies that the stiffness mismatch caused by the adherend termination is less and the associated stress concentration is reduced. A similar situation occurs in testing coupons (in tension) using beveled tabs. The bevel in the tabs reduces the local stresses and helps eliminate the possibility of specimen failure at the tab termination. With this background, it is easy to deduce that, by decreasing the stiffness mismatch between the flange

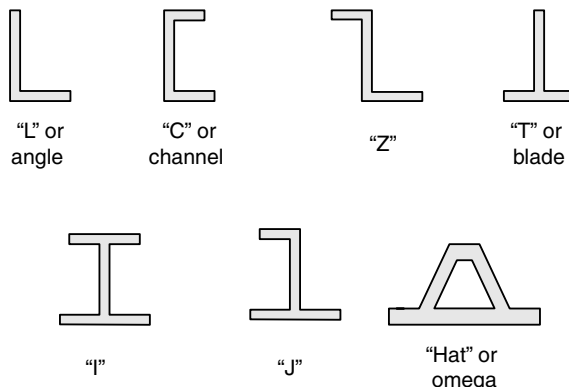


Figure 8.1 Typical beam cross-sections

next to the skin and the skin itself, the possibility of skin failure or flange/skin separation is reduced. This means that: (a) the flange should be made as thin as possible, still meeting other load requirements; and (b) the stiffness of the flange should be as close as possible to that of the skin.

Finally, to improve performance against shear loads (parallel to the web axis) the web must have high strength and stiffness under shear loads, which means it should consist mostly of 45° plies. The importance of 45° plies is discussed later in Section 8.5.1 where the pertinent stiffness term Q_{66} is shown to be maximum for 45° plies.

Combining these into a design would result in the preliminary configuration shown in Figure 8.3. The flange away from the skin consists of only 0° plies (for increased stiffness away from the neutral axes). The flange next to the skin consists of a combination of some 0° plies, for increased stiffness, sandwiched between the two halves of the skin layup in order to minimize the stiffness mismatch between skin and flange. The web consists of 45 and -45° plies for increased shear stiffness and strength.

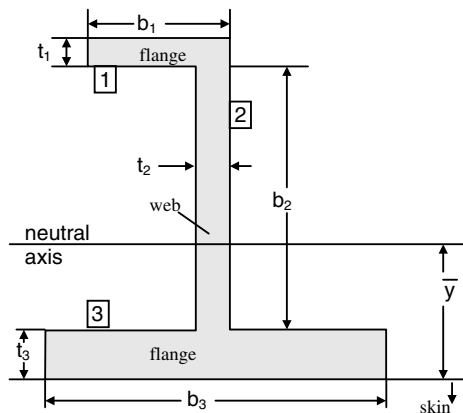


Figure 8.2 J stiffener cross-section

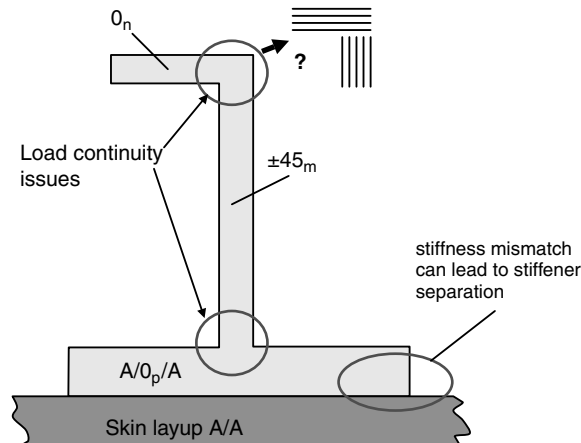


Figure 8.3 Preliminary design of stiffener cross-section based on first (crude) guidelines

As it stands, the design of Figure 8.3 is inadequate. There are several issues readily apparent: (a) at the two corners where the web meets the flanges, dissimilar plies meet and load transfer would rely on the matrix, which is grossly inefficient; (b) the layup of the flange next to the skin may be too thick if the number p of 0° plies is too high and/or still have very different stiffness from the skin; (c) using only one ply orientation in the flange away from the skin and the web to satisfy the respective requirements results in less than adequate performance of the beam when (secondary) conditions or requirements other than the ones used here are considered.

To improve on this design, additional guidelines, developed on the basis of experience and good engineering practice, are implemented. In order to get better load continuity, some plies in the web must continue into the flanges. Also, to protect against secondary load cases, ply orientations that cover the basic possible load directions, $0, 45, -45$, and 90 are used. Usually a very small number of load conditions (quite often a single one) are the critical conditions that size a structure. This does not mean that there are no other load conditions, only that their corresponding loads are lower (see for example Section 5.1.1 for the implications of multiple design load cases). If the layup selected were optimized for a single load case (or few load cases) it might not have enough fibers in other load directions where the loads may be significantly lower, but could still lead to premature failure if not enough fibers are present in those directions. Finally, robust performance under impact requires $+45/-45^\circ$ plies to be placed on the outside of laminates susceptible to impact. (This is more a consequence of the observation that layups with 45° fabric material on the outside tend to more effectively contain impact damage and minimize ply splitting).

Introducing these requirements to the design of Figure 8.3, results in the improved configuration of Figure 8.4.

In this case, a $45/-45$ pair is on the outside to improve impact resistance. It is not, however, clear whether this is sufficient especially in view of the complete layup of, say, the top flange where four 0° plies are stacked next to the two outer 45° plies. Also, it is known that stacking too many plies of the same orientation next to each other leads to the creation of sizeable microcracks during cure or during loading perpendicular to the fibers. The reason is that a matrix crack forming between fibers in a ply can progress easily to the next ply since there are

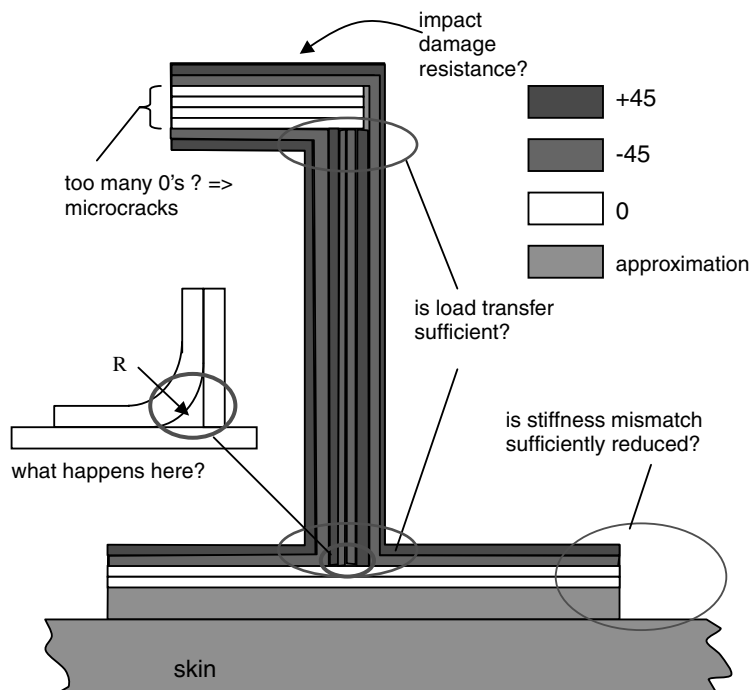


Figure 8.4 Improved stiffener cross-section design (See Plate 17 for the colour figure)

no fibers perpendicular to it in the next ply to stop or slow down its growth. So the improved design of Figure 8.4 still has issues associated with the layup of the flanges.

Furthermore, the continuity of plies around the corners may or may not be sufficient and it will depend on the applied loads. At the top and bottom of the web several plies terminate causing stress concentrations. In particular, adjacent to the terminated plies are plies turning away from the web and into the flange. Typically, it is very hard to force the turning plies to conform perfectly to the 90° turn, and a small radius as shown in the enlarged detail of Figure 8.4 will be present. The resulting gap between terminated and turned plies is usually filled with resin, creating a weak spot for the entire cross-section.

Finally, reaching a compromise layup for the flange next to the skin so that the stiffness mismatch at the flange termination is minimized, is difficult and more information about applied loading and skin layup is needed for further improvement. The design configuration of Figure 8.4 will be periodically revisited and improved upon in future chapters as a better understanding of designing to specific requirements is developed.

8.2 Cross-sectional Properties

The axial (EA) and bending (EI) stiffnesses of a beam are very often used in design and analysis of such structures and, therefore, accurate determination of their values for a composite cross-section is very important. There are some significant differences from metal cross-sections

stemming from the fact that, for a cross-section made using composite materials, the different members may have different layups and thus stiffnesses.

These differences become evident in the calculation of the location of the neutral axis for a cross-section made up of composite materials. With reference to Figure 8.2, the neutral axis is located at

$$\bar{y} = \frac{\sum (EAy)_j}{\sum (EA)_j} \quad (8.1)$$

Note that E here is either the membrane or bending modulus of each member (see Section 3.3 and Equations 3.65). The two moduli are, in general, different. This means that one should differentiate between axial and bending problems and use the appropriate moduli. In what follows, the axial stiffness EA (= modulus \times cross-sectional area), which is a quantity needed in uniaxial loading situations, is calculated first and the bending stiffness EI (= modulus \times moment of inertia), which is used in bending problems, is calculated afterwards.

In order to determine the axial stiffness (EA) of a cross-section, assume, for simplicity, that the layup of each member is symmetric and balanced. Then, denoting the beam axis as the x axis, a uniaxial loading situation for member i is represented by:

$$\begin{aligned} (N_x)_i &= (A_{11})_i(\varepsilon_x)_i + (A_{12})_i(\varepsilon_y)_i \\ (N_y)_i &= (A_{12})_i(\varepsilon_x)_i + (A_{22})_i(\varepsilon_y)_i \end{aligned} \quad (8.2)$$

where the subscript i denotes the i th member. This is the same as Equation (3.49) adjusted to uniaxial loading ($N_{xy} = 0$) and symmetric and balanced layups (B matrix $= A_{16} = A_{26} = 0$).

If now only load N_x is applied, $N_y = 0$ and substituting in Equation (8.2) and solving for $(\varepsilon_y)_i$ gives

$$(\varepsilon_y)_i = - \left(\frac{A_{12}}{A_{22}} \right)_i (\varepsilon_x)_i \quad (8.3)$$

This result can now be substituted into the first of Equations (8.2) to obtain:

$$(N_x)_i = \left(A_{11} - \frac{A_{12}^2}{A_{22}} \right)_i (\varepsilon_x)_i \quad (8.4)$$

If both sides of Equation (8.4) are divided by the thickness of the member t_i the left-hand side becomes the applied stress:

$$(\sigma_x)_i = \underbrace{\frac{1}{t_i} \left(A_{11} - \frac{A_{12}^2}{A_{22}} \right)}_{E_i} (\varepsilon_x)_i \quad (8.5)$$

It can be seen by inspection of Equation (8.5) that the quantity multiplying the strain on the right-hand side is the equivalent axial modulus of the member, which was also given in Section 3.3, Equation (3.59), as a slightly different (but equivalent) expression:

$$E_i = \frac{1}{t_i} \left(A_{11} - \frac{A_{12}^2}{A_{22}} \right) = \frac{1}{(a_{11})_i t_i} \quad (8.6)$$

with a_{11} the 11 entry of the inverse of the A matrix.

The axial or membrane stiffness EA of member i can now be written as

$$(EA)_i = E_i b_i t_i \quad (8.7)$$

with b_i and t_i the width and thickness of the member, respectively.

Consider now that an axial force F_{TOT} is applied to the entire cross-section. Because of the different EA values for each member, the corresponding forces acting on each member will be different. For the three-member cross-section of Figure 8.2, the total force equals the sum of the forces acting on the individual members,

$$F_{TOT} = F_1 + F_2 + F_3 \quad (8.8)$$

but the force F acting on each member is related to the corresponding force per unit width N_x via

$$(N_x)_i = \frac{F_i}{b_i} \quad (8.9)$$

Now for a uniaxial loading case with the load applied at the neutral axis, uniform extension or compression results, which means the strains in all members of the cross-section are equal:

$$(\varepsilon_x)_1 = (\varepsilon_x)_2 = (\varepsilon_x)_3 = \varepsilon_a \quad (8.10)$$

Combining equations (8.4), (8.6), (8.7), (8.9) and (8.10) it can be shown that

$$\frac{F_1}{(EA)_1} = \frac{F_2}{(EA)_2} = \frac{F_3}{(EA)_3} = \frac{F_{TOT}}{(EA)_{eq}} \quad (8.11)$$

with $(EA)_{eq}$ the equivalent membrane stiffness for the entire cross-section.

Combining Equations (8.11) with equation (8.8) and solving for the individual forces on each member it can be shown that the force on member i is given by,

$$F_i = \frac{(EA)_i}{\sum_{j=1}^3 (EA)_j} F_{TOT} = \frac{E_i b_i t_i}{\sum_{j=1}^3 E_j b_j t_j} F_{TOT} \quad (8.12)$$

with $(EA)_j$ given by Equation (8.7).

Equations (8.11) and (8.12) can be combined in order to determine the equivalent axial stiffness for the entire cross-section. Eliminating the forces gives,

$$(EA)_{eq} = \sum_j (EA)_j \quad (8.13)$$

The situation for pure bending is shown in Figure 8.5. Each member contributes to the EI calculation for the entire cross-section according to

$$(EI)_i = E_b \left[\frac{(\text{width})_i (\text{height})_i^3}{12} + A_i d_i^2 \right] \quad (8.14)$$

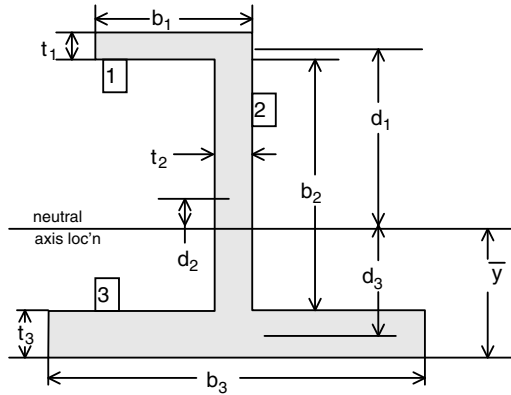


Figure 8.5 Definition of pertinent quantities for a beam cross-section in bending

where A_i is the area of the i th member ($= b_i t_i$) and d_i is the distance of the neutral axis of the i th member from the neutral axis of the entire cross-section determined by Equation (8.1) and the bending modulus is given by Equation (3.63),

$$E_{bi} = \frac{12}{t_i^3 (d_{11})_i} \quad (8.15)$$

If a bending moment M_{TOT} is applied to the beam, the individual bending moments and overall bending stiffness of the cross-section are calculated in a manner analogous to the case of uniaxial loading. However, instead of the strain compatibility condition that required that the strains in all members be equal, here the requirement is that the radii of curvature R_{ci} for all members are all equal to that of the neutral axis of the entire cross-section. Therefore,

$$R_{c1} = R_{c2} = R_{c3} = R_{ca} \quad (8.16)$$

In addition,

$$M_{TOT} = M_1 + M_2 + M_3 \quad (8.17)$$

Also, the local radius of curvature is given by the well-known moment-curvature relation of simple beam theory,

$$R_{ci} = \frac{(EI)_i}{M_i} \quad (8.18)$$

Combining Equations (8.16)–(8.18) and solving for the moments acting on each individual member, gives

$$M_i = \frac{(EI)_i}{\sum_{j=1}^3 (EI)_j} M_{TOT} \quad (8.19)$$

with $(EI)_i$ given by Equation (8.14). This relation is the analogous relation to Equation (8.12) for the axial forces on the members of the cross-section.

With the individual moments given by Equation (8.19), the overall bending stiffness of the cross-section can be obtained from Equations (8.16), (8.18), (8.19):

$$(EI)_{eq} = \sum_j (EI)_j \quad (8.20)$$

In the preceding discussion, axial and bending behaviors were completely uncoupled, which was very convenient since the same layup would undergo each type of deformation (axial or bending) exhibiting a different modulus value. Care must be exercised if both modes of deformation occur simultaneously and are coupled. This issue was first mentioned in Section 7.2.1 and points to a problem associated with attempting to oversimplify the design and analysis of composite structures. In such cases it is better to resort to the constitutive relations involving the A , B , and D matrices (see for example Equation 3.49). As a simpler, less accurate, but conservative approach, one may select the one of the two moduli (membrane or bending) that leads to more conservative results (for example higher post-buckling deflections which are caused by using the lower of the two moduli).

As an example showing the implications of the equations presented so far in this section consider a comparison of the cross-section of Figure 8.4 with an aluminum cross-section with the same dimensions. The (graphite/epoxy) composite cross-section with the flange next to the skin completely defined now is shown in Figure 8.6. For this configuration, the pertinent quantities are shown in Table 8.1.

Using Equation (8.1) the neutral axis is found to be located 7.17 mm away from the outer edge of the bottom flange (Figure 8.6). Using Table 8.1 and Equations (8.13) and (8.20) the membrane (EA) and bending (EI) stiffnesses of the cross-section of Figure 8.6 are found and compared with the case of aluminum with the exact same geometry in Table 8.2.

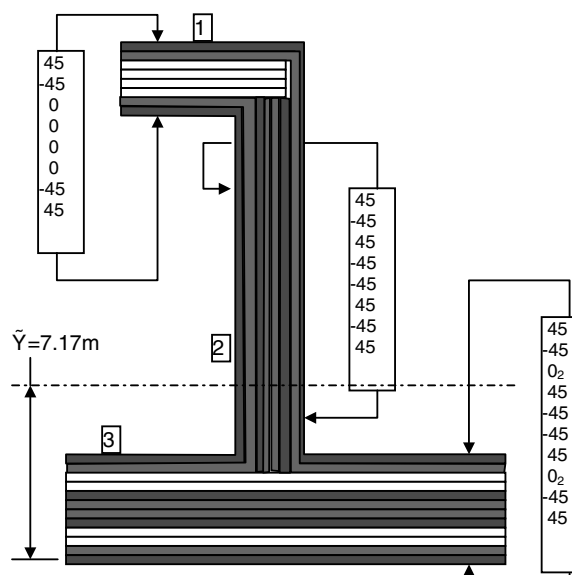


Figure 8.6 Baseline J stiffener cross-section made out of composite materials (See Plate 18 for the colour figure)

Table 8.1 Properties for baseline composite configuration of Figure 8.6

Member	<i>b</i> (mm)	<i>t</i> (mm)	<i>E_m</i> (GPa)	<i>E_b</i> (GPa)
1	12.7	1.2192	75.6	32.4
2	31.75	1.2192	18.2	17.9
3	38.1	1.8288	56.5	47.9

Table 8.2 Composite versus same geometry aluminum

	A	Comp	$\Delta(\%)$
<i>EA</i> (kN)	8525	5803	46.9
<i>EI</i> (N m ²)	1401	631	121.8

Table 8.2 shows that the same geometry made with aluminum has significantly higher stiffness both in-plane (47% higher) and bending (122% higher). Since the geometries are identical between aluminum and composite, it is easy to compare the respective weights. The weight ratio will equal the density ratio. The density of aluminum is 2774 kg/m³ while the density of graphite/epoxy is 1609 kg/m³. This means that the aluminum configuration is 72% heavier.

For a more insightful comparison, design the graphite/epoxy cross-section to have the same stiffnesses as the aluminum design and then compare the weights. Since *EA* for aluminum is 46.9% higher (see Table 8.2), the ply thickness of the graphite/epoxy material is increased by 46.9% and a minor reshuffling of the stacking sequence of the flange away from the skin is done. The changes are shown in Table 8.3.

The only change in layup is in the flange away from the skin where the starting 45/-45 combination is now split by moving the pair of 0 plies between them. The *b* values stay the same but the thicknesses are all increased by a factor of 1.67. As a result the bending stiffness of the flange away from the skin is now increased from 32.4 to 62.7 GPa. It should be noted that simply scaling the ply thickness as was suggested here is not usually possible. The raw material is available only in limited ply thicknesses, so increasing to a specified value would require rounding up to the next integral multiple of ply thickness. So the results of this example are only approximate.

With the changes of Table 8.3, the graphite/epoxy cross-section now matches (or is very close to) the stiffnesses of the aluminum cross-section as is shown in Table 8.4.

Table 8.3 Revised Gr/Ep configuration to match aluminum stiffnesses

Member	Layup before	Layup now	<i>b</i> (mm)	<i>t</i> (mm)	<i>E_m</i> (stays same)	<i>E_b</i> before (GPa)	<i>E_b</i> now (GPa)
1	[45/-45/0] _s	[45/0 ₂ /-45] _s	12.7	1.791	75.6	32.4	62.7
2	[(45/-45) ₂] _s	[(45/-5) ₂] _s	31.75	1.791	18.2	17.9	17.9
3	[45/-45/0 ₂ /45/-45] _s	[45/-45/0 ₂ /45/-45] _s	38.1	2.687	56.5	47.9	47.9

Table 8.4 Comparison of Aluminum and G/E stiffnesses for revised configuration

	Al	Comp	$\Delta(\%)$
EA (kN)	8525	8525	0.0
EI (N m ²)	1401	1441	-2.8

Now the weight comparison includes both the density and thickness difference. The weight ratio of the two configurations is given by:

$$\frac{W_{Gr/Ep}}{W_{Al}} = 0.58 \frac{1.469}{1} = 0.852$$

↑
density ratio for carbon/epoxy

or, the composite design is, approximately, 15 % lighter.

The previous example points to the important fact that, once the design and best-practices rules and other constraints are imposed on the composite design, the weight savings are drastically reduced compared with the nominal savings one would obtain based on the tension or compression strength of a unidirectional ply. The savings of 15% found here is typical of the performance of modern composite materials when used on airframe structures. A somewhat higher value of 38% savings was found in Section 6.2 for a buckling application. In general, the weight savings rarely exceeds 30% and not without detailed evaluation of all possible failure modes and use of a good, robust optimization scheme.

8.3 Column Buckling

In column buckling a beam under compression suddenly deflects perpendicular to its axis. With EI defined in the previous section, the standard buckling expressions can be used for the two cases shown in Figure 8.7. It should be noted that, for buckling load calculations, the membrane modulus E_m given by Equation (8.6) should be used.

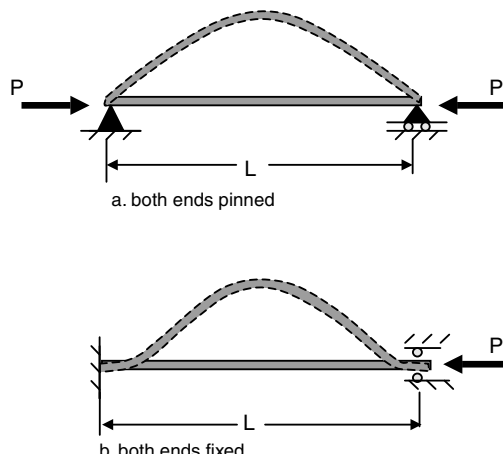
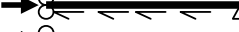
**Figure 8.7** Buckling of simply supported (pinned) and clamped (fixed) beams

Table 8.5 Buckling load coefficient for various boundary conditions and loadings

Configuration	BC at left, right end	c
	pinned, pinned	1.88
	fixed, fixed	7.56
	fixed, pinned	2.05
	fixed, pinned	5.32
	fixed, free	0.25
	fixed, free	0.80

The solutions for the buckling loads are well known and can be found elsewhere in the literature, e.g. [3, 4]. For convenience, they are provided here without derivation.

$$P_{cr} = \frac{\pi^2 EI}{L^2} \text{ (pinned ends)} \quad (8.21)$$

$$P_{cr} = \frac{4\pi^2 EI}{L^2} \text{ (fixed ends)} \quad (8.22)$$

As is seen from the coefficient in the right-hand side of Equations (8.21) and (8.22), the boundary conditions at the beam ends play a big role in the value of the buckling load. A brief compilation of buckling load values for different boundary conditions and loadings is given in Table 8.5. In all cases the buckling load is given by

$$P_{cr} = \frac{c\pi^2 EI}{L^2} \quad (8.23)$$

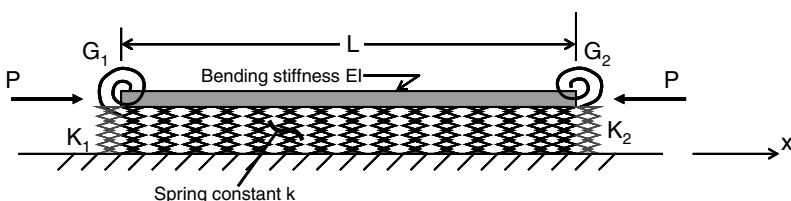
and the coefficient c is given in Table 8.5.

The physical meaning of the boundary conditions in Table 8.5 is as follows:

- free: free rotation and free translation
- pinned: free rotation and fixed translation
- fixed: fixed rotation and fixed translation

8.4 Beam on an Elastic Foundation under Compression

The situation is shown in Figure 8.8. A beam rests on an elastic foundation which has a spring constant k . In general, the beam ends have linear (K_1 and K_2) and torsional (G_1 and G_2) springs

**Figure 8.8** Beam on an elastic foundation

restraining them. Depending on the spring stiffnesses, the end boundary conditions can range from free to clamped, and can achieve any intermediate value.

To gain insight to the problem, the case of a simply supported beam ($G_1 = G_2 = 0$, $K_1 = K_2 = \infty$) is solved first in detail. This is done using energy methods.

Referring to the discussion of Section 5.4 the one-dimensional counterpart of the energy expression is

$$\Pi_c = \frac{1}{2} \int_0^L EI \left(\frac{d^2w}{dx^2} \right)^2 dx + \frac{1}{2} \int_0^L (-P) \left(\frac{dw}{dx} \right)^2 dx + \frac{1}{2} \int_0^L kw^2 dx \quad (8.24)$$

where w is the out-of-plane displacement of the beam.

The first term in the right-hand side of Equation (8.24) is the potential energy stored in bending the beam. The second term is the work done by the external force P and the third term is the energy stored in the spring foundation. The units of k are force/area.

An expression for w is assumed such that the boundary conditions that $w = 0$ at the two ends of the beam are satisfied:

$$w = \sum A_m \sin \frac{m\pi x}{L} \quad (8.25)$$

where L is the length of the beam and A_m are unknown coefficients.

Substituting in the energy expression (8.24) and performing the integrations results in,

$$\Pi_c = \sum \left[\frac{(EI)m^4\pi^4}{4L^3} - \frac{Pm^2\pi^2}{4L} + \frac{kL}{4} \right] A_m^2 \quad (8.26)$$

The energy must be minimized with respect to the unknowns A_m which leads to

$$\frac{\partial \Pi_c}{\partial A_m} = 0 \quad (8.27)$$

Carrying out the differentiation and setting the result equal to zero yields the following equation:

$$2 \left[\frac{(EI)m^4\pi^4}{4L^3} - \frac{Pm^2\pi^2}{4L} + \frac{kL}{4} \right] A_m = 0 \quad (8.28)$$

This is a matrix equation with a diagonal matrix multiplying the vector A_m :

$$\begin{bmatrix} \frac{EI\pi^4}{4L^3} + \frac{kL}{4} - \frac{P\pi^2}{4L} & 0 & 0 & \dots \\ 0 & \frac{EI(16)\pi^4}{4L^3} + \frac{kL}{4} - \frac{P(4)\pi^2}{4L} & 0 & \dots \\ 0 & 0 & \frac{EI(81)\pi^4}{4L^3} + \frac{kL}{4} - \frac{P(9)\pi^2}{4L} & \dots \\ \dots & \dots & \dots & \dots \end{bmatrix} \begin{Bmatrix} A_1 \\ A_2 \\ A_3 \\ A_4 \\ \vdots \end{Bmatrix} = 0$$

The obvious possibility, $A_m = 0$ corresponds to the uniform compression pre-buckling case. Therefore, for out-of-plane deflections to be possible (A_m must be different from zero) the determinant of this matrix must equal zero. Defining,

$$K_{mm} = \frac{\pi^2 EI}{L^2} \left(m^2 + \frac{kL^4}{\pi^4 (EI)m^2} \right) \quad (8.29)$$

the matrix equation can be rewritten in the form:

$$\begin{bmatrix} K_{11} - P & 0 & 0 & 0 & 0 \\ 0 & K_{22} - P & 0 & 0 & 0 \\ 0 & 0 & K_{33} - P & 0 & 0 \\ 0 & 0 & 0 & \dots & \\ 0 & 0 & \dots & \dots & \dots \end{bmatrix} \begin{Bmatrix} A_1 \\ A_2 \\ \dots \\ \dots \\ \dots \end{Bmatrix} = 0 \quad (8.30)$$

Since the matrix on the left-hand side is diagonal, setting its determinant equal to zero is equivalent to setting the product of the diagonal terms equal to zero:

$$(K_{11} - P)(K_{22} - P)(K_{33} - P) \dots = 0 \quad (8.31)$$

There are as many solutions to Equation (8.31) as there are terms. Of them, the solution that results in the lowest buckling load $P = P_{cr}$ is selected:

$$P_{cr} = \min(K_{ii}) \quad (8.32)$$

From Equations (8.31) and (8.29), the buckling load has the form,

$$\frac{P_{cr}}{\frac{\pi^2 EI}{L^2}} = m^2 + \frac{kL^4}{\pi^4 EI} \frac{1}{m^2} \quad (8.33)$$

where K_{mm} from Equation (8.29) was rearranged to bring the term $\pi^2 EI/L^2$ to the left-hand side.

As a special case of Equation (8.33) consider the situation in which $k = 0$. This would be the case of a pinned beam under compression. Then, the critical buckling load would be given by

$$P_{cr} = \frac{\pi^2 EI}{L^2} m^2 \quad (8.34)$$

which is minimized for $m = 1$. If $m = 1$, Equation (8.34) is identical to (8.21) and the exact solution for this case is recovered.

In the general case when $k \neq 0$, the value of m that minimizes the right-hand side of Equation (8.32) or (8.33) depends on the value of k itself. This can be seen more easily graphically where the normalized buckling load (left-hand side of Equation 8.33) is plotted as a function of the parameter $kL^4/(\pi^4 EI)$ which appears on the right-hand side of Equation (8.33). This plot is shown in Figure 8.9.

For each value of m , the right-hand side of Equation (8.33) is a straight line. The straight lines corresponding to different values of m are shown in Figure 8.9. The bold black line giving the envelope of the lowest values of the buckling load defines the critical buckling load for a given value of the parameter $kL^4/(\pi^4 EI)$. It is seen that for low values of this parameter, $m = 1$ (one half-wave over the entire length of the beam) gives the lowest buckling load. As the value of this parameter increases, the buckling mode progressively switches to $m = 2$ (two half-waves along the beam length), $m = 3$, etc. Unlike the case of no elastic foundation where the beam always

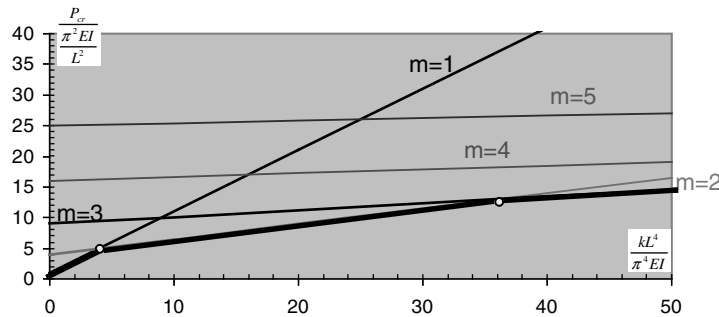


Figure 8.9 Buckling load of a beam on elastic foundation

buckles in one half-wave ($m = 1$), the presence of an elastic foundation changes the buckling mode. The higher the value of $kL^4/(\pi^4 EI)$, the higher the number of half-waves (value of m) into which the beam buckles.

For boundary conditions other than pinned ends, the governing equation

$$EI \frac{d^4 w}{dx^4} + P \frac{d^2 w}{dx^2} + kw = 0 \quad (8.35)$$

can be solved. The solution has the form

$$w = Ae^{px} \quad (8.36)$$

with the exponent p given by

$$p = \pm \sqrt{\frac{-\frac{P}{EI} \pm \sqrt{\left(\frac{P}{EI}\right)^2 - \frac{4k}{EI}}}{2}} \quad (8.37)$$

Thus, there are four solutions of the form (8.36):

$$w = A_1 e^{p_1 x} + A_2 e^{p_2 x} + A_3 e^{p_3 x} + A_4 e^{p_4 x} \quad (8.38)$$

The four coefficients A_1 – A_4 are determined from the boundary conditions at the two ends of the beam:

$$\begin{aligned} -EI \frac{d^2 w}{dx^2} + G_1 \frac{dw}{dx} &= 0 \\ EI \frac{d^3 w}{dx^3} + P \frac{dw}{dx} + K_1 w &= 0 \\ -EI \frac{d^2 w}{dx^2} + G_2 \frac{dw}{dx} &= 0 \\ EI \frac{d^3 w}{dx^3} + P \frac{dw}{dx} + K_2 w &= 0 \end{aligned} \quad (8.39a-d)$$

Equations (8.39) and (8.39c) are statements of moment equilibrium at the two beam ends respectively, i.e. the moment caused by the torsional spring $G(dw/dx)$ equals the beam bending

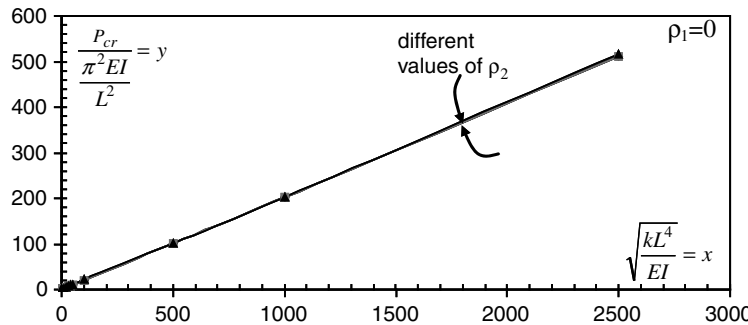


Figure 8.10 Buckling load of beam on elastic foundation pinned at one end and with variable rotational restraint at the other

moment at that end. Equations (8.39b) and (8.39d) express shear force equilibrium at the same locations.

Detailed results for various values of the spring constants G_1 , G_2 , K_1 , and K_2 , can be found in [5]. Following the approach in that reference, the following parameters are defined (subscript $i = 1, 2$ denotes end $x = 0$ or end $x = L$):

$$R_i = \frac{G_i L}{EI}$$

$$\rho_i = \frac{1}{1 + \frac{3}{R_i}} \quad (8.40)$$

Then, $\rho_i = 0$ implies no torsional stiffness at end i , or the beam is free to attain any slope locally (pinned end). Also, $\rho_i = 1$ implies infinite torsional stiffness at end i , or the beam has zero slope at that end (fixed end). As an example, the case where the beam is pinned at the left end and has variable stiffness at the other end is shown in Figures 8.10 and 8.11.

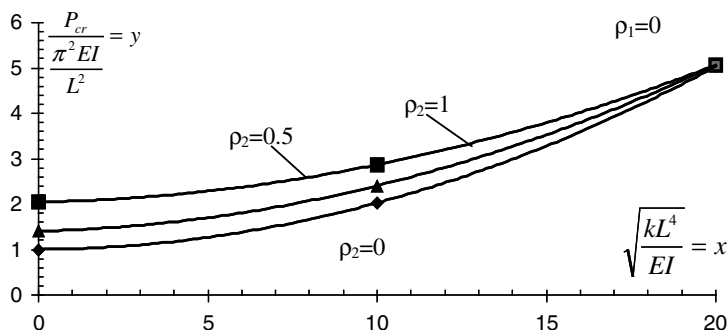


Figure 8.11 Buckling load of beam on elastic foundation pinned at one end and with variable rotation restraint at the other (detail of Figure 8.10 for low values of x)

Table 8.6 Buckling load y as a function of elastic foundation stiffness x and boundary rigidity $\rho_1=0$

ρ_2	x	y	r^2 (goodness of fit)
0	$0 \leq x \leq 20$	$0.0099x^2 + 0.0041x + 1$	1.0000
0	$20 \leq x \leq 100$	$0.0004x^2 + 0.1517x + 1.6658$	0.9987
0.5	$0 \leq x \leq 20$	$0.0004x^2 + 0.0169x + 1.4069$	1.0000
0.5	$20 \leq x \leq 100$	$0.0002x^2 + 0.1714x + 1.4518$	0.9988
1	$0 \leq x \leq 20$	$0.0069x^2 + 0.01134x + 2.046$	1.0000
1	$20 \leq x \leq 100$	$7 \times 10^{-5}x^2 + 0.1924x + 1.2722$	0.9998

$\rho_1 = \rho_2$	x	y	r^2 (goodness of fit)
0.2	$0 \leq x \leq 20$	$0.099x^2 + 0.0039x + 1.28$	1.0000
0.2	$20 < x \leq 100$	$0.0004x^2 + 0.1517x + 1.9512$	0.9987
0.5	$0 \leq x \leq 20$	$0.0099x^2 + 0.0019x + 1.916$	1.0000
0.5	$20 < x \leq 100$	$0.0003x^2 + 0.1539x + 2.5361$	0.999
1	$0 \leq x \leq 20$	$0.0051x^2 + 0.0265x + 4$	1.0000
1	$20 < x \leq 100$	$-0.0003x^2 + 0.2385x + 2.3368$	0.9943

In addition to Figures 8.10 and 8.11, approximate equations for a range of values of the parameters were obtained by best-fitting the results in [5]. These approximate equations are given in Table 8.6.

8.5 Crippling

Crippling is a stability failure where a flange of a stiffener locally buckles and then collapses. This is shown graphically in Figure 8.12. Under compressive load one (or more) of the flanges buckles locally with a half-wavelength ℓ , which is much smaller than the length L of the stiffener. Once the flange buckles it can support very little load in the post-buckling regime and fails (collapses). Its load is then shared by other members of the cross-section (if they have not failed) until the entire cross-section collapses.

Crippling is one of the most common failure modes in a composite airframe. It may occur on stiffeners, stringers, panel breakers, beams, ribs, frame caps, and all other members that are

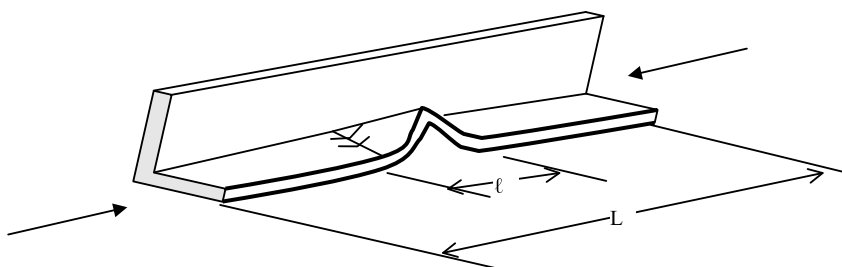


Figure 8.12 Stiffener flange crippling

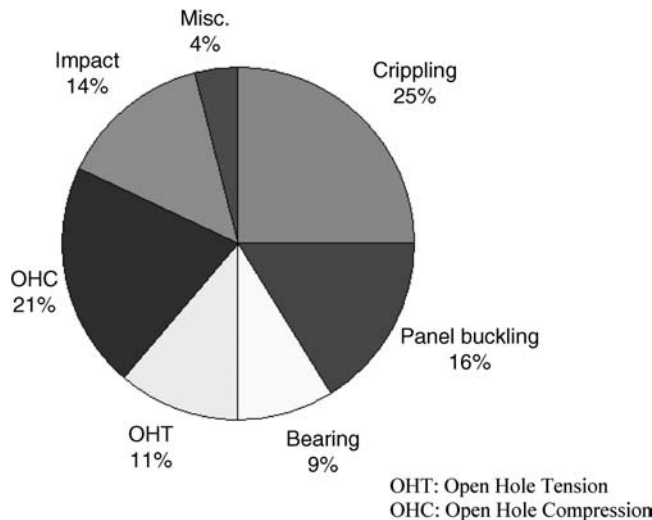


Figure 8.13 Failure modes in a composite airframe

stability critical and do not fail by global buckling. An approximate distribution of failure modes for fuselage and wing of an aircraft is shown in Figure 8.13.

It can be seen from Figure 8.13 that crippling designs as much as one quarter of the parts in a composite airframe. The distribution in Figure 8.13 should not be viewed as exact and it will vary significantly from one application to the next. The main message however, about the importance of certain failure modes such as crippling, carries over to most applications.

In a one-dimensional structure under compression such as a stiffener, crippling competes with (at least) two other failure modes: material failure and column buckling. Typically, for a robust design, material failure (not preceded by some stability failure) is not the driver because it leads to heavy designs. Between crippling and column buckling failure, crippling is preferred as the primary failure mode. The reason is that it typically occurs on one member (or portion of a member in bending situations as will be discussed in Section 8.5.3) and when the crippled flange collapses there is a good chance that the remaining members of the cross-section may be able to absorb some or all of the load originally in the failed flange, thus precluding or delaying complete failure of the stiffener. In column buckling the whole stiffener fails. As a result, crippling has a better chance of leading to a robust design, and is preferred as the designing failure mode. This does not mean that there are no cases where column buckling is the driver, especially in long beams. In such cases, if a weight-competitive design can be generated, the approach is to either increase the bending stiffness of the entire cross-section or shorten the unsupported length of the beam so that column buckling happens at a higher load than flange crippling.

To analyze crippling in detail one would first have to obtain the portion of the total load that acts on each flange and then determine the corresponding buckling load. The flange in that case would be modeled as a long plate with three edges simply supported and one edge free. Then, a post-buckling solution similar to that in Chapter 7 would have to be carried out to determine deflections, strains and stresses and some failure criterion applied to determine the load for final collapse. Such an approach is cumbersome and relies on many simplifying assumptions to make the solution tractable. As a result the solution is not accurate enough. In addition, there are issues with

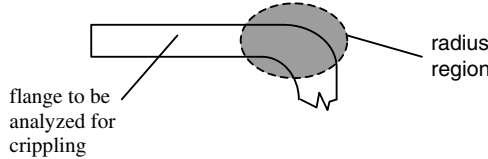


Figure 8.14 Radius region at root of a flange

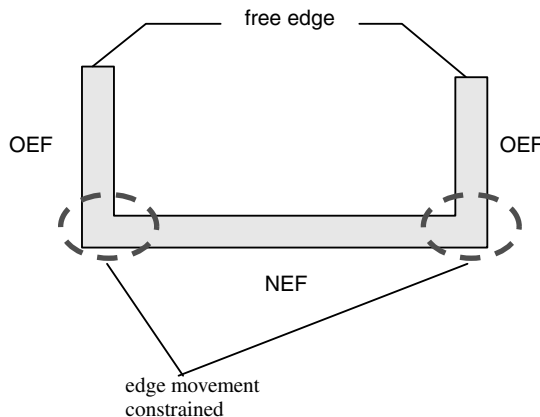


Figure 8.15 One-edge-free and no-edge-free flanges in a cross-section

modeling the boundary condition at the root of the flange. Typically there is a radius region (Figure 8.14) and there is some finite stiffness, meaning the boundary condition is somewhere between simply supported and clamped. The exact type of boundary condition depends on the radius, thickness, layup, and in- and out-of-plane stiffnesses in a complex way further complicating the possibility of generating accurate analytical predictions for this failure mode.

For isotropic configurations, attempts have been made [6] to account for the local specifics of the boundary conditions, in particular for beams that are nominally cantilevered. But more work is needed in this area with an extension to composites before more accurate analytical models for crippling analysis can be developed.

A semi-empirical approach has been favored instead. Two cases are distinguished as shown in Figure 8.15: (a) one-edge-free (OEF) and (b) no-edge-free (NEF). In the OEF case, one end of the flange is constrained, for example by being attached to a web or other member, and the other end is free. In the NEF case, both flange ends are constrained from moving.

8.5.1 One-Edge-Free (OEF) Crippling

Consider the situation shown in Figure 8.16. The cross-section has three OEF flanges, one at the top and two at the bottom on either side of the vertical web. The buckling load for each flange corresponds to that of a long plate with three sides simply supported and one side free. This case was addressed in Chapter 6 for finite and infinite flange length (see Equations 6.12a and 6.13a).

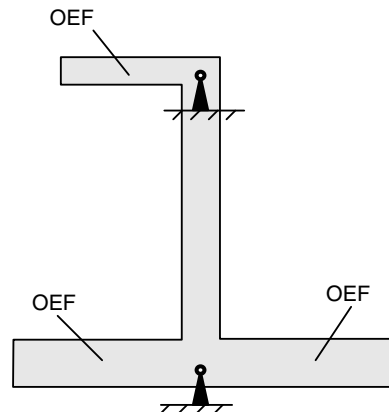


Figure 8.16 OEF flanges in a “J” stiffener

For convenience, the buckling load (infinitely long flange) is repeated here:

$$N_{xcrit} = \frac{12D_{66}}{b^2} \quad (6.13a)$$

Looking at Equation (6.13a), for a given flange width b , to maximize the buckling load one should maximize the twisting stiffness D_{66} . One way to see how D_{66} can be maximized for a given laminate thickness is to consider how each ply contributes to the D_{66} term for the entire laminate.

Consider the situation shown in Figure 8.17 for a symmetric and balanced laminate.

The equation that determines the contribution of the i th ply to the D_{66} term for that laminate (Equation 3.47) can be recast into the form

$$(D_{66})_c = 2D_{66}^{(i)} + 2A_{66}^{(i)}d_i^2 \quad (8.41)$$

where the superscript (i) denotes quantities for the i th ply with respect to its own midplane. Equation (8.41) is essentially the same as Equation (8.14) per unit width with the first term of (8.14) being replaced by the corresponding D term of the i th ply and the second term replaced by the EA term of the i th ply. The factors of 2 on the right-hand side of Equation (8.41) account for the contribution of two plies symmetrically located with respect to the midplane of the laminate.

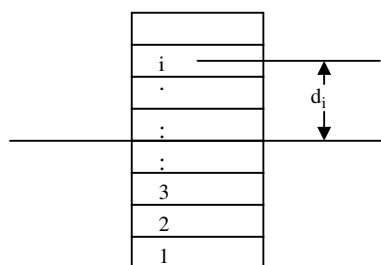


Figure 8.17 Section cut of a symmetric and balanced laminate

Based on Equation (8.41), the biggest contribution to the D_{66} term for the entire laminate comes from the second term in the right-hand side of Equation (8.41) because of the presence of the distance d_i . Terms away from the midplane contribute more. Therefore, one should place material with the high A_{66} term as far away from the midplane as possible. Now maximizing A_{66} for a single ply amounts to maximizing the corresponding expression for Q_{66} (see Equation 3.33d repeated below):

$$Q_{66} = (Q_{xx} + Q_{yy} - 2(Q_{xy} + Q_{ss})\sin^2\theta \cos^2\theta + Q_{66}(\sin^4\theta + \cos^4\theta)) \quad (3.33d)$$

By differentiating the right-hand side with respect to θ and setting the result equal to zero, it can be shown that Q_{66} and, therefore, A_{66} , is maximized when $\theta = 45^\circ$. Therefore, on the basis of Equation (6.13a), to maximize crippling performance one should select a flange layup that has the 45° plies as far from the midplane as possible.

This conclusion contradicts another of the design guidelines, stated in Section 8.1, that the 0° plies should be placed as far from the midplane as possible. This is not an inconsistency as the 0° ply guideline is for increasing the bending stiffness D_{11} and applies to column buckling while the 45° ply guideline is for increasing the bending stiffness D_{66} and applies to crippling. This situation occurs frequently in practice where different design requirements point to different directions and a compromise between them must be reached. In addition, as will be discussed below, the requirement of as many 45° plies away from the midplane as possible is not sufficient to guarantee optimum crippling performance and other ply orientations are also necessary.

Equation (6.13a) is compared with test results for various layups and stiffener geometries in Figure 8.18. It is customary and insightful to plot crippling stress normalized by the compressive strength of the respective layup as a function of the ratio b/t (width divided by thickness) for the respective flange. For low b/t values the crippling strength is essentially the same as the compressive strength of the flange. This would be the case of a thick flange where buckling is delayed because of the high bending stiffness and material strength is the operative failure mode. For high b/t values the crippling strength drops rapidly as b/t increases, showing the sensitivity to reduced bending stiffnesses of the flange.

As is seen from Figure 8.18, the theoretical prediction of Equation (6.13a) is higher than the test results for low b/t values ($b/t < 6$) but close to them. However, it becomes very conservative for high b/t values. The reasons for this, as already mentioned above, are related to the boundary

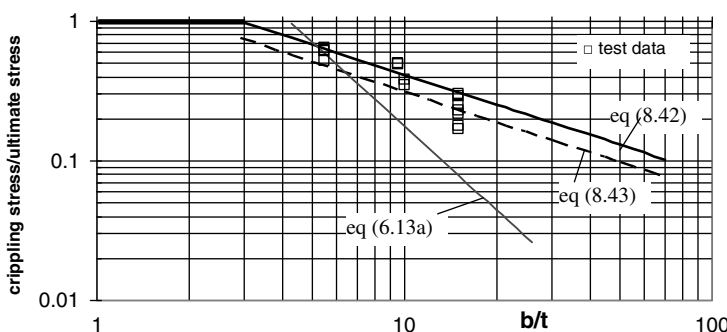


Figure 8.18 OEF crippling test results compared to buckling predictions

conditions at the edge of the flange that are not captured by Equation (6.13a), which assumes a simply supported edge, and to the post-buckling capability of the flange, which becomes more and more pronounced for larger b values. This would be the case where the flange stops behaving as a one-dimensional structure and behaves more like a plate, which, as was discussed in relation to Figure 7.2 in the previous chapter, would result in improved post-buckling load carrying ability.

In view of these differences between analysis and experimental results and the difficulties associated with improving the analysis without resorting to expensive computational approaches, a semi-empirical approach has been adopted where the crippling strength is correlated with the b/t ratio. Over a large set of test results with different materials and layups, it has been found [7] that the following expression fits the data well:

$$\frac{\sigma_{crip}}{\sigma_c^u} = \frac{2.151}{\left(\frac{b}{t}\right)^{0.717}} \quad (8.42)$$

valid for $b \geq 2.91t$; for $b < 2.91t$, $\sigma_{crip} = \sigma_c^u$.

The two constants in Equation (8.42) are determined by best-fitting the data. For design, Equation (8.42) is modified to guarantee that at least 90% of the tests are higher than the prediction (see B-Basis definition in Section 5.1.3 and Figure 5.8). The design equation is, then:

$$\frac{\sigma_{crip}}{\sigma_c^u} = \frac{1.63}{\left(\frac{b}{t}\right)^{0.717}} \quad (8.43)$$

valid for $b \geq 1.98t$; for $b < 1.98t$, $\sigma_{crip} = \sigma_c^u$.

In Equations (8.42) and (8.43) σ_c^u is the ultimate compressive strength of the flange which can be determined, for example, as the first-ply failure of the flange under compression (see Chapter 4 for first-ply-failure criteria). The predictions of these two equations are also shown in Figure 8.18. It can be seen that Equation (8.42) fits the present data well while Equation (8.43) is below most of the data and thus could be used as a design equation. It is important to note that the test results shown in Figure 8.18 were not used in generating the semi-empirical curves of Equations (8.42) or (8.43) so the agreement seems to reinforce the usefulness and applicability of these two equations.

An important note on applicability: As the test data on which Equations (8.42) and (8.43) are based come from laminates with at least 25% 0° plies and 25% 45° plies, these equations should be used only with layups that fall in this category. Extending to other layups with less 0° and/or 45° plies is not recommended. In any case, most flange designs do obey this requirement of at least 25% 0° and at least 25% 45° plies as a compromise between the two design requirements, already presented, of 0° plies for high D_{11} and 45° plies for high D_{66} and respective high $EA \times d^2$ contribution.

A final point relating to the presence of 0° and 45° plies is in order. As was mentioned above, 45° plies away from the laminate midplane maximize D_{66} and thus the buckling load of the flange as given by Equation (6.13a). However, especially for large b/t values where the flange behaves as a plate and has significant post-buckling capability, using mostly 45° plies in the flange is not recommended. 0° plies are also required to increase the post-buckling strength. This is captured in Equation (8.43) in σ_c^u , the compression strength of the flange. As a result, in

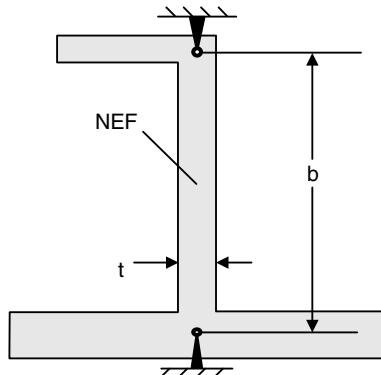


Figure 8.19 NEF web in a J stiffener

practice flange layups with at least 25% 0° and 25% 45° plies are used. They have been demonstrated by test to have better crippling performance.

8.5.2 No-Edge-Free (NEF) Crippling

The situation is shown in Figure 8.19. The vertical web in this Figure is supported at the two ends by the flanges and is treated as no-edge-free (NEF) web.

The web in this case can be modeled as a long plate that is simply supported all around its boundary. This case was examined in detail in Section 6.2. Starting from the buckling load given by Equation (6.7),

$$N_o = \frac{\pi^2}{a^2} \left[D_{11}m^2 + 2(D_{12} + 2D_{66})(AR)^2 + D_{22} \frac{(AR)^4}{m^2} \right] \quad (6.7)$$

the corresponding expression for a very long plate ($a \rightarrow \infty$) can be determined as follows: The term a^2 is brought inside the brackets and a factor b^2 is factored out using the fact that $AR = a/b$. Also, the square root of the product $D_{11}D_{22}$ if factored out, giving

$$N_{xcrit} = \frac{\pi^2}{b^2} \sqrt{D_{11}D_{22}} \left[\frac{m^2 b^2}{a^2 \sqrt{D_{22}}} + \frac{2(D_{12} + 2D_{66})}{\sqrt{D_{11}D_{22}}} + \sqrt{\frac{D_{22}}{D_{11}}} \frac{a^2}{b^2 m^2} \right] \quad (8.44)$$

To determine the number of half-waves m that minimizes Equation (8.46), the right-hand side is differentiated with respect to m and the result set equal to zero. This results in the equation,

$$\frac{mb^2}{a^2 \sqrt{\frac{D_{22}}{D_{11}}}} = \frac{a^2}{b^2 m^3} \sqrt{\frac{D_{22}}{D_{11}}}$$

and solving for m ,

$$m = \frac{a}{b} \left(\frac{D_{22}}{D_{11}} \right)^{1/4} \quad (8.45)$$

Note that, since m is an integer, the right-hand side of Equation (8.45) must be rounded up or down to the next (or previous) integer, whichever minimizes the right-hand side of Equation (8.44). For a long plate, (dimension a is large) m is large and using Equation (8.45) instead of the nearest integer that minimizes Equation (8.44) is justified. Then, using Equation (8.45) to substitute in Equation (8.44) gives,

$$N_{xcrit} = \frac{2\pi^2}{b^2} [\sqrt{D_{11}D_{22}} + (D_{12} + 2D_{66})] \quad (8.46)$$

Equation (8.46) gives the buckling load of a long plate under compression, and can be used to correlate with NEF crippling test results. It is the counterpart of Equation (6.13a), which was used to predict buckling of OEF flanges in the previous section. It is interesting to note that, in terms of laminate stiffnesses, the right-hand side of Equation (8.46) is most sensitive to D_{66} because of the factor of 2 multiplying that term. A fractional change in any other of the terms, D_{11} , D_{22} , or D_{12} will result in smaller increase of the buckling load for the same fractional change in D_{66} . Thus, similar to the OEF case, to maximize the crippling load one should maximize the D_{66} term which, as was shown in the previous section is equivalent to maximizing the number of $45^\circ/-45^\circ$ plies and locating them as far from the midplane as possible.

Equation (8.46) is compared with test results for NEF crippling in Figure 8.20. Just as for the OEF case, the test results are slightly lower for low b/t values ($b/t < 15$) and significantly higher at high b/t values. The same arguments presented in the previous section for OEF flanges are also valid here. The post-buckling ability of the web or flange (not accounted for by Equation 8.46) and the specifics of the boundary condition at the roots of the web or flange are two of the main reasons for the discrepancy between the prediction and test results in Figure 8.20.

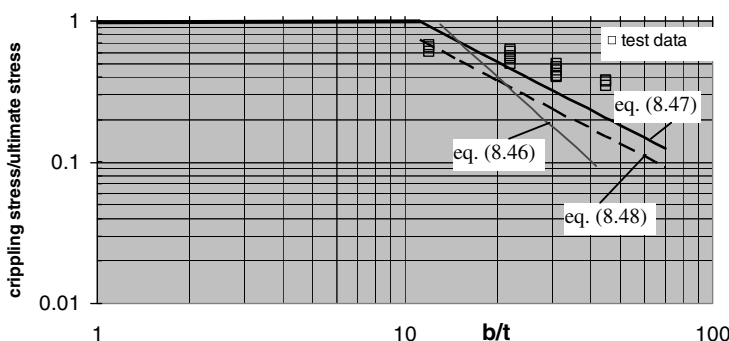


Figure 8.20 NEF crippling test results compared to buckling predictions

Fitting a curve to the test data [8] results in the expression:

$$\frac{\sigma_{crip}}{\sigma_c^u} = \frac{14.92}{\left(\frac{b}{t}\right)^{1.124}} \quad (8.47)$$

where σ_c^u is the compression strength of the flange. Equation (8.47) is valid for $b \geq 11.07t$. For $b < 11.07t$, $\sigma_{crip} = \sigma_c^u$.

For design, a curve that is lower than 90% of the test results (B-Basis value) is used and is given by [8]:

$$\frac{\sigma_{crip}}{\sigma_c^u} = \frac{11.0}{\left(\frac{b}{t}\right)^{1.124}} \quad (8.48)$$

for $b \geq 8.443t$ and $\sigma_{crip} = \sigma_c^u$ for $b < 8.443t$.

Both Equations (8.47) and (8.48) give improved predictions over Equation (8.46). Equation (8.47) matches test results well up to b/t of 25 but then becomes conservative. Equation 8.48 has all test data lying above it and is, therefore, a good equation to use for design. It should be emphasized that the test data in Figure 8.20 were not included in the creation of the semi-empirical Equations (8.47) and (8.48) so the agreement between test results and these equations suggests that the equations have a fairly wide range of applicability. It should be noted that, as Equations (8.47) and (8.48) were derived for flanges with at least 25% 0° and 25% 45° plies, use of these equations for layups that do not fall in this category should be avoided. The tradeoff between 0° and 45° plies that was discussed for OEF flanges in the previous section carries over to this section also. Adding 45° plies away from the midplane increases D_{66} and thus the buckling load. Adding 0° plies increases the compression strength. Both are needed for an optimum design. The final mix of 0° and 45° plies will be a function of applied load and geometry.

Finally, by comparing the test results between Figures 8.18 and 8.20, it can be seen that a NEF flange has always greater crippling strength (as a fraction of the compression strength) than a OEF flange with the same b/t ratio.

8.5.3 Crippling Under Bending Loads

If bending loads are applied to a stiffener (Figure 8.21), then some of the flanges or portions of flanges may still be under compression and can still be crippling-critical.

The recommended approach is to determine the portion of the flange that is under compressive loads and use that portion as the b value in the crippling analysis. Also, as applied load, the average compressive load exerted on that portion is used. This is shown in Figure 8.22 for a case of combined compression and bending loading. For this case, the portion that is under compression is a fraction of the entire flange and is denoted by b in Figure 8.22. Also, the minimum compressive stress σ_{cmin} is zero. Then, the average compressive stress acting over b is given by:

$$\sigma_c = \frac{\sigma_{cmax} + \sigma_{cmin}}{2} = \frac{\sigma_{cmax}}{2} \quad (8.49)$$

The analysis then would consist of determining the crippling stress σ_{crip} for a NEF or OEF flange (depending on the case; it is NEF for the example of Figure 8.22) and comparing it with

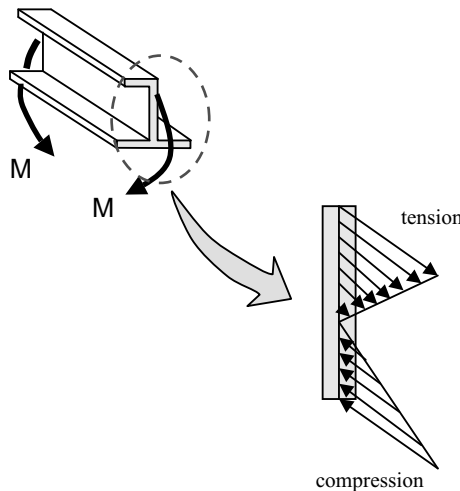


Figure 8.21 Stiffener under bending loads

the applied stress σ_c given by Equation (8.49). If the crippling stress exceeds σ_c then there is no failure.

Note that the example of Figure 8.22 assumes that the bending moment M is large enough to create high tension on the upper end of the flange which exceeds the compression stress due to the applied load P . If M were not high enough the entire flange would be under compression. In

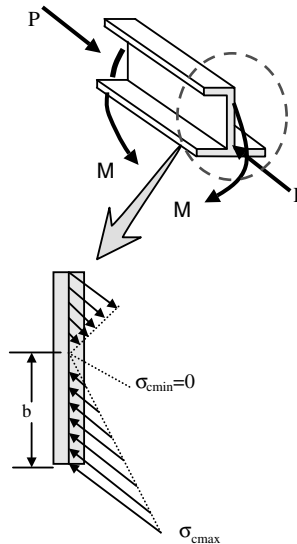


Figure 8.22 Stiffener cross-section under combined compression and bending

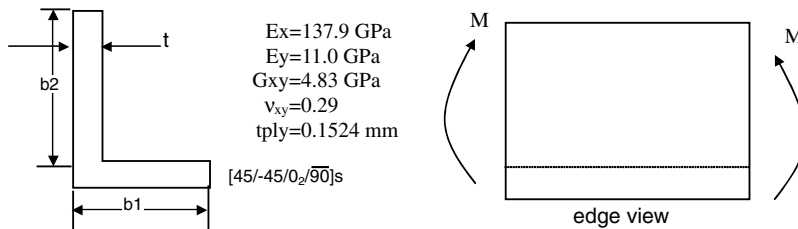


Figure 8.23 Stiffener under bending moment

that case $\sigma_{c\min}$ is not zero, but equal to

$$\sigma_{c\min} = \frac{P}{A} - \frac{Mc}{I}$$

with A and I the area and moment of inertia of the entire cross-section and c half the height. Also, in this case b is equal to the entire width of the web and not a portion of it.

8.5.3.1 Application: Stiffener Design Under Bending Loads

Consider the L stiffener under bending moment $M = 22.6 \text{ N m}$ shown in Figure 8.23. The stiffener layup is the same for both members: $[45/-45/0/90]_s$ with the 0° fibers aligned with the axis of the stiffener (perpendicular to the plane of Figure 8.23). The ultimate strain for this layup at room temperature ambient (RTA) conditions is $12000 \mu\text{s}$. The width b_1 of the horizontal flange is fixed at 17.78 mm . Determine the maximum value of b_2 so that the stiffener does not fail in crippling.

Using classical laminated-plate theory, the elastic properties of the stiffener flange and web are as follows:

$A_{11} (\text{N/mm})$	113015	$D_{11} (\text{Nmm})$	12893.18	$E_{1\text{memb}}$	75.2	GPa
$A_{12} (\text{N/mm})$	23327.5	$D_{12} (\text{Nmm})$	6219.661	$E_{1\text{bend}}$	38.1	GPa
$A_{22} (\text{N/mm})$	54670	$D_{22} (\text{Nmm})$	8265.409	t	1.3716	mm
$A_{66} (\text{N/mm})$	25532.5	$D_{66} (\text{Nmm})$	6564.006			

where axis 1 is aligned with the stiffener axis and axis 2 is in the plane of the web or flange accordingly.

Using Figure 8.24, the stiffener cross-sectional properties are determined as follows:

$$\bar{y} = \frac{b_2 t \left(t + \frac{b_2}{2} \right) + b_1 t \frac{t}{2}}{b_1 t + b_2 t} = \frac{t \left(b_2 + \frac{b_1}{2} \right) + \frac{b_2^2}{2}}{b_1 + b_2}$$

$$I = \frac{tb_2^3}{12} + b_2 t \left(t + \frac{b_2}{2} - \bar{y} \right)^2 + \frac{b_1 t^3}{12} + b_1 t \left(\bar{y} - \frac{t}{2} \right)^2$$

with t the thickness of the laminate used ($=1.3716 \text{ mm}$).

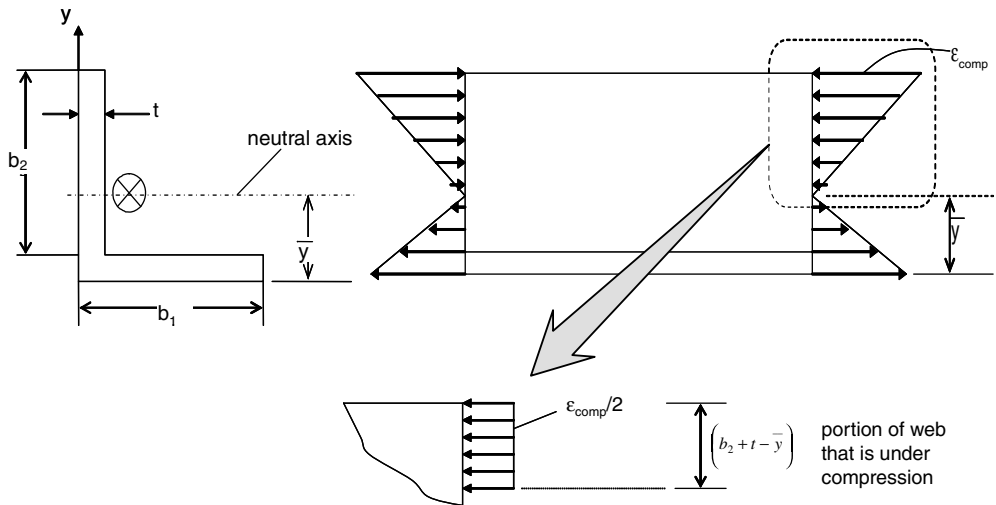


Figure 8.24 Stiffener geometry and neutral axis location

Assuming engineering bending theory is valid, the maximum compressive stress and strain in the stiffener can be shown to be:

$$\sigma_{comp} = \frac{M(b_2 + t - \bar{y})}{I}$$

$$\epsilon_{comp} = \frac{\sigma_{comp}}{E_{1bend}} = \frac{M(b_2 + t - \bar{y})}{E_{1bend}I}$$

Note that for small t values, using E_{1memb} is more representative than E_{1bend} .

The upper portion of the web in Figure 8.24 is under compression and the lower portion, along with the flange, are under tension. Therefore, only the portion above the neutral axis in Figure 8.24 can fail in crippling. This means that the length of the web that may fail in crippling is (see insert of Figure 8.24) $b_2 + t - \bar{y}$. The linear strain distribution shown in Figure 8.24 is approximated as a constant compressive strain equal to the average compressive strain over the portion of the stiffener web that is under compression (see insert of Figure 8.24).

The portion of the stiffener web that is under compression is stabilized at the neutral axis and free at the top so it is OEF. Using Equation (8.43),

$$\frac{\sigma_{crip}}{\sigma_c^u} = \frac{1.63}{\left(\frac{b}{t}\right)^{0.717}}$$

By multiplying numerator and denominator by the axial stiffness E , the crippling equation in terms of strains can be obtained:

$$\frac{\sigma_{crip}}{\sigma_{ult}} = \frac{E\epsilon_{crip}}{E\epsilon_{ult}} = \frac{\epsilon_{crip}}{\epsilon_{ult}} = \frac{1.63}{\left(1 + \frac{b_2 - \bar{y}}{t}\right)^{0.717}}$$

where $b = b_2 + t - \bar{y}$ was substituted in the equation.

The design ultimate strain can be obtained from the ultimate strain at RTA conditions using the knockdowns provided in Section 5.1.6 for material scatter, environmental sensitivity and impact damage. This gives:

$$\epsilon_{ult} = (0.8)(0.8)(0.65)12000 = 4992 \mu\epsilon$$

The not-to-exceed strain at which the web cripes is then given by

$$\epsilon_{crip} = \frac{1.63(0.004992)}{\left(1 + \frac{b_2 - \bar{y}}{t}\right)^{0.717}}$$

which is a function of the web height b_2 .

The applied strain ϵ_{comp} was calculated earlier as a function of the applied moment M and stiffener geometry. That strain must be below the crippling strain ϵ_{crip} to avoid failure. A plot of the applied and crippling strains is shown in Figure 8.25 as a function of the web height b_2 .

As can be seen from Figure 8.25, the crippling strain is lower than the applied strain for small b_2 values. In that range, the applied strain exceeds the crippling strain and failure occurs. This is because the moment of inertia I of the stiffener is low and, as a result, the bending strains are high. Now as b_2 increases, the crippling strain is reduced, which would be expected from the form of the crippling strain equation with b_2 in the denominator. Therefore, the situation would get ‘worse’ from a crippling perspective. However, the rate at which the crippling strain decreases is much lower than the rate at which the applied strain decreases. This is because a change in b_2 increases the moment of inertia (and thus decreases the applied strain) to a larger

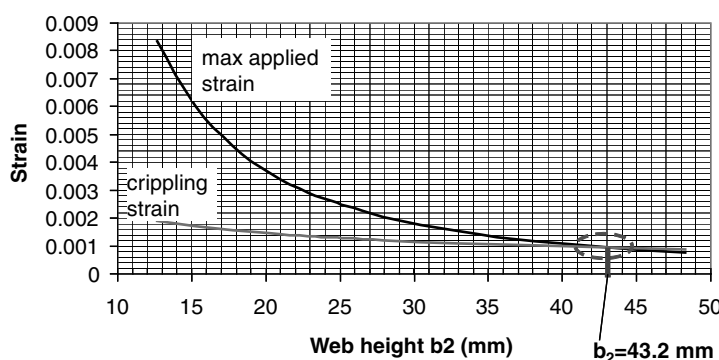


Figure 8.25 Comparison of maximum applied strain to the crippling strain of a stiffener under bending moment

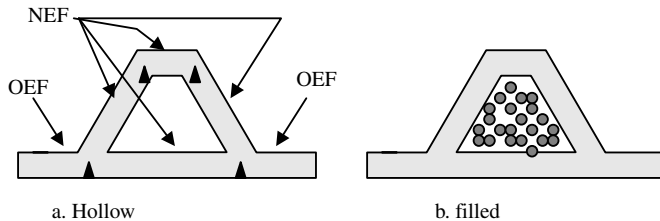


Figure 8.26 Closed cross-section stiffeners (crippling considerations)

extent than the same change decreases the crippling strain. As a result, a value of b_2 can be found, 43.2 mm beyond which the applied strain is lower than the crippling strain and no failure occurs. Therefore, the minimum allowable value of b_2 is 43.2 mm.

8.5.4 Crippling of Closed-Section Beams

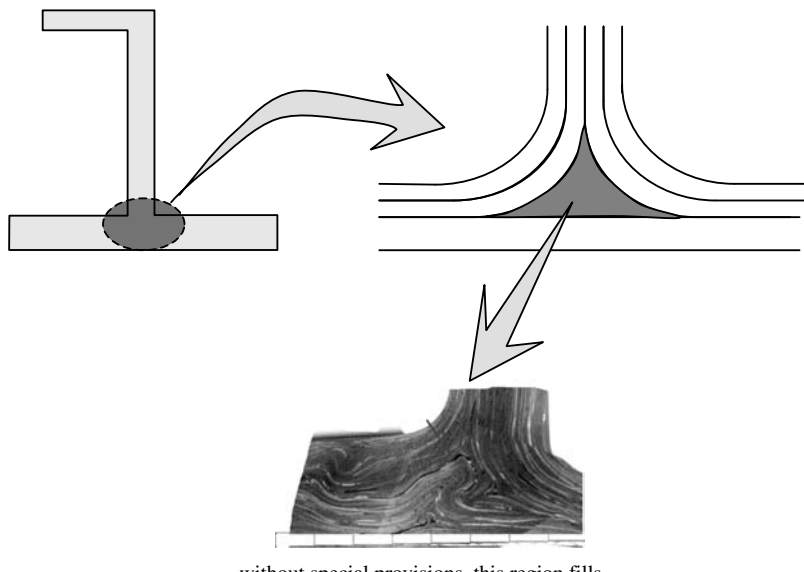
For closed-section beams such as the hat stiffener shown in Figure 8.26, two cases are distinguished: (a) the beam is hollow, and (b) the beam is filled by foam or other material. In the first case, the crippling analysis proceeds as in the previous sections by analyzing each flange of the closed section as NEF. In the second case, an analysis of a beam on an elastic foundation can be carried out (provided a reliable post-buckling analysis is available) or, which is preferred, each flange is treated as a facesheet of a sandwich failing in wrinkling (see Section 10.3).

8.6 Importance of Radius Regions at Flange Intersections

It was briefly mentioned in Section 8.1 (see also Figure 8.4) that turning plies around 90° corners at flange/web intersections is very difficult without the creation of a ‘pocket’. This happens irrespective of the fiber orientation, but is most pronounced in the case of 90° plies and least in the case of 0° plies (where 0° is the direction perpendicular to the page of Figure 8.27). This situation is shown (exaggerated and not to scale) in Figure 8.27.

Wavy fibers in the radius region compromise the strength of the cross-section. Resin-rich areas in the radius region suggest that there are resin-starved areas in adjacent plies, again leading to reduced strength and stiffness, especially under compression or shear. The size of the ‘pocket’ is a function of the layup (plies with fibers aligned with the turn are harder to turn 90° corners following a tight radius), tooling (concave tooling into which the material is placed results in larger pockets, as opposed to convex tooling over which material is draped), cure pressure (higher pressures tend to decrease the size of the pocket), resin flow and bleeding during cure, etc.

Since the existence of the pocket is unavoidable in such configurations, efforts are usually made to reinforce it by incorporating a piece of unidirectional tape or roving material. With reference to Figure 8.28, the area of the ‘pocket’ is found to be:



without special provisions, this region fills with wavy fibers and/or pure resin

Figure 8.27 Resin pocket formed at web/flange intersection of a stiffener (See Plate 19 for the colour figure)

$$A_f = 2 \left[R_i + \frac{t}{2} \right]^2 \left(1 - \frac{\pi}{4} \right) \quad (8.50)$$

where R_i and $t/2$ are the inner radius and thickness of the turning flange respectively.

For the case of uniaxial tension or (pre-buckling) compression, strain compatibility requires that the strain in the pocket be the same as the strain in every other member of the cross-section. Then, using Equation (8.12) the force in the pocket can be found to be:

$$F_f = \frac{E_f A_f}{\sum E_j A_j} F_{TOT} \quad (8.51)$$

The significance of the force absorbed by the filler material can best be seen through an example. Consider the stiffener cross-section shown in Figure 8.29. It is assumed that the

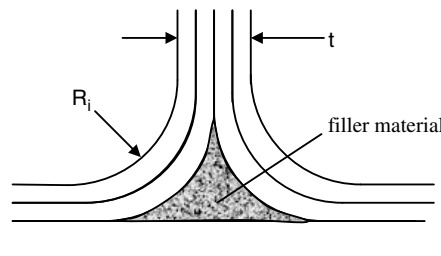


Figure 8.28 Pocket geometry

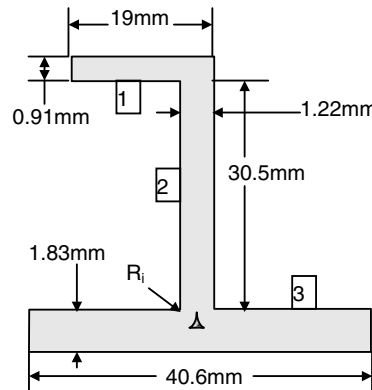


Figure 8.29 Stiffener cross-section with filler material at the interface of the web and bottom flange

material used is typical graphite/epoxy. Then, for typical layups, the axial stiffness of the web and flanges is given by $E_1 = 89.6 \text{ GPa}$, $E_2 = 31.0 \text{ GPa}$, $E_3 = 48.3 \text{ GPa}$, with the subscripts referring to the three members in Figure 8.29. The filler material can be anything from pure resin (no filler) whose stiffness is $E_f = 3 \text{ GPa}$, to completely filled by unidirectional material, in which case the stiffness would be $E_f = 138 \text{ GPa}$. Finally, the inside radius R_i of the turning flange (see Figure 8.28) is assumed to vary in a typical range of 2.5–6.35 mm.

Using Equation (8.51) the force acting in the filler region can be determined as a fraction of the total applied force. The results are shown in Figure 8.30. It can be seen that the force on the filler can be a significant fraction of the total applied force, especially when it is filled with unidirectional material. In general, even when unidirectional or roving material is used, the force on the filler is neglected during the design phase. This increases the load on the other members of the cross-section, making the design more conservative. For a detailed analysis and for comparison with test results the force on the filler must be taken into account.

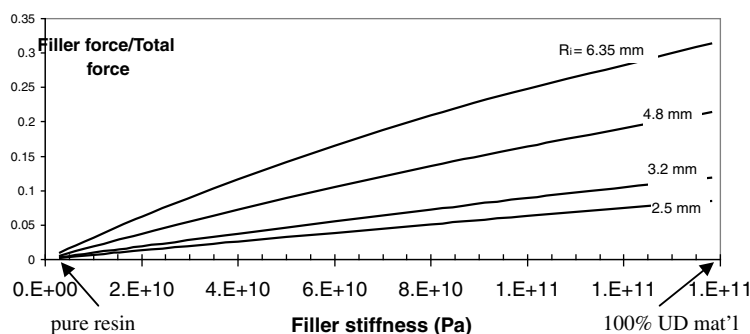


Figure 8.30 Force on filler region as a function of filler stiffness and flange inside radius

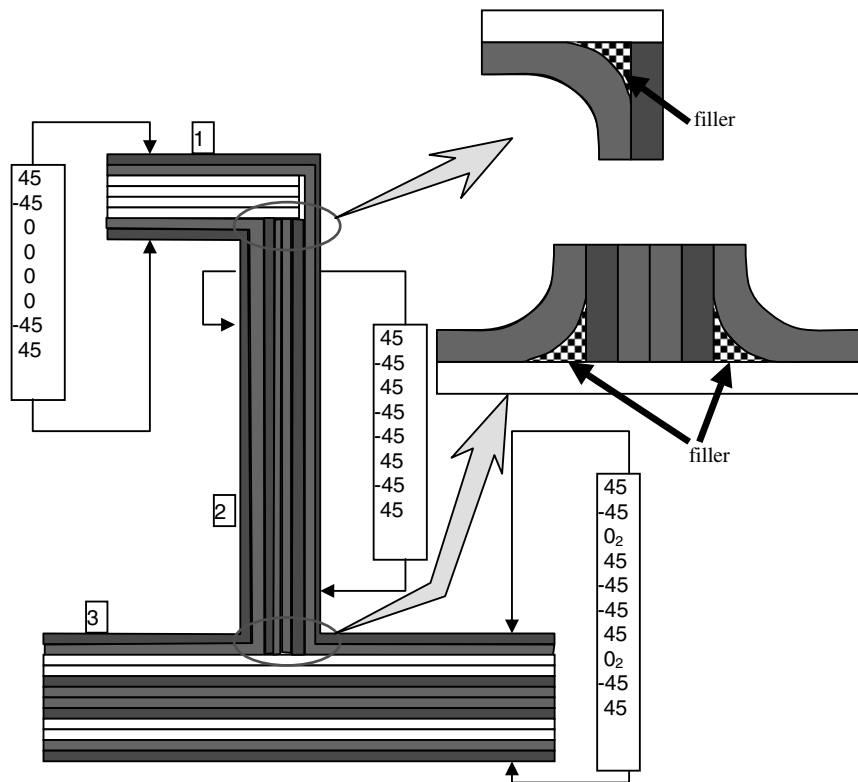


Figure 8.31 J stiffener cross-section with filler material (See Plate 20 for the colour figure)

In view of the importance of the filler material in load sharing and alleviating some of the load in the stiffener web and flanges, the design of the J cross-section from Figure 8.6 is now revisited in Figure 8.31. Besides a filler material, the conclusions of the discussion on crippling have been applied to the flange and an attempt has been made to combine, in the bottom flange, 45° plies (for increased D_{66}) with 0° plies (for increased moment of inertia and compressive strength which, in turn increases the crippling strength).

8.7 Inter-rivet Buckling of Stiffener Flanges

In addition to material failure, column buckling, and crippling, a flange under compression may buckle in a mode where the half-wave is confined between adjacent fasteners. This is shown in Figure 8.32.

In a design, efforts are made to avoid the use of fasteners because of the associated increase in cost and, depending on the fastener type and spacing, increase in weight. However, in situations where co-curing or bonding is not deemed sufficient, fasteners may be the only option. In addition, for post-buckled panels, fasteners may be used (typically near the stiffener ends only) to keep the skin from peeling away from the flange.

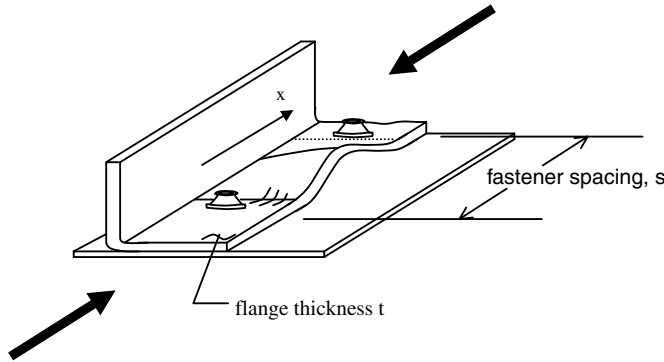


Figure 8.32 Flange inter-rivet buckling

To obtain the design condition for this failure mode, the flange is treated as a beam with the x axis running along its length (Figure 8.32). Also, the 0° direction is aligned with the x axis. Assuming the flange to be symmetric and have $D_{16} = D_{26} = 0$, the governing equation for the out-of-plane displacements w is given by Equation 5.16 applied to a one-dimensional problem ($\partial/\partial y = 0$) with no distributed loads ($p_x = p_y = p_z = 0$):

$$\begin{aligned} D_{11} \frac{\partial^4 w}{\partial x^4} + 2(D_{12} + 2D_{66}) \cancel{\frac{\partial^4 w}{\partial x^2 \partial y^2}} + D_{22} \cancel{\frac{\partial^4 w}{\partial y^4}} &= N_x \frac{\partial^2 w}{\partial x^2} + 2N \cancel{\frac{\partial^2 w}{\partial x \partial y}} \\ + N_y \cancel{\frac{\partial^2 w}{\partial y^2}} - p_x \cancel{\frac{\partial w}{\partial x}} - p_y \cancel{\frac{\partial w}{\partial y}} + p_z &\cancel{=} 0 \end{aligned} \quad (5.16)$$

which, for a compressive load $N_o = -N_x$ simplifies to:

$$D_{11} \frac{\partial^4 w}{\partial x^4} + N_o \frac{\partial^2 w}{\partial x^2} = 0 \quad (8.52)$$

which has the general solution:

$$w = C_o + C_1 x + C_2 \sin\left(\sqrt{\frac{N_o}{D_{11}}} x\right) + C_3 \cos\left(\sqrt{\frac{N_o}{D_{11}}} x\right) \quad (8.53)$$

Note that the partial derivatives of Equation (8.52) are, in fact, total derivatives in this case because there is no dependence on y .

If the fasteners are assumed to provide simple support to the flange at $x = 0$ and $x = s$, the boundary conditions are:

$$\begin{aligned} w(x = 0) = w(x = s) &= 0 \\ -D_{11} \frac{d^2 w}{dx^2} &= M = 0 \quad \text{at } x = 0, x = s \end{aligned} \quad (8.54)$$

Substituting in Equation (8.54):

$$w(x = 0) = 0 \Rightarrow C_o + C_3 = 0$$

$$w(x = s) = 0 \Rightarrow C_o + C_{1s} + C_2 \sin\left(\sqrt{\frac{N_o}{D_{11}}}s\right) + C_3 \cos\left(\sqrt{\frac{N_o}{D_{11}}}s\right) = 0 \quad (8.55a-d)$$

$$-D_{11} \frac{d^2 w}{dx^2}(x = 0) \Rightarrow C_3 \frac{N_0}{D_{11}} = 0$$

$$-D_{11} \frac{d^2 w}{dx^2}(x = s) \Rightarrow C_2 \frac{N_0}{D_{11}} \sin\left(\sqrt{\frac{N_o}{D_{11}}}s\right) + C_3 \frac{N_0}{D_{11}} \cos\left(\sqrt{\frac{N_o}{D_{11}}}s\right) = 0$$

From Equation (8.55c),

$$C_3 = 0$$

which substituted in (8.55a) gives

$$C_o = 0$$

Then, Equation (8.55b) can be used to obtain a relation between C_1 and C_2 :

$$C_1 = -C_2 \frac{1}{s} \sin\left(\sqrt{\frac{N_o}{D_{11}}}s\right)$$

Finally, Equation 8.55d gives:

$$\sin\left(\sqrt{\frac{N_o}{D_{11}}}s\right) = 0 \Rightarrow \sqrt{\frac{N_o}{D_{11}}}s = n\pi \Rightarrow N_o = \frac{n^2\pi^2}{s^2}D_{11}$$

which gives the buckling load N_o for the flange. The lowest buckling load ($n = 1$) is the one of interest. Therefore, the inter-rivet (buckling) stress is

$$\sigma_{ir} = \frac{N_o}{t} = \frac{\pi^2 D_{11}}{ts^2}$$

where t is the flange thickness.

This equation corresponds to simply supported ends at the fasteners. However, depending on the type of fastener, the support provided at the ends can be more restricting than a simple support with the slope locally constrained to a degree. The edge condition can range from simply supported (countersunk fasteners) to nearly fixed (protruding fasteners). This range of boundary conditions is represented by a coefficient of fixity c and the inter-rivet stress expression is generalized to:

$$\sigma_{ir} = \frac{c\pi^2 D_{11}}{ts^2} \quad (8.56)$$

with $c = 1$ for countersunk fasteners and $c = 3$ for protruding-head fasteners.

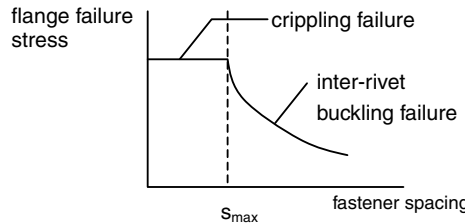


Figure 8.33 Flange failure modes as a function of fastener spacing

The fastener spacing and flange stiffness determine the failure mode of the flange. Contrasting inter-rivet buckling with crippling for example, it can be seen that for relatively wide fastener spacings and soft flanges (s large and D_{11} small) the flange will fail by inter-rivet buckling. For narrow spacings and large bending stiffness the flange will fail in crippling. This means that, given a flange layup, there is a threshold fastener spacing value that, if exceeded, the failure mode switches from crippling to inter-rivet buckling. This is shown schematically in Figure 8.33.

Typically, the flange attached to the skin that may fail by inter-rivet buckling is of the one-edge-free (OEF) type. Then, Equations (8.43) and (8.56) can be combined to determine the critical fastener spacing. Equating the inter-rivet buckling stress to the crippling stress and solving for s gives,

$$s_{\max} = \sqrt{\frac{c\pi^2 D_{11}}{1.63t\sigma_c^u} \left(\frac{b}{t}\right)^{0.717}} \quad (8.57)$$

which gives the maximum fastener spacing for crippling to occur.

The implications of Equation (8.57) can be seen more clearly through an example. Consider the two flange layups given in Table 8.7. The first is a stiff flange and the second a very soft flange.

The maximum fastener spacing determined from Equation (8.57) is plotted in Figure 8.34 for the first layup, $[45/0_2/-45/0_4]_s$. As the width to thickness ratio b/t for the flange increases the value of s_{\max} increases.

The maximum fastener spacing for the soft layup, $[(\pm 45)/(0/90)/(\pm 45)]$, is shown in Figure 8.35. The trends are the same as in Figure 8.34, but an important problem not present in the stiff flange of Figure 8.34 is now evident: The maximum allowed fastener spacing is too small for typical b/t ratios. Fastener spacing values less than 20 mm are avoided in practice because the interaction between adjacent fasteners leads to increased bearing loads. For a (protruding-head) fastener spacing of 20 mm, Figure 8.35 suggests a b/t value of about 25 which corresponds to very low crippling failure loads (see Figure 8.18). The situation is even worse for countersunk fasteners.

Table 8.7 Properties of two potential flange layups

Layup	$[45/0_2/-45/0_4]_s$	$[(\pm 45)/(0/90)/(\pm 45)]$
σ_c^u (MPa)	762	529
D_{11} (Nm)	67.5	0.66
t (mm)	2.032	0.572

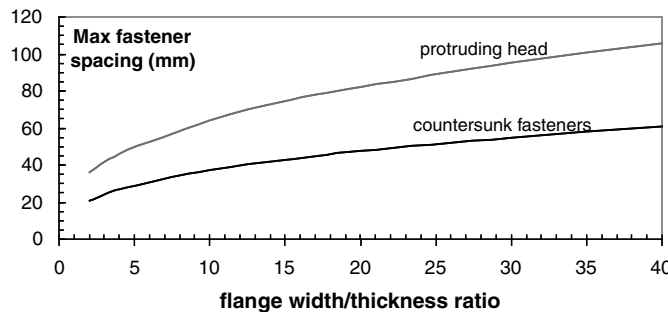


Figure 8.34 Fastener spacing to cause inter-rivet buckling for $[45/0_2/-45/0_4]_s$ flange

This discussion brought to the surface some of the issues associated with fasteners and fastener spacing. While the interaction between inter-rivet buckling and crippling suggests that relatively large fastener spacings may be necessary, bolted joint analysis of multi-fastener joints shows that, for composites, lower fastener spacings should be preferred because they tend to maximize the net section strength [9]. As is often the case when multiple failure modes and constraints come into play, design guidelines can be generated that, at times, conflict with one another. Care must be exercised in such situations to generate designs that yield the best compromise. While an exhaustive discussion of bolted joints is beyond the scope of this book, some basic guidelines derived from the above discussion and more elaborate analyses of fastener joints [9–11] are summarized below.

1. If no other requirements dominate, use a fastener spacing of $4\text{--}5D$ (where D is the diameter of the fastener)
2. Minimum fastener spacing should be no less than 20 mm
3. Use skin thickness/diameter ratio $< 1/3$ to minimize fastener bending
4. Use skin thickness/countersunk depth $> 2/3$ to avoid pulling countersunk fastener through the skin when loads perpendicular to the skin are applied
5. Use at least 40% 45/–45 plies around fasteners for better load transfer

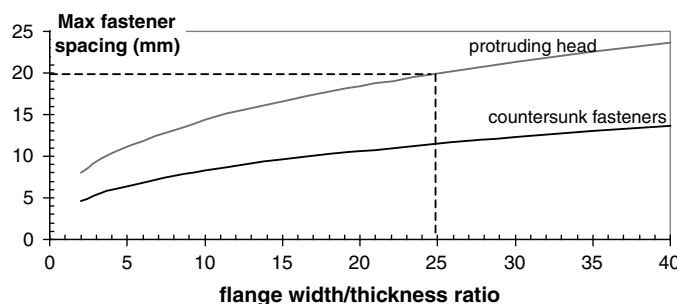


Figure 8.35 Fastener spacing to cause inter-rivet buckling for $[(\pm 45)/(0/90)/(\pm 45)]$ flange

8.8 Application: Analysis of Stiffeners in a Stiffened Panel under Compression

A highly loaded stiffened panel is shown in Figure 8.36. The stiffener cross-section is the same, in terms of layup, as in Figure 8.31. The effect of the filler material at the radius regions is neglected. Skin and stiffener properties are summarized in Table 8.8. The axial stiffness of the skin is found from Equation (8.6) to be $E_{\text{skin}} = 41.15 \text{ GPa}$. The portion of skin under compression, b_{eff} if the post-buckling load distribution is represented by a piecewise constant distribution, is given by Equation (7.15), resulting in $b_{\text{eff}} = 0.292a = 4.45 \text{ cm}$.

Using Equation (6.7), the buckling load of the skin between the stiffeners is found to be $N_o = 182 \text{ N/mm}$. This corresponds to a total force of $182 \times 457 = 83\,174 \text{ N}$. So, under the applied load of 100 kN, the skin buckles and the PB ratio is $100/83.17 = 1.20$. It is now assumed that, once the skin buckles all the excess load (between 100 and 83 kN) is taken by the stiffeners and b_{eff} skin next to them. So the load on each cross-section of Figure 8.37 is the buckling load on the b_{eff} portion of the skin and the total load minus the buckling load acting on the stiffener plus the b_{eff} skin portion. Since there are four stiffener/skin combinations as in Figure 8.37, the load in the skin due to skin buckling is $83\,174/4 = 20794 \text{ N}$. The load beyond buckling acting on

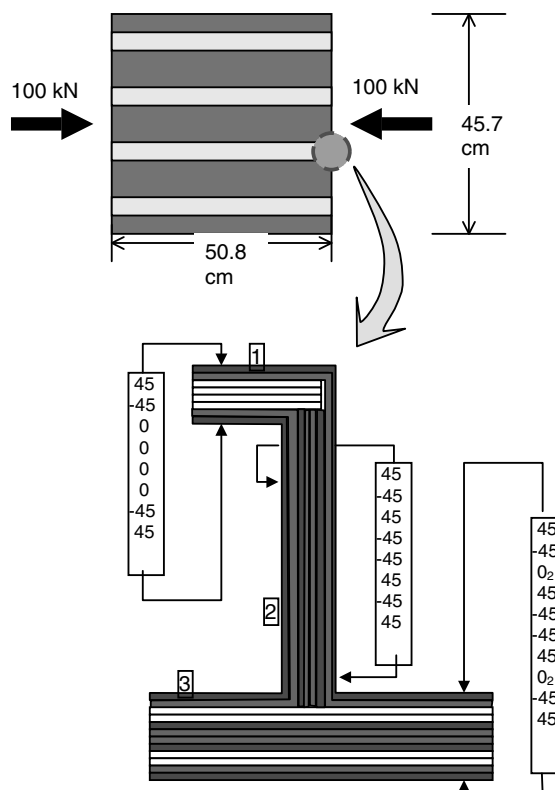


Figure 8.36 Skin-stiffened panel under compression (See Plate 21 for the colour figure)

Table 8.8 Skin and stiffener properties

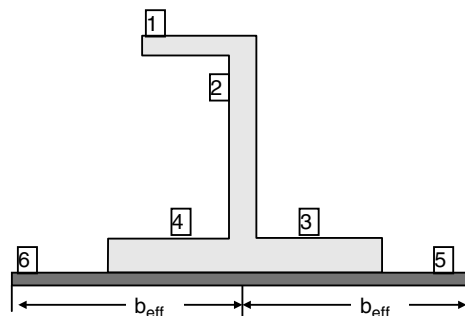
SKIN				
D_{11}	659.7	Nmm		
D_{12}	466.9	Nmm		
D_{22}	659.7	Nmm		
D_{66}	494.0	Nmm		
skin thickness = 0.57mm				
A_{11}	28912.44	N/mm		
A_{12}	12491.43	N/mm		
A_{22}	28912.44	N/mm		
A_{66}	13468.58	N/mm		
STIFFENER				
Member	b (mm)	t (mm)	E_m (Gpa)	E_b (GPa)
1	12.7	1.2192	75.6	32.4
2	31.75	1.2192	18.2	17.9
3	38.1	1.8288	56.5	47.9

each stiffener/skin combination is $(100\ 000 - 83\ 174)/4 = 4207$ N. The situation is shown in Figure 8.38.

The skin buckling load of 20 794 N is shown in Figure 8.38 acting through the skin neutral axis to emphasize the fact that it is caused by skin buckling and stays in the skin (does not transfer into the stiffener). The remaining load of 4207 N is acting through the neutral axis of the entire combination of stiffener and effective skin.

Using the geometry of Table 8.8 and the crippling equations (8.43) and (8.48) the crippling stresses in each member of the cross-section can be determined as a fraction of the compression strength of each member. Then, a first-ply failure criterion (Tsai-Wu failure theory, see Section 4.4) is used to determine the compression strength of each member and, from that, the crippling failure stresses in each member. The results are shown in Table 8.9.

Equation (8.12) can be used to determine the applied load on each of the members of the cross-section. This equation is applied to the 4207N load (see Figure 8.38) while the 20794 N

**Figure 8.37** Cross-section carrying load in the post-buckling regime

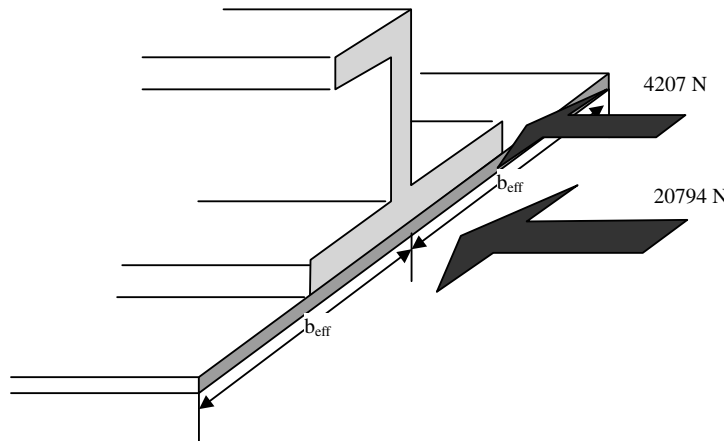


Figure 8.38 Loads on representative cross-section after the skin buckles

load is added to the skin members 5 and 6 in addition to the contribution coming from the 4207 N load. The resulting loads are given in Table 8.10.

The last column of Table 8.9 gives the stress at which the corresponding member will fail (allowable stress). The last column of Table 8.10 gives the applied stress. The ratio of the two stresses is shown in Table 8.11. If the ratio of applied to allowable (also termed the loading index) is greater than 1, the corresponding member fails. As can be seen from Table 8.11, the last two members, i.e. the effective skin portion will fail in crippling.

Table 8.9 Crippling analysis of members of the cross-section

Member	b (mm)	t (mm)	OEF/NEF	b/t	$\sigma_{\text{crip}}/\sigma_{\text{cu}}$	$\sigma_{\text{cu}}(\text{N/mm}^2)$	$\sigma_{\text{fail}}(\text{N/mm}^2)$
1	12.7	1.22	OEF	10.42	0.304	494.64	150.2344
2	31.75	1.22	NEF	26.04	0.282	283.88	80.04247
3	19.05	1.83	OEF	10.42	0.304	351.75	106.8331
4	19.05	1.83	OEF	10.42	0.304	351.75	106.8331
5	44.5	0.57	NEF	78.07	0.082	529.14	43.43236
6	44.5	0.57	NEF	78.07	0.082	529.14	43.43236

Table 8.10 Applied loads on the members of the cross-section

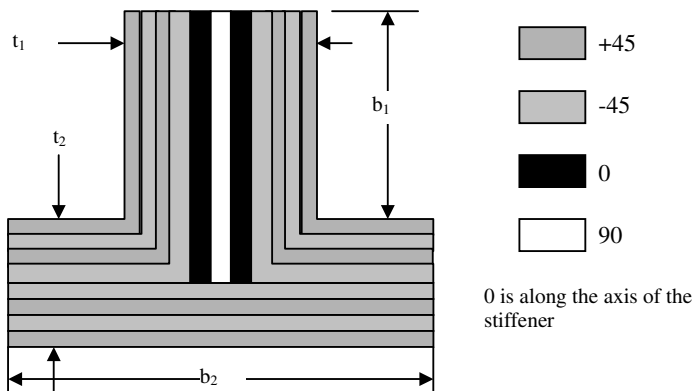
Member	b (mm)	t (mm)	E (N/m^2)	A (mm^2)	EA (N)	F_i/F_{tot}	Applied F (N)	σ_{applied} (N/mm^2)
1	12.7	1.22	7.56E + 10	15.48	1.17E + 05	0.148	623.42	40.26
2	31.75	1.22	1.82E + 10	38.71	7.05E + 04	0.089	375.20	9.69
3	19.05	1.83	5.65E + 10	34.84	1.97E + 05	0.249	1048.31	30.09
4	19.05	1.83	5.65E + 10	34.84	1.97E + 05	0.249	1048.31	30.09
5	44.5	0.57	4.12E + 10	25.37	1.04E + 05	0.132	10952.88	431.81
6	44.5	0.57	4.12E + 10	25.37	1.04E + 05	0.132	10952.88	431.81

Table 8.11 Failure index (applied/allowable stress) for members of the cross-section

Member	Applied/allowable
1	0.268
2	0.121
3	0.282
4	0.282
5	9.942
6	9.942

Exercises

8.1 A T stiffener is used in a compression application. It has the following configuration:



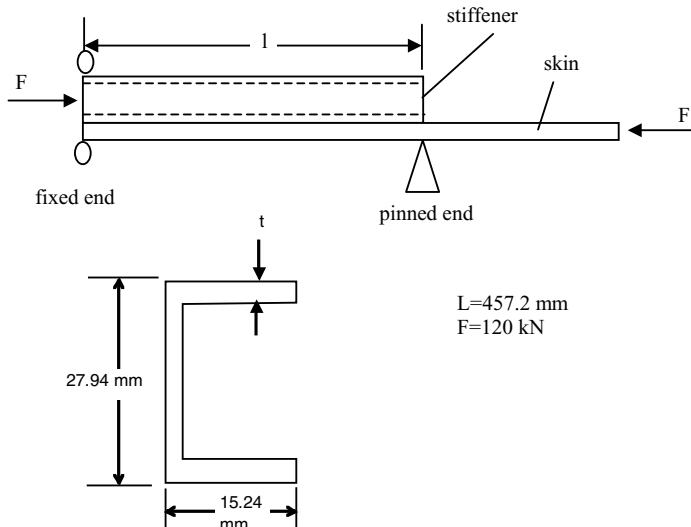
The material used has the properties:

$$\begin{aligned} E_x &= 137.9 \text{ GPa} \\ E_y &= 11.0 \text{ GPa} \\ G_{xy} &= 4.82 \text{ GPa} \\ v_{xy} &= 0.29 \\ t_{\text{ply}} &= 0.1524 \text{ mm} \end{aligned}$$

The length L of the stiffener is 304.8 mm. The stiffener is pinned at the two ends and rests on an elastic foundation of spring constant k . Manufacturing considerations do not permit b_2 to be smaller than 19.05 mm or b_1 to be smaller than 12.7 mm. (a) If k is allowed to vary between 1378 800 N/m² and 5515 200 N/m², create a plot that shows how b_1 and b_2 vary with k so that the weight is minimized and the stiffener does not buckle below 31.115 kN. (b) What is the optimum value of k to use in this application (taking ‘optimum’ to mean the value that minimizes the stiffener weight)?

8.2 A stiffener terminates in the middle of nowhere on a skin. The stiffener is loaded on one end by a compressive load of 22.2 kN. The outer mold line of the stiffener cross-section (i.e. the outer shape) is fixed because a tool to make it is already available. But the stiffener thickness is variable. The situation is shown in the Figure below.

The basic material properties are the same as in Exercise 8.1.



Use only 45, -45, 0, and 90° plies to create a symmetric and balanced laminate, which includes at least one of each of these principal four orientations, to determine the lowest thickness laminate that does not buckle under the applied load.

- 8.3 You are now given the basic strength values for the material of Exercise 8.2:

$$X^t = 2068 \text{ MPa} \text{ (tension strength parallel to the fibers)}$$

$$X^c = 1378 \text{ MPa} \text{ (compression strength parallel to the fibers)}$$

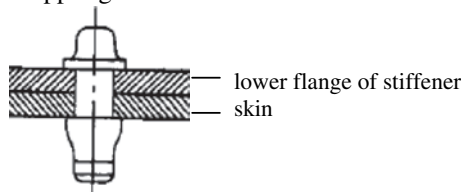
$$Y^t = 103.4 \text{ MPa} \text{ (tension strength perpendicular to the fibers)}$$

$$Y^c = 310.2 \text{ MPa} \text{ (compression strength perpendicular to the fibers)}$$

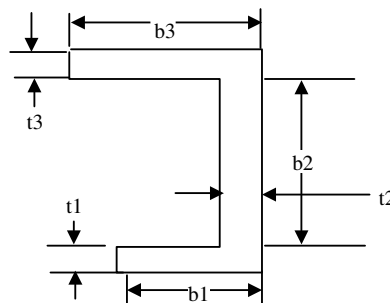
$$S = 124.1 \text{ MPa} \text{ (shear strength)}$$

Check your solution of Exercise 8.3 for crippling of the upper flange (flange away from the skin) and the vertical web. If your solution fails in crippling, discuss how you would go about changing different parameters of the problem (layups, lengths, widths) to avoid failure with the lowest possible weight increase. If your solution does not fail in crippling, discuss what parameters of the problem (layups, length, widths, etc) you should change to reduce the weight of the structure as much as possible without failing in crippling or buckling. Do not run any numbers, simply discuss what you should change and why you think it is the most effective.

- 8.4 The stiffener of Exercise 8.3 is riveted to the skin. Using the layup you obtained in Exercise 8.3, determine the maximum allowed rivet spacing for the rivets shown below. For this problem, disregard the crippling failure.



8.5 A C (or channel) stiffener is used in a compression application (see Figure)



Member 1 is next to the skin and its layup is fixed to: [45/-45/0/90/0/-45/45] with 0 running along the axis of the stiffener. The dimension b_1 is also fixed at 19.05 mm. The basic material properties are as follows:

E_x	1.31E + 11 Pa	X^T	1.7235E + 09 Pa
E_y	1.14E + 10 Pa	X^C	1.379E + 09 Pa
G_{xy}	4.83E + 09 Pa	Y^T	8.273E + 07 Pa
v_{uxy}	2.90E-01	Y^C	3.033E + 08 Pa
t_{ply}	1.52E-01 mm	S	8.809E + 07 Pa

Dimensions b_2 and b_3 are allowed to vary between 12.7 and 48.26 mm. Use the layup for member 1 above and change it (if needed) according to the following rules:

- (a) No fewer plies than the base layup are allowed
- (b) Keep +45/-45 on the outside
- (c) Layup is symmetric
- (d) At least one 0° and one 90° ply are present in the layup
- (e) Only 45, -45, 0, and 90° degree plies are used
- (f) No layup has more than a total of 13 plies

to create candidate layups for members 2 and 3.

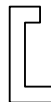
- (a) (you will need access to do first ply failure analysis). If the total compressive load applied to the cross-section is 26.67 kN, determine the optimum layup(s) and dimensions for members 2 and 3 so that the cross-section does not fail in crippling. Note that member 1, being next to the skin is reinforced by the effective skin and is assumed not to fail in crippling (so you do not need to do any failure analysis for member 1). For crippling equations, assume that the general equations given in this chapter are valid even if, for some of your layups, the requirement of at least 25% 0, 25% 45° plies is not satisfied. Optimum here means that for each set of layups that do not fail in crippling, determine the one with the lowest cross-sectional area. Do not reduce the strength value calculated to account for environmental effects, impact, and material scatter.
- (b) Among the optimum layups determined in part (a) determine, as the best layup(s) to use, the one(s) that make most sense from a robust design and manufacturing perspective.

8.6 You are to design the cross-sectional shape and layup for a composite stiffener for an application under compressive load.

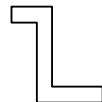
Of the seven shapes below select three (if the hat stiffener is not included in your selection) or two (if the hat stiffener is one of them). Also note that you are not allowed to include both the C and Z stiffeners in your selection. If you like both the C and the Z you must only include one of them in your analysis.



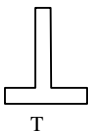
L



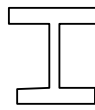
C



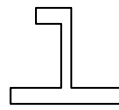
Z



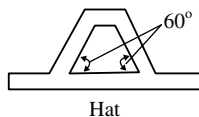
T



I

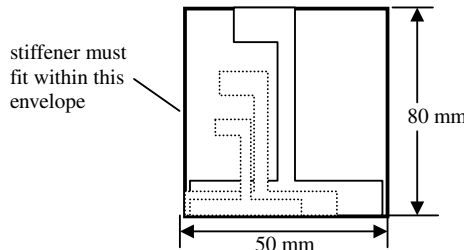


J



Hat

The stiffeners must fit within a rectangle of height 80 mm and width 50 mm. These are the maximum dimensions, but they can be smaller than that.



The applied load is 35000 N (assume it is acting at the center of gravity of the selected cross-section). The length ℓ of the stiffener is 550 mm.

Two composite materials are available, with properties as follows:

Unidirectional tape Gr/Epoxy	Plain weave fabric Gr/Epoxy
$E_x = 131 \text{ GPa}$	68.9 GPa
$E_y = 11.4 \text{ GPa}$	68.9 GPa
$v_{xy} = 0.31$	0.05
$G_{xy} = 5.17 \text{ GPa}$	5.31 GPa
$t_{\text{ply}} = 0.1524 \text{ mm}$	0.1905 mm
$\rho = 1611 \text{ kg/m}^3$	1611 kg/m ³

You are allowed to use any of the two graphit/epoxy materials or a combination thereof. Finally, assume a compression strain allowable (accounting for environment, damage, and material scatter) of $4500 \mu\text{s}$.

1. Determine the layup of each member of each stiffener and its dimensions, observing as many of the design rules as possible.
2. Provide a simple sketch of the cross-section of stiffeners that shows the plies, layup, dimensions, etc.
3. Calculate the corresponding weights for the stiffeners and compare. Based on the comparison, select the ‘best’ design.

References

1. Hart-Smith, L.J. The key to designing durable adhesively bonded joints, *Composites*, **25**, 895–898 (1994).
2. Kairouz, K.C. and Matthews, F.L, Strength and failure modes of bonded single lap joints between cross-ply adherends *Composites*, **24**, 475–484 (1993).
3. Rivello, R.M., *Theory and Analysis of Flight Structures*, McGraw-Hill Book Co., 1969, Chapter 14.
4. Timoshenko, S.M., and Gere, J.M., *Theory of Elastic Stability*, McGraw-Hill Book Co., 1961, Section 2.1.
5. Aristizabal-Ochoa, J.D. Classical stability of beam columns with semi-grid connections on elastic foundation, 16–18 July 2003, Paper 67.
6. O'Donnell, W.J., The Additional Deflection of a Cantilever Due to the Elasticity of the Support, *ASME Journal of Applied Mechanics*, **27**, 461 (1960).
7. *Mil-Hdbk 17-3F*, vol. 3, chap. 5, Fig 5.7.2.h, 17 June 2002.
8. *Mil-Hdbk 17-3F*, vol. 3, chap. 5, Fig 5.7.2.f, 17 June 2002.
9. Hart-Smith, L.J., The key to designing efficient bolted composite joints, *Composites*, **25**, 835–837 (1994).
10. Hart-Smith, L.J., Bolted Joints in Graphite/Epoxy Composites, *McDonnell-Douglas Corporation, Report A600503*, June 1976.
11. Ramkumar, R.L., Saether, E.S. and Cheng, D., Design Guide for Bolted Joints in Composite Structures, *Air Force Wright Aeronautical Report AFWAL-TR-86-3035*, March 1986.

9

Skin-Stiffened Structure

The individual constituents, skin and stiffeners have been examined in previous chapters. Based on that discussion, the behavior and the design of a stiffened panel such as the one shown in Figure 9.1 can be summarized as follows: The skin takes pressure loads via in-plane stretching (membrane action) and shear loads. It also takes compression loads up to buckling. Beyond buckling extra care must be exercised to account for the skin deformations and additional failure modes, not examined so far, such as the skin/stiffener separation, which is discussed in this chapter. The stiffeners take bending and compression loads. It is readily apparent that the robustness and efficiency of a design will strongly depend on how one can 'sequence' the various failure modes so benign failures occur first and load can be shared by the rest of the structure, and how one can eliminate certain failure modes without unduly increasing the weight of the entire panel.

In this chapter, some aspects that manifest themselves at the component level, with both skin and stiffeners present, are examined. This includes modeling aspects such as smearing of stiffness properties and additional failure modes such as the skin/stiffener separation.

9.1 Smearing of Stiffness Properties (Equivalent Stiffness)

If the number of stiffeners is sufficiently large and/or their spacing is sufficiently narrow, accurate results for the overall panel performance can be obtained by smearing the skin and stiffener properties in combined, equivalent stiffness, expressions. This can be done for both in-plane (membrane) and out-of-plane (bending) properties.

9.1.1 Equivalent Membrane Stiffnesses

A composite stiffened panel is shown in Figure 9.2. The stiffener spacing is d_s and the width of the panel is b_p .

As can be seen from Equation (8.13), the equivalent in-plane stiffness of the skin–stiffener combination is the sum of the individual stiffnesses of skin and stiffeners. This means that the

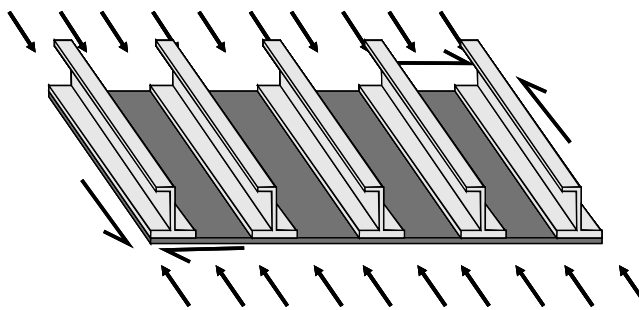


Figure 9.1 Stiffened panel under combined loads

A matrix for the entire panel, which is the membrane stiffness per unit width, is given by the sum of the corresponding terms for skin and stiffeners considered separately:

$$(A_{ij})_{eq} = (A_{ij})_{skin} + (A_{ij})_{stiffeners} \quad (9.1)$$

with the subscript ij denoting the ij element of the A matrix. Also, again from Equation (8.13),

$$(A_{ij})_{stiffeners} = n_s (A_{ij})_{singlestiff} \quad (9.2)$$

where n_s is the number of the stiffeners.

Determining the number of the stiffeners involves some approximation caused by the presence or lack of stiffeners at the panel edges. If there are stiffeners right at the panel edges as in Figure 9.2, the number of stiffeners is given by:

$$n_s = \text{int}\left[\frac{b_p}{d_s}\right] + 1 \quad (9.3)$$

where $\text{int}[\dots]$ denotes the integer that is obtained when the quantity in brackets is rounded down to the nearest integer.

If the stiffener spacing is sufficiently small, the second term in the right-hand side of Equation (9.3) can be neglected and the number of stiffeners approximated by,

$$n_s \approx \frac{b_p}{d_s} \quad (9.4)$$

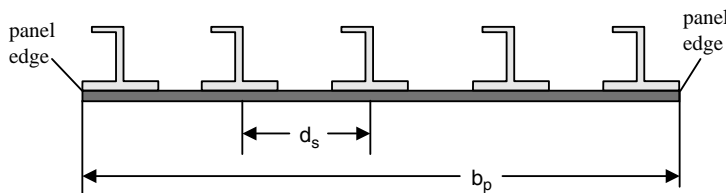


Figure 9.2 Section cut of a composite stiffened panel

If there are no stiffeners at the panel edges, i.e. the skin overhangs on either side of the panel, b_s in Equation (9.3) must be reduced by the total amount of overhang. Again, for sufficiently large b_s and/or small d_s Equation (9.4) can be used. Note that Equation (9.4) typically is a rational number as the division b_s/d_s is an integer only for judiciously chosen values of b_p and d_s . But, for the purpose of stiffness estimation, using the rational number obtained from Equation (9.4) without round-off is a reasonable approximation.

Now the A_{ij} term for a single stiffener can be estimated by averaging the corresponding membrane stiffness of the stiffener over the skin width b_p . For the case of A_{11} this gives

$$(A_{11})_{\text{singlestiff}} = \frac{(EA)_{\text{stiff}}}{b_p} \quad (9.5)$$

Placing Equations (9.2), (9.4), and (9.5) into Equation (9.1) and recognizing that a one-dimensional stiffener has negligible contribution to stiffnesses other than the one parallel to its own axis, gives the A matrix terms:

$$\begin{aligned} (A_{11})_{eq} &\approx (A_{11})_{\text{skin}} + \frac{(EA)_{\text{stiff}}}{d_s} \\ (A_{12})_{eq} &\approx (A_{12})_{\text{skin}} \\ (A_{22})_{eq} &\approx (A_{22})_{\text{skin}} \\ (A_{66})_{eq} &\approx (A_{66})_{\text{skin}} \end{aligned} \quad (9.6)$$

9.1.2 Equivalent Bending Stiffnesses

The derivation of the bending stiffnesses proceeds in a similar fashion. Based on Equation (8.20) the bending stiffnesses per unit width can be written as:

$$(D_{ij})_{eq} = (D_{ij})_{\text{skin}} + (D_{ij})_{\text{stiffeners}} \quad (9.7)$$

with

$$(D_{ij})_{\text{stiffeners}} = n_s (D_{ij})_{\text{singlestiff}} \quad (9.8)$$

The bending stiffness D_{11} for a single stiffener can be determined by smearing its contribution over the entire width b_p :

$$(D_{11})_{\text{singlestiff}} = \frac{(EI)_{\text{stif}}}{b_p} \quad (9.9)$$

While there are no contributions to the D_{12} and D_{22} terms because the bending stiffness contribution from the stiffeners is negligible in these directions, the contribution to D_{66} requires a detailed derivation.

Consider the situation shown in Figure 9.3 where a laminate deforms under an applied torque.

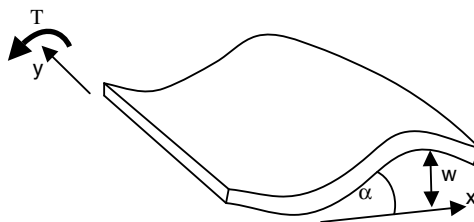


Figure 9.3 Laminate under applied torque

The angle α is given by

$$\alpha = \frac{\partial w}{\partial x} \quad (9.10)$$

From torsion theory [1], the rate of change of angle α as a function of y is given by

$$\frac{d\alpha}{dy} = \frac{T}{GJ} \quad (9.11)$$

where T is the applied torque, G the shear modulus and J the polar moment of inertia. Combining Equations (9.10) and (9.11) gives

$$\frac{d\alpha}{dy} = \frac{\partial^2 w}{\partial x \partial y} = \frac{T}{GJ} \quad (9.12)$$

Now from classical laminated-plate theory (see Equation 3.49 and assuming no coupling is present) the torque per unit width M_{xy} is given by

$$M_{xy} = -2D_{66} \frac{\partial^2 w}{\partial x \partial y} \quad (9.13)$$

Since now

$$\frac{T}{b_p} = -M_{xy} \quad (9.14)$$

Equations (9.12), (9.13), and (9.14) can be combined and applied to a single stiffener to give:

$$(D_{66})_{\text{singlestiff}} = \frac{(GJ)_{\text{stif}}}{2b_p} \quad (9.15)$$

This equation is analogous to Equation (9.9), but there is a factor of 2 in the denominator. Summing up the contributions of all stiffeners and using Equation (9.4), the contribution of all stiffeners to D_{66} for the combined skin/stiffener configuration is

$$D_{66} = n_s (D_{66})_{\text{singlestiff}} = \frac{(GJ)_{\text{stif}}}{2d_s} \quad (9.16)$$

Finally, combining Equations (9.7)–(9.9) and (9.16) gives the final approximate expressions for the bending stiffnesses of a stiffened panel:

$$\begin{aligned}
 (D_{11})_{eq} &\approx (D_{11})_{skin} + \frac{(EI)_{stif}}{d_s} \\
 (D_{12})_{eq} &\approx (D_{12})_{skin} \\
 (D_{22})_{eq} &\approx (D_{22})_{skin} \\
 (D_{66})_{eq} &\approx (D_{66})_{skin} + \frac{(GJ)_{stif}}{2d_s}
 \end{aligned} \tag{9.17}$$

which are analogous to Equations (9.6) in the previous section.

If the stiffeners have an open cross-section (such as *L*, *C*, *Z*, *T*, *I*, *J*, etc.) the polar moment of inertia *J* in the last of Equations (9.17) is negligibly small and the stiffener contribution (second term in that equation) can be neglected altogether. If the stiffeners have a closed cross-section (such as a hat stiffener) the second term in the last of Equations (9.17) is significant and cannot be neglected.

In addition to the approximation introduced by Equation (9.4) when the number of stiffeners is small, there is an approximation in Equations (9.17) introduced by the fact that stretching–bending coupling terms (*B* matrix contribution) were neglected. The skin–stiffener cross-section in Figure 9.2 is asymmetric and there is a contribution to the bending stiffnesses coming from the axial stiffnesses of the stiffeners and skin. These are analogous to the *B* matrix terms of an asymmetric laminate and they become more significant as the stiffeners become bigger (greater web heights for example). Only in a situation where the stiffeners are mirrored to the other side of the skin, giving a symmetric configuration with respect to the skin midplane, will these coupling terms be exactly zero and no additional correction terms needed in Equation (9.17).

9.2 Failure Modes of a Stiffened Panel

Failure modes that are specific to the individual constituents, skin and stiffeners, were examined in previous chapters. Here, a summary of all failure modes, including those pertaining to the interaction between the skin and stiffeners, is given. The most important failure modes are presented in Figure 9.4. Of these, the material strength failure modes (either for the stiffener or for the skin) are typically covered by a first-ply failure analysis (see Chapter 4) supported and modified by test results. They were also briefly invoked in the discussion on crippling (Section 8.5) and skin post-buckling (see Sections 7.1 and 7.2). Flange crippling was examined in Section 8.5. Inter-rivet buckling was discussed in Section 8.7. Panel buckling failure modes were discussed in Chapter 6 for plates and Section 8.3 for beams. Whichever buckling model occurs first, overall buckling of the panel or buckling of the skin between stiffeners is a function of the relative stiffnesses and geometry of skin and stiffeners, and conditions ensuring precedence of one buckling mode over another are discussed in this chapter. Finally, the skin–stiffener separation mode was briefly mentioned in association with post-buckling (at the start of Chapter 7) and will be examined in detail in this chapter.

As might be expected, unless explicitly designed for this, failure modes do not occur simultaneously. In certain situations, designing so that some (or all) failure modes occur at the same time gives the most efficient design in the sense that no component is over-designed. This

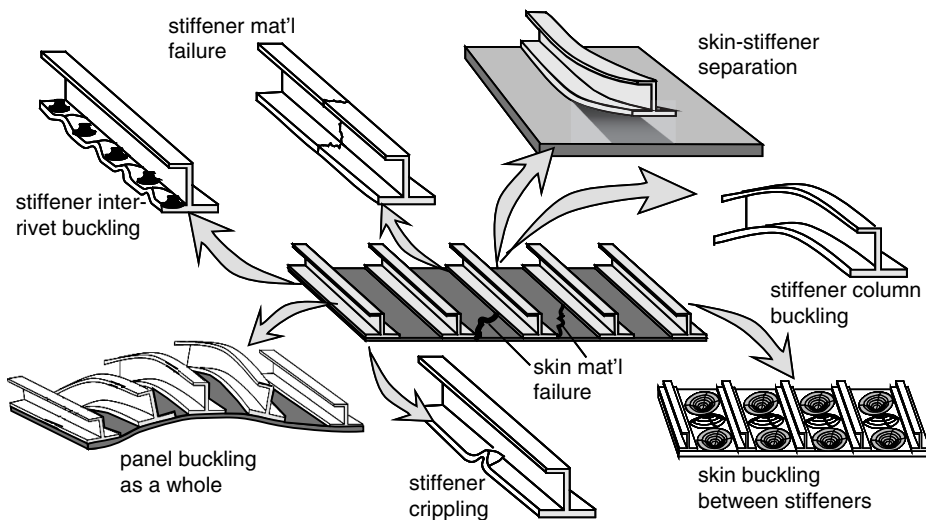


Figure 9.4 Failure modes of a stiffened panel

is not always true. It assumes that different components are used to take different types of loading and fail in different failure modes that are independent from one another. In general, formal optimization shows that the lightest designs are not always the ones where the critical failure modes occur simultaneously.

In view of this, knowing when one failure mode may switch to another is critical. In addition, sequencing failure modes so they occur in a predetermined sequence is also very useful for the creation of robust designs. For example, relatively benign failure modes such as crippling (as opposed to column buckling) and local buckling between stiffeners as (opposed to overall buckling) contribute to creating a damage tolerant design, in the sense that catastrophic failure is delayed and some load sharing with components that have not yet failed occurs. One such case of finding when one failure mode changes to another was examined in Section 8.7 where the condition for switching from crippling to inter-rivet buckling was determined.

9.2.1 Local Buckling (Between Stiffeners) Versus Overall Panel Buckling (the Panel Breaker Condition)

As mentioned in the previous section, confining the buckling mode between stiffeners is preferable. In general it leads to lighter designs and keeps the overall panel from buckling, which, typically, leads to catastrophic failure. From a qualitative point of view, as the bending stiffness of the stiffeners increases, it becomes harder for them to bend. Then under compressive loading for example, if the stiffeners are sufficiently stiff, the skin between the stiffeners will buckle first. The stiffeners remain straight and act as 'panel breakers'. For a given stiffener stiffness, this behaviour can be assured if the stiffener spacing is sufficiently wide. Then, even for relatively soft stiffeners, the skin between them will buckle first. This means that the panel breaker condition will involve both the stiffness and spacing of the stiffeners compared with the skin stiffness and its overall dimensions.

There are two main scenarios to quantify this sequence of events. In the first, a non-buckling design is all that is required (no post-buckling capability). In such a case, the stiffeners must have properties such that the buckling load of the panel as a whole equals the buckling load of the skin between stiffeners. The two failure modes, local and global buckling, occur simultaneously. In the second scenario, the skin is allowed to buckle. This means that the stiffeners must stay intact and not bend, until the skin reaches the desired post-buckling load and fails.

9.2.1.1 Global Buckling = Local Buckling (Compression Loading)

It is important to recognize that the total applied force F_{TOT} is distributed between the skin and stiffeners according to their respective in-plane EA stiffnesses. This was expressed by Equation (8.12). With reference to Figure 9.5, the membrane stiffness EA of the skin is approximated by bA_{11} . Note that a more accurate expression would be $b(A_{11} - A_{12}^2/A_{22})$, as is indicated by Equations (8.5) and (8.6), but the second term is neglected here, assuming the skin has at least 40% 0° plies aligned with the load so that $A_{12} \ll A_{11}$. If this requirement is not satisfied, the equations that follow can be modified accordingly.

Using Equation (8.12), the force acting on the skin alone can be determined as

$$F_{skin} = \frac{bA_{11}}{bA_{11} + b\frac{EA}{d_s}} F_{TOT} = \frac{A_{11}}{A_{11} + \frac{EA}{d_s}} F_{TOT} \quad (9.18)$$

Then, the force per unit length acting on the skin alone is

$$N_{xskin} = \frac{F_{skin}}{b} \quad (9.19)$$

If the skin between stiffeners is assumed to be simply supported, its buckling load can be obtained from Equation (6.7):

$$N_{xskin} = \frac{\pi^2}{a^2} \left[D_{11}k^2 + 2(D_{12} + 2D_{66})(\bar{AR})^2 + D_{22} \frac{(\bar{AR})^4}{k^2} \right] \quad (9.20)$$

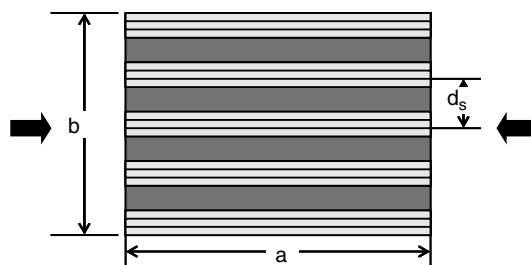


Figure 9.5 Stiffened skin under compression

where k is the number of half-waves into which the skin buckles, D_{ij} are skin bending stiffnesses and \overline{AR} is the aspect ratio a/d_s .

Combining Equations (9.18)–(9.20) and solving for the total force F_{TOT} , gives:

$$F_{TOT} = \frac{A_{11} + \frac{EA}{d_s}}{A_{11}} \frac{\pi^2 b}{a^2} \left[D_{11} k^2 + 2(D_{12} + 2D_{66}) (\overline{AR})^2 + D_{22} \frac{(\overline{AR})^4}{k^2} \right] \quad (9.21)$$

where A_{11} is the skin membrane stiffness and EA is the stiffener membrane stiffness.

Assuming now that the panel as a whole is simply supported all around its boundary, its buckling load will also be given by Equation (6.7),

$$N_{panel} = \frac{\pi^2}{a^2} \left[(D_{11})_p m^2 + 2((D_{12})_p + 2(D_{66})_p) (AR)^2 + (D_{22})_p \frac{(AR)^4}{m^2} \right] \quad (9.22)$$

where m is the number of half-waves into which the entire panel would buckle (note that m for the overall panel and k for the skin between the stiffeners can be different) and the subscript p denotes the entire panel. The aspect ratio AR of the panel is a/b . The bending stiffnesses $(D_{ij})_p$ for the panel are given by Equation (9.17).

The force per unit length N_{panel} is given by

$$N_{panel} = \frac{F_{TOT}}{b} \quad (9.23)$$

Combining Equations (9.22) and (9.23) and solving for F_{TOT} gives:

$$F_{TOT} = \frac{b\pi^2}{a^2} \left[(D_{11})_p m^2 + 2((D_{12})_p + 2(D_{66})_p) (AR)^2 + (D_{22})_p \frac{(AR)^4}{m^2} \right] \quad (9.24)$$

Equations (9.21) and (9.24) imply that the total load at which the skin between stiffeners buckles and the panel as a whole buckles is the same. Therefore, equating the right-hand sides of Equations (9.21) and (9.24) gives:

$$\begin{aligned} & \frac{A_{11} + \frac{EA}{d_s}}{A_{11}} \frac{\pi^2 b}{a^2} \left[D_{11} k^2 + 2(D_{12} + 2D_{66}) (\overline{AR})^2 + D_{22} \frac{(\overline{AR})^4}{k^2} \right] \\ &= \frac{b\pi^2}{a^2} \left[(D_{11})_p m^2 + 2((D_{12})_p + 2(D_{66})_p) (AR)^2 + (D_{22})_p \frac{(AR)^4}{m^2} \right] \end{aligned} \quad (9.25)$$

Equation (9.25) can be simplified by canceling out common factors and using Equation (9.17) to express the panel bending stiffnesses EI . Here, it will be assumed that the stiffener has an open cross-section so its GJ is very small and does not contribute to the panel D_{66} value. Then, Equation (9.25) reads,

$$\begin{aligned}
& \frac{A_{11} + \frac{EA}{d_s}}{A_{11}} \left[D_{11}k^2 + 2(D_{12} + 2D_{66})(\overline{AR})^2 + D_{22} \frac{(\overline{AR})^4}{k^2} \right] \\
&= \left[\left(D_{11} + \frac{EI}{d_s} \right) m^2 + 2(D_{12} + 2D_{66})(AR)^2 + D_{22} \frac{(AR)^4}{m^2} \right]
\end{aligned} \tag{9.26}$$

Note that, in Equation (9.26), EA and EI both refer to stiffener quantities.

Further simplification is possible if the values of k and m are approximated. As mentioned in Section 6.2, k and m are the integer values of half-waves that minimize the corresponding buckling loads (skin between stiffeners or entire panel). If k and m were continuous variables (instead of only taking integer values) differentiating the corresponding buckling expressions and setting the result equal to zero would give the values to use (see the derivation of Equation 8.45 in the previous chapter). Since they are integers, the rational expression resulting from differentiation would have to be rounded up or down to the nearest adjacent integer that minimizes the buckling load.

Differentiating the right-hand side of Equation (9.20) with respect to k and setting the result equal to zero gives:

$$\frac{dN_{xskin}}{dk} = 0 \Rightarrow k^* = \left(\frac{D_{22}}{D_{11}} \right)^{1/4} \left(\frac{a}{d_s} \right) \tag{9.27}$$

where k^* denotes the continuous variable ($k = k^*$ when the right-hand side of Equation (9.27) is an integer).

Using Equation (9.27), the value of k is given by either,

$$k = \text{int}[k^*]$$

or

$$k = \text{int}[k^*] + 1$$

whichever of the two minimizes the right-hand side of Equation (9.20). The symbol $\text{int}[x]$ denotes the integer obtained if x is rounded down to the next integer.

Similarly for m ,

$$m^* = \left(\frac{D_{22}}{D_{11} + \frac{EI}{d_s}} \right)^{1/4} \left(\frac{a}{b} \right) \tag{9.28}$$

By necessity, if either of k^* or m^* is less than 1, the corresponding value of k or m will be set equal to 1.

Now for typical applications of panels under compression, the quantity $D_{11} + EI/d_s$ is greater than D_{22} because of the contribution of the stiffeners EI/d_s and the tendency to align fibers with the load direction which would give $D_{11} \geq D_{22}$. So unless, $a/b \gg 1$ the quantity in the right-hand side of Equation (9.28) is less than 1 and m will be equal to 1.

To proceed, set $k = k^*$ as obtained from Equation (9.27). Then, substituting for k and m in Equation (9.26)

$$D_{11} + \frac{(EI)_{stif}}{d_s} + 2[D_{12} + 2D_{66}](AR)^2 + D_{22}(AR)^4 \\ = \underbrace{\frac{A_{11} + \frac{EA}{d_s}}{A_{11}}}_{\lambda} \left[D_{11} \sqrt{\frac{D_{22}}{D_{11}} \overline{AR}^2 + 2[D_{12} + 2D_{66}] (\overline{AR})^2 + D_{22} \frac{(\overline{AR})^4}{\sqrt{\frac{D_{22}}{D_{11}} \overline{AR}^2}}} \right] \quad (9.29)$$

Denoting by λ the term multiplying the quantity in brackets on the right-hand side, solving for the stiffener EI , and dropping the subscript ‘stiff’, for convenience, gives the final expression:

$$EI = D_{11}d_s \left[\sqrt{\frac{D_{22}}{D_{11}} \left(2\lambda \overline{AR}^2 - \sqrt{\frac{D_{22}}{D_{11}} (AR)^4} \right)} + \frac{2(D_{12} + 2D_{66})}{D_{11}} \left(\lambda \overline{AR}^2 - (AR)^2 \right) - 1 \right] \quad (9.30)$$

Equation (9.30) gives the minimum bending stiffness EI that the stiffeners must have in order for buckling of the skin between stiffeners to occur at the same time as overall buckling of the stiffened panel. If EI is greater than the right-hand side of Equation (9.30), the skin between stiffeners buckles first.

9.2.1.2 Stiffener Buckling = PB × Buckling of Skin Between Stiffeners (Compression Loading)

This scenario covers the case where skin is allowed to post-buckle. It is assumed that the skin is loaded over the b_{eff} portion, which was determined in Section 7.1. The stiffener must stay straight all the way up to the load that fails the skin. That load is given by the buckling load of the skin between stiffeners multiplied by the post-buckling ratio PB.

In general, when the skin has buckled the compressive load on it is not constant (see Figure 7.8 for example) and the skin strains are not constant across its width. If the skin is replaced by the b_{eff} portion shown in Figure 9.6, then, the skin load is constant over b_{eff} and the strain, given by inverting Equation (8.4) is also constant. Thus, strain compatibility can be applied.

Considering a $2b_{eff}$ portion of skin and its corresponding stiffener as shown in Figure 9.6, and using Equation (8.12), the individual forces on skin and stiffener can be found to be:

$$F_{skin} = \frac{A_{11} \frac{b}{d_s} 2b_{eff}}{2A_{11} \frac{b}{d_s} b_{eff} + EA \frac{b}{d_s}} F_{TOT} \Rightarrow F_{skin} = \frac{2A_{11}b_{eff}}{2A_{11}b_{eff} + EA} F_{TOT} \quad (9.31)$$

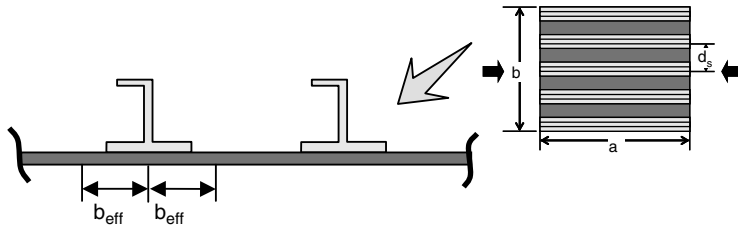


Figure 9.6 Effective skin in the vicinity of a stiffener in a post-buckled stiffened panel

$$F_{stiffeners} = \frac{EA}{2A_{11}b_{eff} + EA} F_{TOT} \quad (9.32)$$

where EA is the membrane stiffness of each stiffener (=membrane modulus \times cross-sectional area)

For a single stiffener, dividing the right-hand side of Equation (9.32) by the number of stiffeners given by Equation (9.4) gives,

$$F_{stif} = \frac{d_s}{b} \frac{EA}{2A_{11}b_{eff} + EA} F_{TOT} \quad (9.33)$$

Now, the column buckling load of a stiffener is, for simply supported ends, given by Equation (8.21), repeated here for convenience:

$$F_{stiffb} = \frac{\pi^2 EI}{a^2} \quad (9.34)$$

Equating the right-hand sides of Equations (9.33) and (9.34) relates the load in each stiffener to the buckling load of that stiffener, and can be solved for the total force on the panel F_{TOT} :

$$\frac{d_s}{b} \frac{EA}{2A_{11}b_{eff} + EA} F_{TOT} = \frac{\pi^2 EI}{a^2} \Rightarrow F_{TOT} = \frac{\pi^2 EI}{a^2} \frac{b}{d_s} \frac{2A_{11}b_{eff} + EA}{EA} \quad (9.35)$$

Now it is postulated that final failure occurs when the required post-buckling ratio PB is reached. At that point, the force in the skin F_{skin} must equal the buckling load of the skin between the stiffeners multiplied by PB :

$$F_{skin} = F_{skin\ buckling}(PB) \quad (9.36)$$

The skin buckling load $F_{skin\ buckling}$ is given by Equation (9.20) multiplied by the panel width b to convert the force per unit width N_{xskin} into force:

$$F_{skin\ buckling} = b \frac{\pi^2}{a^2} \left[(D_{11})k^2 + 2[(D_{12}) + 2(D_{66})](\overline{AR})^2 + (D_{22}) \frac{(\overline{AR})^4}{k^2} \right] \quad (9.37)$$

with all terms as defined before.

Combining Equation (9.31) with (9.36) and (9.37) relates the total force to the skin buckling load:

$$F_{TOT} = \frac{2A_{11}b_{eff} + EA}{2A_{11}b_{eff}} b \frac{\pi^2}{a^2} \left[(D_{11})k^2 + 2[(D_{12}) + 2(D_{66})](\overline{AR})^2 + (D_{22}) \frac{(\overline{AR})^4}{k^2} \right] (PB) \quad (9.38)$$

Equations (9.35) and (9.38) can now be combined to yield the condition for column buckling of the stiffeners occurring when the final PB is reached:

$$\frac{EI}{d_s EA} = \frac{(PB)}{2A_{11}b_{eff}} \left[D_{11}k^2 + 2[D_{12} + 2D_{66}](\overline{AR})^2 + D_{22} \frac{(\overline{AR})^4}{k^2} \right] \quad (9.39)$$

which relates stiffener properties on the left-hand side with skin properties on the right-hand side.

Equation (9.39) can be further manipulated using the definition of the parameter λ that was introduced when Equation (9.29) was derived. Using that definition, it can be shown that,

$$\lambda = \frac{A_{11} + \frac{EA}{d_s}}{A_{11}} \Rightarrow \lambda A_{11} - A_{11} = \frac{EA}{d_s} \Rightarrow A_{11}(\lambda - 1) = \frac{EA}{d_s} \Rightarrow \frac{EA}{d_s} = (\lambda - 1)d_s \quad (9.40)$$

Introducing this result in Equation (9.39) and solving for the stiffener bending stiffness EI results in the expression:

$$EI = (\lambda - 1)(PB)d_s \frac{d_s}{2b_{eff}} \left[D_{11}k^2 + 2[D_{12} + 2D_{66}](\overline{AR})^2 + D_{22} \frac{(\overline{AR})^4}{k^2} \right] \quad (9.41)$$

Also note that using the expression for b_{eff} , Equation (7.15) derived earlier (assuming the boundary conditions for the skin between stiffeners reasonably approximate those used in Section 7.1) the following can be shown:

$$\frac{d_s}{b_{eff}} = 2 \left[1 + 2 \left(1 + \frac{A_{12}}{A_{11}} \right) \left(1 - \frac{1}{(PB)} \right) \frac{A_{11}}{A_{11} + 3A_{22}} \right] \quad (9.42)$$

which can be substituted in Equation (9.41).

Equation (9.41) determines the minimum bending stiffness of the stiffeners so that they do not buckle until the final failure load in the post-buckling regime is reached. This would guarantee that the stiffeners will stay straight, and thus act as panel breakers, all the way to the failure load of the panel. It should be noted that EI in Equation (9.42) is related to the stiffener EA through the parameter λ so the two are not entirely independent and some iterations may be needed between stiffener geometry and layup to arrive at the required bending stiffness.

9.2.1.3 Example

As an application of the two conditions (9.30) and (9.41) consider a skin panel with dimensions $a = 508$ mm and $b = 762$ mm loaded in compression parallel to dimension a as shown in Figure 9.7. The skin layup is $[(\pm 45)/(0/90)/(\pm 45)]$ with stiffness properties given in Figure 9.7. The stiffener spacing, geometry, and layup are unknown. The minimum EI for the stiffeners must be determined subject to conditions (9.30) and (9.41).

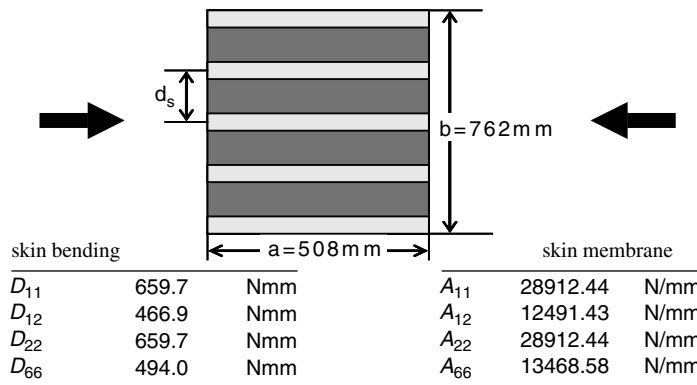


Figure 9.7 Example of stiffened panel under compression

The procedure is as follows: First a value of the parameter λ is selected. Then, for that value, the stiffener spacing d_s is varied between 75 and 300 mm. For each value of d_s the aspect ratio (\overline{AR}) is calculated and the corresponding buckling load of the skin between the stiffeners is determined using Equation (9.20). Finally, the minimum EI required is determined using Equations (9.30) and (9.41). When using Equation (9.41) a PB ratio of 5 is assumed. The results are shown in Figure 9.8 for two different λ values.

It can be seen from Figure 9.8 that the minimum bending stiffness for the stiffener decreases as the stiffener spacing increases. This is due to the fact that, as the stiffener spacing increases, the buckling load of the skin between the stiffeners decreases. This implies that the total load at which the skin buckles is lower and the corresponding load applied to the stiffeners is lower. So the stiffener requirement must be satisfied for a lower load and thus lower bending stiffness is needed.

It is also evident from Figure 9.8 that as λ decreases the required bending stiffness for the stiffener decreases. This is because, for a given skin (and thus A_{11} value) the only way to decrease λ is by decreasing the stiffener EA (see Equation (9.40)). But if the stiffener EA decreases, less load is absorbed by the stiffeners (see Equation (9.32)) and more by the skin.

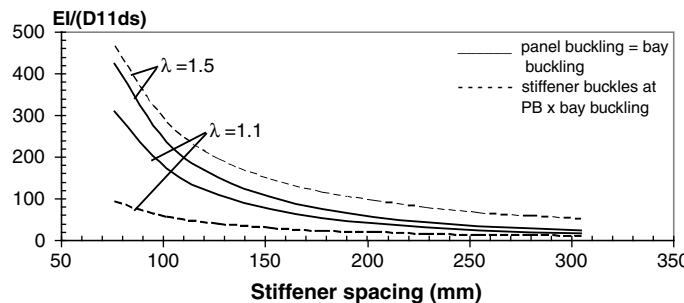


Figure 9.8 Normalized minimum bending stiffness required for stiffeners of a stiffened panel under compression (PB = 5)

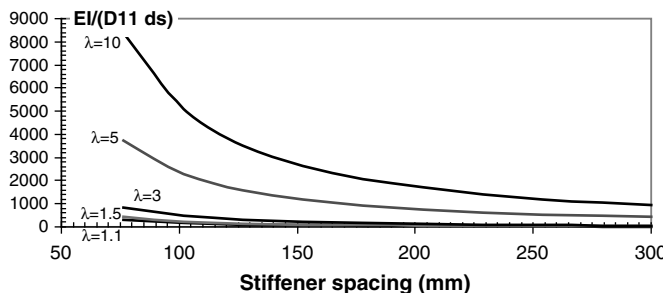


Figure 9.9 Normalized minimum bending stiffness of stiffeners for various λ values ($PB = 5$)

Again, since the load carried by each stiffener is lower, the required bending stiffness will also be lower.

The last observation related to the trends of Figure 9.8 is that a value of λ is reached beyond which the condition that the stiffeners buckle at $PB \times$ bay buckling dominates. This is demonstrated by the fact that the continuous curve is above the dashed curve for $\lambda = 1.1$, but below the dashed curve for $\lambda = 1.5$. This means that, for a given stiffener spacing, there is a λ value between 1.1 and 1.5 at which the design driver switches from Equation (9.30) to Equation (9.41). This means that one should check both conditions, (9.30) and (9.41), and use the one that gives the more conservative results. Unless, of course, no post-buckling is allowed in the design, in which case, only condition (9.30) should be used.

Selecting the more critical of the two conditions, for each value of λ , results in the curves of Figure 9.9. The lowest 3 curves ($\lambda = 1.1, 1.5, 3.0$) correspond to Equation (9.30) dominating the design and the highest 2 curves ($\lambda = 5.0, 10.$) correspond to Equation (9.40) dominating the design.

9.2.2 Skin–Stiffener Separation

As load is transferred between skin and stiffeners, out-of-plane loads develop at their interface or at the flange edges. These loads develop, even when the applied loads are in the plane of the skin and they can lead to separation of the stiffener from the skins. There are two main mechanisms for the development of these out-of-plane stresses. The first is associated with the presence of any stress-free edges such as the flange edges [2–7]. Load present in one component such as the flange has to transfer to the other as the free edge is approached. The local stiffness mismatch caused by the presence of the free edge (and the differences in stacking sequence between flange and skin) creates out-of-plane stresses which are the main culprit for separation of the flange from the skin. This is shown in Figure 9.10.

Away from the flange edge, closer to the location where the stiffener web meets the flange, a two-dimensional state of stress develops that can be determined with the use of classical-laminated plate theory once the local loads are known. A section including the flange edge and the skin below can be cut off and placed in equilibrium (bottom left part of Figure 9.10). If then, the flange alone is sectioned off (bottom right of Figure 9.10), it is not in equilibrium unless out-of-plane shear and normal stresses develop at the interface between the flange and skin.

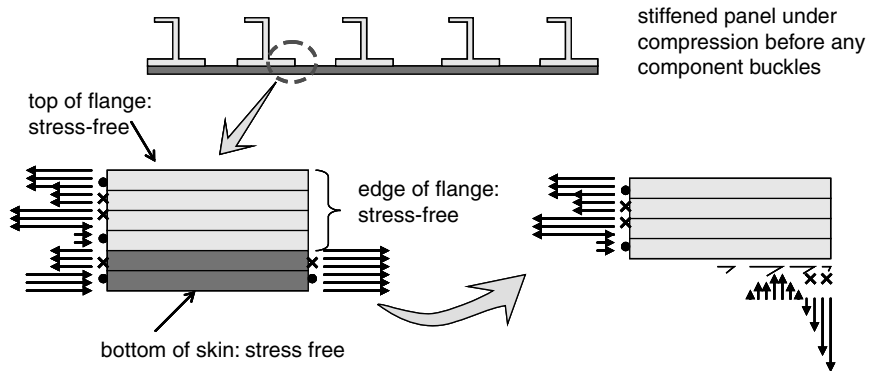


Figure 9.10 Development of out-of-plane stresses at the interface between flange and skin prior to buckling

This is the only location where this can happen since the top of the flange and the right edge of the flange are, by definition, stress-free. Zooming to the sectioned detail at the bottom right of Figure 9.10 gives the situation shown in Figure 9.11.

For the purposes of discussion, the skin and stiffener in Figures 9.10 and 9.11 are assumed to be under compression. A local coordinate system is established in Figure 9.11 to facilitate the discussion. As shown in Figure 9.11, to maintain force equilibrium in the y direction, an interlaminar shear stress τ_{yz} must develop at the flange–skin interface (bottom of flange in Figure 9.11). Also, the presence of in-plane shear stresses at the left end of the flange, as predicted by classical laminated-plate theory leads to a net force in the x direction. In order to balance that force, an interlaminar shear stress τ_{xz} must also develop at the flange–skin interface. Finally, to balance the moments (about the bottom right corner of the flange say), an out-of-plane normal stress σ_z must develop at the flange–skin interface. However, since there is no net force in the z direction in Figure 9.11, the σ_z stress must be self-equilibrating. Thus, it will be tensile over a portion of the region over which it acts and compressive over the remaining portion. This is why σ_z is shown as both tensile and compressive in Figure 9.11.

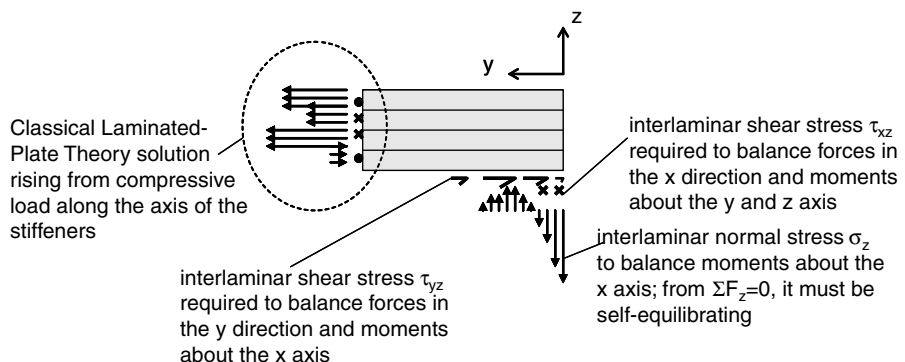


Figure 9.11 Free-body diagram of the flange

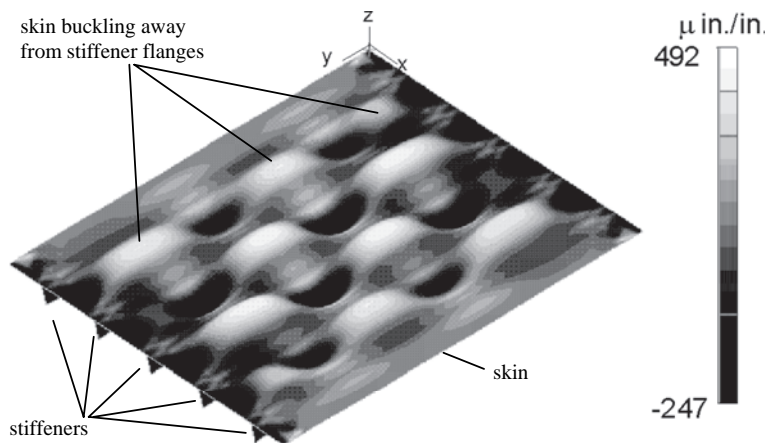


Figure 9.12 Post-buckled shape of blade-stiffened panel under compression

The second mechanism that gives rise to these separation stresses is associated with the skin deformation after buckling in a post-buckling situation. This is shown in Figure 9.12 based on an example from reference [8].

The stiffened panel of Figure 9.12 is shown with the stiffeners at the bottom so the skin deformations are more easily seen without stiffeners blocking the view. As shown in Figure 9.12 a portion of the buckling pattern has the skin moving away from the stiffeners. This would give rise to ‘peeling’ stresses at the skin–stiffener interface and could lead to skin–stiffener separation. The resulting failure for this situation is shown in Figure 9.13.

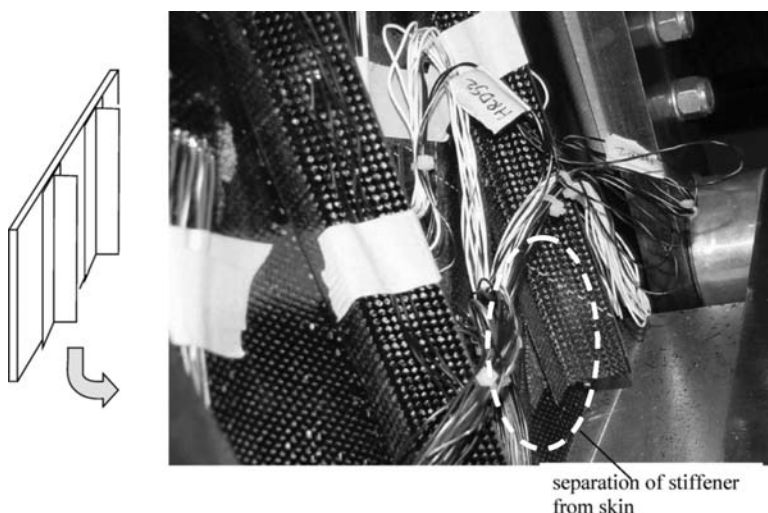


Figure 9.13 Skin–stiffener separation failure mode (See Plate 22 for the colour figure)

The separated stiffener is highlighted with a red ellipse. It is important to bear in mind that, for this mechanism to occur, bucking of the skin (under compression, shear, or combined loads) is a prerequisite [9].

Many different solutions to the problem of determining the stresses between the skin and stiffener given a loading situation have been proposed [2–12]. The highest accuracy is obtained with detailed finite element methods [8–12] at a relatively high computational cost. The required mesh refinement in the region (or interface) of interest makes it difficult to use this approach in a design environment where many configurations must be rapidly compared with each other for the best candidates to emerge. Simpler methods [2–6] can be used for screening candidate designs and performing a first evaluation. Once the best candidates are selected, more detailed analysis methods using finite elements can be used for more accurate predictions.

In general, solutions that calculate the stresses at the skin–stiffener interface assume a perfect bond between stiffener flange and the skin and require the use of some out-of-plane failure criterion [13, 14] to determine when delamination starts. This can be quite conservative as a delamination starting at the skin–stiffener interface rarely grows in an unstable fashion to cause final failure. To model the presence of a delamination and to determine when it will grow, methods based on energy release rate calculations [10–12] are very useful. In what follows, only the problem of determining the out-of-plane stresses in a pristine structure will be presented.

The approach is adapted from [3, 4] and can be applied to any situation for which the loads away from the flange edge are known, irrespective of whether the structure is post-buckled or not. The situation is shown in Figure 9.14. The flange end is isolated from the rest of the stiffener and a portion of the skin below it is shown.

Two coordinate systems are used in Figure 9.14, one for the flange and one for the skin. They have a common origin at the end of the flange where it interfaces with the skin. The z axis (out-of-plane) for the flange is going up and it is going down for the skin. The y axis is moving away from the flange edge towards the stiffener web and the x axis is aligned with the axis of the stiffener. The stresses away from the origin of the coordinate systems, at the far left and right end in Figure 9.14, are assumed known. They would be the result of classical laminated-plate theory and/or other two-dimensional solutions. For the solution discussed here, these far-field stresses are assumed to be only in-plane stresses. This means that the three-dimensional stresses that arise in the vicinity of the flange termination die out in the far-field so the known solution at the left and right end of Figure 9.14 can be recovered.

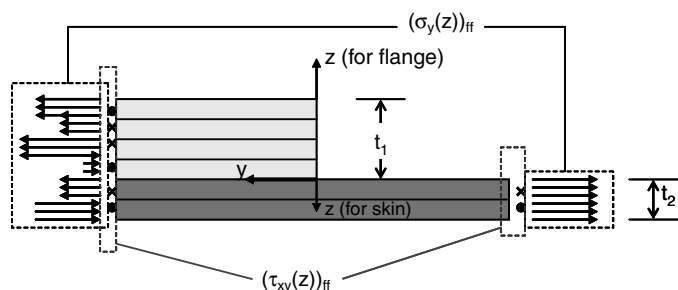


Figure 9.14 Geometry and coordinate systems for the skin–stiffener separation problem

Note that out-of-plane stresses at the far field can, if present, be added following the same procedure as the one outlined below.

It is assumed that the structure shown in Figure 9.14 is long in the x direction (perpendicular to the plane of the figure) so no quantity depends on the x coordinate, i.e.,

$$\frac{\partial(\dots)}{\partial x} = 0$$

With this assumption, the equilibrium equations (5.2) become

$$\begin{aligned}\frac{\partial \tau_{xy}}{\partial y} + \frac{\partial \tau_{xz}}{\partial z} &= 0 \\ \frac{\partial \sigma_y}{\partial y} + \frac{\partial \tau_{yz}}{\partial z} &= 0 \\ \frac{\partial \tau_{yz}}{\partial y} + \frac{\partial \sigma_z}{\partial z} &= 0\end{aligned}\tag{9.43a-c}$$

This means that the first equilibrium equation, (9.43a), uncouples from the other two. This, in turn, suggests that if one of the stresses τ_{xy} or τ_{xz} were somehow known, Equation (9.43a) could be used to determine the other. Similarly, if one of the stresses σ_y , τ_{yz} , or σ_z were known, the other two could be determined from Equations (9.43b) and (9.43c).

Pursuing this line of thought, a fairly general assumption is made for τ_{xy} and σ_y in the form:

$$\sigma_y = (\sigma_y(z))_{ff} + f(y)F(z)\tag{9.44}$$

$$\tau_{xy} = (\tau_{xy}(z))_{ff} + g(y)G(z)\tag{9.45}$$

where $f(y)$, $g(y)$, $F(z)$ and $G(z)$ are unknown functions of the respective coordinates and $(\sigma_y(z))_{ff}$ and $(\tau_{xy}(z))_{ff}$ are the known far-field stresses away from the flange edge (i.e. at large positive or negative y values).

The solution remains quite general if $F(z)$ and $G(z)$ are assumed to be Fourier sine and cosine series. Concentrating on the flange, Equations (9.44) and (9.45) can be written as:

$$\sigma_y = (\sigma_y(z))_{ff} + f(y) \left[\sum_{m=1}^{\infty} A_m \sin \frac{m\pi z}{t_1} + \sum_{n=1}^{\infty} B_n \cos \frac{n\pi z}{t_1} \right]\tag{9.44a}$$

$$\tau_{xy} = (\tau_{xy}(z))_{ff} + g(y) \left[\sum_{p=1}^{\infty} C_{1p} \sin \frac{p\pi z}{t_1} + \sum_{q=1}^{\infty} C_{2q} \cos \frac{q\pi z}{t_1} \right]\tag{9.45a}$$

Here a simplification is introduced by truncating the infinite series in Equations (9.44a) and (9.44b) after the first term. This will give good solutions in terms of trends and will simplify the algebra considerably. Additional terms may be included for more accurate solutions. Then the two stresses in the flange have the form:

$$\sigma_y = (\sigma_y(z))_{ff} + f(y) \left[A_1 \sin \frac{\pi z}{t_1} + B_1 \cos \frac{\pi z}{t_1} \right] \quad (9.44b)$$

$$\tau_{xy} = (\tau_{xy}(z))_{ff} + g(y) \left[C_1 \sin \frac{\pi z}{t_1} + C_2 \cos \frac{\pi z}{t_1} \right] \quad (9.45b)$$

where, for simplicity, we set $C_1 = C_{11}$ and $C_2 = C_{21}$. The coefficients A_1 , B_1 , C_1 , and C_2 and the functions $f(y)$ and $g(y)$ are unknown at this point.

Now use Equation (9.44b) to substitute in (9.43b) to obtain

$$\frac{\partial \tau_{yz}}{\partial z} = -f' \left(A_1 \sin \frac{\pi z}{t_1} + B_1 \cos \frac{\pi z}{t_1} \right) \quad (9.46)$$

where $f' = df/dy$.

Integrating (9.46) with respect to z gives,

$$\tau_{yz} = -f' \left(-A_1 \frac{t_1}{\pi} \cos \frac{\pi z}{t_1} + B_1 \frac{t_1}{\pi} \sin \frac{\pi z}{t_1} \right) + P_1(y) \quad (9.47)$$

where $P_1(y)$ is an unknown function of y .

Now the top of the flange is stress free, which means that $\tau_{yz}(z=t_1)=0$ or,

$$-f' \left(A_1 \frac{t_1}{\pi} \right) + P_1(y) = 0 \Rightarrow P_1(y) = f' \left(A_1 \frac{t_1}{\pi} \right) \quad (9.48)$$

and $P_1(y)$ is determined. This would give the following expression for τ_{yz} :

$$\tau_{yz} = f' \left(A_1 \frac{t_1}{\pi} \left(1 + \cos \frac{\pi z}{t_1} \right) - B_1 \frac{t_1}{\pi} \sin \frac{\pi z}{t_1} \right) \quad (9.49)$$

In a similar fashion, Equation (9.49) can be used to substitute for τ_{yz} in (9.43c) to obtain:

$$\frac{\partial \sigma_z}{\partial z} = -f'' \left(A_1 \frac{t_1}{\pi} \left(1 + \cos \frac{\pi z}{t_1} \right) - B_1 \frac{t_1}{\pi} \sin \frac{\pi z}{t_1} \right) \quad (9.50)$$

which can be integrated with respect to z to give:

$$\sigma_z = -f'' \left(A_1 \frac{t_1}{\pi} \left(z + \frac{t_1}{\pi} \sin \frac{\pi z}{t_1} \right) + B_1 \left(\frac{t_1}{\pi} \right)^2 \cos \frac{\pi z}{t_1} \right) + P_2(y) \quad (9.51)$$

where $f'' = d^2f/dy^2$ and $P_2(y)$ is an unknown function.

Again, the requirement that the top of the flange be stress free leads to $\sigma_z(z=t_1)=0$ or,

$$-f'' \left(A_1 \frac{t_1}{\pi} (t_1) + B_1 \left(\frac{t_1}{\pi} \right)^2 \cos \pi \right) + P_2(y) = 0 \Rightarrow P_2(y) = f'' \left(A_1 \frac{t_1^2}{\pi} - B_1 \left(\frac{t_1}{\pi} \right)^2 \right) \quad (9.52)$$

With $P_2(y)$ known, the final expression for σ_z can be obtained:

$$\sigma_z = f'' \left(A_1 \frac{t_1}{\pi} \left(t_1 - z - \frac{t_1}{\pi} \sin \frac{\pi z}{t_1} \right) - B_1 \left(\frac{t_1}{\pi} \right)^2 \left(1 + \cos \frac{\pi z}{t_1} \right) \right) \quad (9.53)$$

In a completely analogous fashion, placing Equation (9.45b) into (9.43a) and solving for τ_{xz} gives

$$\tau_{xz} = g' \left[C_1 \frac{t_1}{\pi} \left(1 + \cos \frac{\pi z}{t_1} \right) - C_2 \frac{t_1}{\pi} \sin \frac{\pi z}{t_1} \right] \quad (9.54)$$

Equations (9.44b), (9.45b), (9.49), (9.51), and (9.54) determine the stresses σ_y , τ_{xy} , τ_{yz} , σ_z , and τ_{xz} to within some unknown constants and the two unknown functions f and g and their derivatives. At this point the stress σ_x is unknown. It does not appear in the equilibrium equations (9.43a–c) and other means must be invoked for its determination.

By inverting the stress–strain equations (5.4), the following relations are obtained:

$$\begin{Bmatrix} \varepsilon_x \\ \varepsilon_y \\ \varepsilon_z \\ \gamma_{yz} \\ \gamma_{xz} \\ \gamma_{xy} \end{Bmatrix} = \begin{bmatrix} S_{11} & S_{12} & S_{13} & 0 & 0 & S_{16} \\ S_{12} & S_{22} & S_{23} & 0 & 0 & S_{26} \\ S_{13} & S_{23} & S_{33} & 0 & 0 & S_{36} \\ 0 & 0 & 0 & S_{44} & S_{45} & 0 \\ 0 & 0 & 0 & S_{45} & S_{55} & 0 \\ S_{16} & S_{26} & S_{36} & 0 & 0 & S_{66} \end{bmatrix} \begin{Bmatrix} \sigma_x \\ \sigma_y \\ \sigma_z \\ \tau_{yz} \\ \tau_{xz} \\ \tau_{xy} \end{Bmatrix} \quad (9.55)$$

where S_{ij} ($i, j = 1–6$) are compliances for the flange as a whole. They can be computed as thickness-averaged sums of the corresponding compliances for the individual plies, and the compliances of the individual plies are obtained using standard tensor transformation equations (Equations 3.8–3.10).

In addition, the strain compatibility relations (5.10) and (5.12) can be rewritten as:

$$\frac{\partial^2 \gamma_{xy}}{\partial x \partial y} = \frac{\partial^2 \varepsilon_x}{\partial y^2} + \frac{\partial^2 \varepsilon_y}{\partial x^2} \quad (9.56)$$

$$\frac{\partial^2 \gamma_{xz}}{\partial x \partial z} = \frac{\partial^2 \varepsilon_x}{\partial z^2} + \frac{\partial^2 \varepsilon_z}{\partial x^2} \quad (9.57)$$

As was mentioned earlier, there is no dependence on the x coordinate so all derivatives with respect to x are zero and Equations (9.56) and (9.57) simplify to:

$$0 = \frac{\partial^2 \varepsilon_x}{\partial y^2} \quad (9.58)$$

$$0 = \frac{\partial^2 \varepsilon_x}{\partial z^2} \quad (9.59)$$

The first of Equations (9.55) can be combined with Equations (9.58) and (9.59) to give:

$$\frac{\partial^2}{\partial y^2} [S_{11}\sigma_x + S_{12}\sigma_y + S_{13}\sigma_z + S_{16}\tau_{xy}] = 0 \quad (9.60)$$

$$\frac{\partial^2}{\partial z^2} [S_{11}\sigma_x + S_{12}\sigma_y + S_{13}\sigma_z + S_{16}\tau_{xy}] = 0 \quad (9.61)$$

The quantity in brackets is the same for both Equations (9.60) and (9.61). The only way these two equations can be compatible with each other is if the quantity in brackets has the following form:

$$S_{11}\sigma_x + S_{12}\sigma_y + S_{13}\sigma_z + S_{16}\tau_{xy} = yG_1(z) + G_2(z) \quad (9.62)$$

with $G_1(z)$ and $G_2(z)$ unknown functions of z .

Using Equation (9.62) to substitute in (9.61) gives:

$$y \frac{d^2G_1(z)}{dz^2} + \frac{d^2G_2(z)}{dz^2} = 0$$

from which

$$G_1(z) = k_o + k_1 z$$

$$G_2(z) = k_3 + k_4 z$$

with k_o , k_1 , k_3 , and k_4 unknown constants.

Using this result and Equation (9.62) to solve for σ_x gives

$$\sigma_x = K_o + K_1 y + K_2 z + K_3 y z - \frac{S_{12}}{S_{11}} \sigma_y - \frac{S_{13}}{S_{11}} \sigma_z - \frac{S_{16}}{S_{11}} \tau_{xy} \quad (9.63)$$

with K_o , K_1 , K_2 , and K_3 new unknown constants (combinations of $k_o - k_4$).

Equation (9.63) determines σ_x as a function of the other stresses σ_y , σ_z , and τ_{xy} which were determined earlier. The unknown coefficients $K_o - K_3$ are determined from matching the far-field solution. That is, Equation (9.63) is evaluated for large values of y and compared with the known solution there.

At this point, all stresses in the flange have been determined to within some unknown coefficients and two unknown functions $f(y)$ and $g(y)$. The stresses in the skin for $y > 0$ are determined in a completely analogous fashion. One additional set of conditions is imposed here, namely, stress continuity at the flange–skin interface. By using an overbar to denote skin quantities, these conditions have the form:

$$\begin{aligned} \tau_{xz}(z = 0) &= -\overline{\tau_{xz}}(z = 0) \\ \tau_{yz}(z = 0) &= -\overline{\tau_{yz}}(z = 0) \\ \sigma_z(z = 0) &= \overline{\sigma_z}(z = 0) \end{aligned} \quad (9.64)$$

Note that a minus sign is needed in front of the shear stresses on the right-hand side to account for the orientation of the coordinate systems in Figure 9.14. As a result of Equations (9.64), the unknown functions $f(y)$ and $g(y)$ have to be the same for both flange and skin. In addition, the coefficients A_1 , B_1 , etc. for the skin, corresponding to the coefficients present in Equations (9.44b), (9.45b), (9.49), (9.51) and (9.54) for the flange, are also determined from Equations (9.64).

In order to determine the unknown functions $f(y)$ and $g(y)$, the principle of minimum complementary energy (see Section 5.4) is invoked. This means that the quantity,

$$\Pi_C = \frac{1}{2} \int \int \int \underline{\sigma}^T \underline{S} \underline{\sigma} dy dx dz + \frac{1}{2} \int \int \int \bar{\underline{\sigma}}^T \bar{\underline{S}} \bar{\underline{\sigma}} dy dx dz - \int \int \underline{T}^T \underline{u}^* dy dz \quad (9.65)$$

must be minimized. Underscores denote vectors and matrices. Overbars, as already mentioned denote skin quantities. Specifically,

$$\underline{\sigma}^T = [\sigma_x \quad \sigma_y \quad \sigma_z \quad \tau_{yz} \quad \tau_{xz} \quad \tau_{xy}]$$

and \underline{S} was given in Equation (9.55) above.

The last term of Equation (9.65) is the work term. It consists of the tractions \underline{T} multiplying the prescribed displacements \underline{u}^* .

The stress expressions already determined are used to substitute in Equation (9.65). The x and z integrations can be carried out without difficulty because they only involve either powers or sines and cosines of the variables. Thus, after x and z integration, an expression for the energy is obtained in the form:

$$\Pi_C = \frac{1}{2} \int H \left(\frac{d^2 f}{dy^2}, \frac{df}{dy}, f, \frac{dg}{dy}, g, y \right) dy \quad (9.66)$$

The problem has thus been recast as one in which the functions $f(y)$ and $g(y)$ must be determined such that the integral in the right-hand side of Equation (9.66) is minimized. This can be done by using the calculus of variations [15]. The general form of the Euler equations for f and g is as follows:

$$\frac{d^2}{dy^2} \left(\frac{\partial H}{\partial f''} \right) - \frac{d}{dy} \left(\frac{\partial H}{\partial f'} \right) + \frac{\partial H}{\partial f} = 0 \quad (9.67)$$

$$\frac{\partial H}{\partial g} - \frac{d}{dy} \left[\frac{\partial H}{\partial g'} \right] = 0 \quad (9.68)$$

Using the detailed expression of H to substitute in Equations (9.67) and (9.68) yields the two equations:

$$\frac{d^4 f}{dy^4} + R_1 \frac{d^2 f}{dy^2} + R_2 f + R_3 \frac{d^2 g}{dy^2} + R_4 g = 0 \quad (9.67a)$$

$$\frac{d^2 g}{dy^2} + R_5 g + R_6 \frac{d^2 f}{dy^2} + R_7 f = 0 \quad (9.68b)$$

where R_1-R_7 are constants obtained from the x and z integrations implied by Equation (9.65) and can be found in [2].

It should be noted that Equations (9.67a) and (9.68a) are given as homogenous equations. In fact, Equations (9.67) and (9.68) would yield a nonhomogeneous term, i.e. the right-hand side of Equations (9.67a) and (9.68a) is, in general, nonzero. However, it can be shown [2] that the nonhomogeneous terms affect only the far-field behavior of the stresses which is already

incorporated in the stress expressions. So the nonhomogeneous part of the solution can be neglected without loss of generality.

The two equations (9.67a) and (9.68a) are coupled ordinary differential equations with constant coefficients. Following standard procedures the solutions can be written using exponentials:

$$f(y) = S_{1f}e^{-\phi_1 y} + S_{2f}e^{-\phi_2 y} + S_{3f}e^{-\phi_3 y} \quad (9.69)$$

$$g(y) = S_{1g}e^{-\phi_1 y} + S_{2g}e^{-\phi_2 y} + S_{3g}e^{-\phi_3 y} \quad (9.70)$$

where the exponents ϕ_i are solutions to:

$$\phi^6 + (R_1 + R_5 - R_3 R_6)\phi^4 + (R_1 R_5 + R_2 - R_3 R_7 - R_4 R_6)\phi^2 + R_2 R_5 - R_4 R_7 = 0 \quad (9.71)$$

There are, in general six solutions to Equation (9.71), but because only even powers of ϕ are present, they will appear in positive and negative pairs. Positive values of ϕ (or ϕ values with positive real parts) imply that f and g grow indefinitely as y increases, which implies that the interlaminar stresses containing f and g and their derivatives will tend to infinity for large values of y . This, however, is unacceptable as the interlaminar stresses must go to zero for large values of y in order for the far-field solution to be recovered. This is the reason for the negative exponents in Equations (9.69) and (9.70). It is assumed that ϕ_1 , ϕ_2 , and ϕ_3 correspond to the positive solutions of Equation (9.71) (or those with positive real parts) so that the expressions for f and g are in terms of decaying exponentials.

One additional comment pertaining to the limits of the integral in Equation (9.66) is in order. The lower limit is zero, the edge of the flange. The upper limit is any large but finite value of y , corresponding to a point where the far-field stresses are recovered. Of course, if the flange of the stiffener is very narrow, the negative exponentials in Equations (9.69) and (9.70) have not died out and those two expressions for f and g must be modified to include the remaining three ϕ solutions of (9.71) which correspond to increasing exponentials. As already alluded to, some of the solutions to Equation (9.71) may be complex, in which case, expressions (9.69) and (9.70) will include complex conjugates.

Proceeding with the solution to the system of the two equations (9.67a) and (9.68a) it can be shown that

$$\frac{S_{if}}{S_{ig}} = -\frac{\phi_i^2 + R_5}{R_6\phi_i^2 + R_7} \quad (9.72)$$

which relates the coefficients in function $f(y)$ to those in function $g(y)$.

At this point in the solution, the following unknowns remain: S_{1f} , S_{2f} , S_{3f} , B_1 , and C_2 in the flange and \bar{C}_2 in the skin. To determine these, the remaining boundary conditions, namely that the flange edge is stress free are imposed:

$$\begin{aligned} \sigma_y(y=0) &= 0 \\ \tau_{xy}(y=0) &= 0 \\ \tau_{yz}(y=0) &= 0 \end{aligned} \quad (9.73)$$

which, using the expressions for the stresses and the solution to the governing equations for f and g become:

$$(S_{1f} + S_{2f} + S_{3f}) \left(A_1 \sin \frac{\pi z}{t_1} + B_1 \cos \frac{\pi z}{t_1} \right) + (\sigma_y(z))_{ff} = 0$$

$$(S_{1g} + S_{2g} + S_{3g}) \left(C_1 \sin \frac{\pi z}{t_1} + C_2 \cos \frac{\pi z}{t_1} \right) + (\tau_{xy}(z))_{ff} = 0 \quad (9.74a-c)$$

$$(\phi_1 S_{1f} + \phi_2 S_{2f} + \phi_3 S_{3f}) \left(A_1 \frac{t_1}{\pi} \left(1 + \cos \frac{\pi z}{t_1} \right) - B_1 \frac{t_1}{\pi} \sin \frac{\pi z}{t_1} \right) = 0$$

Since Equations (9.74a–c) involve sines and cosines of the variable z , the far-field stresses $(\sigma_y(z))_{ff}$ and $(\tau_{xy}(z))_{ff}$ are expanded in Fourier series and the first terms used to match the corresponding terms in Equations (9.74a–c). This introduces an additional approximation in the solution, but the results are still accurate enough to give reliable trends of the behavior.

Once Equations (9.74a–c) are solved, all unknown constants in the stress expressions are determined except for \bar{C}_2 in the skin. This, again, is determined by energy minimization

$$\frac{\partial \Pi_c}{\partial \bar{C}_2} = 0$$

which yields a linear equation for \bar{C}_2 . The details of the algebra can be found in [2].

The predictions of the method presented here have been compared with finite element results [2–4] and shown to be in good to excellent agreement. Discrepancies and reasons for them are discussed in the references. In what follows, the solution will be used to generate trend curves and discuss the implications for design.

To gain insight on how different parameters affect the tendency of a stiffener to peel away from a skin, a typical flange and skin portion of a stiffened panel is isolated in Figure 9.15. The applied loading is simplified to an applied moment M . This could be the result of bending loads (e.g. pressure) applied on the panel, or even post-buckling where local in-plane axial and/or shear loads are neglected.

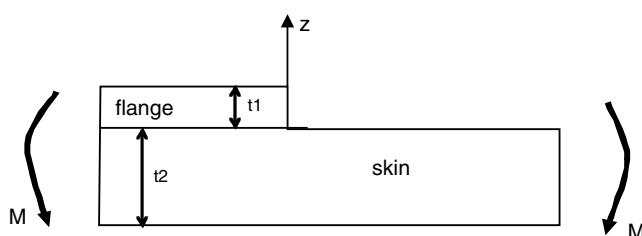


Figure 9.15 Skin–flange configuration under bending load

The basic material properties are as follows:

$$\begin{array}{ll}
 E_x = 137.9 \text{ GPa} & E_z = 11.03 \text{ GPa} \\
 E_y = 11.03 \text{ GPa} & G_{xz} = 4.826 \text{ GPa} \\
 G_{xy} = 4.826 \text{ GPa} & G_{yz} = 3.447 \text{ GPa} \\
 v_{xy} = 0.29 & v_{xz} = 0.29 \\
 t_{\text{ply}} = 0.152 \text{ mm} & v_{yz} = 0.4
 \end{array}$$

Note that, for this type of problem where out-of-plane stresses are involved, the out-of-plane stiffness properties E_z , G_{xz} , G_{yz} , v_{xz} and v_{yz} of the basic ply are also needed.

For the first set of results, the skin and flange layup are assumed to be the same [45/-45/-45/45]n in order to eliminate stiffness mismatch due to differences in moduli in the flange and skin. Only the thicknesses of skin and flange are allowed to vary by specifying different values of n . The normal stress σ_z at the interface between skin and flange is plotted against distance from the flange edge for different values of the ratio t_1/t_2 in Figure 9.16. It is normalized with the maximum tensile value of σ_z at the far field which is given by

$$\sigma_{z\max} = \frac{6M}{(t_1 + t_2)^2}$$

with M the applied moment per unit of stiffener length.

As expected from the qualitative discussion in association with Figure 9.11 at the beginning of this section, the normal stress has a maximum value at the edge of the flange and then reduces rapidly to negative values and decays to zero. The higher the value of t_1/t_2 the more rapidly the stress decays to zero. The distance over which the normal stress decays to zero does not exceed 10 flange thicknesses as is shown in Figure 9.16.

It is also apparent from Figure 9.16 that starting from low t_1/t_2 values and going up, the peak stress at the flange edge increases. However, this trend is not monotonic. As is shown in Figure 9.17, for the same skin and flange layups as in Figure 9.16, the highest peaks are reached for t_1/t_2 values between 1 and 1.5 and then decrease again. This means that flange thicknesses close to the skin thickness should be avoided because they maximize the normal stresses at the interface.

The discussion so far has attempted to isolate the effect of geometry by keeping the layup of the flange and skin the same. Now, the thicknesses of the flange and skin are fixed to the

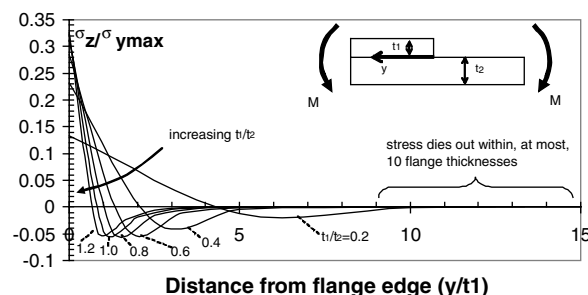


Figure 9.16 Normal stress as a function of distance from flange end for various thickness ratios

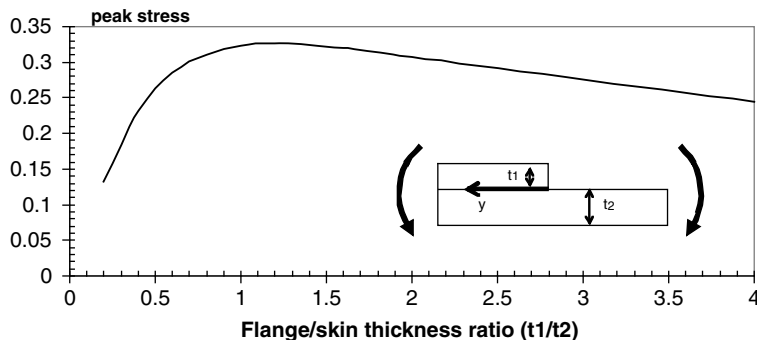


Figure 9.17 Peak normal stress at the flange edge as a function of flange to skin thickness ratio

same value and the layup is varied. This is shown in Figure 9.18 where the case of [45/-45]_s flange and skin is compared with the extreme case of an all 0° flange, [0₄], on an all 90° skin, [90₄]. This is the most extreme case because it has the largest stiffness mismatch between skin and flange. Note that the 0 direction is taken to be parallel to the y axis for this example.

The [0₄] flange on [90₄] skin has a peak normal stress that is twice as high as the peak stress when skin and flange are both [45/-45]_s. And, because the peak value is higher, the stress decays to zero faster than in the case of [45/-45]_s skin and flange. An attempt to combine the effect of layup and geometry is shown in Figure 9.19 where the peak stress is plotted as a function of the ratio t_1/t_2 for the two layups of Figure 9.18.

Again, the highest peaks occur for t_1/t_2 ratios between 1 and 1.5. In addition, the 0° flange on 90° skin has much higher peaks (as much as 2 times higher) than a situation where flange and skin have the same layup. Only for t_1/t_2 values lower than 0.3 do the two cases approach each other but, even for $t_1/t_2 = 0.2$ the 0° flange on 90° skin has 40% higher peak normal stress at the flange edge.

The results presented in Figures 9.16–9.19 were based on a case where only a bending moment M was applied. Similar results are obtained for other types of loading (but see exercise 9.5 for some important differences). The trends can be summarized into the following recommendations or guidelines for design.

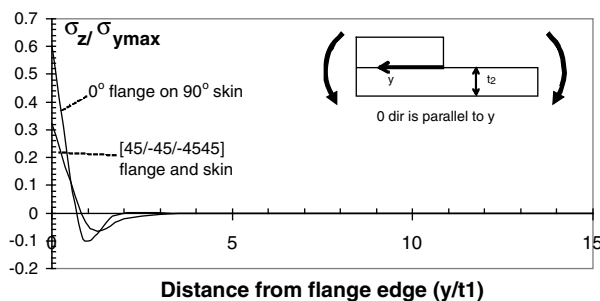


Figure 9.18 Dependence of interface normal stress on layup

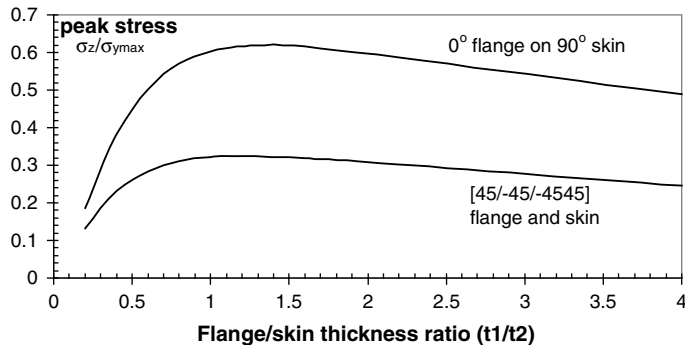


Figure 9.19 Peak normal stress as a function of thickness ratio (t_1/t_2) for two different layup configurations.

1. The interlaminar stresses die out within 10–15 flange thicknesses away from the flanged edge.
2. The interlaminar normal stress peaks at the flange edge and decays rapidly to zero.
3. The flange thickness must be either less than the skin thickness or at least 1.5 times greater to minimize the peak stress at the flange edge.
4. The closer the stiffness of the flange is to that of the skin, the lower the interlaminar stresses at the flange skin interface. Since the thicknesses have to be different, this suggests a situation where the flange and skin have the same repeating base layup and only the number of times it repeats in one is different than in the other.

These implications for design rely heavily on the peak value of the normal stress at the flange–skin interface. This value occurs at the edge of the flange. It is important to note that the exact value at that location is not easy to determine. While the method presented in this section gives a well-defined value for the peak stress, the approximations and assumptions made in the derivation suggest that it may not be sufficiently accurate. On the other hand, finite element solutions show that the value at the edge itself is a function of the mesh size. In general, the finer the mesh near the flange edge, the higher the value. This is a well-known problem associated with free edges in composite materials [16, 17] and displacement-based formulations have difficulty in obtaining accurate stresses because the stress-free boundary condition is implemented in an average sense [17, 18]. In addition, exact anisotropic elasticity solutions for simple laminates [19, 20] have shown that, indeed, the stresses are, in general, singular at the free edge. However, in most cases, the strength of the singularity is so low that it becomes significant over a range equivalent to a few fiber diameters. In such a case, the main assumption of homogeneity in the elasticity solution breaks down and the two different constituents, fiber and matrix must be modeled separately. As a result, the elasticity solution is no more reliable than finite element solutions or the approach presented in this section.

From a design perspective, any method that gives accurate stresses near the free edge of the flange (but not necessarily the flange edge itself) can be used to differentiate between design candidates. Configurations with higher peak values at the edge are expected to have inferior performance. Predicting the exact load at which a delamination will start requires the use of

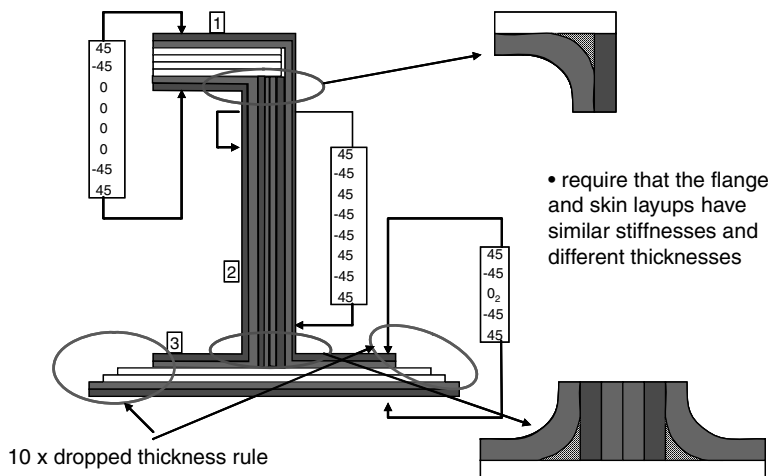


Figure 9.20 Stiffener cross-section design incorporating guidelines from this section

some failure criterion [13, 14] and some test results to adjust any discrepancies between the value predicted at the edge by the analysis method used and the actual test value.

The design guidelines presented in this section can now be used to revisit and upgrade the design of the stiffener cross-section that was last reviewed in Figure 8.36. The revised design is shown in Figure 9.20. The two main differences from Figure 8.36 are the stepped flange next to the skin where plies are dropped with the distance between drops at least 10 times the height of the dropped ply (or plies if more than one plies are dropped at the same location) and the requirement that the skin and flange thicknesses be different $t_{\text{flange}}/t_{\text{skin}} < 1$ or > 1.5) with layups that are, if possible, multiples of the same base layup to keep the respective in-plane stiffnesses as close as possible.

It is recognized, of course, that by using a stepped flange next to the skin the manufacturing cost increases significantly. A tradeoff between the increased cost associated with the stepped flange and the improvement in performance (and thus decreased weight) is necessary in such cases. Alternatives to the stepped flange are shown in Figure 9.21. While they all improve the performance of the skin-stiffened panel, they all carry a significant cost penalty with them.

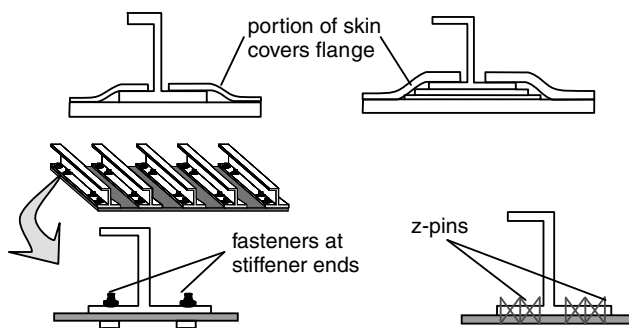


Figure 9.21 Different options for delaying skin–stiffener separation

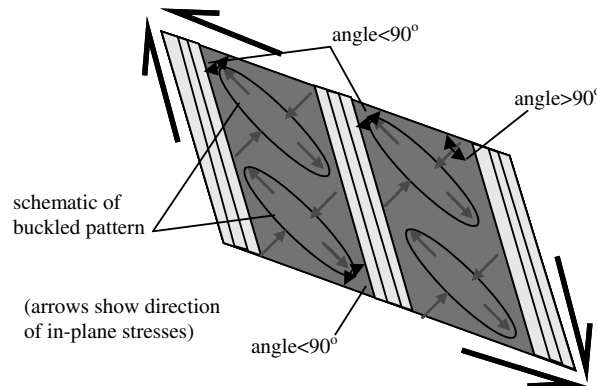


Figure 9.22 Local tension and compression regions in skin under shear

9.3 Additional Considerations for Stiffened Panels

9.3.1 ‘Pinching’ of Skin

With shear loads present, the skin between stiffeners goes into diagonal tension (see Section 7.2). Resolving the shear load in biaxial tension and compression as was done in Section 7.2 results in the situation shown in Figure 9.22. Only the base flanges of the stiffeners are shown in this figure for clarity.

Of particular importance during testing of such configurations are the compression regions at the top left and bottom right of each bay (the term bay here refers to the section between stiffeners). Locally there, an originally rectangular piece of skin deforms such that the angle at the corners of interest is less than 90° (Figure 9.22). If the applied load is sufficiently high, this can cause the skin to fail in compression. This ‘pinching’ phenomenon is more pronounced on components isolated from the surrounding structure during, for example, testing of individual panels. In a complete structure such as a fuselage or wing skin, the conditions at the edges of the panel in Figure 9.22 are different from when it is isolated in a test fixture and the compliance of the adjacent structure relieves this phenomenon.

Pinching of skin at the corners may lead to a premature failure when testing in the laboratory. This can happen even before the skin buckles and it can be exacerbated by local eccentricities that may introduce additional bending moments in the region where the skin is under compression. For this reason special fixtures and specimen geometries have been designed to eliminate this problem [21].

9.3.2 Co-Curing Versus Bonding Versus Fastening

The discussion in this book has mostly been confined to generating designs that meet the loads at low weights. Other than Chapter 2 and Sections 5.1.1, 5.1.2, and 9.2.2, little attention has been paid to the cost associated with some of the designs that result from the approaches presented. The subject of skin-stiffened structure is ideal for bringing up some additional considerations relative to assembly cost and how different concepts can be traded with cost as an additional driver.

There are three major ways in which a stiffened panel can be assembled: (a) co-curing, (b) bonding, (c) fastening. There are variations or combinations of those such as co-bonding (where one or both of skin and stiffeners are staged and then cured with adhesive present), bonding and fastening, etc., but these three major options are a good starting point for cost tradeoffs.

To discuss these approaches some basic aspects and experience-based conclusions should be laid down first:

1. In general, the larger the part the lower the cost per unit weight. There are economies of scale, elimination of secondary process steps (such as off-line part preparation), and, most importantly, elimination of assembly time required to put together the final product if it is made in smaller pieces instead of one larger part.
2. Eliminating additional cure cycles reduces the cost. Ideally, one should have one cure cycle (or cure at room temperature if materials and loads permit).
3. The higher the complexity of the part being made the higher the cost.
4. If the process requires additional inspection to assure structural integrity and to check that tolerances are met, the cost increases.
5. The risk associated with something going wrong during fabrication adds to the cost. This risk is higher for parts of greater complexity and size. Thus, complex parts have a higher rework and scrap rate than simpler parts, which add to their cost.
6. Automated processes are more accurate and reliable and have lower recurring cost, but can be limited by how complex a part they can make. Also, the nonrecurring cost associated with acquiring the equipment (e.g. an automated fiber/tow placement machine) can be high and not easily justifiable for relatively short production runs.

In co-curing, the skin and stiffeners are cured at the same time. This requires detailed (and costly) tooling to accurately locate the stiffeners during cure, and to ensure uniform pressure everywhere. So the nonrecurring cost associated with tooling is relatively high. The recurring cost (labor hours) per unit weight is relatively low according to item (1) above. On the other hand, the risk of something going wrong during cure of the combined skin and stiffeners is relatively high, which, according to item (5) above, adds to the cost.

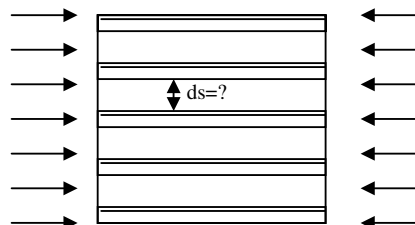
In a bonded configuration, skin and stiffeners are made separately which minimizes the risk. But bonding requires the extra assembly step of skin and stiffeners thus adding to the cost. In addition, there are currently no reliable consistent nondestructive inspection methods to verify that the bond is everywhere effective and meets minimum strength requirements. This means that additional process steps ensuring proper surface preparation of the surfaces to be bonded, full coverage with adhesive, cleanliness and avoidance of contamination, etc. have to be in place to guarantee a good bondline. This adds to the cost. In some cases, to protect against defective bondlines that were missed during fabrication and inspection, it is required to demonstrate that the structure can meet limit load with a significant portion of the bondline ineffective, which adds to the weight of the structure.

Fastening of the stiffeners to the skin eliminates the problems associated with bonding and improves the post-buckling performance. However, the extra assembly time associated with fastening is a significant cost increase. In addition, the use of fasteners typically increases the weight.

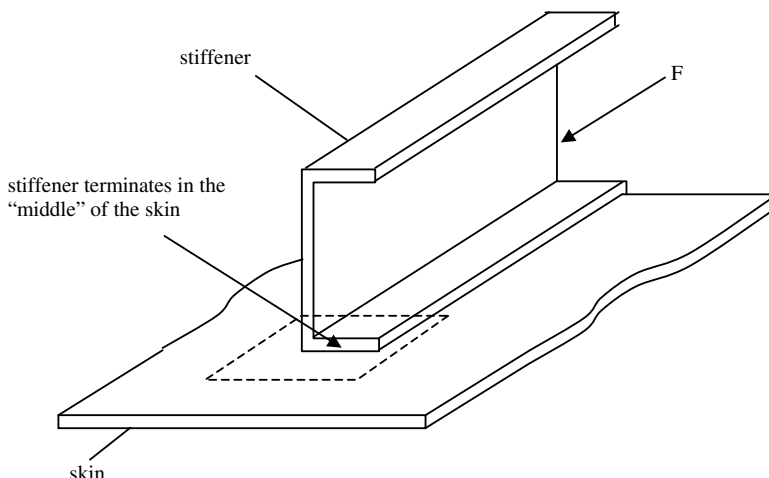
It can be seen from the previous discussion that each of the three approaches has advantages and disadvantages, and deciding which approach to follow is a function of the amount of risk to be undertaken and which process steps a particular facility is more comfortable with and more efficient in. It is possible, for example, if the assembly process steps are streamlined and automated, that the cost associated with them is only a small fraction of the total and can lead to overall cost savings compared with a co-cured configuration [22].

Exercises

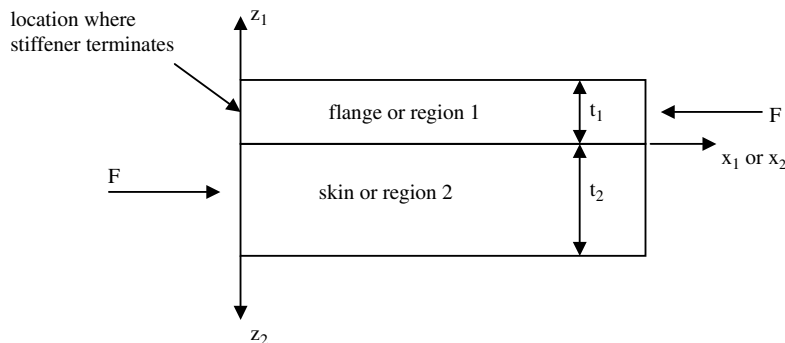
- 9.1 Assume that the stiffener used in the application in Section 8.5.3.1 is to be used on a square skin panel of dimensions 508×508 mm loaded in compression. The skin layup is $[45/-45]_s$ (same material as the stiffener). Determine the largest stiffener spacing (and thus the spacing that minimizes the number of stiffeners and therefore the fabrication cost) such that the overall buckling load equals the buckling load of the skin portion between the stiffeners.



- 9.2 Consider the stiffener terminating somewhere on a skin as shown in the figure.



Further isolating the flange and skin portions included in the dashed rectangle above and viewing them from the side (enlarged):



Note the following:

- (a) The load F applied to the stiffener in the first figure, when transmitted to the flange in the second figure would, in general, also exert a moment. To simplify the calculations this moment is neglected. There are applications where this is valid (when the stiffener is also attached to a very stiff part which absorbs the bending moment). Similarly, going from the applied F on the flange in the second figure to the reacting F on the skin on the left would again, in general, result in a bending moment which is neglected for the same reasons.
- (b) The flange is called region 1, meaning all the quantities relating to the flange will have a subscript 1 from now on. Similarly, the skin is region 2 and all skin-related quantities will have a subscript 2. Note there are two coordinate systems one in region 1 and one in region 2. Also note that the z directions in these two coordinate systems are opposite each other.
- (c) The left edge of the flange in the second figure above, where the stiffener terminates has no loads applied and therefore stresses are zero there. All stresses in the flange transfer to the skin as that edge is approached.
- (d) The flange and skin are assumed to be wide in the y direction (perpendicular to the plane of the figure and, therefore, there is no dependence on y_1 or y_2 .

It is assumed that far from the terminating flange edge (i.e. for high values of x_1) the classical laminated plate theory is recovered according to which the average stress in the flange σ_1 is given by

$$\sigma_1 = \frac{F}{t_1 b_1} = A_1$$

where b_1 is the flange width.

It is now assumed that the normal stress σ_{x1} in the flange is given by the following expression:

$$\sigma_{x1} = f \left(\sin \frac{\pi z}{2t_1} + D_1 \sin \frac{3\pi z}{2t_1} \right) + A_1$$

where f is an unknown function of x_1 and D_1 is an unknown constant.

Note that this expression can be viewed as consisting of the first few terms of a Fourier series. The requirement, of course, is that f , for large x_1 , tend to zero so $\sigma_{x1} \rightarrow A_1$ away from the flange termination.

Use the equilibrium equations to determine the stresses τ_{xz1} and σ_{z1} (all other stresses are zero or close to zero in the flange). To do this you will also need to make sure that $\tau_{xz1} = 0$ and $\sigma_{z1} = 0$ at the top of the flange. Also, write the corresponding stress expressions for region 2 (by analogy with region 1).

Require that τ_{xz} and σ_z are continuous at the flange/skin interface (i.e. the value of τ_{xz} obtained at the flange skin interface coming from the flange equals the value of τ_{xz} obtained at the same location coming from the skin, and similarly for σ_z) and obtain the values of D_1 and D_2 . (Watch out for the definition of the coordinate systems and the z direction.)

- 9.3 Continuing from Exercise 9.2, the function f is still unknown. To determine it you need to minimize the energy in the flange/skin system. The energy has the form:

$$\Pi = U - W$$

where the internal potential energy U is the sum of U_1 and U_2 and W is the external work. It turns out that W does not contribute to the solution so neglect it.

Now U_1 is given by

$$U_1 = \frac{1}{2} \iiint [S_{11}\sigma_x^2 + 2S_{13}\sigma_x\sigma_z + S_{33}\sigma_z^2 + S_{55}\tau_{xz}^2] dx dy dz$$

where, all quantities in the right-hand side should have an additional subscript 1 to denote the flange (omitted here for simplicity) and the quantities S_{ij} are compliances (obtained from inverting the stiffness matrix for the entire flange).

The y integration only yields a constant b_1 , the width of the flange since there is no dependence on y .

Without substituting for D_1 (and D_2) use your expressions for the stresses obtained in Exercise 9.2 and perform the z integrations in the expression for U_1 . Note that, because these involve sines and cosines, quite a few of the integrals are zero and you can derive simple expressions for those that are not.

Write the analogous expression for U_2 and perform the z integration. Note that the y integration in the skin will also yield a constant multiplier of b_1 because we are assuming the the skin/flange portion we have isolated for analysis is of width b_1 both for the flange and the skin.

If you substitute in the expression for $\Pi = U_1 + U_2$ you will now have a long integral with respect to x only (y and z integrations already performed) which will be a function of f and its first two derivatives.

- 9.4 Continuing from Exercise 9.3, using the calculus of variations write down the Euler equation for this problem and derive the governing equation for f so that the energy is minimized. Write the governing equation in the form

$$R_1(d^n f / dx^n) + R_2(d^{n-1} f / dx^{n-1}) + \dots = 0$$

Start with R_1 with the highest derivative of f , and neglect the constant term (because it does not contribute to the solution). Write down the expressions for R_1, R_2, \dots .

Solve the equation obtained writing down the solution in the form:

$$f = C_1 e^{m_1 x} + C_2 e^{m_2 x} + \dots$$

Also write down the expression for m_i .

9.5 (Continuing from Exercise 9.4) At this point, the fact that none of the stresses can increase with increasing x is invoked and only exponentials with negative real parts are used. In addition, the boundary conditions that require $\tau_{xz1} = 0$ and $\sigma_{x1} = 0$ at $x = 0$ are invoked (the second one approximately only) and the constants C_1, C_2, \dots are determined. After that is done, one notices that at $x_1 = 0$ at the flange–skin interface, the interlaminar shear stresses τ_{xz1} and τ_{xz2} are zero and only the normal stress σ_{z1} or σ_{z2} are nonzero. Therefore, the only stress that contributes to delamination is σ_{z1} (or σ_{z2} which is the same at the flange–skin interface by stress continuity).

Substituting in the stress expressions and evaluating σ_{z1} at $x = z = 0$ show that

$$\sigma_{zcrit} = \frac{-8A_1}{\pi} \left(1 - \frac{t_2}{3t_1} \right) \sqrt{\frac{(S_{11})_1 \left(1 + \frac{D_1^2}{2} \right) + (S_{11})_2 \frac{t_2}{t_1} \left(1 + \frac{D_2^2}{2} \right)}{2(S_{33})_1 \left[T_1 + \left(\frac{t_2}{t_1} \right)^5 T_2 \right]}}$$

where the compliances for each laminate (flange or skin) can be obtained by averaging the compliances over all plies (springs in series):

$$\frac{t_1}{(S_{ij})_1} = \sum \frac{t_i}{(S_{ij})_{ithply}}$$

with an analogous expression for region 2, and the compliances for each ply of orientation θ are given by the following expressions where quantities with superscript 0 refer to a 0° ply of the material being used.

$$S_{11} = S_{11}^0 \cos^4 \theta + (2S_{12}^0 + S_{66}^0) \sin^2 \theta \cos^2 \theta + S_{22}^0 \sin^4 \theta$$

$$S_{13} = S_{13}^0 \cos^2 \theta + S_{23}^0 \sin^2 \theta$$

$$S_{33} = S_{33}^0$$

$$S_{55} = S_{55}^0 \cos^2 \theta + S_{44}^0 \sin^2 \theta$$

$$S_{11}^0 = \frac{1}{E_{11}}$$

$$S_{12}^0 = -\frac{v_{12}}{E_{11}}$$

$$S_{66}^0 = \frac{1}{G_{12}}$$

$$S_{22}^0 = \frac{1}{E_{22}}$$

$$S_{13}^0 = -\frac{v_{13}}{E_{11}}$$

$$S_{23}^0 = -\frac{v_{23}}{E_{22}}$$

$$S_{33}^0 = \frac{1}{E_{33}}$$

$$S_{44}^0 = \frac{1}{G_{23}}$$

$$S_{55}^0 = \frac{1}{G_{13}}$$

$$T_1 = \frac{3}{2} - \frac{4}{\pi} + \frac{D_1^2}{81} \left(\frac{3}{2} - \frac{4}{3\pi} \right) + \frac{2D_1}{9} \left(1 - \frac{8}{3\pi} \right)$$

$$T_2 = \frac{3}{2} - \frac{4}{\pi} + \frac{D_2^2}{81} \left(\frac{3}{2} - \frac{4}{3\pi} \right) + \frac{2D_2}{9} \left(1 - \frac{8}{3\pi} \right)$$

A material is made available with the following properties:

$$E_{11} = 137.88 \text{ GPa}$$

$$E_{22} = E_{33} = 11.72 \text{ GPa}$$

$$G_{12} = G_{13} = 4.825 \text{ GPa}$$

$$G_{23} = 4.0 \text{ GPa}$$

$$v_{12} = v_{13} = 0.3$$

$$v_{23} = 0.45$$

$$t_{\text{ply}} = 0.1524 \text{ mm}$$

$$X^t = 2068 \text{ MPa}$$

$$X^c = 1379 \text{ MPa}$$

$$Y^t = 68.94 \text{ MPa}$$

$$Y^c = 310.2 \text{ MPa}$$

$$S = 124.1 \text{ MPa}$$

It is also given that the skin at the location of interest has the following layup: [45/-45/0/90]_{s4}.

- 9.6 (a) If the skin is not to exceed 4500 μ s, determine the value of F that barely fails the skin.
 (b) Assume that the flange is made from one of the three layups: [0/90]_{s n} , or [45/-45]_{s m} or [45/-45/0/90]_{s p} . Select a value of n, m , and p and plot the value of $\sigma_{z\text{crit}}$ as a function of t_2/t_1 . Which value(s) of t_2/t_1 would you recommend to use in this case and why? (c) Use your results in (a) and (b) to select the lightest flange layup you should use.

References

1. Megson, T.H.G., *Aircraft Structures for Engineering Students*, Elsevier, 2007, Chapter 3.
2. Kassapoglou, C., Stress Determination at Skin-Stiffener Interfaces of Composite Stiffened Panels Under Generalized Loading, *Journal of Reinforced Plastics and Composites*, **13**, 1555–1572 (1994).
3. Kassapoglou, C., Calculation of Stresses at Skin-Stiffener Interfaces of Composite Stiffened Panels Under Shear Loads, *International Journal of Solids and Structures*, **30**, 1491–1503 (1993).
4. Kassapoglou C. and DiNicola A.J., Efficient Stress Solutions at Skin Stiffener Interfaces of Composite Stiffened Panels, *AIAA Journal*, July 1992, pp 1833–1839.
5. Hyer, M.W. and Cohen, D., Calculation of Stresses and Forces Between the Skin and Stiffener in Composite Panels, *AIAA Paper 87-0731, 28th SDM Conference*, Monterey CA, April 1987.
6. Cohen, D. and Hyer, M.W., Influence of Geometric Non-linearities on Skin-Stiffener Interface Stresses, *AIAA Paper 88-2217, 29th SDM Conference*, Williamsburg VA, April 1988.
7. Volpert, Y., and Gottesman, T., Skin-stiffener interface stresses in tapered composite panel, *Composite Structures*, **33**, 1–6 (1995).
8. Baker, D.J. and Kassapoglou, C., Post buckled composite panels for helicopter fuselages: Design, analysis, fabrication and testing. *Presented at the American Helicopter Society International Structures Specialists' Meeting, Hampton Roads Chapter, Structures Specialists Meeting*, Williamsburg VA, 30 October–1 November 2001.
9. Wiggenraad, J.F.M. and Bauld, N.R., Global/Local Interlaminar Stress Analysis of a Grid-Stiffened Composite Panel, *Journal of Reinforced Plastics and Composites*, **12**, 237–253 (1993).
10. Minguet, P.J. and O'Brien, T.K., Analysis of Test Methods for Characterizing Skin/Stringer Debonding Failures in Reinforced Composite Panels, in: *Composite Materials: Testing and Design ASTM STP 1274* R. B. Deo and C. R. Saff (eds), American Society for Testing and Materials, 1996, pp 105–124.
11. Wang, J.T. and Raju, I.S., Strain Energy Release Rate Formulae for Skin-Stiffener Debond Modeled with Plate Elements, *Engineering Fracture Mechanics*, **54**, 211–228 (1996).
12. Wang, J.T., Raju, I.S. and Sleight, D.W., Composite Skin-Stiffener Debond Analyses, Using Fracture Mechanics Approach with Shell Elements, *Composites Engineering*, **5**, 277–296 (1995).
13. Brewer, J.C. and Lagace, P.A., Quadratic Stress Criterion for Initiation of Delamination, *Journal of Composite Materials*, **22**, 1141–1155 (1988).
14. Fenske, M.T., and Vizzini, A.J., The Inclusion of In-Plane Stresses in Delamination Criteria, *Journal of Composite Materials*, **35**, 1325–1342 (2001).
15. Hildebrandt, F.B. *Advanced Calculus for Applications*, Prentice Hall, Englewood Cliffs, NJ, 1976, Section 7.8.
16. Wang, A.S.D. and Crossman, F.W. Some new results on edge effect in symmetric composite laminates. *Journal of Composite Materials*, **11**, 92–106 (1977).
17. Bauld, N.R., Goree, J.G. and Tzeng, L-S., A comparison of finite-difference and finite element methods for calculating free edge stresses in composites, *Composites and Structures*, **20**, 897–914 (1985).
18. Spilker, R.L and Chou, S.C., Edge Effects in Symmetric Composite Laminates: Importance of Satisfying the Traction-Free-Edge Condition, *Journal of Composite Materials*, **14**, 2–20 (1980).
19. Wang, S.S. and Choi, I., Boundary-layer effects in composite laminates, Part I – free edge stress solutions and basic characteristics, *ASME Transactions Applied Mechanics*, **49**, 541–548 (1982).
20. Wang, S.S. and Choi, I., Boundary-layer effects in composite laminates, Part II – free edge stress solutions and basic characteristics, *ASME Transactions Applied Mechanics*, **49**, 549–560 (1982).
21. Farley, G.L. and Baker, D.J., In-Plane Shear Test of Thin Panels, *Experimental Mechanics*, **23**, 81–88 (1983).
22. Apostolopoulos, P. and Kassapoglou, C., Cost Minimization of Composite Laminated Structures – Optimum Part Size as a Function of Learning Curve Effects and Assembly, *Journal of Composite Materials*, **36**(4), 501–518 (2002).

10

Sandwich Structure

A sandwich structure (Figure 10.1) typically consists of two facesheets separated by light-weight core. Usually, the facesheets are bonded to the core with the use of adhesive but, under certain circumstances (for example using X-cor® or K-cor® [1,2] it is possible to eliminate the use of adhesive.

Composite laminates make up the facesheets. There is a variety of materials and configurations used for the core depending on the application and the desired properties: foam, honeycomb, low density foaming aluminum, etc. Most core materials, in particular honeycombs, are anisotropic. They have different stiffness and strength in different directions. In general, the purpose of the core is to increase the bending stiffness of the sandwich by moving material away from the neutral axis of the cross-section. The stiffness (and strength) of the core are, typically, much lower than those of the facesheets. As a result, for general loading situations such as that shown in Figure 10.1, with applied bending moment M and in-plane axial and shear loads N and V , respectively, all the load is taken by the facesheets. The bending moment (per unit width) is resolved into a force couple where one facesheet is loaded by a positive force per unit width N_m and the other by an equal and opposite force per unit width $-N_m$. The magnitude of that force is such that the force couple generates a moment equal to M :

$$N_m = \frac{M}{t_c + t_f}$$

The axial load N and the shear load V are divided equally between the two facesheets.

The core must still have minimum strength and stiffness in certain directions so that: (i) the sandwich does not collapse under pressure during cure; (ii) load can be transferred between facesheets; and (iii) core ramp-downs, where the core gradually transitions to monolithic laminate for attachment to adjacent structure, do not fail prematurely. With reference to Figure 10.2, aside from the core thickness t_c which determines the overall bending stiffnesses of the sandwich, the most important core properties are: The transverse shear stiffnesses G_{xz} and G_{yz} , the corresponding transverse shear strengths Z_{xz} , Z_{yz} , the out-of-plane Young's modulus E_c , and the corresponding (flatwise) tension and compression strengths Z^t and Z^c respectively. Finally, for the case of honeycomb core such as that shown in Figure 10.2, the core cell size s

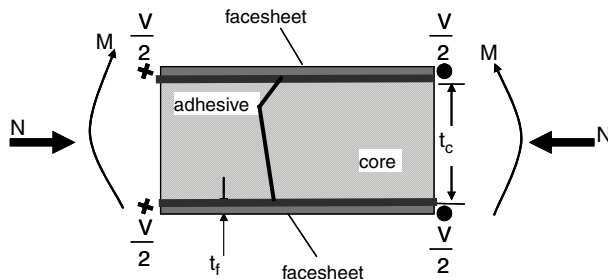


Figure 10.1 Sandwich configuration

plays a role in some of the failure modes. A thorough investigation of sandwich structures with isotropic facesheets can be found in reference [3].

10.1 Sandwich Bending Stiffnesses

A sandwich can be treated as a laminate where the core is just another ply with negligible stiffness and strength properties, and thickness equal to the core thickness. Standard classical laminated-plate theory (see Section 3.3) can be used to determine the corresponding A , B and D matrices. The presence of the core does not change the A matrix, but will affect the B (if the total layup is unsymmetric) and D matrices significantly. This can be seen by applying Equation (8.14) to obtain the D matrix of a sandwich. Rewriting Equation (8.14) it can be shown that for a sandwich with identical facesheets,

$$D_{ij} = 2(D_{ij})_f + 2(A_{ij})_f \left(\frac{t_c + t_f}{2} \right)^2 \quad (10.1)$$

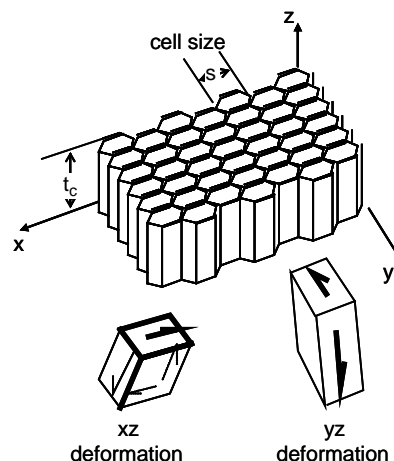


Figure 10.2 Honeycomb core geometry

where the multiplicative factors of 2 appearing on the right-hand side account for the presence of two facesheets. The first term on the right-hand side of Equation (10.1) is the same as the EI term in Equation (8.14) with the stiffness E incorporated in the corresponding D_{ij} term. The second term is the product of the stiffness and the distance from the neutral axis present in Equation (8.14) with the modulus this time lumped in the A_{ij} term.

To see the effect of the core on increasing the bending stiffness of a sandwich, consider two facesheets of layup $(\pm 45)/(0/90)/(\pm 45)$ separated by a core of varying core thickness. The individual A and D matrices for each facesheet are given by:

A_{11}	28912.44	N/mm	D_{11}	659.7	Nmm
A_{12}	12491.43	N/mm	D_{12}	466.9	Nmm
A_{22}	28912.44	N/mm	D_{22}	659.7	Nmm
A_{66}	13468.58	N/mm	D_{66}	494.0	Nmm

Using Equation (10.1), the ratio of D_{11} for the entire sandwich divided by D_{11} for each facesheet can be determined as a function of varying core thickness. The result is shown in Figure 10.3.

It can be seen from Figure 10.3 that even very small core thicknesses (5 mm) result in a thousand-fold increase of the bending stiffness. The range of typical core thicknesses used in many applications is also shown in Figure 10.3, indicating that, for such applications, the core increases the bending stiffness anywhere between 4000 and 15 000 times.

This kind of improvement at a relatively small increase in weight, due to the presence of the core and adhesive, makes sandwich structure ideal for many stability-driven applications where high buckling loads are important. In fact, judicious selection of facesheet material and layup and core material and thickness would result in sandwich being the most weight-efficient structure if it weren't for a variety of new failure modes associated with such configurations. Each of the components – facesheet, adhesive, or core, can fail and there are more than one failure modes for each component. Some of these failure modes are quite limiting and tend to drive the design. The result is that sandwich is not always more efficient than the alternative(s) such as a skin-stiffened structure. It depends on the geometry, loading, and design philosophy (e.g. whether post-buckling is allowed and at how high a post-buckling ratio). The most important of these failure modes are examined in subsequent sections.

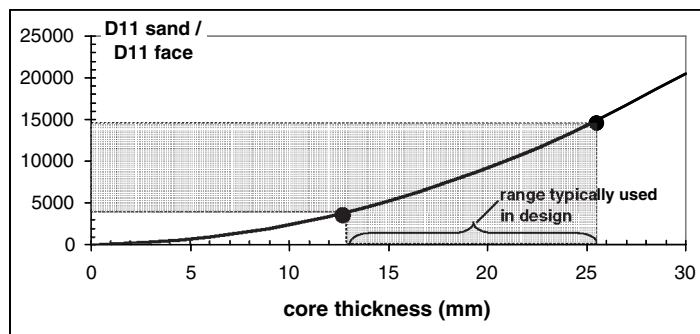


Figure 10.3 Variation of sandwich bending stiffness as a function of core thickness

In addition, it should be pointed out that in many applications where sandwich is selected, ramp-downs are used at the edges of the sandwich for attachment to adjacent structure. Ramp-downs are briefly discussed in Section 10.6.1. They tend to increase cost and introduce additional failure modes that must be checked to make sure they do not lead to premature failure of the entire structure.

10.2 Buckling of Sandwich Structure

Buckling is one of the critical failure modes for sandwich structure in particular for relatively large panels. The reason is that it is hard to design against all possible failure modes in the post-buckling regime and, as a result, buckling is usually considered to coincide with final failure.

10.2.1 Buckling of Sandwich Under Compression

The procedure to determine the buckling load of a sandwich structure is very similar to that presented in Chapter 6 for monolithic laminates, with one important difference. The presence of the core makes the effects of transverse shear very important. If they are not properly accounted for, the predicted buckling load is very unconservative (higher than the case where transverse shear effects are accounted for).

In a uniform thickness plate where transverse shear effects are significant the Kirchoff hypothesis is no longer valid. Plane sections remain plane, but are no longer perpendicular to the plate midplane. This is shown schematically in Figure 10.4.

The sandwich under compression is treated as a wide beam. Following the derivation in [4] for isotropic beams, the buckling load is given by:

$$N_{crit} = \frac{N_{Ecrit}}{1 + \frac{kN_{Ecrit}}{t_c G_c}} \quad (10.2)$$

In Equation (10.2), N_{Ecrit} is the buckling load N_o of the sandwich if transverse shear effects are neglected, given, for simply supported edges by Equation (6.7) repeated below for convenience:

$$N_{Ecrit} = \frac{\pi^2}{a^2} \left[D_{11}m^2 + 2(D_{12} + 2D_{66})(AR)^2 + D_{22} \frac{(AR)^4}{m^2} \right] \quad (6.7)$$

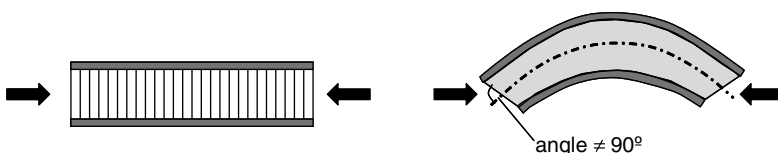


Figure 10.4 Bending of a sandwich panel under compression

Also, t_c and G_c are the core thickness and transverse shear stiffness respectively. It is important to note that G_c is the value of the shear modulus (typically G_{xz} or G_{yz}) aligned with the loading direction.

Finally, k in Equation (10.2) is the shear correction factor. The shear correction factor is introduced to reconcile the inconsistency between the derived and assumed transverse shear stress distributions through the thickness of the plate. Engineering bending theory leads to a quadratic distribution of shear stress through the thickness while first-order shear deformation theory assumes the shear strain (and thus the shear stress) is independent of the through-thickness coordinate. This inconsistency [5] is reconciled by requiring that the work done following either formulation is the same. This leads to an expression for the transverse shear force (per unit width) of the form [5],

$$Q_x = kG_{xz}h\gamma = \frac{5}{6}G_{xz}h\gamma$$

where the shear correction factor is $k = 5/6$ in this case, h is the plate thickness and γ is the transverse shear strain.

As mentioned earlier, most sandwich structures use core with very small shear stiffness G_{xz} compared with that of the facesheets. As a result, the shear stress through the thickness is very nearly uniform. This is consistent with the fact that bending stresses are not linearly distributed through the thickness of the core because, as was mentioned earlier, bending moments are transmitted through a sandwich as a force couple. Thus, there is (almost) no inconsistency between bending theory and first-order shear deformation theory and $k \approx 1$. Thus,

$$N_{crit} = \frac{N_{Ecrit}}{1 + \frac{N_{Ecrit}}{t_c G_c}} \quad (10.3)$$

An example would help illustrate the importance of transverse shear in a sandwich. The same facesheet properties as those in Section 10.1 and Figure 10.3 are used here. The core material is assumed to have a shear stiffness $G_{xz} = 42.1 \text{ N/mm}^2$. Equation (10.3) is used to calculate the buckling load of a square sandwich panel of side 508 mm and compare it with Equation (6.7), i.e. without accounting for transverse shear. This is done for different core thicknesses and the results are shown in Figure 10.5.

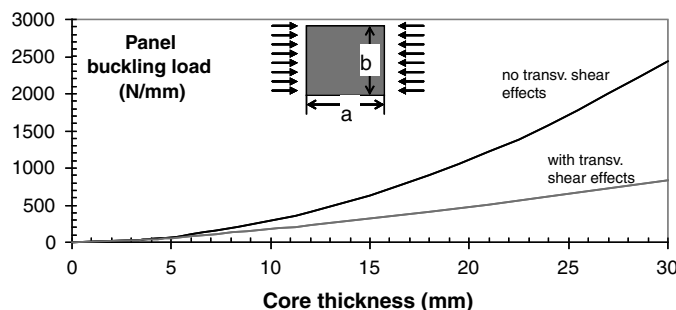


Figure 10.5 Buckling load of a sandwich with and without transverse shear effects as a function of core thickness

It can be seen that once the core thickness exceeds 5 mm, the buckling load including transverse shear effects diverges drastically from the buckling load without transverse shear effects. If transverse shear effects are included the buckling load is always lower. Even for a core thickness of 3 mm the two buckling loads (with and without transverse shear effects) differ by 21%.

10.2.2 Buckling of Sandwich Under Shear

The situation is shown in Figure 10.6. The form of the equation predicting buckling of a simply supported sandwich under shear is the same as Equation (10.3):

$$N_{xycrit} = \frac{N_{xyc}}{1 + \frac{N_{xyc}}{t_c G_{45}}} \quad (10.4)$$

where N_{xyc} is the shear buckling load without transverse shear effects (see for example Sections 6.3–6.5) and G_{45} is the core shear modulus in the 45° direction, as shown in Figure 10.6.

The shear modulus G_{45} is used because it is the one mostly opposing the tendency of the panel to buckle. Since a pure shear loading is equivalent to biaxial loading with tension in one direction and compression in the other (see for example Section 7.2), the tendency for buckled half-waves to form is along the 45° line in Figure 10.6 (the direction of maximum compression) and G_{45} , the core shear stiffness in that direction, opposes that tendency.

To determine G_{45} standard tensor transformation equations are used (Section 3.2, Equation 3.8). The result is

$$G_{45} = \sin^2 45 G_{yz} + \cos^2 45 G_{xz} = \frac{G_{yz} + G_{xz}}{2} \quad (10.5)$$

Using this result to substitute in Equation (10.4) and rearranging leads to:

$$N_{xycrit} = \frac{\frac{(G_{xz} + G_{yz})}{t_c}}{\frac{(G_{xz} + G_{yz})}{t_c} + 2} N_{xyc} \quad (10.6)$$

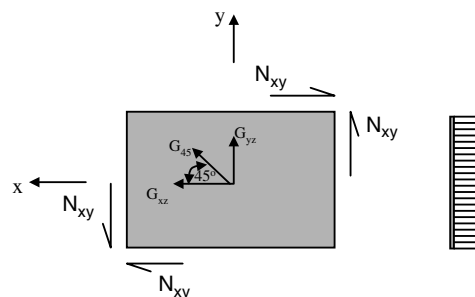


Figure 10.6 Sandwich panel under shear load

10.2.3 Buckling of Sandwich Under Combined Loading

For combined loading situations the same interaction curves as those presented in Sections 6.5 and 6.6 can be used, provided the individual buckling loads are corrected for transverse shear effects as presented in the two previous sections.

10.3 Sandwich Wrinkling

Wrinkling is a local buckling phenomenon where the facesheet of a sandwich buckles over a characteristic half-wavelength ℓ , which is unrelated to the overall length or width of the panel. There are three possible modes, symmetric, antisymmetric and mixed-mode wrinkling. These are shown schematically in Figure 10.7 for applied compression, but can also occur under applied shear or combined loads.

10.3.1 Sandwich Wrinkling Under Compression

The symmetric wrinkling case is examined here in detail (see also [6]). A sandwich compression specimen, which failed in wrinkling, is shown in Figure 10.8.

The deformed shape after the facesheet has buckled in the wrinkling mode is idealized in Figure 10.9. This shape extends through the width of the sandwich (perpendicular to the plane of Figure 10.9). It is assumed that the sandwich is very long in the y direction. It is also assumed that at the edges of the buckled shape, at $x=0$ and $x=\ell$, the boundary conditions on the facesheet are those of simple support, i.e. $w=0$ there.

One important aspect of the formulation is modeling the behavior of the core. Assuming perfect bonding between core and facesheet, it is obvious from Figure 10.9 that the core deforms under the buckled facesheet. In the case shown in Figure 10.9, the core extends perpendicular to the x axis. If the core were very thick, there would be a region near the midplane of the core where

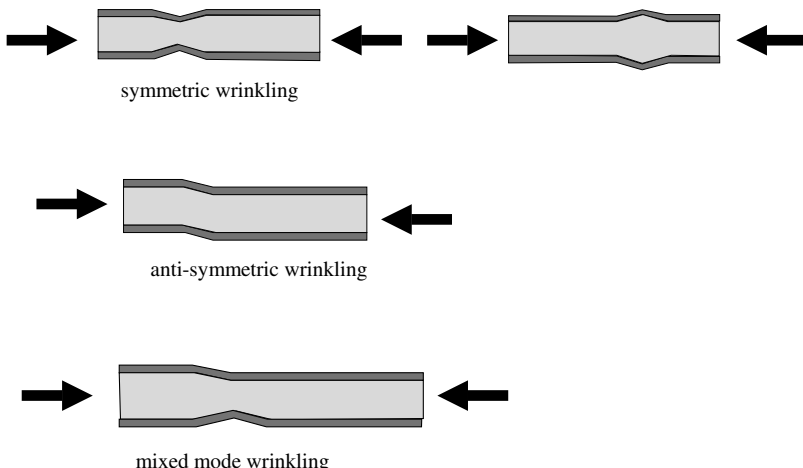


Figure 10.7 Sandwich wrinkling modes

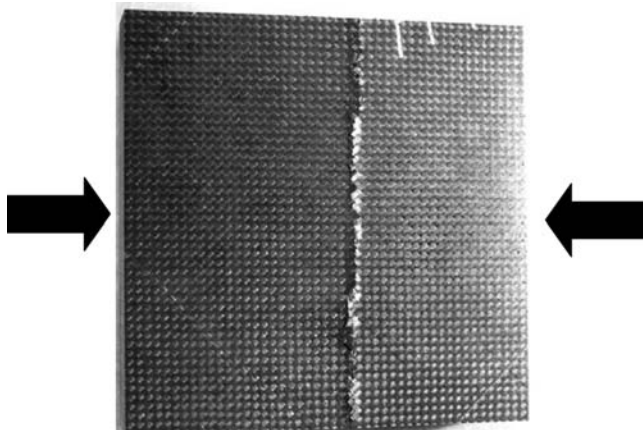


Figure 10.8 Wrinkling failure of sandwich tested in compression

the core would not deform. So the core deformations are confined in a region close to the facesheet. It is assumed that this region has width z_c (Figure 10.9) where z_c is unknown at this point. It is also assumed that the core deflections in the z direction vary linearly with z .

Combining the assumption of simply supported ends for the deformed facesheet and linear variation of deflection for the core, the following expression for w is introduced:

$$w = A \frac{z}{z_c} \sin \frac{\pi x}{\ell} \quad (10.7)$$

Equation (10.7) satisfies the requirement that $w = 0$ at $x = 0$ and $x = \ell$. It also satisfies the linear variation of w as a function of z with $w = 0$ at $z = 0$ (i.e. at the interface where core deformations seize to be significant) and reproducing the facesheet sinusoidal deformation at $z = z_c$, which is the intersection of the core with the facesheet.

The wrinkling load is determined by energy minimization. During wrinkling, energy is stored in bending the facesheet and extending the core. So the energy expression has the form:

$$\Pi_c = 2U_f + U_c - 2W \quad (10.8)$$

where U_f is the energy in each facesheet and U_c is the energy stored in the core. W is the work done by the applied load on one end of the sandwich. The factors of 2 in this equation account for the presence of two (identical) facesheets.

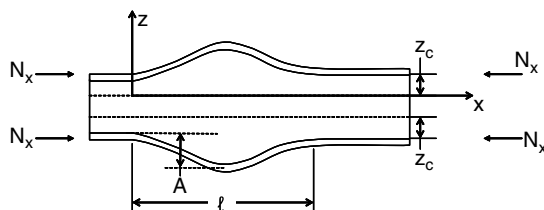


Figure 10.9 Deformed configuration of sandwich undergoing symmetric wrinkling

Neglecting deformations u and v in the plane of the facesheet, the strain and stress in the facesheet can be obtained from Equations (5.6), (5.7), and (5.4):

$$\begin{aligned}\varepsilon_x &= -z \frac{\partial^2 w}{\partial x^2} \\ \sigma_x &= E_f \varepsilon_x\end{aligned}\tag{10.9}$$

where E_f is the facesheet membrane modulus obtained from Equation (8.6).

Then,

$$\sigma_x \varepsilon_x = E_f z^2 \left(\frac{\partial^2 w}{\partial x^2} \right)^2$$

Thus, the facesheet energy can be written as,

$$U_f = \frac{1}{2} \iint E_f z^2 \left[\left(\frac{\partial^2 w}{\partial x^2} \right)^2 \right]_{z=z_c} dz dx = \frac{1}{2} E_f \bar{I} \int_0^\ell \left[\left(\frac{\partial^2 w}{\partial x^2} \right)^2 \right]_{z=z_c} dx = \frac{(E\bar{I})_f}{2} \int_0^\ell \left[\left(\frac{\partial^2 w}{\partial x^2} \right)^2 \right]_{z=z_c} dx\tag{10.10}$$

where \bar{I} is the moment of inertia of the facesheet per unit width b . It should be noted that this expression can also be obtained from Equation (5.62) assuming a symmetric facesheet and noticing that only the D_{11} term contributes with $D_{11} = EI/b$ where b is the width of the facesheet perpendicular to the plane of Figure 10.9.

The strain–displacement and stress–strain equations (5.9) and (5.4) applied to the core, give

$$\begin{aligned}\varepsilon_z &= \frac{\partial w}{\partial z} \\ \gamma_{xz} &= \frac{\partial w}{\partial x} + \frac{\partial u}{\partial z} \\ \sigma_z &= E_c \varepsilon_z \\ \tau_{xz} &= G_{xz} \gamma_{xz}\end{aligned}$$

where E_c is the core modulus in the z direction and G_{xz} is the transverse shear modulus of the core for shearing in the xz plane (see Figure 10.9).

As already mentioned, the u deflection of the core is negligible. Then, the above equations can be combined to

$$\begin{aligned}\sigma_z \varepsilon_z &= E_c \left(\frac{\partial w}{\partial z} \right)^2 \\ \tau_{xz} \gamma_{xz} &= G_{xz} \left(\frac{\partial w}{\partial x} \right)^2\end{aligned}$$

which, in turn, can be substituted for in the core energy expression:

$$U_c = \frac{1}{2} \int_0^\ell \int_0^{z_c} (E_c \sigma_z \varepsilon_z + G_{xz} \tau_{xz} \gamma_{xz}) dz dx = \int_0^\ell \int_0^{z_c} \left(E_c \left(\frac{\partial w}{\partial z} \right)^2 + G_{xz} \left(\frac{\partial w}{\partial x} \right)^2 \right) dz dx \quad (10.11)$$

Note the factor of 2 in front of the second integral, which is introduced to account for the fact that there are two portions of the core (one above and one below the midplane) both of thickness z_c that contribute to the core energy.

The external work done by the applied load N_x per facesheet per unit width is given by

$$\begin{aligned} W &= N_x \delta \\ \delta &= \ell - \int_0^\ell dx \end{aligned}$$

with δ the deflection at the edge of the sandwich portion considered, i.e. at $x=0$ and $x=\ell$.

Considering the deformed shape of the facesheet shown in Figure 10.10, the deflection δ can be calculated using Pythagoras' theorem and assuming small deflections w .

By Pythagoras' theorem,

$$(dx)^2 + (dw)^2 = (ds)^2 \Rightarrow dx = ds \sqrt{1 - \left(\frac{dw}{ds} \right)^2}$$

The quantity involving the square root can be expanded into the first two terms of a Taylor series (valid for small $(dw/ds)^2$) to give,

$$\sqrt{1 - \left(\frac{dw}{ds} \right)^2} \approx 1 - \frac{1}{2} \left(\frac{dw}{ds} \right)^2 \quad \text{for small } \left(\frac{dw}{ds} \right)^2$$

and for small deflections w

$$\frac{dw}{ds} \approx \frac{dw}{dx}$$

Therefore, substituting in the expression for δ ,

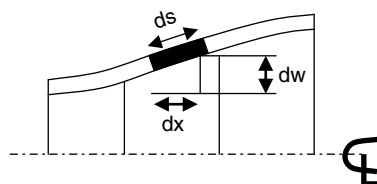


Figure 10.10 Deformed facesheet and local geometry

$$W = \frac{N_x}{2} \int_0^\ell \left(\frac{\partial w}{\partial x} \right)^2 \Big|_{z=z_c} dx$$

At this point, the relevant w derivatives present in the energy expression are evaluated:

$$\left(\frac{\partial w}{\partial x} \right)^2 = \frac{A^2 z^2}{z_c^2} \frac{\pi^2}{2\ell^2} \left(1 + \cos \frac{2\pi x}{\ell} \right)$$

$$\left(\frac{\partial w}{\partial z} \right)^2 = \frac{A^2}{z_c^2} \frac{1}{2} \left(1 - \cos \frac{2\pi x}{\ell} \right)$$

$$\left(\frac{\partial^2 w}{\partial x^2} \right)^2 = \frac{A^2 z^2}{z_c^2} \frac{\pi^4}{2\ell^4} \left(1 - \cos \frac{2\pi x}{\ell} \right)$$

and substituted in Equation (10.8). Evaluating the integrals gives,

$$\Pi_c = \frac{\pi^4}{2\ell^3} (\bar{EI})_f A^2 + \frac{1}{2} \left[\frac{E_c \ell}{z_c} + \frac{1}{3} G_{xz} z_c \frac{\pi^2}{\ell} \right] A^2 - N_x \frac{A^2 \pi^2}{2\ell} \quad (10.12)$$

Equation (10.12) must be minimized with respect to the unknown amplitude A . This implies,

$$\frac{\partial \Pi_c}{\partial A} = 0 \Rightarrow 2A \left[\frac{\pi^4}{2\ell^3} (\bar{EI})_f + \frac{1}{2} \left[\frac{E_c \ell}{z_c} + \frac{1}{3} G_{xz} z_c \frac{\pi^2}{\ell} \right] - N_x \frac{\pi^2}{2\ell} \right] = 0 \quad (10.13)$$

For nonzero values of A , the quantity in brackets must be zero. This gives a condition for the wrinkling load N_x . Denoting the wrinkling load by N_{xwr} :

$$N_{xwr} = \frac{\pi^2 (\bar{EI})_f}{\ell^2} + \frac{E_c \ell^2}{\pi^2 z_c} + G_{xz} \frac{z_c}{3} \quad (10.14)$$

Examining Equation (10.14) it can be seen that the first term of the right-hand side is the buckling load of a beam column (per unit width). The second term is the contribution to the buckling load of a beam by an elastic foundation when the stiffness of the foundation k equals E_c/z_c . This can be readily seen by comparing this term with Equation (8.33) when $m = 1$. The third term is the contribution of the elastic foundation when it consists of torsional instead of extensional springs.

This expression for the wrinkling load is still in terms of two unknowns: ℓ the half wavelength during wrinkling, and z_c the portion of the core undergoing deformations during wrinkling. Each of them is determined by noticing that if N_x starts increasing from zero, then wrinkling will occur at the lowest possible value that Equation (10.14) allows as a function of ℓ and z_c . Therefore, minimizing N_{xwr} with respect to ℓ gives:

$$\frac{\partial N_{xwr}}{\partial \ell} = 0 \Rightarrow \ell = \pi \left(\frac{(E\bar{I})_f}{E_c} z_c \right)^{1/4} \quad (10.15)$$

which gives a condition relating ℓ and z_c . Using it to eliminate ℓ from Equation (10.14) results in

$$N_{xwr} = \frac{2\sqrt{E_c(E\bar{I})_f}}{\sqrt{z_c}} + \frac{G_{xz}z_c}{3} \quad (10.16)$$

which is only in terms of z_c . Differentiating now with respect to z_c and setting the result equal to 0 gives,

$$\frac{\partial N_{xwr}}{\partial z_c} = 0 \Rightarrow z_c = 3^{2/3} \left(\frac{E_c(E\bar{I})_f}{G_{xz}^2} \right)^{1/3} \quad (10.17)$$

Now the moment of inertia per unit width

$$\bar{I} = \frac{t_f^3}{12}$$

is used to substitute in Equation (10.17) to obtain the final expression for z_c

$$z_c = \frac{3^{2/3}}{12} t_f \left(\frac{E_c E_f}{G_{xz}^2} \right)^{1/3} = 0.91 t_f \left(\frac{E_c E_f}{G_{xz}^2} \right)^{1/3} \quad (10.18)$$

This expression can now be used to substitute in Equation (10.15) to get the final value for the half-wavelength:

$$\ell = \frac{\pi 3^{1/6}}{12^{1/3}} t_f \left(\frac{E_f}{\sqrt{E_c G_{xz}}} \right)^{1/3} = 1.648 t_f \left(\frac{E_f}{\sqrt{E_c G_{xz}}} \right)^{1/3} \quad (10.19)$$

Finally, Equation (10.18) can be used to substitute in Equation (10.16) to obtain the wrinkling load,

$$N_{xwr} = 0.91 t_f (E_f E_c G_{xz})^{1/3} \quad (10.20)$$

Equation (10.20) has been derived in many different ways [6,7]. In fact, depending on the assumptions, the form of the equation remains the same and only the coefficient in the right-hand side changes [7].

It is important to keep in mind that the derivation so far has assumed that the core was sufficiently thick that the portion z_c of the core undergoing deformations is less than or equal to half the core thickness $t_c/2$. If z_c given by Equation (10.18) is greater than half the core thickness, then the entire core deforms during wrinkling and

$$z_c = \frac{t_c}{2} \quad (10.18a)$$

With this new value of z_c new values of ℓ and N_{xwr} must be calculated. Following the same procedure as before, z_c is substituted for in Equation (10.15) to get

$$\ell = \frac{\pi}{24^{1/4}} \left(\frac{E_f}{E_c} t_f^3 t_c \right)^{1/4} \quad \text{for } z_c = \frac{t_c}{2} \quad (10.19a)$$

Then, the new value of z_c is substituted in Equation (10.16) to obtain

$$N_{xwr} = 0.816 \sqrt{\frac{E_f E_c t_f^3}{t_c}} + G_{xz} \frac{t_c}{6} \quad (10.20a)$$

The condition for the full depth of the core being involved in the wrinkling deformations can be obtained from Equation (10.18). If the right-hand side of Equation (10.18) is greater than $t_c/2$, then the entire core thickness deforms. Therefore, if

$$t_c < 1.817 t_f \left(\frac{E_f E_c}{G_{xz}^2} \right)^{1/3} \quad (10.21)$$

the core deforms in its entirety, and Equations (10.18a), (10.19a), and (10.20a) are valid. Otherwise, only a portion z_c of the core deforms and Equations (10.18), (10.19) and (10.20) are valid.

It should be noted that, according to Equation (10.20a), as the core thickness increases the wrinkling load decreases. So it would be expected that wrinkling would become the primary failure mode beyond a certain core thickness. However, this is only true as long as Equation (10.21) is satisfied. Once the core thickness exceeds the right-hand side of Equation (10.21) the governing Equation is (10.20), which is independent of the core thickness.

For antisymmetric wrinkling, an analogous approach to that presented above, but with a different expression for the w deflection of the core in order to satisfy the different boundary conditions, leads to the following results [6,8]:

$$N_{xwr} = 0.51 t_f \left(E_f E_c G_{xz} \right)^{1/3} + \frac{G_{xz} t_c}{3} \quad (10.22)$$

$$\ell = 2.15 t_f \left(\frac{E_f^2}{E_c G_{xz}} \right)^{1/6} \quad (10.23)$$

$$z_c = \frac{3}{2} t_f \left(\frac{E_f E_c}{G_{xz}^2} \right)^{1/3} \quad (10.24)$$

for sufficiently thick core, i.e. when

$$t_c \geq 3 t_f \left(\frac{E_f E_c}{G_{xz}^2} \right)^{1/3} \quad (10.25)$$

or, when the entire core thickness undergoes deformations (core is relatively thin),

$$N_{xwr} = 0.59 t_f^{3/2} \sqrt{\frac{E_f E_c}{t_c}} + 0.378 G_{xz} t_c \quad (10.22a)$$

$$\ell = 1.67 t_f \left(\frac{E_f t_c}{E_c t_f} \right)^{1/4} \quad (10.23a)$$

valid when

$$t_c < 3 t_f \left(\frac{E_f E_c}{G_{xz}^2} \right)^{1/3} \quad (10.25a)$$

In practice, one would have to evaluate both symmetric and antisymmetric wrinkling loads for a given application and use the lowest of the two. However, it can be demonstrated, (see Exercise 10.1) that only for very thin cores is antisymmetric wrinkling possible. For typical core thicknesses, symmetric wrinkling is the mode of failure.

Comparison of the predictions for symmetric and antisymmetric wrinkling with experimental results is difficult to do with the equations presented so far. The main reason is that sandwich structure is most often fabricated by co-curing core, adhesive, and facesheets all at once. As a result of this process the facesheets are not perfectly flat, but have some waviness. This waviness is not included in the analysis presented so far. Only if the facesheets are pre-cured separately and then bonded on a perfectly flat core will the waviness be (mostly) eliminated.

For this reason, the predictions presented so far are compared with finite element models in which the facesheets are perfectly flat. Such a comparison can be found in reference [9] and its conclusions are summarized here.

A sandwich with 25.4 mm honeycomb core and facesheets made with four plain weave fabric plies and layup $[(\pm 45)(0/90)_2/(\pm 45)]$ was modeled under compression using finite elements. The facesheet stiffness E_f was 64 GPa. Since the core was thick, only symmetric wrinkling predictions were used. The pertinent core properties and a comparison or prediction from Equations (10.19) and (10.20) are shown in Table 10.1 for three different core materials with the same facesheet.

It can be seen that the predictions for the wrinkling stress N_{xwr}/t_f and the corresponding half-wavelength ℓ are in good agreement with finite elements with the highest discrepancy being less than 20%. It should be noted that the predicted wrinkling loads are always less than the finite element result. Also, the greatest discrepancy in wrinkling stress (case 2) does not correspond to the case with the greatest discrepancy in the half-wavelength (case 3). The discrepancies are attributed to a combination of finite element modeling issues related to proper load introduction and boundary conditions, and to the fact that Equation (10.7) is an approximation, especially considering the assumed linear variation with out-of-plane coordinate z .

The discussion so far has not explicitly accounted for the fact that the facesheets are made of composite materials. Only by substituting the appropriate value for the facesheet in-plane

Table 10.1 Analytical predictions versus FE results for sandwich wrinkling

E_c (MPa)	G_{xz} (MPa)	N_{xwr}/t_f (MPa) present	N_{xwr}/t_f (MPa) FE	$\Delta\%$	ℓ (mm) present	ℓ (mm) FE	$\Delta\%$
133	42	646	658	-1.8	11.3	11.4	-0.9
266	42	842	1033	-18.5	9.5	8.9	+6.7
133	84	808	821	-1.6	10.6	13.2	-19.7

stiffness E_f in the equations derived does one account for composite laminates. For more accurate values for E_f in case of composite facesheets, the following expression can be used [7]:

$$E_f = \frac{12(1 - v_{xy}v_{yx})D_{11f}}{t_f^3} \quad (10.26)$$

where v_{xy} , v_{yx} , and D_{11f} are Poisson's ratios and bending stiffness of the facesheet.

Other models explicitly incorporating composite layups can be found in the literature. For example, symmetric wrinkling was determined by Pearce and Webber [10] as:

$$N_{xwr} = \frac{\pi^2}{a^2} \left[(D_{11})_f m^2 + 2 \left((D_{12})_f + 2(D_{66})_f \right) \left(\frac{a}{b} \right)^2 + \frac{(D_{22})_f}{m^2} \left(\frac{a}{b} \right)^4 \right] + \frac{2E_c a^2}{m^2 \pi^2 t_c} \quad (10.27)$$

Comparing Equation (10.27) with Equation (8.33) suggests that the wrinkling load consists of two parts, the buckling load of the facesheet and a contribution from the core acting as an elastic foundation with spring constant $k = 2E_c/t_c$. Indeed, the first part of Equation (10.27) is identical to the buckling load of a simply supported plate under compression given by Equation (6.7). Finally, comparing Equation (10.27) with the wrinkling expression (10.14) derived earlier without explicitly incorporating the fact that the facesheet is composite, it is seen that the first two terms of Equation (10.14) have a one-to-one correspondence with the two terms of Equation (10.27). The first term corresponds to buckling of the facesheet and the second to the core acting as an elastic foundation and storing energy in deformation in the z direction. However, Equation (10.14) has an additional term dependent on the core shear stiffness which represents core shear deformations. This term is not present in Equation (10.27). It is, therefore, expected that Equation (10.27) may not be as accurate when the core shear deformations are appreciable.

As already alluded to, the fact that sandwich structures are usually co-cured results in facesheet waviness, which may significantly affect the performance of the sandwich and limit the usefulness of the design equations presented so far. One attempt to include the effect of waviness can be found in [9]. A typical cross-section of a $([\pm 45]/(0/90)/[\pm 45])$ facesheet on honeycomb core is shown in Figure 10.11 (taken from [9]).

Using Figure 10.11, the waviness of the facesheet at that section cut through the specimen was measured and plotted in Figure 10.12 (taken from [9]). It is evident from Figure 10.12 that the waviness can be significant and its amplitude can approach one-quarter to one-third of the facesheet thickness t_f ($=0.5717$ mm in this case).

Even though there is an element of randomness in the waviness of Figure 10.12, a main sinusoidal component of a specific amplitude and wavelength can be estimated. Assuming that component is present everywhere in the facesheet, a new model of facesheet deformations under compression accounting for the waviness can be created [9]. This model assumes a sinusoidal shape of the facesheet shown schematically in Figure 10.13. This model permits accounting for the presence of facesheet (light grey color in Figure 10.13), adhesive (dark grey color in Figure 10.13), and core and their respective failure modes relatively easily. The model assumes that the waviness shown in Figure 10.13 extends all the way to the edges of the sandwich (perpendicular to the plane of the Figure).

Each of the failure modes shown in Figure 10.13, core tension, core compression, core shear, adhesive tension, adhesive shear, and facesheet bending must be checked for, and the most critical will give the failure prediction. This requires accurate knowledge of the corresponding allowables.

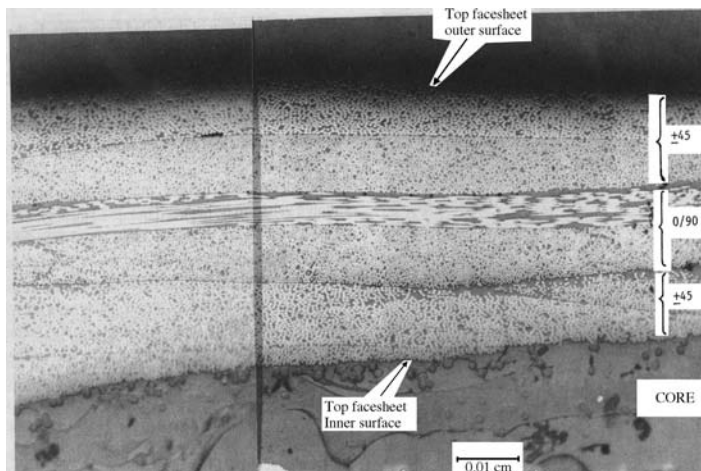


Figure 10.11 Sandwich cross-section showing facesheet and portion of the core (200 \times magnification from [9])

A comparison of this model to test results, taken from [9], is shown in Table 10.2. Here, three different facesheet layups and three different cores were used. The predictions range from excellent to barely acceptable (for the last case in Table 10.2). The main reasons for the discrepancies from test results are: (a) not so accurate knowledge of all allowables for the

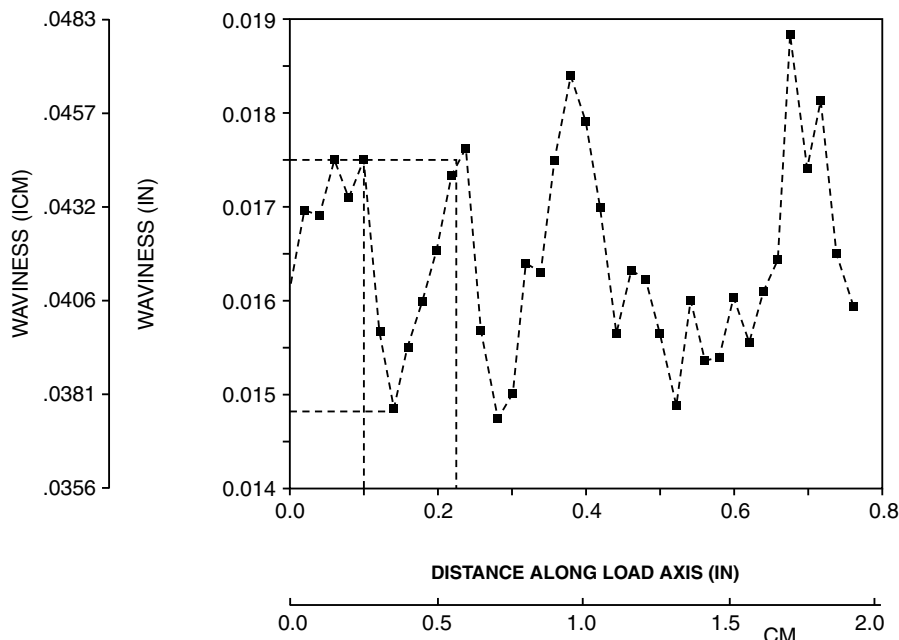


Figure 10.12 Waviness of outer surface of facesheet of Figure 10.11 (from [9])

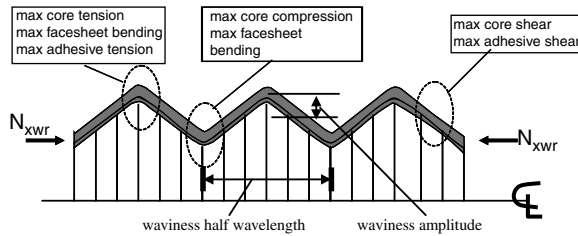


Figure 10.13 Sandwich with waviness

failure modes mentioned above; and (b) in all cases, one amplitude and waviness were used obtained from Figure 10.12, which is not sufficiently accurate for some of the cores and facesheet layups in Table 10.2. Still, using a waviness model is promising and, combined with accurate allowables, can yield very reliable predictions.

To account for the effect of (usually unknown) waviness and other complicating factors, it is customary to knockdown the predictions of Equation (10.20) for symmetric wrinkling by reducing the coefficient in the right-hand side [11]:

$$N_{xwr} = 0.43t_f(E_f E_c G_{xz})^{1/3} \quad (10.28)$$

Similarly, for antisymmetric wrinkling which, as already mentioned, occurs only in thin cores, Equation (10.22a) is modified as follows [12]:

$$N_{xwr} = 0.33t_f E_f \sqrt{\frac{E_c t_f}{E_f t_c}} \quad (10.29)$$

Equations (10.28) and (10.29) have been shown to be (sometimes very) conservative over a wide variety of facesheet and core materials, including metals.

What has been presented so far is only a small portion of sandwich wrinkling modeling approaches. There are many more models, each with its own range of applicability. A discussion of the accuracy of the various models and their applicability can be found in [13].

Table 10.2 Comparison of wrinkling predictions obtained with a waviness model to test results

Facesheet	Core	Predicted wr. stress (MPa)	Test wr. stress (MPa)	$\Delta\%$
(±45)/(0/90)	Nomex®HRH 10-1/8-3.0	295	313	-5.8
(±45)/(0/90)/(±45)	Nomex®HRH 10-1/8-3.0	264	297	-11.2
(±45)/(0/90) ₂ /(±45)	Nomex®HRH 10-1/8-3.0	426	337	+26.4
(±45)/(0/90)	Phenolic HFT 3/16-3.0	344	350	-1.8
(±45)/(0/90)/(±45)	Phenolic HFT 3/16-3.0	255	349	-26.9
(±45)/(0/90) ₂ /(±45)	Phenolic HFT 3/16-3.0	309	382	-19.0
(±45)/(0/90)/(±45)	Korex® 1/8-3.0	246	365	-32.7

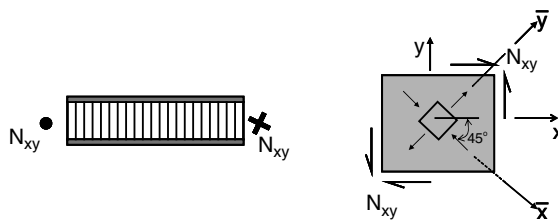


Figure 10.14 Sandwich under shear with shear load resolved into compression and tension loads

10.3.2 Sandwich Wrinkling Under Shear

Wrinkling of a sandwich structure can also occur under applied shear load. Since pure shear can be resolved in compression in one direction and tension in the other, the compression portion can cause wrinkling of the sandwich along a line at 45° to the applied shear load (see Figure 10.14). A conservative way to estimate the wrinkling load under shear is to analyze the sandwich as loaded under compression along the 45° line and neglect the tension load. The reason is that in biaxial loading situations with compression and tension, the tension load tends to stabilize the structure and the buckling load is higher than if only compression were applied. This was demonstrated in Figure 6.3 where the buckling load was higher for compression and tension than for biaxial compression.

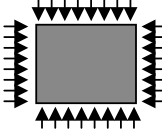
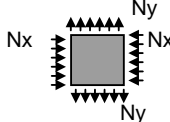
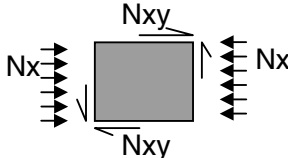
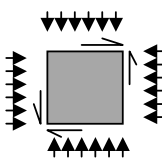
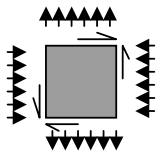
Therefore, conservatively, the equations derived in the previous section for wrinkling under compression can also be used here, provided the relevant quantities E_f , E_c , and G_{xz} are rotated to the direction of applied compression. Of these, the core Young's modulus in the z direction E_c remains unaffected. The facesheet modulus E_f is rotated by 45° by simply rotating the stacking sequence by that angle and calculating the corresponding membrane modulus of the resulting laminate in that direction using Equation (8.6). The core shear modulus G_{45} also changes if the core is not isotropic in its plane. The corresponding transformation was given by Equation (10.5). So, in the coordinate system $\bar{x}\bar{y}$, with compression parallel to the \bar{x} axis, the rotated core shear stiffnesses are:

$$\begin{aligned} G_{\bar{x}z} &= \sin^2 \theta G_{yz} + \cos^2 \theta G_{xz} = \frac{G_{yz} + G_{xz}}{2} \quad \text{for } \theta = -45^\circ \\ G_{\bar{y}z} &= \cos^2 \theta G_{yz} + \sin^2 \theta G_{xz} = \frac{G_{yz} + G_{xz}}{2} \quad \text{for } \theta = -45^\circ \end{aligned} \quad (10.5a)$$

10.3.3 Sandwich Wrinkling Under Combined Loads

Wrinkling under combined loads is analyzed using interaction curves [7,14], which are very similar to the interaction curves for buckling of monolithic plates presented in Sections 6.5 and 6.6. A summary of the most common cases is given in Table 10.3. To use Table 10.3 the following ratios are defined:

Table 10.3 Interaction curves for sandwich wrinkling under combined loads

Case	Loading	Design equation
Biaxial compression		$N_x = \frac{N_{xwr}}{\left(1 + \left(\frac{N_y}{N_x}\right)^3\right)^{1/3}}$
Compression in x direction and tension in y direction		$N_x = N_{xwr}$
Combined compression and shear		$R_c + R_s^2 = 1$
Biaxial compression and shear		$R_c + R_s^2 = 1$ $R_c = N_x/N_{xwr}$ $R_s = N_{xy}/N_{xywr}$ N_{xwr} is wrinkling load in major core direction when biaxial compression acts alone (1 st case in this table)
Compression in x direction, tension in y direction, and shear		$R_c + R_s^2 = 1$ $R_c = N_x/N_{xwr}$ $R_s = N_{xy}/N_{xywr}$ N_{xwr} is wrinkling load in x direction when compression acts alone.

For compression alone,

$$R_c = N_x/N_{xwr} \quad (10.30)$$

where N_{xwr} is the wrinkling load under compression

For shear alone,

$$R_s = N_{xy}/N_{xywr} \quad (10.31)$$

where N_{xywr} is the wrinkling load under shear

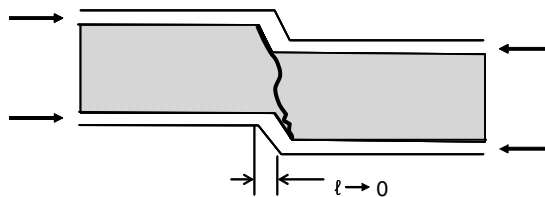


Figure 10.15 Sandwich crimping

10.4 Sandwich Crimping

This failure mode is shown in Figure 10.15. It occurs when the core shear stiffness is very low and is quite sensitive to the presence of eccentricities (e.g. when the core thickness is not uniform or if there is an abrupt change in the facesheet thickness when many plies are dropped).

This is a failure mode that is similar to antisymmetric wrinkling with, essentially, zero wavelength ($\ell \rightarrow 0$).

10.4.1 Sandwich Crimping Under Compression

If the wavelength ℓ of the buckling mode tends to zero, the corresponding buckling load tends to infinity since the buckling load is proportional to $1/\ell^2$. Then, the basic buckling equation for a sandwich under compression Equation (10.3) can be used,

$$N_{crit} = \frac{N_{Ecrit}}{1 + \frac{N_{Ecrit}}{t_c G_c}} \quad (10.3)$$

letting N_{Ecrit} tend to infinity.

It can be seen that Equation (10.3) is of the form ∞/∞ as $N_{Ecrit} \rightarrow \infty$, so l'Hopital's rule can be used to determine the limit of N_{crit} . Differentiating numerator and denominator with respect to N_{Ecrit} and, subsequently letting N_{Ecrit} tend to infinity, the crimping load N_{crit} is shown to be:

$$N_{crit} = t_c G_c \quad (10.32)$$

where G_c is either G_{xz} or G_{yz} , whichever is aligned with the direction of the load.

10.4.2 Sandwich Crimping Under Shear

A semi-empirical formula is used in this case, which is analogous to Equation (10.32):

$$N_{xycrim} = t_c \sqrt{G_{xz} G_{yz}} \quad (10.33)$$

10.5 Sandwich Intracellular Buckling (Dimpling) under Compression

This is a failure mode specific to honeycomb or other open-cell cores. Representative such cores are shown in Figure 10.16. Flex and double-flex core are used in structures with single or

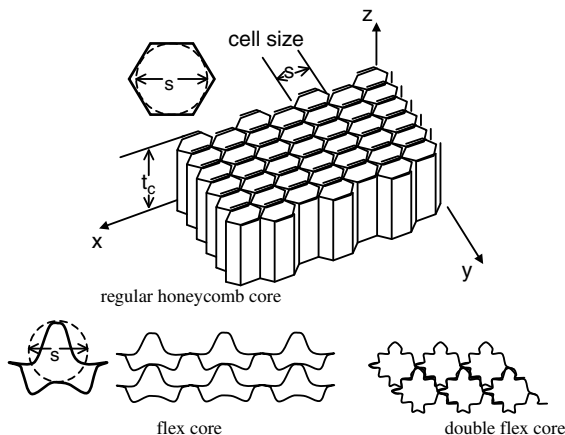


Figure 10.16 Cores susceptible to dimpling

compound curvature to allow the sandwich to conform to the curved shape and eliminate anticlastic curvature effects.

When cores as those shown in Figure 10.16 are used, if the cell size is big enough it is possible for the unsupported facesheet between the cell walls to buckle. To analyze this intracellular buckling or dimpling mode requires developing a buckling solution for a composite facesheet with hexagonal or highly irregular (for flex or double-flex cores in Figure 10.16) boundaries. The complexity of such solution is prohibitive. Instead, a one-dimensional column-buckling type solution combining Equations (8.56) and (10.26) with a semi-empirical factor is used:

$$N_{x \text{ dim}} = 2 \frac{E_f t_f^3}{1 - v_{xy} v_{yx}} \frac{1}{s^2} \quad (10.34a)$$

or

$$N_{x \text{ dim}} = 24 \frac{D_{11f}}{s^2} \quad (10.34b)$$

where s is the core cell size shown in Figure 10.16.

10.6 Attaching Sandwich Structures

As mentioned in Section 10.1, sandwich has superior bending stiffness properties and would be the preferred design configuration had it not been for several failure modes such as wrinkling or crimping that limit its performance. Another problem that limits the usage of sandwich structure is the difficulty of attaching it to adjacent structure with adequate load transfer at the attachment region without undue increase in weight and cost. While it is relatively easy to attach sandwich structure when the applied loads are low, it is quite a challenge to do so for highly loaded structure. Some considerations and options are discussed in the following two sections.

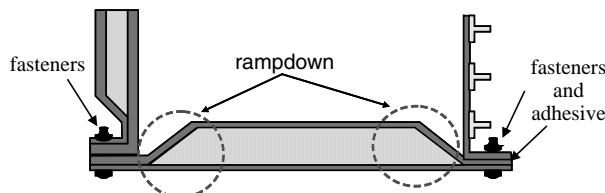


Figure 10.17 Attaching sandwich structure through the use of ramp-downs

10.6.1 Core Ramp-Down Regions

One of the most common methods of providing adequate means of attachment is through the use of a ramp-down. By eliminating the core at the attachment region one does not have to deal with the fact that core has low compression and shear strengths which would compromise the strength of an attachment. As seen in Figure 10.17, the attachment can be through fasteners or adhesive (or both) connecting monolithic laminates at the edge of the ramp-down region.

The monolithic laminate created by eliminating the core (consisting of the two facesheets) may not be sufficient if the loads are high, and local reinforcement may be necessary to transfer bearing and shear loads (Figure 10.18). This creates the additional problem of deciding how and where the extra plies will be dropped off, transitioning to the full depth of the core. Clearly, they cannot all terminate at the edge of the core ramp because the resulting stiffness mismatch would lead to premature failure. In fact, a number of plies must go up the ramp to stiffen it and thus attract some of the load to the upper facesheet in Figure 10.18. This is of particular importance for relatively large values of the ramp angle θ ($15^\circ < \theta < 40^\circ$).

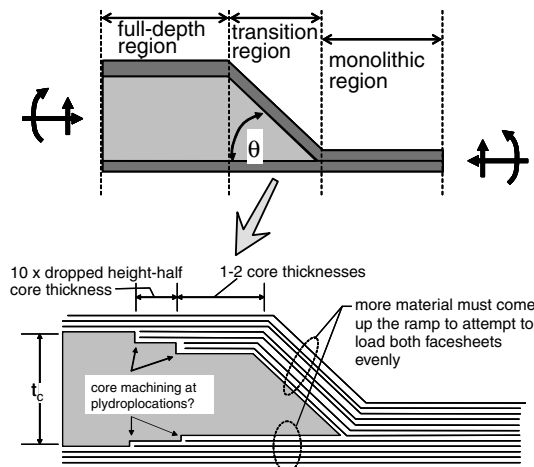


Figure 10.18 Transitioning from monolithic laminate to full-depth core

Consider a situation where some in-plane load, for example compression, is applied at the edge where the monolithic laminate is. The loading is eccentric in that it acts at the neutral axis of the monolithic laminate which is offset from the neutral axis of the full-depth core. This causes a bending moment. At low loads, the entire compressive load stays in the flat facesheet, the bottom facesheet in Figure 10.18. At higher loads, bending of the full-depth core is more pronounced, and a significant fraction of the applied load starts to get transmitted up the ramp into the ramped facesheet (top facesheet in Figure 10.18). This is the reason plies must go up the ramp and into the upper facesheet, to transfer that load without failure. For typical designs of ramped sandwich under compression, 60% of the load stays in the straight (bottom) facesheet and 40% is transmitted up the ramp to the top facesheet.

Since the monolithic region is typically designed for bearing strength (at least when fasteners are used to connect to adjacent structure) and the facesheets away from the ramped regions are designed for buckling and notched strength requirements, the thickness of the monolithic region is, usually, significantly higher than the sum of the thicknesses of the two facesheets. This poses the problem of smoothly transitioning the thicker monolithic laminate to the thinner facesheets. A typical transition with some guidelines is shown in Figure 10.18. Successive plydrops are separated by at least 10 times the thickness of the dropped plies. This is in agreement with the findings of Figure 9.16. At the same time, again consistent with the results of Section 9.2.2, dropping a large number of plies should be avoided because of the high normal and shear stresses created. In addition, dropping many plies at the same location may require machining a step into the core, as shown in Figure 10.18, to accommodate them. Dropping no more than 3–4 plies at one location usually does not require special provisions such as locally machining the core.

If the thickness difference between the monolithic laminate at the panel edges and the facesheets at the full-thickness portion of the core is large it will be necessary to have a number of plydrop locations transitioning from the edge without core to the full-depth core. It is customary to separate successive plydrops by distances roughly equal to the core thickness, provided other requirements such as the minimum distance between drops = $10 \times$ plydrop thickness are not violated. Also, plydrops along the ramped itself are usually avoided.

The discussion so far has been qualitative and draws mostly on previous results from Chapter 9. A detailed analytical approach for evaluating ramp-down regions can be found in [15]. The possibility of facesheet and/or core failures in the ramp region are examined in that reference.

A final word related to the ramp-down angle θ is in order. If the ramp angle is large (Figure 10.19a) the ramp is closer to vertical and it is hard to transfer load to the upper facesheet.

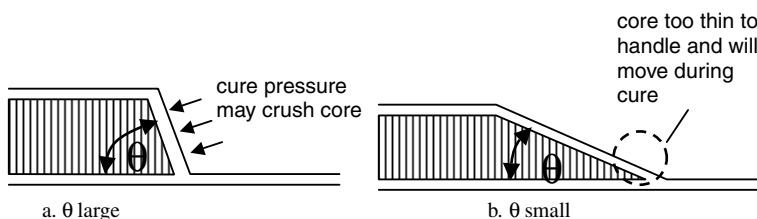


Figure 10.19 Steep versus shallow ramp-down regions

Furthermore, the pressure during cure tends to crush the core. For ramp angles between 30° and 45° , curing an extra layer of adhesive prior to curing the facesheets stabilizes the core and eliminates the crushing problem (at the expense of an extra cure cycle for the adhesive layer). On the other hand, large ramp angles take up less space. If the ramp angle is shallow (Figure 10.19b) the ramp is closer to the horizontal, and transferring load to the upper facesheet is easier. However, small ramp angles result in long ramp-down regions which means significant portions of the sandwich panel have core with lower thickness and thus lower bending stiffness. This can cause stability problems. In addition, for small ramp angles, the end of the core, where the monolithic laminate starts, ends up being very thin. This causes handling problems during fabrication and it is hard to keep the core edge from moving and/or getting crushed under pressure during cure.

The optimum ramp angle will depend on which of the factors mentioned above are favored for a given design and by specific factory practices. Lightly loaded ramps and situations with limited available space tend to favor larger values of θ , while more highly loaded applications will favor lower values of θ which approach a more even distribution of load between the facesheets, provided the local loss of bending stiffness is not prohibitive. For applied bending loads on small panels, where the ramped portions on either side of the panel are a significant fraction of the total panel size, it can be shown that the optimum value of θ is $12\text{--}18^\circ$ (depending on panel size) [15]. This is a result of two opposing tendencies. For large values of θ the core shear and normal stresses are high, and lead to failure. For low values of θ , the core stresses are low, but the deformations are high due to reduced bending stiffness, and they cause failure. The best compromise is reached at intermediate θ values.

10.6.2 Alternatives to Core Ramp-Down

While using a ramp-down has certain advantages, especially for highly loaded situations, it does not come without a price, in particular because of the additional failure modes (core compression or shear) in the ramp-down region that require detailed analysis. Alternatives have been used for a long time and are based on the experience with metal cores [16].

These methods make use of inserts and bushings that span the full depth of the core so there is no need for ramp-down (Figure 10.20). Locally, the core may be densified with higher-density

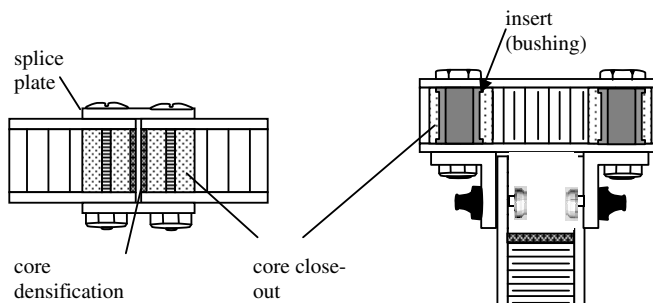


Figure 10.20 Attachments of sandwich parts without ramp-downs

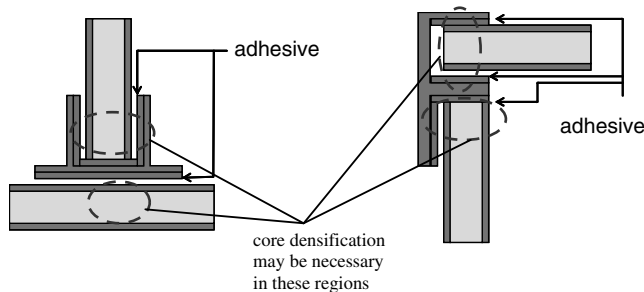
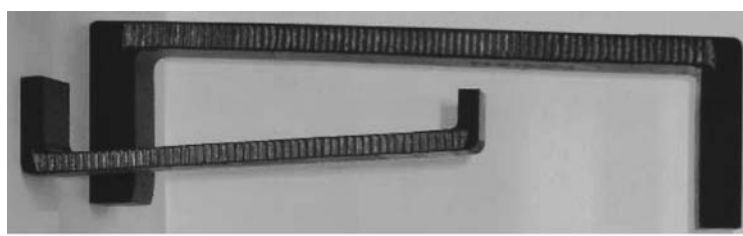


Figure 10.21 Alternate means of joining sandwich structures (See Plate 23 for the colour figure)

core or other material that has the required compression and shear stiffness to meet the loads exerted by clamp-up of bolts or other localized loads.

In addition to these, bonded configurations making use of special purpose joints such as the “pi” and “F” joints shown in Figure 10.21 can be used. Again, local densification of the core may be necessary. Due to the difficulty in accurately controlling the final thickness of the parts to be connected, and the width of the opening of the “pi” or “F” joint (mainly due to spring-back after cure), paste adhesive is used. Controlling the thickness of the bondline and making sure it is within the required range (too thin leads to early failure, too thick causes eccentricities that lead to high bending-induced loads) is the major challenge for these configurations. In addition, the lack of a reliable nondestructive inspection (NDI) technique, that determines whether the bond has the required strength or not, may either force the designer to use fasteners or to build into the configuration sufficient strength and alternate load paths so that, if a significant portion of the bond is compromised, the remainder can still meet limit load requirements. Despite these issues, bonded joints similar to those in Figure 10.21 have been used successfully in airframe structures (see for example [17,18]).

Finally, for relatively thin cores, transitioning to a thick monolithic laminate that forms an “F” joint is also a possibility and has been used successfully (Figure 10.22).



(Courtesy: Aurora Flight Sciences)

Figure 10.22 Core transitioning to monolithic laminate without ramp-down (Courtesy Aurora Flight Sciences) (See Plate 24 for the colour figure)

Exercises

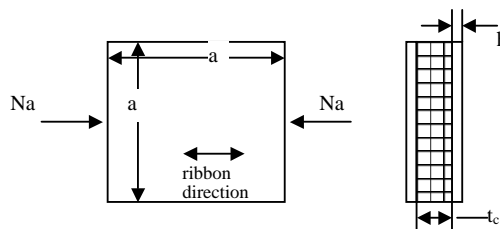
- 10.1 Prove that for antisymmetric wrinkling to occur, the core thickness must satisfy the following relation:

$$t_c < 1.047 f \left(\frac{E_f E_c}{G_{xz}^2} \right)^{1/3}$$

- 10.2a Prove that for a simply supported square composite panel for which $D_{11} = D_{22}$, the number of half-waves m into which the panel buckles under compression is always 1. What should the condition be between D_{11} and D_{22} for the square panel to buckle in two half-waves?

- 10.2b Assume a layup consists of n plies of the same material all at the same orientation (not necessarily 0°). Let E the Young's modulus of a single ply at that orientation, G the corresponding shear modulus, and ν_{12} , ν_{21} the two Poisson's ratios. Derive analytical expressions for $A_{11}, A_{12}, A_{22}, A_{66}, D_{11}, D_{12}, D_{22}, D_{66}$ as functions of E , G , ν_{12} , ν_{21} , and the thickness h of the laminates (still having all plies with the same fiber orientation).

- 10.2c A simply supported square sandwich panel of dimension a and core thickness t_c is under a compression load N_a (units: force/width). Use the results of Exercises 10.2a and 10.2b to express the buckling load N_{crit} as a function of E , G , ν_{12} , ν_{21} , h and t_c . Assume now that the material used is plain weave fabric for which $E_x = E_y$ and simplify the expression you derived (ν_{12} , ν_{21} are replaced by a single Poisson's ratio ν).



- 10.2d In certain circumstances, optimizing a structure that is likely to fail in more than one failure modes with corresponding loads 'reasonably' close to each other, is equivalent to making sure that all failure modes occur simultaneously since this guarantees that the structure is not over-designed (and thus heavier than it needs to be) for any of the failure modes. This is not true in general, but it is true in quite a few cases. Assuming that the wrinkling failure and the buckling failure for the simply supported sandwich of Exercise 10.2c above occur at the same time, derive an expression for the facesheet thickness h (independent of t_c) and the core thickness t_c (which will be a function of h).

- 10.2e Let $a = 381$ mm, $N_a = 175$ N/mm. For the facesheet material assume that $E_x = E_y = 68.94$ GPa, $G_{xy} = 4.826$ GPa, $\nu_{xy} = 0.05$, and $t_{\text{ply}} = 0.1905$ mm. For the core assume $E_c = 133.05$ MPa, (out-of-plane stiffness) and $G_{xz} = 42.05$ MPa (shear stiffness in the ribbon direction). If the ribbon direction is aligned with the loading N_a and the facesheet consists exclusively of (± 45) plies, use the results of Exercise 10.2d to determine the minimum number of plies and minimum facesheet thickness needed. Is this the minimum weight configuration (i.e. is there another pair of values of h, t_c that gives lower weight)?

For the optimum solution you found are the crimping and intracellular buckling requirements also satisfied? (For the latter assume a core cell size of 6.35 mm.)

- 10.3a A skin panel has dimensions 1270×1016 mm and is loaded in compression (along the long dimension of the panel) with $N_x = 121.45$ N/mm. A sandwich design is proposed for this application. The skin layup has been fixed to [45/-45/0/core/0/-45/45]. The facesheet material has the following properties:

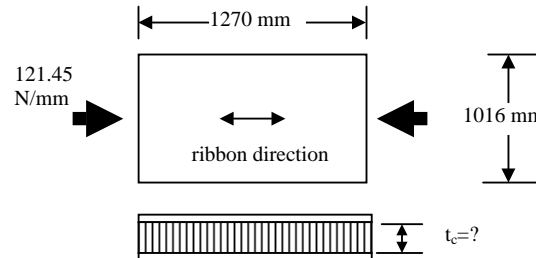
$$\begin{aligned}E_x &= 137.88 \text{ GPa} \\E_y &= 11.03 \text{ GPa} \\G_{xy} &= 4.826 \text{ GPa} \\v_{xy} &= 0.29 \\t_{\text{ply}} &= 0.1524 \text{ mm}\end{aligned}$$

Two Nomex honeycomb materials are proposed with the properties given below:

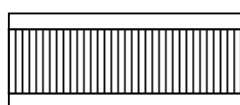
Material	E_c (MPa)	G_{xz} (MPa) (ribbon direction)	G_{yz} (MPa)
HRH-1/8-3.0	133.1	42.05	24.12
HRH-3/16-3.0	122.7	39.29	24.12

Note that in the core material designation, 1/8 and 3/16 denote the cell size (in inches!) and the 3.0 the density (in units of lb/ft³). The second material is cheaper than the first and this is the only reason it is considered as a candidate.

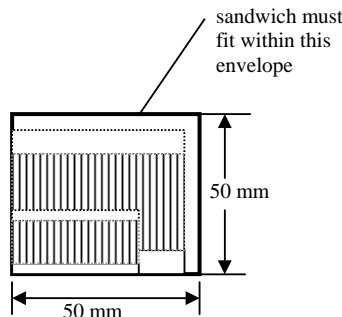
Given the ribbon direction call-out shown below, determine the minimum core thickness needed for each type of core material for the sandwich panel not to fail.



- 10.3b The manufacturing personnel in the factory who will fabricate this panel are very sloppy and careless. The engineer designing the panel is concerned that they will mis-orient the core in the panel and the ribbon direction will be perpendicular to the load. What is the minimum core thickness needed in this case (which will cover all possible errors in core placement during fabrication)? (Do this problem *only* for the first of the two core materials).
- 10.4 (may be done in conjunction with Exercise 8.6 which has the exact same requirements for a stiffener.) Design a sandwich configuration to represent a composite stiffener under compression.



The sandwich design for each stiffener must fit within a 50×50 mm rectangle.



The applied load is 35000 N (assume it is acting at the center of gravity of the selected cross-section). The length ℓ of the stiffener is 550 mm.

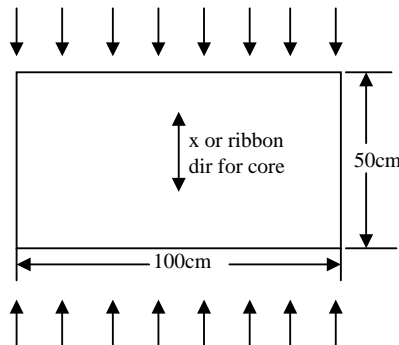
Two composite materials are available, and one core material with properties as follows:

Unidirectional tape graphite/epoxy	Plain weave fabric graphite/epoxy	Nomex core
$E_x = 131$ GPa	68.9 GPa	
$E_y = 11.4$ GPa	68.9 GPa	
$v_{xy} = 0.31$	0.05	
$G_{xy} = 5.17$ GPa	5.31 GPa	
$t_{ply} = 0.1524$ mm	0.1905 mm	
$\rho = 1611$ kg/m ³	1611 kg/m ³	48.2 kg/m ³

Also assume that the honeycomb core is attached to the facesheet (on either side) with an adhesive layer of density 0.147 kg/m². (Watch out for the units!) You are allowed to use any of the two graphite/epoxy materials or a combination thereof. Do not worry about any analysis for the adhesive, it is included here only for the weight calculation. Finally, assume a compression strain allowable (accounting for environment, damage, and material scatter) of 4500 μs .

Determine the layup and core thickness of the sandwich, observing as many of the design rules as possible. (Note that the core is only allowed to take thickness values that are integral multiples of 3.175 mm; this is to save on machining costs.) Provide a simple sketch of the cross-section of stiffeners and sandwich that shows the plies, layup, dimensions, etc. Calculate the corresponding weight. If available, compare with the answer from Exercise 8.6.

- 10.5 (may be done in conjunction with Exercise 7.6.) You are to design a composite panel under compressive load, using sandwich construction. The panel dimensions are 100 \times 50 cm and the applied load is 1750 N/mm acting parallel to the 50 cm dimension.

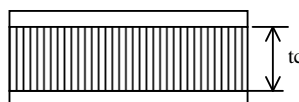


Two composite materials are available, and one core material with properties as follows:

Unidirectional tape graphite/epoxy	Plain weave fabric graphite/epoxy	Nomex core
$E_x = 131 \text{ GPa}$	68.9 GPa	
$E_y = 11.4 \text{ GPa}$	68.9 GPa	$E_c = 133 \text{ MPa}$
$N_{xy} = 0.31$	0.05	
$G_{xy} = 5.17 \text{ GPa}$	5.31 GPa	$G_{xz} = 42.0 \text{ MPa}$
$T_{\text{ply}} = 0.1524 \text{ mm}$	0.1905 mm	Core cell size = 3.2 mm
$X_t = 2068 \text{ MPa}$	1378.8 MPa	
$X_c = 1723 \text{ MPa}$	1378.8 MPa	
$Y_t = 68.9 \text{ MPa}$	1378.8 MPa	
$Y_c = 303.3 \text{ MPa}$	1378.8 MPa	
$S = 124.1 \text{ MPa}$	119.0 MPa	
$\rho = 1611 \text{ kg/m}^3$	1611 kg/m ³	48.2 kg/m ³

Once you determine any strength values needed for any of the layups selected you are to assume the same knockdowns mentioned in Section 5.1.6 for environment, material scatter and damage, i.e. any first-ply failure values should be reduced to the design (or allowable) values by multiplying them by $0.8 \times 0.65 \times 0.8 = 0.416$.

Determine the facesheet layup and core thickness for the sandwich panel not to buckle or fail in any other failure mode up to the applied load of 1750 N/mm. Also assume that the honeycomb core is attached to the facesheet (above and below) with an adhesive layer of density 0.147 kg/m^2 . (Watch out for the units!) For the facesheet, you are allowed to use any of the two graphite/epoxy materials or a combination thereof. Do not worry about any analysis for the adhesive, it is included here only for the weight calculation. The core thickness cannot exceed 5 cm and cannot be any less than 6 mm. Each of the facesheets cannot be thinner than 0.57 mm.



Determine the layup and core thickness of the sandwich, observing as many of the design rules as possible. Provide a simple sketch of the cross-section of the sandwich that shows the plies, layup, dimensions, etc. Calculate the corresponding weight and, if available compare with the post-buckled design of Exercise 7.6.

References

1. Carstensen, T., Cournoyer, D., Kunkel, E. and Magee, C., X-cor® Advanced Sandwich Core Material, *Proc. 33rd Int. SAMPE Conf.*, Seattle, WA, November 2001.
2. Marasco, A.M., Cartié, D.D.R., Partridge, I.K. and Rezai, A., Mechanical Properties Balance in Novel Z-Pinned Sandwich Panels: Out-of-Plane Properties, *Composites Part A: Applied Science and Manufacturing*, **37**, 295–302 (2006).
3. Plantema, F.J., *Sandwich Construction*, John Wiley & Sons, NY, 1966.
4. Timoshenko, S.P. and Gere, J.M., *Theory of Elastic Stability*, McGraw-Hill, NY, 1961, p. 351.
5. Whitney, J.M. and Pagano, N.J., (1970). Shear Deformation in Heterogeneous Anisotropic Plates, *Journal of Applied Mechanics*, **37**, 1031–1036 (1970).
6. Hoff, N.J., Mautner, S.E., The Buckling of Sandwich-Type Panels, *Journal of Aeronautical Sciences*, July 1945, 285–297.
7. Ley, R.P., Lin, W. and Mbanefo, U., Facesheet Wrinkling in Sandwich Structures, *NASA/CR-1999-208994*, January 1999.
8. Vadakke, V. and Carlsson, L.A., Experimental Investigation of Compression Failure Mechanisms of Composite Faced Foam Core Sandwich Specimens, *Journal of Sandwich Structures and Materials*, **6**, 327–342 (2004).
9. Kassapoglou, C., Fantle, S.C. and Chou, J.C., Wrinkling of Composite Sandwich Structures Under Compression, *Journal of Composites Technology and Research*, **17**, 308–316 (1995).
10. Pearce, T.R.A. and Webber, J.P.H., Buckling of Sandwich Panels with Laminated Face Plates, *Aeronautical Quarterly*, **23**, 148–160 (1972).
11. Bruhn, E.F., *Analysis and Design of Flight Vehicle Structures*, S.R. Jacobs & Assoc, Indianapolis, IN, 1973, Section C12.10.3.
12. Sullins, R.T., Smith, G.W. and Spier, D.D, Manual for Structural Stability Analysis of Sandwich Plates and Shells, *NASA CR 1457*, 1969, Section 2.
13. Dobyns, A., Correlation of Sandwich Facesheet Wrinkling Test Results with Several Analysis Methods, *51st American Helicopter Society (AHS) Forum*, Fort Worth, TX, 9–11 May 1995.
14. Birman, V. and Bert, C.W., Wrinkling of Composite Facing Sandwich Panels Under Biaxial Loading, *Journal of Sandwich Structures and Materials*, **6**, 217–237 (2004).
15. Kassapoglou, C., Stress Determination and Core Failure Analysis in Sandwich Rampdown Structures Under Bending Loads, *Fracture of Composites*, E. Armanios (ed.), TransTech Publications, Switzerland, 1996, pp 307–326.
16. Bruhn, E.F., *Analysis and Design of Flight Vehicle Structures*, S.R. Jacobs & Assoc., Indianapolis IN, 1973, Section C12.50.
17. Wong, R., Sandwich Construction in the Starship, *Proc. 37th International SAMPE Symposium and Exhibition*, Anaheim CA, 9–12 March 1992, pp 186–197.
18. Jonas, P., and Aldag, T., Certification of Bonded Composite Structure, *SAE Technical Paper Series, Paper 871022*, 1987; also presented at *SAE General Aviation Aircraft Meeting and Exposition*, Wichita KS, 28–30 April 1987.

11

Good Design Practices and Design ‘Rules of Thumb’

Throughout the previous chapters, several guidelines that result in robust designs have been presented and, in some cases, analytical models that support them were given. In this chapter, all the rules already mentioned in this book are collected and some new ones added to provide a framework within which most composite designs can perform successfully.

Design guidelines are a result of analysis and trending, test results and experience. As such, they typically have a range of applicability (especially in terms of the stacking sequences to which they apply) outside of which they may or may not be as successful. There is no reason why any and all of the guidelines should be closely followed. Deviations and departures from them are often necessary. As long as the reasons for deviation are understood and test results and accurate analysis are available to support that deviation, there is no reason to limit the designs by following these guidelines. In fact, there is a motivation to open up or reformulate some of these guidelines in order to generate more efficient and/or more robust designs in the future [1].

The most important guidelines with a brief discussion are listed below. Other guidelines and/or variations of the ones presented below can be found in the literature, for example, in reference [2].

11.1 Layup/stacking Sequence-related

1. The *layup* (stacking sequence) of a laminate *should be symmetric*. This eliminates unwanted (and difficult to analyze) membrane/bending coupling (B matrix is zero).
2. The *layup should be balanced* (for every $+\theta$ ply there should be a $-\theta$ ply of the same material and thickness somewhere in the laminate). This eliminates stretching/shearing coupling ($A_{16}=A_{26}=0$).
3. *Bending/twisting coupling should be avoided*. One way to achieve this is to use antisymmetric layups, but this violates guideline number 1. Another is to use fabric materials and unidirectional materials exclusively in the 0 and 90° directions. When these options are not

possible, layups where D_{16} and D_{26} are small compared with the remaining terms of the D matrix should be preferred. To that end, $+θ$ and $-θ$ plies should be grouped together. Also, special classes of laminates with negligible D_{16} and D_{26} are possible [3].

4. *The 10% rule.* At least 10% of the fibers in every layup should be lined up with each of the four principal directions: 0, 45, -45, and 90. This protects against secondary load cases, which have small load magnitudes and thus are not included in the design effort, but could lead to premature failure if there are no fibers in one of the four principal directions. In some cases, instead of 10% other values (12, 15%) are also used.
5. *Minimization of the number of unidirectional plies with same orientation next to each other.* If there is a number of unidirectional (UD) plies of the same orientation next to each other, then a matrix crack forming in them can grow easily in the matrix and extend from one end of the identical ply stack to the other without being arrested. Such cracks can be caused by thermal stresses during cure or due to transverse loading during service (transverse to the orientation of the fibers in the ply stack in question). It is recommended to avoid ply stacks of the same ply orientation that exceed 0.6–0.8 mm (corresponding to 4–5 plies for typical UD materials). Interrupting the ply stack with plies of different orientation (preferably with at least 45° difference from the plies in the ply stack) provides a means to arrest microcracks. The probability of microcracks coalescing and/or creating delaminations is minimized.

11.2 Loading and Performance-related

6. To improve the *bending stiffness of a one-dimensional composite structure* place 0° plies as far away from the neutral axes as possible (this maximizes D_{11}).
7. *Panel buckling and crippling improvement.* Place 45/-45 plies as far away from the neutral axis as possible (this maximizes D_{66}).
8. *Fastener rule 1.* Maintain skin thickness/fastener diameter ratio <1/3 to minimize fastener bending (Figure 11.1a).
9. *Fastener rule 2 (countersunk fasteners).* Maintain skin thickness/to countersunk depth >2/3 to avoid pulling the fastener through the skin under out-of-plane loads (Figure 11.1b).
10. *45° fabric plies on the outside.* To improve damage resistance, i.e. to limit the amount of damage caused by low speed impact, fabric plies should be placed on the outside of a stacking sequence. They limit the amount of fiber splitting and help contain splits created in the first (impacted) or last ply.
11. *Skin layup should be dominated by 45/-45 plies.* Using 45 and -45° plies improves the shear stiffness and strength of the layup. This is also a good rule to follow for beam or stiffener webs under shear loads in the plane of the web.
12. *Fastener rule 3.* For improved load transfer around fasteners in bolted joints, at least 40% of the fibers should be in the +45° and -45° directions relative to the applied axial load.
13. *Fastener rule 4.* To avoid interaction and increased stress concentrations *fastener spacing* should be at least 4–5D where D is the fastener diameter (Figure 11.1c). This only ensures that the full by-pass load is developed between fasteners, and the load distribution around one fastener does not affect that around its neighbors. This decreases

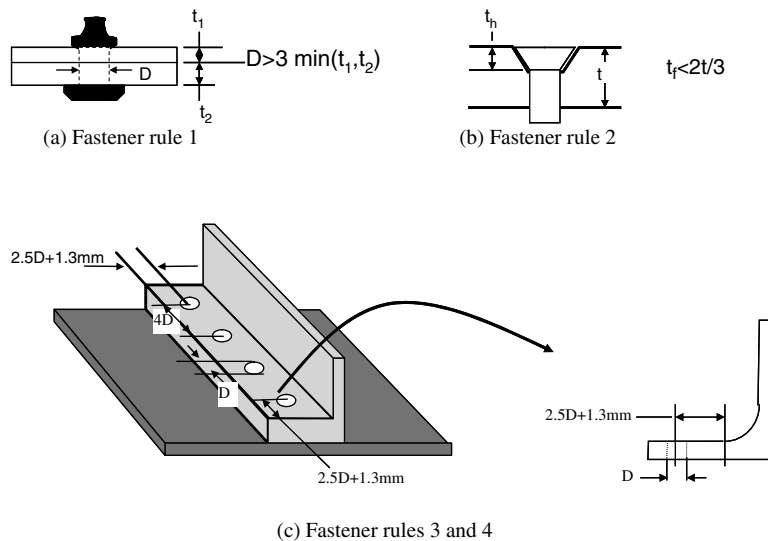


Figure 11.1 Fastener rules of thumb

the stress concentration effect. It does not account for other considerations such as inter-fastener buckling (see Section 8.7) or potential improvements in bolted joint performance with lower spacings alluded to in Section 8.7. Specific requirements of each design might supersede this guideline

14. *Fastener rule 5 (edge distance).* To minimize edge effects (so that the load distribution around the fastener approaches that of a fastener in an infinite plate) the edge distance between a fastener and the edge of a part should be no less than $2.5D + 1.3$ mm where D is the fastener diameter (see Figure 11.1c). This includes the distance of a fastener from the tangency point of the radius region of a web transitioning to a flange (see Figure 11.1c).
 15. *Plydrop guidelines.* See Figure 11.2.
 - a. Avoid external plydrops. The tendency to delaminate at the edge of the terminating ply is high. Plydrops should be as close to the midplane of the laminate as possible.
 - b. For more than one plydrop, try to drop plies symmetrically with respect to the midplane of the laminate.
 - c. Avoid dropping more than 0.5 mm worth of plies at the same location to minimize the interlaminar stresses created (see typical results in Section 9.2.2).
 - d. The distance between successive plydrops should be at least 10 or 15 times the dropped height to avoid constructive interference (enhancement of stresses) between the stresses at the different plydrop sites (see Section 9.2.2).
 16. *Anti-peel fasteners.* For highly post-buckled stiffened panels with co-cured stiffeners, using two fasteners at each stiffener end postpones or eliminates the skin-stiffener separation failure mode (see Section 9.2.2 and Figure 9.21).

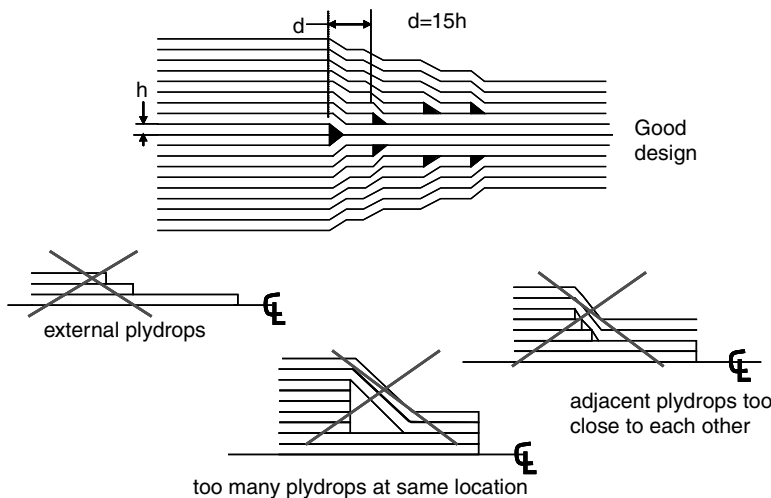


Figure 11.2 Plydrop guidelines

11.3 Guidelines Related to Environmental Sensitivity and Manufacturing Constraints

17. *Minimum gage.* For lightly loaded structure, the thickness should be no lower than 0.5–0.6 mm to keep moisture from seeping into the structure. For lower thicknesses, additional coating protecting against moisture should be used.
18. *Minimum flange width.*
 - a. *Fastener rule 6.* If fastened, the minimum flange width is the sum of edge distances from guideline 14: $5D + 2.6$ mm from the flange edge to the tangency point of the web-to-flange transition.
 - b. If *co-cured or bonded* the minimum flange width for lightly loaded structure is 12.7 mm and for highly loaded structure is 19 mm. These values are the minimum required for the load shearing through the flange to reach at least 95% of its far field value.
19. *Minimum web height.* To avoid damage during handling and to make fabrication easier, the minimum web height should be 18 mm. This is particularly important for stiffeners with flanges at both ends of the web (I, J, C, Z) where access to the web is limited.
20. *Bridging avoidance.* Avoid 90° plies going around corners (see Figure 11.3) in particular when convex tools are used during layup. It is very hard to make the stiff 90° fibers conform to the shape of the tool and, usually, bridging occurs where a void and/or resin pocket is created.

11.4 Configuration and Layout-related

21. *Preferred stiffener shapes.* Unless the structure is lightly loaded, stiffeners with a one-sided flange (L, C, Z) on the skin side should be avoided and stiffeners with flanges on

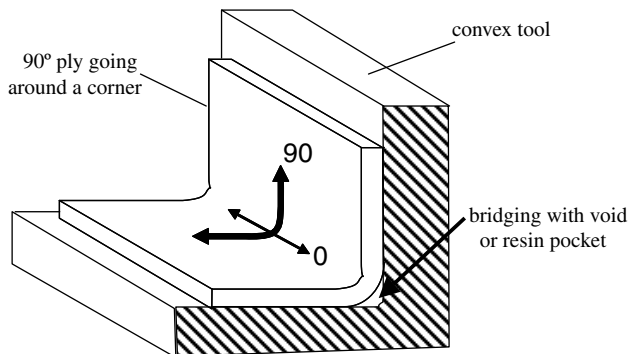


Figure 11.3 Bridging at a corner

either side of the web should be preferred (T, I, J, Hat). This protects the resin pocket present at the web flange corner (see Figure 11.4) from moisture and contamination and minimizes the possibility that matrix cracks may develop there and coalesce into delaminations under fatigue loading.

22. *Stiffener and frame spacing.* While the optimum spacing of frames and stiffeners will be dictated by the design loads and cost and weight considerations, a configuration that has been found to be robust and reasonably efficient is frame spacing of 500–510 mm and stiffener spacing of 150–160 mm. This is, approximately, the same configuration used in many metal structures and combines relatively low cost and weight. While lower stiffener spacing can lead to lower weights the cost can be prohibitive as it increases rapidly with the number of stiffeners. At the other end of the spectrum, using high stiffener spacing reduces the cost, but increases the weight since the skin thickness must increase to meet buckling and post-buckling requirements and the stiffener thickness must increase to maintain the desired ratio of stiffener to skin loads.

At this point, with all the design guidelines in place, the J stiffener cross-section that has been used all along as an example last discussed in Section 9.2.2, Figure 9.20, can be revisited and the preliminary configuration can be finalized. This is shown in Figure 11.5. This is preliminary in the sense that no specific load has been used to design it. The final dimensions and layup would depend on the applied loads. What is shown in Figure 11.5 is just a good starting point

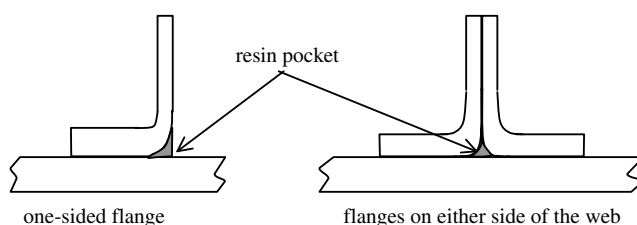


Figure 11.4 Exposed resin pockets may lead to delaminations easily

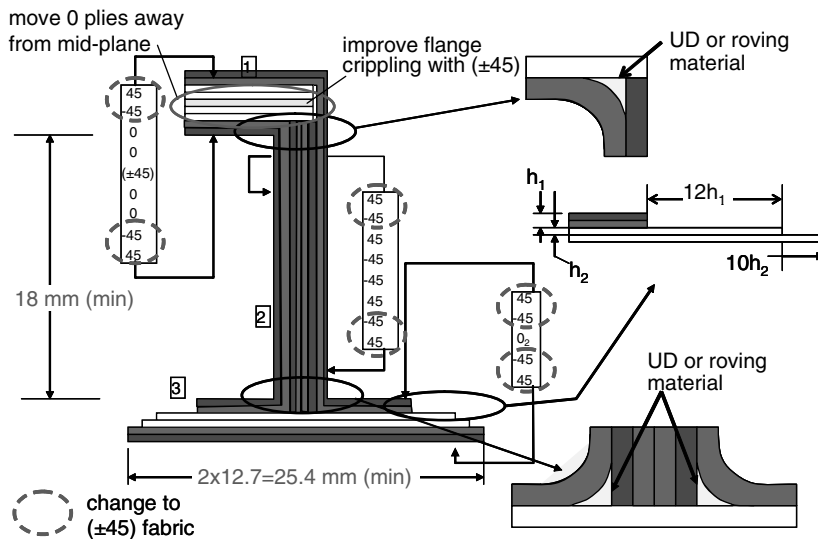
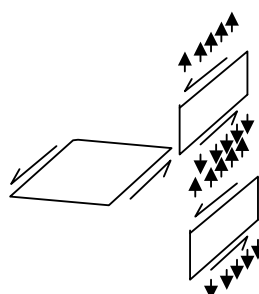


Figure 11.5 Stiffener cross-section created on the basis of design guidelines

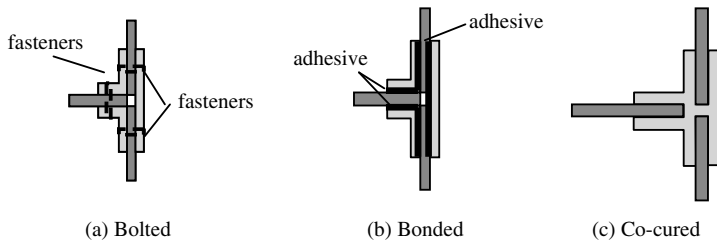
applicable to lightly loaded stiffeners. Note that what is shown in Figure 11.5 does not satisfy the 10% rule.

Exercises

11.1 Consider three composite parts intersecting at right angles as shown in the figure below. They are under tension and shear loads as shown.



Three different methods for assembling them together are proposed, shown below: (a) bolted connections, (b) bonded connections, and (c) co-cured with the use of a 3-D preform.



Discuss the merits and disadvantages of each of the three approaches from a weight and cost perspective. Combine the material from this chapter with that from Chapter 2. Include in your discussion (but do not limit it to) assembly cost associated with fastener installation, weight impact of use of fasteners, bearing load requirements, bondline thickness control, inspection issues of adhesive, use of RTM with 3-D preforms and associated tooling cost, effect of process on final strength and stiffness, etc.

- 11.2 Referring to Figure 11.4, determine which of the design guidelines presented in this chapter are not satisfied and discuss the implications. (For example, the web layup does not satisfy the 10% rule.)

References

1. Abdalla, MM, Kassapoglou, C. and Gurdal Z., Formulation of Composite Laminate Robustness Constraint in Lamination Parameters Space, *Proc. 50th AIAA/ASME/ASCE/AHS/ASC Structures, Structural Dynamics and Materials Conf.*, Palm Springs CA, 4–7 May 2009.
2. Beckwith, SW, Designing with Composites: Suggested 'Best Practices' Rules, *SAMPE Journal*, **45**, 36–37 (2009).
3. Caprino, F. and Crivelli Visconti, I., A Note on Specially Orthotropic Laminates, *Journal of Composite Materials*, **16**, 395–399 (1982).

Index

- A-Basis values, 75, 78, 79, 113
adhesive, 82, 179, 252, 259–61, 272, 282–3, 286–7, 295
airframe, 20–1, 63–5, 72, 77, 81, 188, 194–5, 283
allowable, 57–8, 78–9, 138, 169, 217, 218
antisymmetric laminate, 289
aspect ratio, 121, 123, 128–9, 131, 136–7, 157, 174
automated fiber/tow placement, 12, 13, 14, 20

balanced laminate, 34, 39, 219
B-Basis values, 75, 78–80, 113, 115, 199, 202, 230, 235
beam, 1, 4, 5, 21, 28, 29, 64, 119, 138, 179, 262
 beam cross-section properties, 182–8
bearing of fasteners, 71, 72, 213, 280–1, 295
bending stiffness of laminate, 47, 165, 183–7, 225–7, 260–1, 290
black aluminium, 63, 81
boundary conditions, 81, 107, 148
 effect on plates, 138, 141
 effect on beams, 189
 effect on beams on elastic foundation, 192–94
bolts (see fasteners)
buckling, 28, 70–2, 228, 262–5, 290
 beams, 188–94
 beams on elastic foundation, 189–94
 plates, 119
bulkhead, 5, 21, 27–8, 64, 70
BVID, 77–9

calculus of variations, 244, 255
cell size, 258–9, 285, 287

closed-section beams, 148
 on plates, 227
 crippling, 207
column buckling, 147–8, 188–9, 195, 228, 279
complexity, 4, 9–10, 18–22
core, 3, 17, 23, 70, 82, 259
 double-flex core, 278–9
 flex core, 279
 stabilization, 282
corrosion resistance, 5, 64–5
cost, 1, 9, 63–7, 77, 79, 81, 115, 143, 211, 250–3, 258, 279, 286, 293, 295
assembly, 11, 251, 295
labor, 10, 15, 23, 65, 252
raw material, 10–1, 14, 28–9
cure cycle, 27, 252, 282
crimping (see shear crimping)
crippling, 70, 71, 147–8, 170, 194, 219–20, 229, 290, 294
 one-edge-free crippling, 195–6
 no-edge-free crippling, 196, 200
 under bending loads, 202–4
cross-ply laminate, 34, 44
cross-section, 147, 148, 176–9, 227, 230, 250
 properties, 182–8, 204
curvature, 46–8, 51, 56, 84, 88, 90, 91, 108–9, 185

damage, 19, 28, 55, 65, 76–80, 103, 148, 174–6, 181–2, 206, 228, 286–7, 290
deck, 21, 23–4, 26, 28, 64, 71
delamination, 18, 55, 61, 70–1, 76, 145, 147, 239, 249, 256, 258, 290, 293

- design, 9, 18, 28, 50, 63, 145, 179–224, 261, 262
 guidelines, 289–94
 process, 20, 64–9
 requirements, 63–7, 198–9
 values, 78–80
 diagonal tension, 162–8, 168, 172–3, 177, 251
 doors, 21, 23–8, 64, 71
 dimpling, 82, 278–9
 equivalent properties, 155, 183, 223–7
 membrane stiffness, 51, 84, 110, 165, 184, 223–5
 bending stiffness, 47, 165, 183–7, 225–7, 234–6, 260–2, 290
 effective skin, 216, 220, 233
 eigenvalue problem, 127–41
 generalized, 135
 standard, 135–6
 elastic foundation (see buckling)
 energy, 106–13, 130, 133, 143, 190, 244, 255, 266
 potential energy, 106–7, 130, 133, 190, 255
 complementary energy, 106–7, 110, 244
 environmental effects, 57, 75–6, 78–81, 174–5
 equilibrium equations, 82–3, 89–90, 96, 106, 240, 242, 255
 external work, 107, 110, 255, 268
 Euler equations, 244, 255
 failure, 55–61, 81, 82, 148, 227–8, 290
 first-ply, 56, 60, 199, 220, 287
 material, 148, 195
 failure index, 218
 failure mode, 18–55, 60, 81–2, 148, 194–6, 211, 213, 227–8
 fasteners, 63, 81, 210–4, 250, 280–1, 290–1, 295
 filament winding, 12, 14, 29–30
 filler, 208–15
 finite element method, 68, 82, 98, 239, 246, 249, 272
 first-ply failure (*see* failure)
 fit, form, and function, 64, 65, 67
 fitting, 14, 15, 21, 23–29, 60, 64, 71
 fixity coefficient, 212
 flange of stiffener, 162, 163, 176, 179–82, 205–57, 291–94
 floor, 21, 23, 28, 64, 71
 frame, 14, 21, 22, 26–8, 64, 70, 92, 160, 163–5, 169–71, 293
 frequency placement, 1, 65
 handling problems, 282, 292
 holes, 31, 66, 117
 honeycomb, 259–60, 272–3, 278–9, 285–7
 impact damage, 2, 77–8, 103, 117, 181–2, 206
 intercostals, 21, 29, 64, 71
 interface of skin/stiffener, 236–49
 interlaminar stresses, 245, 249, 258, 291
 interphase of fiber/matrix, 55–6
 inter-rivet buckling, 70, 210–4, 227–8
 intracellular buckling, 70, 82, 278–9
 K-cor®, 259
 Kirchhoff hypothesis, 46, 262
 layup, 33–35, 77–81, 99–104, 157–9, 179–83, 249, 289–90
 lightening holes, 66
 limit load, 73, 77–8, 147, 252, 283
 loading index, 82, 217
 load transfer, 66, 69, 179, 181–2, 214, 279, 290
 loads, 46, 48, 65–9, 72–5, 132, 137–9, 147, 162–3, 202, 276, 290
 margin of safety, 82, 31, 175
 material scatter, 57, 73–5, 78–9, 114, 124, 143, 175–6, 206, 222, 286–7
 matrix cracks, 55–6, 293
 matrix pocket, 208, 292–3
 maximum strain failure criterion, 58
 maximum stress failure criterion, 57
 membrane deformations, 46, 48, 50
 membrane stiffness of laminate, 50–1, 84, 110, 165, 184, 223–225, 233
 microcracking, 181–2, 290
 micromechanics, 55, 60, 61
 midplane strains, 48, 56, 84–5, 88, 91, 93, 108–9, 151
 NDI (see nondestructive inspection)
 no-edge-free (see crippling)
 nondestructive inspection, 252, 283
 notch, 70–2, 76, 281
 notch sensitivity, 76

- one-edge-free (see crippling)
- panel breaker condition, 228–36
- part, 1, 7, 10, 16–31, 63–72, 251–4, 294
- part families, 20–27, 63
- pinching of skin, 251
- plates, 86, 107
- buckling, 119–44
 - post-buckling, 145–62
- plydrops, 28, 280–1, 291–2
- post-buckling angle, 162, 164, 169–71
- post-buckling factor, 147, 164, 176
- post-buckling ratio, 147, 154, 158, 164, 232–3, 261
- potential function, 90
- press molding, 14–15, 29
- pultrusion, 14, 21, 26–9
- quasi-isotropic laminate, 34–6, 63, 80–1, 99, 121–6, 156
- radius of curvature, 28, 185
- rate of twist, 226
- resistance to fluids, 65
- resin film infusion, 12, 28
- resin transfer molding, 11, 20–1, 29
- reserve factor, 66, 82, 175
- rib, 21, 28, 29, 64, 71, 142, 194
- ribbon, 175, 284–6
- risk, 1, 6, 19–27, 252
- roving, 207, 209, 294
- sandwich, 3–4, 20–1, 67, 71, 82, 207, 259–88, 272–83
- scatter (see material scatter)
- scrap rate, 28–9, 252
- sequencing of failure modes, 228
- shear correction factor, 263
- shear deformation theory, 263
- shear crimping, 70, 82
- sheet molding compound, 14
- sign convention (forces and moments), 45, 83
- skin–stiffener separation, 119, 145, 170, 227, 236–51, 291
- smeared properties (see equivalent properties)
- sources of uncertainty, 72
- applied loads, 73
 - usage, 73
- material scatter, 73
- spar, 64, 71, 141, 142
- spring constant, 189, 193, 218, 273
- stabilization (see core stabilization)
- stacking sequence, 33–5, 48, 52, 117, 157–8, 236, 289
- steered fibers, 13
- stiffener, 21, 29, 64, 92, 145–8, 169–77, 179–257, 290
- stiffness, 33–51, 223–7, 260–2
- membrane, 50–1, 184, 223–5
 - bending, 47, 51, 183, 185, 225–7, 260–2, 290
- stiffness mismatch, 179–82, 236, 247–8, 280
- strain, 35–7
- compatibility, 85, 90–3, 106–7, 173, 185, 208, 232, 242
 - cutoff 169, 170
 - engineering, 44
 - midplane strain, 48, 56, 84–93, 109, 151
 - tensor, 44
- strain–displacement equations, 82, 85, 89, 106, 109
- stress–strain equations, 43, 82, 84, 93, 106, 110, 167, 242, 267
- stringer, 3, 14, 20–1, 23–4, 26–7, 29, 64, 70, 163–5, 179, 194, 258
- structural configuration, 66–7
- symmetric laminate, 34–5, 49, 51, 227
- technology, 20–7
- technology mix (optimum), 20, 24–7
 - applicability of a technology, 21, 23, 26
- thermal expansion coefficient
- placement, 65
- threshold of detectability, 77
- transverse shear effects, 262–5
- Tsai–Hill failure criterion, 58–60
- Tsai–Wu failure criterion, 59–60, 216
- ultimate load, 73, 77–8, 113
- usage, 64, 72–3
- vacuum-assisted resin transfer molding, 12, 28
- variability (see sources of uncertainty)
- variational calculus (see calculus of variations)

- void content, 76
von Karman plate equations, 86–91
waviness, 272–5
web of stiffener, 205, 210, 236, 239, 290
- wrinkling, 70, 72, 82, 207, 265
symmetric, 265–71, 275
antisymmetric, 265, 271, 272, 275, 278, 284
- X-cor®, 259, 288



Plate 1 Figure 1.1 Akaflieg Phönix FS-24 (Courtesy: Deutsches Segelflugzeugmuseum)



Plate 2 Figure 1.2 Aerospatiale SA 341G Gazelle (Copyright Jenny Coffey printed with permission)



Plate 3 Figure 1.3 Long EZ and Vari-Eze (Vari-Eze, photo: courtesy Stephen Kearney; Long EZ, photo: Courtesy Ray McCrea)



Plate 4 Figure 1.4 Lear Avia LearFan 2100 (Copyright: Thierry Deutsch)



Plate 5 Figure 1.5 Beech (Raytheon Aircraft) Starship I (Photo courtesy Brian Bartlett)



Plate 6 Figure 1.6 Airbus A-320 (Photo courtesy Brian Bartlett)



Plate 7 Figure 1.7 Boeing 777 (Photo courtesy Brian Bartlett)



Plate 8 Figure 1.8 Airbus A-380 (Photo courtesy Bjoern Schmitt – World-of-Aviation.de)



Plate 9 Figure 1.9 Boeing 787 Dreamliner (Courtesy of Agnes Blom)

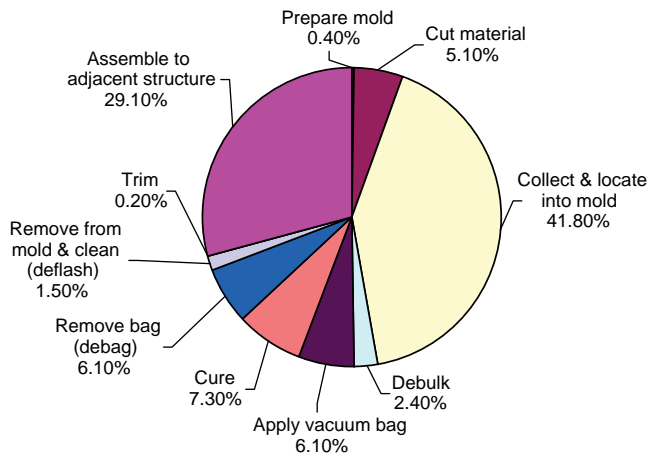


Plate 10 Figure 2.1 Process steps for hand layup and their cost as fractions of total recurring cost [3]

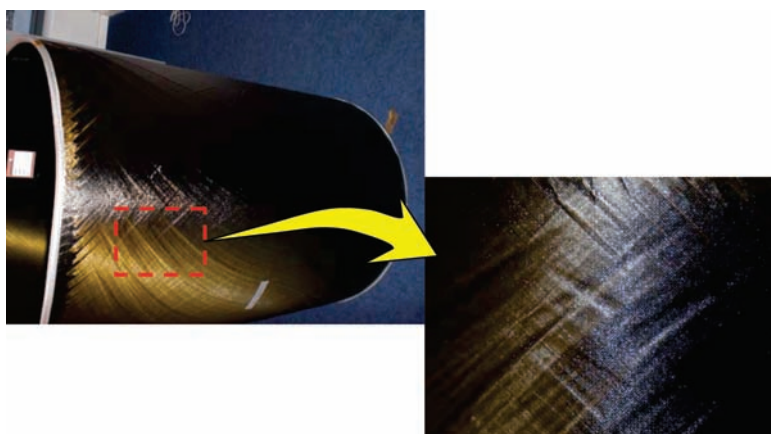


Plate 11 Figure 2.5 Composite cylinder with steered fibers fabricated by automated fiber placement (made in a collaborative effort by TU Delft and NLR)

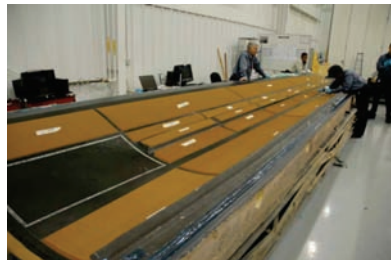


Plate 12 Figure 2.9 Co-cure of large complex parts (Courtesy Aurora Flight Sciences)

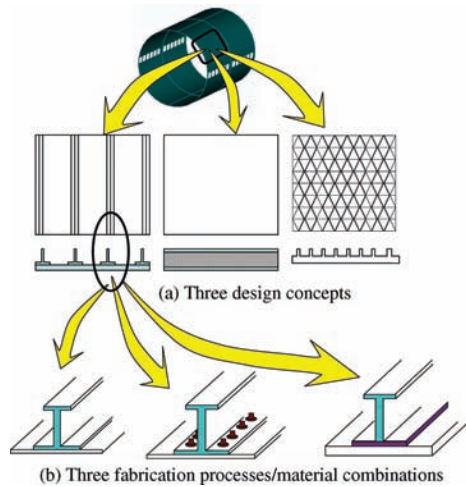


Plate 13 Figure 5.4 Options to be considered during design/analysis of a part

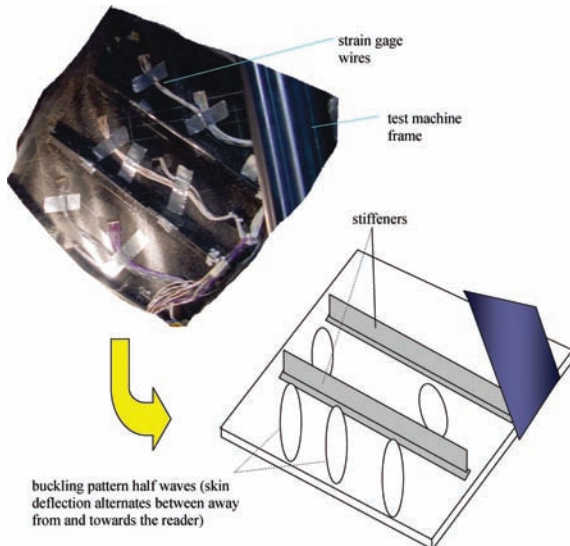


Plate 14 Figure 6.1 Composite stiffened panel buckling under shear

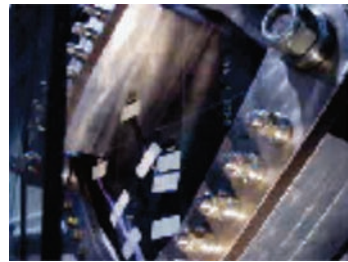


Plate 15 Figure 7.1 Post-buckled curved composite stiffened panel

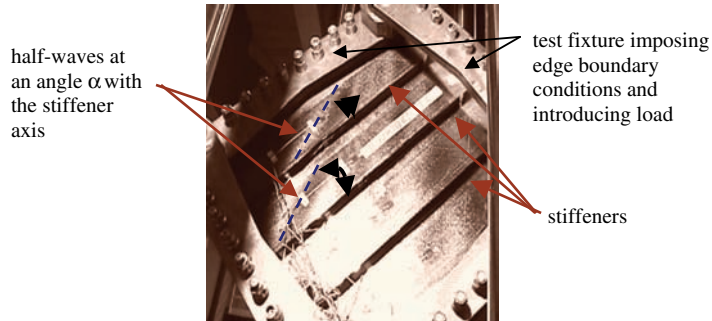


Plate 16 Figure 7.13 Stiffened composite panel in the post-buckling regime

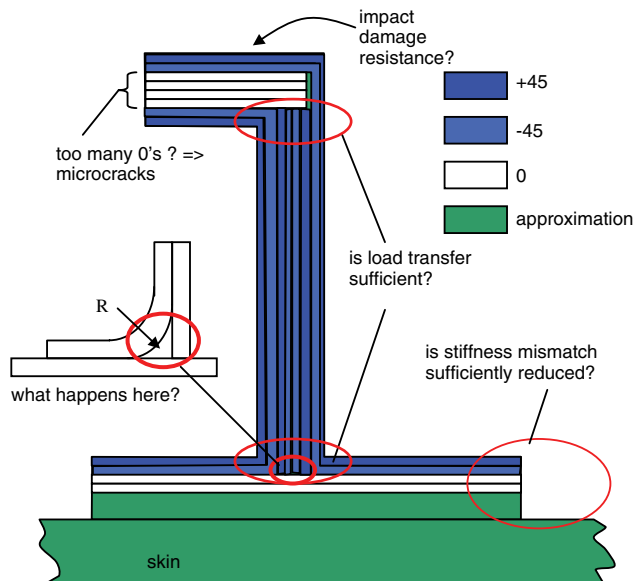


Plate 17 Figure 8.4 Improved stiffener cross-section design

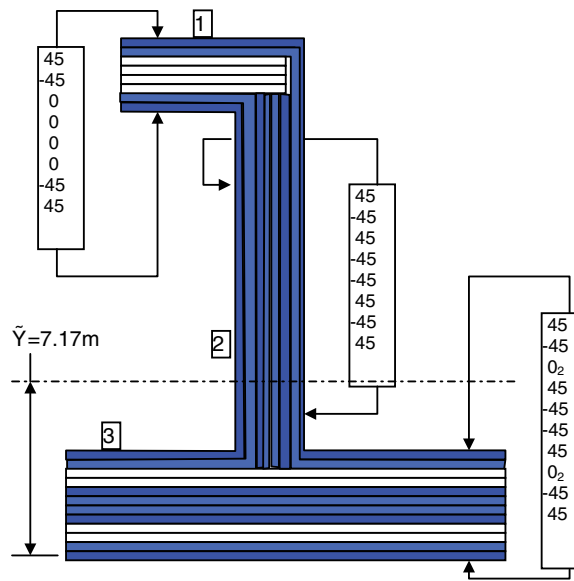
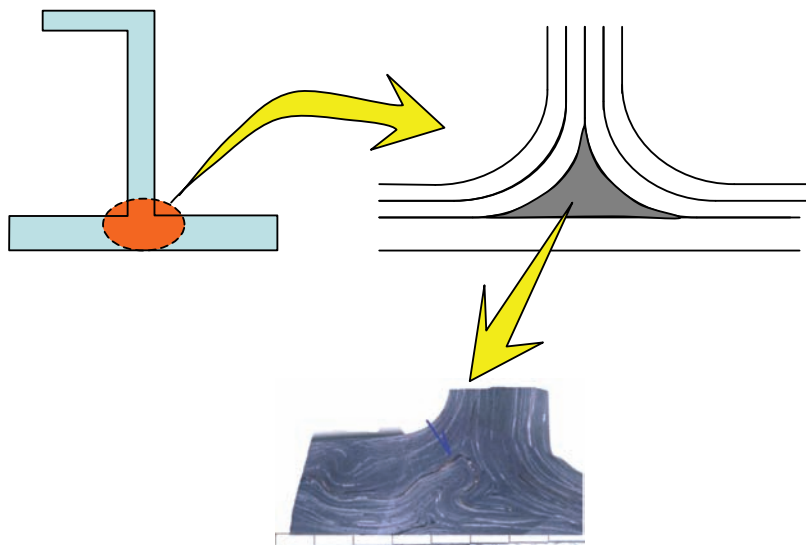


Plate 18 Figure 8.6 Baseline J stiffener cross-section made out of composite materials



without special provisions, this region fills
with wavy fibers and/or pure resin

Plate 19 Figure 8.27 Resin pocket formed at web/flange intersection of a stiffener

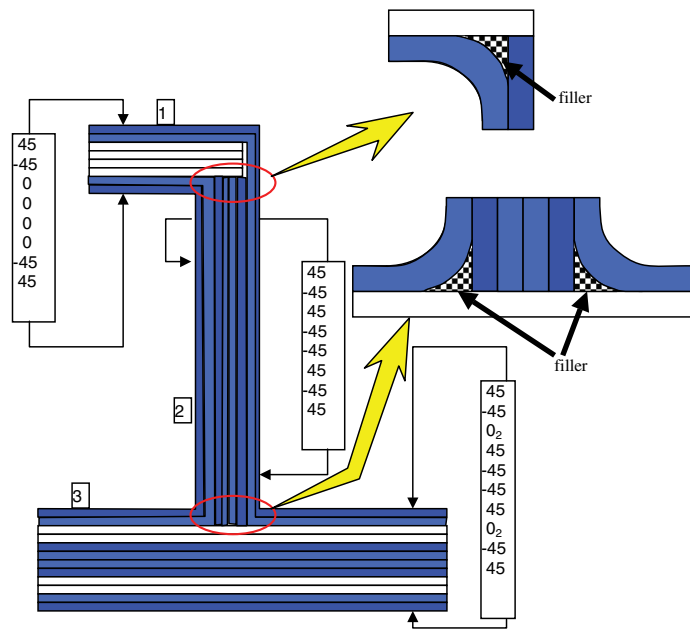


Plate 20 Figure 8.31 J stiffener cross-section with filler material

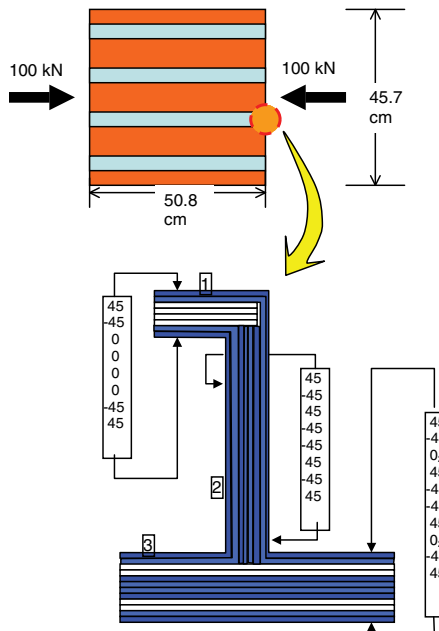


Plate 21 Figure 8.36 Skin-stiffened panel under compression

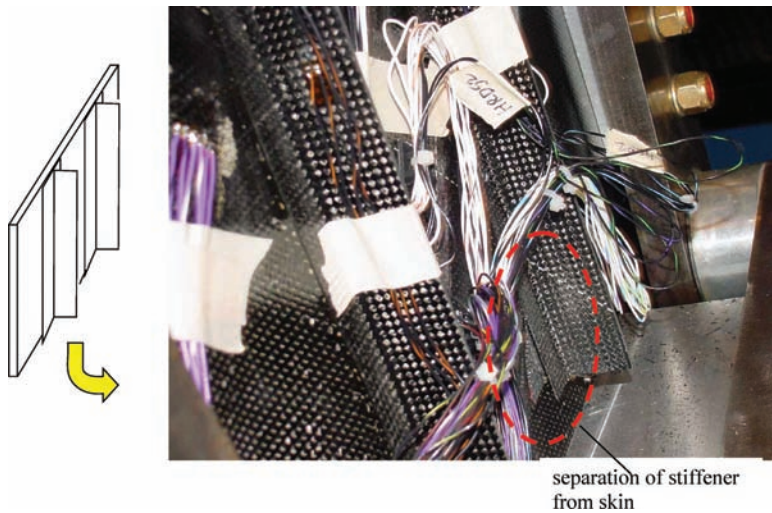


Plate 22 Figure 9.13 Skin–stiffener separation failure mode

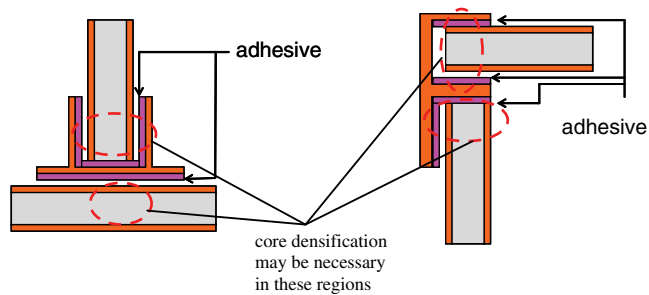


Plate 23 Figure 10.21 Alternate means of joining sandwich structures



(Courtesy: Aurora Flight Sciences)

Plate 24 Figure 10.22 Core transitioning to monolithic laminate without ramp-down (Courtesy Aurora Flight Sciences)